On the Estimation of Center of Gravity Height of Arbitrarily Loaded Articulated Freight Vehicle

Feng Yang

A Thesis

in

The Department

of

Mechanical and Industrial Engineering

Presented in Partial Fulfillment of the Requirements
for the Degree of Master of Applied Science (Mechanical Engineering) at
Concordia University
Montreal, Quebec, Canada

March 7, 2005

Your file Votre référence
ISBN: 0-494-04206-0
Our file Notre référence
ISBN: 0-494-04206-0

ABSTRACT

On the Estimation of Center of Gravity Height of Arbitrarily Loaded Articulated Freight Vehicle

Feng Yang

The accurate prediction of an impending rollover threat of a heavy vehicle forms the essential basis for developing a rollover prevention system. The vehicle roll stability and the rollover predictors are most significantly related to the center of gravity height of the trailer sprung mass, which tends to vary considerably. The developments in the rollover warning devices have been mostly limited due to extreme complexities associated with the onsite measurement of the center of gravity height of an arbitrarily loaded vehicle. In this study, the system identification techniques are applied to obtain an estimate of the c.g. (Center of Gravity) height on the basis of the measured response under a controlled directional maneuver. A simulation model of a five-axle tractor-semitrailer is analyzed in the TruckSim environment to identify the desirable response measure, which is most sensitive to variation in the c.g. height, and the test maneuver for deriving the desired response. A 10 D.O.F. (degree-of-freedom) analytical model of the vehicle is developed and linearized to derive the analytical transfer function relating the steer angle to the desired semitrailer sprung mass roll angle response. A model reduction technique is further applied to obtain a reduced-order analytical transfer function to facilitate its implementation. A compensation function is then formulated to account for possible contribution due to model reduction and model

simplification, on the basis of a target response derived from a well-known Yaw/Roll program. System Identification technique is applied to identify the vehicle transfer function from the measured, representative data. A c.g. height estimation algorithm is developed for estimating the c.g. height of an arbitrarily loaded vehicle by comparing the coefficients of the two transfer functions: compensated analytical and identified transfer functions. The robustness of the proposed algorithm is examined in terms of its effectiveness under varying levels of signal to noise ratio, and variation in selected vehicle parameters. The simulation result shows that the proposed algorithm offers considerable potential for implementations for online estimation of the c.g. height.

ACKNOWLEDGEMENTS

The author wishes to express his sincere appreciation to his thesis supervisors, Dr. Subhash Rakheja and Dr. Ion Stiharu, for initiating the study topic and providing continued guidance thought the course of this investigation.

Finally, the author would like to express his special thanks to his wife, Lilong Chen, for her understanding and encouragement.

TABLE OF CONTENTS

LIST OF FIGURES

LIST OF TABLES

NOMENCLATURE

A_2	Tire spacing of axle 2 (m)
A_3	Tire spacing of axle 3 (m)
A_4	Tire spacing of axle 4 (m)
A_5	Tire spacing of axle 5 (m)
F_1	Load of axle 1 (kN)
F_2	Load of axle 2 (kN)
F_3	Load of axle 3 (kN)
F_4	Load of axle 4 (kN)
F_5	Load of axle 5 (kN)
F	Fifth wheel vertical load applied on tractor (kN)
F'	Fifth wheel vertical load applied on semitrailer (kN)
F_{11}	Suspension force of left spring of axle 1 (kN)
F_{12}	Suspension force of right spring of axle 1 (kN)
F_{21}	Suspension force of left spring of axle 2 (kN)
F_{22}	Suspension force of right spring of axle 2 (kN)
F_{31}	Suspension force of left spring of axle 3 (kN)
F_{32}	Suspension force of right spring of axle 3 (kN)
F_{41}	Suspension force of left spring of axle 4 (kN)
F_{42}	Suspension force of right spring of axle 4 (kN)
F_{51}	Suspension force of left spring of axle 5 (kN)
F_{52}	Suspension force of right spring of axle 5 (kN)
F_{R_1}	Roll center force of axle 1 (kN)
F_{R_2}	Roll center force of axle 2 (kN)
F_{R_3}	Roll center force of axle 3 (kN)
F_{R_4}	Roll center force of axle 4 (kN)
F_{R_5}	Roll center force of axle 5 (kN)
$F_{y_{11}}$	Tire 1 lateral force of axle 1 (kN)
$F_{y_{12}}$	Tire 2 lateral force of axle 1 (kN)
$F_{y_{21}}$	Tire 1 lateral force of axle 2 (kN)

$F_{y_{22}}$ Tire 2 lateral force of axle 2 (kN)

$F_{y_{23}}$ Tire 3 lateral force of axle 2 (kN)

$F_{y_{24}}$ Tire 4 lateral force of axle 2 (kN)

$F_{y_{31}}$ Tire 1 lateral force of axle 3 (kN)

$F_{y_{32}}$ Tire 2 lateral force of axle 3 (kN)

$F_{y_{33}}$ Tire 3 lateral force of axle 3 (kN)

$F_{y_{34}}$ Tire 4 lateral force of axle 3 (kN)

$F_{y_{41}}$ Tire 1 lateral force of axle 4 (kN)

$F_{y_{42}}$ Tire 2 lateral force of axle 4 (kN)

$F_{y_{43}}$ Tire 3 lateral force of axle 4 (kN)

$F_{y_{44}}$ Tire 4 lateral force of axle 4 (kN)

$F_{y_{51}}$ Tire 1 lateral force of axle 5 (kN)

$F_{y_{52}}$ Tire 2 lateral force of axle 5 (kN)

$F_{y_{53}}$ Tire 3 lateral force of axle 5 (kN)

$F_{y_{54}}$ Tire 4 lateral force of axle 5 (kN)

$F_{z_{11}}$ Tire 1 vertical force of axle 1 (kN)

$F_{z_{12}}$ Tire 2 vertical force of axle 1 (kN)

$F_{z_{21}}$ Tire 1 vertical force of axle 2 (kN)

$F_{z_{22}}$ Tire 2 vertical force of axle 2 (kN)

$F_{z_{23}}$ Tire 3 vertical force of axle 2 (kN)

$F_{z_{24}}$ Tire 4 vertical force of axle 2 (kN)

$F_{z_{31}}$ Tire 1 vertical force of axle 3 (kN)

$F_{z_{32}}$ Tire 2 vertical force of axle 3 (kN)

$F_{z_{33}}$ Tire 3 vertical force of axle 3 (kN)

$F_{z_{34}}$ Tire 4 vertical force of axle 3 (kN)

$F_{z_{41}}$ Tire 1 vertical force of axle 4 (kN)

$F_{z_{42}}$ Tire 2 vertical force of axle 4 (kN)

$F_{z_{43}}$ Tire 3 vertical force of axle 4 (kN)

$F_{z_{44}}$ Tire 4 vertical force of axle 4 (kN)

$F_{z_{51}}$ Tire 1 vertical force of axle 5 (kN)

$F_{z_{52}}$ Tire 2 vertical force of axle 5 (kN)

$F_{z_{53}}$ Tire 3 vertical force of axle 5 (kN)

$F_{z_{54}}$ Tire 4 vertical force of axle 5 (kN)

H_{R_1} Roll center height of axle 1 (m)

H_{R_2} Roll center height of axle 2 (m)

H_{R_3} Roll center height of axle 3 (m)

H_{R_4} Roll center height of axle 4 (m)

H_{R_5} Roll center height of axle 5 (m)

K_1 Fifth wheel coupling resultant torsion stiffness (kNm/degree)

KS_1 Equivalent vertical stiffness of suspension spring of axle 1 (kN/cm)

KS_2 Equivalent vertical stiffness of suspension spring of axle 2 (kN/cm)

KS_3 Equivalent vertical stiffness of suspension spring of axle 3 (kN/cm)

KS_4 Equivalent vertical stiffness of suspension spring of axle 4 (kN/cm)

KS_5 Equivalent vertical stiffness of suspension spring of axle 5 (kN/cm)

$KT_{M_{11}}$ Tire 1 aligning stiffness of axle 1 (kNm/degree)

$KT_{M_{12}}$ Tire 2 aligning stiffness of axle 1 (kNm/degree)

$KT_{M_{21}}$ Tire 1 aligning stiffness of axle 2 (kNm/degree)

$KT_{M_{22}}$ Tire 2 aligning stiffness of axle 2 (kNm/degree)

$KT_{M_{23}}$ Tire 3 aligning stiffness of axle 2 (kNm/degree)

$KT_{M_{24}}$ Tire 4 aligning stiffness of axle 2 (kNm/degree)

$KT_{M_{31}}$ Tire 1 aligning stiffness of axle 3 (kNm/degree)

$KT_{M_{32}}$ Tire 2 aligning stiffness of axle 3 (kNm/degree)

$KT_{M_{33}}$ Tire 3 aligning stiffness of axle 3 (kNm/degree)

$KT_{M_{34}}$ Tire 4 aligning stiffness of axle 3 (kNm/degree)

$KT_{M_{41}}$ Tire 1 aligning stiffness of axle 4 (kNm/degree)

$KT_{M_{42}}$ Tire 2 aligning stiffness of axle 4 (kNm/degree)

$KT_{M_{43}}$ Tire 3 aligning stiffness of axle 4 (kNm/degree)

$KT_{M_{44}}$ Tire 4 aligning stiffness of axle 4 (kNm/degree)

$KT_{M_{51}}$ Tire 1 aligning stiffness of axle 5 (kNm/degree)

$KT_{M_{52}}$ Tire 2 aligning stiffness of axle 5 (kNm/degree)

$KT_{M_{53}}$ Tire 3 aligning stiffness of axle 5 (kNm/degree)

$KT_{M_{54}}$ Tire 4 aligning stiffness of axle 5 (kNm/degree)

$KT_{y_{11}}$ Tire 1 cornering stiffness of axle 1 (kN/cm)

$KT_{y_{12}}$ Tire 2 cornering stiffness of axle 1 (kN/cm)

$KT_{y_{21}}$ Tire 1 cornering stiffness of axle 2 (kN/cm)

$KT_{y_{22}}$ Tire 2 cornering stiffness of axle 2 (kN/cm)

$KT_{y_{23}}$ Tire 3 cornering stiffness of axle 2 (kN/cm)

$KT_{y_{24}}$ Tire 4 cornering stiffness of axle 2 (kN/cm)

$KT_{y_{31}}$ Tire 1 cornering stiffness of axle 3 (kN/cm)

$KT_{y_{32}}$ Tire 2 cornering stiffness of axle 3 (kN/cm)

$KT_{y_{33}}$ Tire 3 cornering stiffness of axle 3 (kN/cm)

$KT_{y_{34}}$ Tire 4 cornering stiffness of axle 3 (kN/cm)

$KT_{y_{41}}$ Tire 1 cornering stiffness of axle 4 (kN/cm)

$KT_{y_{42}}$ Tire 2 cornering stiffness of axle 4 (kN/cm)

$KT_{y_{43}}$ Tire 3 cornering stiffness of axle 4 (kN/cm)

$KT_{y_{44}}$ Tire 4 cornering stiffness of axle 4 (kN/cm)

$KT_{y_{51}}$ Tire 1 cornering stiffness of axle 5 (kN/cm)

$KT_{y_{52}}$ Tire 2 cornering stiffness of axle 5 (kN/cm)

$KT_{y_{53}}$ Tire 3 cornering stiffness of axle 5 (kN/cm)

$KT_{y_{54}}$ Tire 4 cornering stiffness of axle 5 (kN/cm)

$KT_{z_{11}}$ Tire 1 vertical stiffness of axle 1 (kN/cm)

$KT_{z_{12}}$ Tire 2 vertical stiffness of axle 1 (kN/cm)

$KT_{z_{21}}$ Tire 1 vertical stiffness of axle 2 (kN/cm)

$KT_{z_{22}}$ Tire 2 vertical stiffness of axle 2 (kN/cm)

$KT_{z_{23}}$ Tire 3 vertical stiffness of axle 2 (kN/cm)

$KT_{z_{24}}$ Tire 4 vertical stiffness of axle 2 (kN/cm)

$KT_{z_{31}}$ Tire 1 vertical stiffness of axle 3 (kN/cm)

$KT_{z_{32}}$ Tire 2 vertical stiffness of axle 3 (kN/cm)

$KT_{z_{33}}$ Tire 3 vertical stiffness of axle 3 (kN/cm)

$KT_{z_{34}}$ Tire 4 vertical stiffness of axle 3 (kN/cm)

$KT_{z_{41}}$ Tire 1 vertical stiffness of axle 4 (kN/cm)

$KT_{z_{42}}$ Tire 2 vertical stiffness of axle 4 (kN/cm)

$KT_{z_{43}}$ Tire 3 vertical stiffness of axle 4 (kN/cm)

$KT_{z_{44}}$ Tire 4 vertical stiffness of axle 4 (kN/cm)

$KT_{z_{51}}$ Tire 1 vertical stiffness of axle 5 (kN/cm)

$KT_{z_{52}}$ Tire 2 vertical stiffness of axle 5 (kN/cm)

$KT_{z_{53}}$	Tire 3 vertical stiffness of axle 5 (kN/cm)
$KT_{z_{54}}$	Tire 4 vertical stiffness of axle 5 (kN/cm)
L_g	Gate length for path (m)
m_0	Mass of unladen semitrailer (kg)
m_p	Payload mass (kg)
m_{s_1}	Tractor sprung mass (kg)
m_{s_2}	Semitrailer sprung mass (kg)
m_{u_1}	Mass of axle 1 (kg)
m_{u_2}	Mass of axle 2 (kg)
m_{u_3}	Mass of axle 3 (kg)
m_{u_4}	Mass of axle 4 (kg)
m_{u_5}	Mass of axle 5 (kg)
M_{11}	Tire 1 aligning moment of axle 1 (kNm)
M_{12}	Tire 2 aligning moment of axle 1 (kNm)
M_{21}	Tire 1 aligning moment of axle 2 (kNm)
M_{22}	Tire 2 aligning moment of axle 2 (kNm)
M_{23}	Tire 3 aligning moment of axle 2 (kNm)
M_{24}	Tire 4 aligning moment of axle 2 (kNm)
M_{31}	Tire 1 aligning moment of axle 3 (kNm)
M_{32}	Tire 2 aligning moment of axle 3 (kNm)
M_{33}	Tire 3 aligning moment of axle 3 (kNm)
M_{34}	Tire 4 aligning moment of axle 3 (kNm)
M_{41}	Tire 1 aligning moment of axle 4 (kNm)
M_{42}	Tire 2 aligning moment of axle 4 (kNm)
M_{43}	Tire 3 aligning moment of axle 4 (kNm)
M_{44}	Tire 4 aligning moment of axle 4 (kNm)
M_{51}	Tire 1 aligning moment of axle 5 (kNm)
M_{52}	Tire 2 aligning moment of axle 5 (kNm)
M_{53}	Tire 3 aligning moment of axle 5 (kNm)
M_{54}	Tire 4 aligning moment of axle 5 (kNm)
p_{s_1}	Tractor sprung mass roll rate (degree/s)
p_{s_2}	Semitrailer sprung mass roll rate (degree/s)

p_{u_1} Axle 1 roll rate (degree/s)

p_{u_2} Axle 2 roll rate (degree/s)

p_{u_3} Axle 3 roll rate (degree/s)

p_{u_4} Axle 4 roll rate (degree/s)

p_{u_5} Axle 5 roll rate (degree/s)

r_{s_1} Tractor sprung mass yaw rate (degree/s)

r_{s_2} Semitrailer sprung mass yaw rate (degree/s)

R_1 Roll center of axle 1

R_2 Roll center of axle 2

R_3 Roll center of axle 3

R_4 Roll center of axle 4

R_5 Roll center of axle 5

S_1 Half of suspension lateral spread of axle 1 (m)

S_2 Half of suspension lateral spread of axle 2 (m)

S_3 Half of suspension lateral spread of axle 3 (m)

S_4 Half of suspension lateral spread of axle 4 (m)

S_5 Half of suspension lateral spread of axle 5 (m)

T_1 Half tire track of axle 1 (m)

T_2 Half tire track of axle 2 (m)

T_3 Half tire track of axle 3 (m)

T_4 Half tire track of axle 4 (m)

T_5 Half tire track of axle 5 (m)

$u_{tire_{11}}$ Tire 1 forward velocity of axle 1 (km/h)

$u_{tire_{12}}$ Tire 2 forward velocity of axle 1 (km/h)

$u_{tire_{21}}$ Tire 1 forward velocity of axle 2 (km/h)

$u_{tire_{22}}$ Tire 2 forward velocity of axle 2 (km/h)

$u_{tire_{23}}$ Tire 3 forward velocity of axle 2 (km/h)

$u_{tire_{24}}$ Tire 4 forward velocity of axle 2 (km/h)

$u_{tire_{31}}$ Tire 1 forward velocity of axle 3 (km/h)

$u_{tire_{32}}$ Tire 2 forward velocity of axle 3 (km/h)

$u_{tire_{33}}$ Tire 3 forward velocity of axle 3 (km/h)

$u_{tire_{34}}$ Tire 4 forward velocity of axle 3 (km/h)

$u_{tire_{41}}$ Tire 1 forward velocity of axle 4 (km/h)

$u_{tire_{42}}$ Tire 2 forward velocity of axle 4 (km/h)

$u_{tire_{43}}$ Tire 3 forward velocity of axle 4 (km/h)

$u_{tire_{44}}$ Tire 4 forward velocity of axle 4 (km/h)

$u_{tire_{51}}$ Tire 1 forward velocity of axle 5 (km/h)

$u_{tire_{52}}$ Tire 2 forward velocity of axle 5 (km/h)

$u_{tire_{53}}$ Tire 3 forward velocity of axle 5 (km/h)

$u_{tire_{54}}$ Tire 4 forward velocity of axle 5 (km/h)

v_{axle_1} Axle 1 lateral velocity (km/h)

v_{axle_2} Axle 2 lateral velocity (km/h)

v_{axle_3} Axle 3 lateral velocity (km/h)

v_{axle_4} Axle 4 lateral velocity (km/h)

v_{axle_5} Axle 5 lateral velocity (km/h)

W_{s_1} Tractor sprung weight (kN)

W_{s_2} Semitrailer sprung weight (kN)

W_{u_1} Unsprung weight of axle 1 (kN)

W_{u_2} Unsprung weight of axle 2 (kN)

W_{u_3} Unsprung weight of axle 3 (kN)

W_{u_4} Unsprung weight of axle 4 (kN)

W_{u_5} Unsprung weight of axle 5 (kN)

X_1 Longitudinal distance of axle 1 to tractor sprung mass c.g. (m)

X_2 Longitudinal distance of axle 2 to tractor sprung mass c.g. (m)

X_3 Longitudinal distance of axle 3 to tractor sprung mass c.g. (m)

X_4 Longitudinal distance of axle 4 to semitrailer sprung mass c.g. (m)

X_5 Longitudinal distance of axle 5 to semitrailer sprung mass c.g. (m)

X_{sc_1} Longitudinal distance of articulation point to tractor sprung mass c.g. (m)

X_{sc_2} Longitudinal distance of articulation point to semitrailer sprung mass c.g. (m)

Z_{R_1} Distance between axle 1 roll center and tractor sprung mass c.g. (m)

Z_{R_2} Distance between axle 2 roll center and tractor sprung mass c.g. (m)

Z_{R_3} Distance between axle 3 roll center and tractor sprung mass c.g. (m)

Z_{R_4} Distance between axle 4 roll center and semitrailer sprung mass c.g. (m)

Z_{R_5} Distance between axle 5 roll center and semitrailer sprung mass c.g. (m)

Z_{u_1} Distance between roll center and c.g. of axle 1 (m)

Z_{u_2} Distance between roll center and c.g. of axle 2 (m)

Z_{u_3} Distance between roll center and c.g. of axle 3 (m)

Z_{u_4} Distance between roll center and c.g. of axle 4 (m)

Z_{u_5} Distance between roll center and c.g. of axle 5 (m)

α_{11} Tire 1 side slide angle of axle 1 (degree)

α_{12} Tire 2 side slide angle of axle 1 (degree)

α_{21} Tire 1 side slide angle of axle 2 (degree)

α_{22} Tire 2 side slide angle of axle 2 (degree)

α_{23} Tire 3 side slide angle of axle 2 (degree)

α_{24} Tire 4 side slide angle of axle 2 (degree)

α_{31} Tire 1 side slide angle of axle 3 (degree)

α_{32} Tire 2 side slide angle of axle 3 (degree)

α_{33} Tire 3 side slide angle of axle 3 (degree)

α_{34} Tire 4 side slide angle of axle 3 (degree)

α_{41} Tire 1 side slide angle of axle 4 (degree)

α_{42} Tire 2 side slide angle of axle 4 (degree)

α_{43} Tire 3 side slide angle of axle 4 (degree)

α_{44} Tire 4 side slide angle of axle 4 (degree)

α_{51} Tire 1 side slide angle of axle 5 (degree)

α_{52} Tire 2 side slide angle of axle 5 (degree)

α_{53} Tire 3 side slide angle of axle 5 (degree)

α_{54} Tire 4 side slide angle of axle 5 (degree)

δ_1 Steer angle of axle 1 (degree)

ψ_{s_1} Yaw angle of tractor sprung mass (degree)

ψ_{s_2} Yaw angle of semitrailer sprung mass (degree)

ϕ_{s_1} Roll angle of tractor sprung mass (degree)

ϕ_{s_2} Roll angle of semitrailer sprung mass (degree)

ϕ_{u_1} Roll angle of axle 1 (degree)

ϕ_{u_2} Roll angle of axle 2 (degree)

ϕ_{u_3} Roll angle of axle 3 (degree)

ϕ_{u_4} Roll angle of axle 4 (degree)

ϕ_{u_5} Roll angle of axle 5 (degree)

$\Delta_{s0_{11}}$ Static deflection of left suspension spring of axle 1 (cm)

$\Delta_{s0_{21}}$ Static deflection of left suspension spring of axle 2 (cm)

$\Delta_{s0_{31}}$ Static deflection of left suspension spring of axle 3 (cm)

$\Delta_{s0_{41}}$ Static deflection of left suspension spring of axle 4 (cm)

$\Delta_{s0_{51}}$ Static deflection of left suspension spring of axle 5 (cm)

$\Delta_{s0_{12}}$ Static deflection of right suspension spring of axle 1 (cm)

$\Delta_{s0_{22}}$ Static deflection of right suspension spring of axle 2 (cm)

$\Delta_{s0_{32}}$ Static deflection of right suspension spring of axle 3 (cm)

$\Delta_{s0_{42}}$ Static deflection of right suspension spring of axle 4 (cm)

$\Delta_{s0_{52}}$ Static deflection of right suspension spring of axle 5 (cm)

$\Delta_{t0_{11}}$ Tire 1 static deflection of axle 1 (cm)

$\Delta_{t0_{12}}$ Tire 2 static deflection of axle 1 (cm)

$\Delta_{t0_{21}}$ Tire 1 static deflection of axle 2 (cm)

$\Delta_{t0_{22}}$ Tire 2 static deflection of axle 2 (cm)

$\Delta_{t0_{23}}$ Tire 3 static deflection of axle 2 (cm)

$\Delta_{t0_{24}}$ Tire 4 static deflection of axle 2 (cm)

$\Delta_{t0_{31}}$ Tire 1 static deflection of axle 3 (cm)

$\Delta_{t0_{32}}$ Tire 2 static deflection of axle 3 (cm)

$\Delta_{t0_{33}}$ Tire 3 static deflection of axle 3 (cm)

$\Delta_{t0_{34}}$ Tire 4 static deflection of axle 3 (cm)

$\Delta_{t0_{41}}$ Tire 1 static deflection of axle 4 (cm)

$\Delta_{t0_{42}}$ Tire 2 static deflection of axle 4 (cm)

$\Delta_{t0_{43}}$ Tire 3 static deflection of axle 4 (cm)

$\Delta_{t0_{44}}$ Tire 4 static deflection of axle 4 (cm)

$\Delta_{t0_{51}}$ Tire 1 static deflection of axle 5 (cm)

$\Delta_{t0_{52}}$ Tire 2 static deflection of axle 5 (cm)

$\Delta_{t0_{53}}$ Tire 3 static deflection of axle 5 (cm)

$\Delta_{t0_{54}}$ Tire 4 static deflection of axle 5 (cm)

$\Delta_{t_{11}}$ Tire 1 deflection of axle 1 (cm)

$\Delta_{t_{12}}$ Tire 2 deflection of axle 1 (cm)

$\Delta_{t_{21}}$ Tire 1 deflection of axle 2 (cm)

$\Delta_{t_{22}}$ Tire 2 deflection of axle 2 (cm)

$\Delta_{t_{23}}$ Tire 3 deflection of axle 2 (cm)

$\Delta_{t_{24}}$ Tire 4 deflection of axle 2 (cm)

$\Delta_{t_{31}}$ Tire 1 deflection of axle 3 (cm)

$\Delta_{t_{32}}$ Tire 2 deflection of axle 3 (cm)

$\Delta_{t_{33}}$ Tire 3 deflection of axle 3 (cm)

$\Delta_{t_{34}}$ Tire 4 deflection of axle 3 (cm)

$\Delta_{t_{41}}$ Tire 1 deflection of axle 4 (cm)

$\Delta_{t_{42}}$ Tire 2 deflection of axle 4 (cm)

$\Delta_{t_{43}}$ Tire 3 deflection of axle 4 (cm)

$\Delta_{t_{44}}$ Tire 4 deflection of axle 4 (cm)

$\Delta_{t_{51}}$ Tire 1 deflection of axle 5 (cm)

$\Delta_{t_{52}}$ Tire 2 deflection of axle 5 (cm)

$\Delta_{t_{53}}$ Tire 3 deflection of axle 5 (cm)

$\Delta_{t_{54}}$ Tire 4 deflection of axle 5 (cm)

CHAPTER 1 LITERATURE REVIEW AND RESEARCH SCOPE

1.1 Introduction

Heavy trucks are much more likely to be involved in fatal vehicle crashes due to their excessive weights, large sizes and high centers of gravity. The latest crash statistics given by NHTSA (National Highway Traffic Safety Administration), "Traffic Safety Facts 2002" [1], report that large trucks accounted for 7.8 percent of the vehicles in fatal crashes in America. Of the 4,542 large trucks involved in fatal crashes, 76 percent were combination trucks, and 13.3 percent were rollover related. Since heavy vehicle rollover accidents could cause serious damages to properties and human lives, the development of rollover prevention system is a subject which has drawn considerable attention. Extensive studies have been conducted in this area in the last three decades, and central to these efforts is the development of early rollover predictor.

A rollover prevention system will work well only if the impending rollover threat can be accurately predicted. It involves the establishment of a dynamic rollover criterion and the identification of motion response parameters that are directly related to the onset of rollover, and therefore can be used for evaluating and predicting the threat of rollover. Vehicle c.g. height is one of the most important factors affecting vehicle roll stability. In particular the c.g. height is used directly in the calculation of Static Stability Factor (SSF) and indirectly in the Side Pull Ratio (SPR) measurement. The definitions of SSF and SPR can be found in the review paper on static rollover metrics written by Chrstos and Guenther [2]. Furthermore,

the knowledge of c.g. height is vital for computing Critical Sliding Velocity (CSV) [3], a dynamic roll stability metric used in evaluating propensity of tripped rollover. Liu [4] concluded that trailer lateral acceleration was a reliable rollover indicator for rollover early warning system development, however, the precondition required the knowledge of trailer c.g. height.

Obviously, vehicle c.g. height is a critical parameter both for roll stability evaluation and for rollover prevention system development. The coordinates of c.g. of the sprung masses of a vehicle combination vary over a wide range due to variations in c.g. heights of such vehicles corresponding to each loading practice and the nature of cargo. Measurement of pattern is quite complex, especially when multiple unit vehicles are involved. It would thus be desirable to explore concepts in developing an online measurement system to efficiently estimate the c.g. height of an arbitrarily loaded vehicle from its dynamic responses under carefully controlled maneuvers. Such a system can be installed on the vehicle, to automatically capture its c.g. height under driver's instruction. The information gained on the vehicle c.g. height can be directly utilized by the rollover prevention system to realize rollover prediction and control. Moreover, knowledge of c.g. height can be directly applied to estimate the rollover threshold of a vehicle, such as Static Safety Factor, to assess the rollover risk by the operators.

Thus far, only one published study can be found on the subject of vehicle c.g. height online measurement [5]. Far more efforts are needed to fill the void in this area. Further investigations on this issue will definitely contribute to the development of a reliable rollover prevention system and the attainment of

enhanced highway safety. This dissertation research is directed towards investigating a concept in online estimation of c.g. height of a five-axle tractor-semitrailer using system identification technique. A brief review of relevant literature is presented in the following sections, and finally the scope of this dissertation is outlined.

1.2 Review of Relevant Literature

Formulations and study of concepts in online estimation of c.g. height involves complex challenges related to directional dynamics of heavy articulated vehicles in view of varying loading and operating practices, rollover dynamics, system identification techniques, etc. The relevant studies reported within these topic areas are reviewed to build essential background and formulate the scope of the dissertation research. The reviewed studies, grouped within the topic area, are systematically discussed below.

1.2.1 Roll dynamics analysis models

A vast number of analytical models have been developed for analyzing the roll dynamic behaviors and for evaluating rollover thresholds of heavy vehicles. These models differ greatly in capability, in complexity, in the number of degrees of freedom considered, and in the amount of input data required. Three of these models are widely adopted in the roll dynamics analysis: static roll plane model, for estimating the steady-turning roll stability limit, yaw/roll model, for deriving the steering responses under constant forward speed, and Phase 4, for deriving the

yaw and roll behavior of vehicle under constant speed operation [6, 8, 10].

Verma et al. [6] developed a nonlinear analytical roll plane model for studying roll dynamics of commercial vehicles on the basis of large displacements and rotations, so that it could be applied for the study of roll dynamics well beyond the limits of wheel lift-off. The vehicle model comprises one sprung mass and one composite unsprung mass consisting of a rigid axle with wheels and dual tires that are represented by separate spring damper combinations. The suspension is characterized by springs having a linear or nonlinear spring rate, backlash, coulomb friction, and frequently, a viscous damper. The reaction of lateral forces through the suspension is represented by a roll center force, which for commercial vehicles generally falls just above the axle center. While the internal load transfer is considered to be negligible, the roll center is assumed to be fixed with respect to the sprung mass c.g. and it could translate with respect to the unsprung mass. The sprung mass is permitted to rotate about the roll center, and the unsprung mass to roll about its own c.g., which could translate horizontally and vertically. The model was validated on the basis of the measured data attained for a five-axle full trailer driven through a double lane-change maneuver at a forward speed of 72 km/h. The study revealed good agreement between the measured and model results in terms of sprung mass roll angle. The proposed model considers the whole vehicle as lumped rigid bodies in a single roll plane, and thus neglects load transfer between the axles and dynamics of articulation mechanism. Moreover, considerable complexities exist in determining the parameters representing the composite characteristics of a combination vehicle, specifically

when different axles comprise dissimilar suspensions.

Mallikarjunarao et al. [7] developed a static roll model to determine the rollover threshold of articulated vehicles during a steady-state turning maneuver. The axles with similar suspension properties are grouped together and sprung masses are distributed over three composite axles, representing the steer, drive and trailer axles. Each composite axle and its suspension supported sprung mass forms a roll plane and the adjacent roll planes are coupled with a torsion spring representing the structure compliance existing in the tractor frame or articulation joint. In each roll plane, the suspension springs are assumed to retain perpendicular to the axle and transmit only compressive or tensile forces; the roll center is permitted to slide freely along an axis perpendicular to the axle; all axle forces acting perpendicular to the axle are taken up by the suspension springs, while all axle forces acting in a direction parallel to the axle are assumed to act through the roll center located at a fixed distance from the sprung mass c.g.. Suspension non-linearity such as backlash and progressively hardening suspension springs are represented by a tabular load-deflection input format. The roll angles of the sprung masses are assumed to be small, and the articulated angle is neglected. The total vertical load carried by each composite axle is assumed to remain constant during the rollover process. In order to accommodate any pitching motion that might take place during rollover, the sprung masses are permitted to take up different vertical deflection at each axle. The static roll model was validated using tilt table test results, and has been widely used to predict static rollover threshold of articulated tractor-semitrailer combinations.

Gillespie and MacAdam [8] introduced a yaw/roll model for predicting the directional and roll responses of single and multiple articulated vehicles engaged in turning maneuvers at a constant forward velocity. Each sprung mass possesses five D.O.F.: lateral, vertical, yaw, roll and pitch; and each unsprung mass can roll and bounce with respect to the sprung mass to which it is attached. The roll centers are assumed to be located at fixed distances beneath the sprung masses. Suspension lash and other nonlinear properties are taken into account in modeling the suspension springs. The cornering force and aligning moment produced by a given tire are considered to be functions of the side-slip angle and vertical load, while the wheel camber effect is ignored. The model can be applied for four different hitch mechanisms, and both the closed-loop (defined path input) and open-loop (defined steer angle input) modes of steering input. The model was validated by comparisons with field tests done by Winkler et al. [9]. The results indicated that the model provides good correlation with the test results up to lateral acceleration of 2 m/s^2, and a conservative estimate under more severe maneuvers.

El-Gindy and Wong [10] described the comprehensive three-dimensional vehicle model developed at University of Michigan Transportation Research Institute, named as Phase 4 Model, for simulating the braking and steering dynamics of single and articulated trucks. The motions of the vehicles are represented by differential equations derived from Newtonian mechanics that are solved for successive time increments by numerical integration. The mathematical model incorporates up to 71 D.O.F. for up to 4 units and brakes. The number of

D.O.F. is dependent on the vehicle configuration and derived from the following:

- Six D.O.F. for the truck/tractor sprung mass;
- Three rotational D.O.F. for each semitrailer;
- Five D.O.F. for each of the two full trailers allowed;
- Two D.O.F. for each of the 13 axles allowed;
- A rotational D.O.F. for each of the 26 wheels allowed.

The program can be operated in either open-loop or close-loop steering inputs, and on roads of specified grade or cross-slope.

1.2.2 Measures of static roll instability

Static Rollover Threshold (SRT) is the basic measure of roll stability, which is defined as the maximum lateral acceleration that a vehicle can sustain without suffering a divergent roll response in a steady-state turning maneuver. Theoretical analysis reveals that the parameters of fundamental importance to SRT include c.g. heights of the sprung masses, the fifth wheel separation moment, and various parameters for the trailer and tractor drive axles, including track width, suspension spring rates and spring lash characteristics, vertical tire stiffness characteristics, auxiliary roll stiffness, and roll center heights.

On the basis of analysis of reported rollover accidents, a strong relationship between the SRT and the chance of rollover accident has been established [11]. The relationship between the rollover risk and the SRT is nonlinear, the chance of rollover asymptotically approaches to zero, as the SRT increases. Conversely, as the stability limit (SRT) decreases, the sensitivity of the probability of rollover

increases rapidly. The measure based upone SRT has thus been widely accepted as the key performance measure for evaluating the likelihood of rollover of a vehicle. The proposed relationship, however, is considered to unreliable for online control of roll instability due to its lack of consideration of directional dynamic responses. A number of studies have also proposed upper bonds of the SRT to ensure acceptable roll stability for heavy vehicles, which range from 0.35 to 0.4 g.

SRT can be evaluated experimentally and theoretically. The experimental methods include road test, side-pull test and tilt table test. The tilt table test is extensively used for measuring SRT of heavy vehicles due to its simplicity and high degree of repeatability [12]. However, the tilt table test has a drawback. As the inclination angle of the table is increased during the measurement, the vertical force acting on the vehicle decreases. This will cause a change in the c.g. height of the vehicle, and thus influence its rollover threshold [2].

A number of alternate measures of static roll stability have also been proposed. The static stability factor (SSF) is perhaps the simplest measure that considers the c.g. height and track width, while the contributions due to the compliant properties of the suspensions, tires and articulation mechanisms are ignored. Piche et al. proposed a compliance factor that could be applied to enhance the prediction accuracy of the SSF. The compliance factor was established on the basis of simulations performed with a wide range of different suspensions and tires. The comparisons of the results attained from the corrected SSF with SRT revealed reasonably good agreement between them.

1.2.3 Measures of dynamic roll instability

The dynamic rollover mechanism can be grouped into two classes: tripped rollover and maneuver-induced rollover. A tripped vehicle rollover can result if the vehicle strikes a curb or other obstacles. A maneuver-induced vehicle rollover occurs during an abrupt vehicle maneuver without the help of a tripping mechanism.

Nalecz et al. [13] proposed an energy based function named Rollover Prevention Energy Reserve (RPER) to describe the vehicle tip-over. RPER is defined as the difference between the energy needed to bring the vehicle to its tip-over position and the rotational kinetic energy, which can be transferred into the gravitational potential energy to lift the vehicle. RPER remains positive for non-rollover cases, and a rollover will occur when RPER approaches a negative value in the absence of a prevention action. A special advantage of RPER is that the same concept can be applied to both tripped and maneuver-induced rollover incidents. The tip-over stability of a vehicle is also assessed in terms of Rollover Prevention Metric (RPM), defined as the difference between the initial lateral translational kinetic energy and the rotational kinetic energy after the impact divided by the initial energy [14]. Another measure used to predict tripped rollover stability is called Critical Sliding Velocity (CSV), which is defined as the minimum lateral velocity required to initiate a rollover [3].

Preston-Thomas and Woodrooffe [15] used the Lateral load Transfer Ratio (LTR) to predict the maneuver-induced rollover threat under dynamic maneuvers. This measure is expressed in terms of fractional change in tire loads between left-

and right-tracks during the maneuver, and thereby the dynamic rollover in terms of tire-road contact.

El-Gindy [16] further described another important dynamic measure of roll stability based upon rearward amplification tendencies of articulated vehicles, referred to as Rearward Amplification Ratio (RA). When the driver of a combination vehicle traveling at highway speeds steers rapidly for any reason, the consequence of this steering input has been shown to be amplified as it moves rearward through successive trailers and converter dollies. The result, at best, is undesirable side to side movement of the last trailer, and at worst, amplification induced trailer rollover. As a performance measure, the rearward amplification ratio describes the peak response of the rearmost trailer in the combination to that of the tractor. A number of design and operating factors are known to influence the rearward amplification characteristics of a vehicle combination, such as vehicle speed, axle loads, gross weight, trailer lengths and number of hitches.

El-Gindy [16] also described a new measure of dynamic rollover, referred to as the Yaw Damping Ratio that directly relates to the rate of decay of the vehicle's oscillatory response. The Yaw Damping Ratio is evaluated at a speed of 100 km/h, by applying a steering wheel pulse of 80 degrees (half sine) over a time interval of 0.1 second. The peak magnitudes of successive oscillations in lateral acceleration response of the rearmost trailer are evaluated to derive the damping ratio, using the logarithmic decrement procedure.

Among the various measures of dynamic rollover, the LTR measure is most widely used as it directly relates the loss of the tire-road contact and thus the

vehicle rollover. The LTR is relatively less sensitive to variations in vehicle design and operating parameters, it considers the lateral load shift of all the vehicle axles, including the steering axles. As the relative rollover condition of an articulated vehicle is satisfied when the tires on one side of the tractor drive and trailer axles lose contact with the road, the LTR may lead to erroneous indication of a relative rollover. Moreover, a specific value of LTR corresponding to the dynamic rollover is not yet known. Liu [4] proposed a Roll Safety Factor (RSF) measure upon recognizing the disadvantage of LTR. The RSF is similar to the LTR, but it only considers the axles which experience wheel lift-off when the instability condition is satisfied, and it approaches a unity value when the vehicle comes up to its relative rollover condition, irrespective of its design and operating factors.

1.2.4 Detection of impending rollover

The roll instability measures, such as LTR or RSF, can provide a reliable prediction of the threat of rollover, but pose extreme complexities in acquiring the online measurement of the dynamic tire forces in motion. Alternatively, considerable attempts are being made to desire other measures that are directly measurable and correlate well with RSF and LTR. Moreover, the identified measures must be relatively insensitive to variations in vehicle design and operation conditions.

Piché [17] attempted to relate the onset of roll instability to various vehicle response parameters and concluded that the vehicle rollover during steady turns can be detected via the vehicle's lateral acceleration response, and the roll angle

response of the semitrailer's trailing axle provides the most reliable information concerning the onset of vehicle rollover at highway speeds.

Liu [4] investigated various potential rollover indicators and classified them in six groups. The study performed systematic evaluations of the measures based upon their measurability, reliability, and early warning feature. The study concluded that no single measure would serve as an appropriate indicator of impending rollover in terms of measurability, reliability and the desirable time margin for the corrective maneuvers. It was also pointed out that if the wheel track, axle load, and tire elastic properties for each axle are known, the onset of vehicle rollover can be detected via monitoring roll angles of tractor rear and trailer axles for a tractor-semitrailer combination; trailer lateral acceleration or roll angle can also be used as a rollover indicator, if further information such as the c.g. height and axle roll stiffness is known. The same conclusion was also made by Piché [17]. A combination of several indicators was thus suggested for detection of impending rollover in views of the difficulties in finding a single indicator with desirable measurability, reliability and available time margin for corrective maneuvers.

Chen et al. [18] proposed a measure referred to as Time-To-Rollover (TTR) metric, which describes the time to an impending rollover incident. By definition TTR is the amount of time over which the vehicle will produce rollover (tire-lift-off) if the current operating state of the vehicle was maintained. It is computed from a simple yaw/roll vehicle model and then corrected by using an artificial neural network. Chen et al. [19] verified a TTR based rollover threat index for two

different SUVs, and concluded that the TTR computed from the simple yaw/roll model is accurate enough due to the fact that vehicle roll angles for SUVs corresponding to tire-lift-off are generally very small.

Trent et al. [20] developed a genetic algorithm predictor for estimating vehicle rollover. The model is used for solving input steering angle for given speed, and roll and yaw rates. The predictor then uses speed, roll and yaw rates, and the derived steering angle as inputs to obtain estimates of the roll angle response at instant of 50 times steps into the future. Preliminary results of the study revealed rollover prediction of 400 ms in advance of the actual event.

All of the rollover indicators that could be directly measurable necessitate the prior knowledge of many vehicle parameters including lateral acceleration, sprung mass roll angle, unsprung mass roll angle and particularly the c.g. height.

1.2.5 Rollover warning/control systems

Owing to the relatively low roll stability limits of heavy vehicles, a number of warning systems and active control systems for preventing rollover in open- and closed-loop manners have been investigated. Rakheja et al. [21] proposed an early warning device based upon online monitoring of key variables that are related to rollover threat for tractor-semitrailer vehicles. In low speed cornering, a threshold lateral acceleration at the onset of trailer tire lift-off is obtained by static analysis of roll stability based on maximum c.g. height of a trailer. While in high-speed maneuvers, the peak axle roll angle at the onset of trailer tire lift-off is used as a roll stability criterion. Both measures, however, revealed considerable

sensitivity to variations in design and operating parameters and required the information of c.g. height.

Dunwoody et al. [22] studied active roll control of a semitrailer using a tilt table fifth wheel. The system comprised a tilt table coupled to the fifth wheel, hydraulic actuators to apply a roll moment to the back axles of the trailer, a hydraulic power supply, sensors to measure the lateral acceleration of the trailer and roll angles of the fifth wheel coupling and the back axles relative to the frame of the trailer, and a controller. The hydraulic actuators applied a corrective roll moment at the rear most axle and the coupling in response to a perceived rollover risk evaluated based on the lateral acceleration and roll angles. The active roll control system was entirely contained within the semitrailer, requiring only electrical power from the tractor. Their calculations showed an increase in rollover threshold of up to 30%.

Lin et al. [23] also investigated the use of active roll control to enhance the roll stability of a tractor-semitrailer. They validated the Yaw/Roll simulation program developed at UMTRI under tilt table, steady turning and lane change tests, on a typical UK 4-axle articulated lorry. A simple linear model was then developed and used to select the gains for the active roll control system with a lateral acceleration controller. The controller used lateral acceleration signals from the tractor and trailer to control active anti-roll bars fitted to the tractor and trailer axles. The system reduced steady-state and transient load transfers by up to 30%. The results of the study were confirmed on the basis of the time domain simulation results from the nonlinear Yaw/Roll model.

Palkovics et al. [24] suggested an alternative system for detection and control of rollover stability of a single unit truck by reprogramming the existing Electronic Braking System (EBS). The EBS regularly applies a small braking force to each of the wheels and monitors the wheel slip response. Excessive slip response to a pulse indicates that a given wheel is lightly loaded and could lead to lift-off. The signal may be used to predict the onset of potential roll instability. It was proposed to activate the brakes momentarily lock the outside wheel of that axle to reduce the lateral tire force so that the axle suddenly slips laterally. A threshold value for the control, however, was not established. The proposed system offers considerable advantages as it can operate on the existing EBS hardware.

Wielenga [25, 26] proposed anti-rollover braking by using differential braking instead of full brake application. The study proposed the use of rebound bumpers to detect tire lift-off during a maneuver. The differential braking was activated to avert the rollover, whenever tire lift-off was detected or lateral acceleration of the vehicle exceeded its threshold value. A computer-controlled differential braking rollover prevention system was further developed by Lewis et al. [27]. The system adjusted the brake forces on the right and left sides of the vehicle independently to stabilize the vehicle. Simulation results showed that the controller could prevent rollover without significantly changing the direction of the vehicle. The proposed system, however, posed significant challenges in deriving an effective algorithm for adjusting the braking system in response to continuous changes that take place in a tractor-semitrailer as it maneuvers around a corner.

1.2.6 CG height measurement

Vehicle c.g. height is a critical parameter both for roll stability evaluation and for rollover prevention system development. It varies considerably with the loading practices and the nature of cargo. The roll stability limit of a vehicle is most sensitive to the c.g. height. A vast numbers of studies on rollover warning and control have concluded that the lack of c.g. height information is the primary deterring factor for further development and implementation of the open-loop rollover warning and control systems. It is thus extremely vital to develop some effective methods for efficient measurement or estimation of c.g. height of an arbitrarily loaded vehicle as it leaves a loading area. An online measurement system would be highly desirable to capture vehicle c.g. height on the basis of vehicle dynamic responses under a carefully controlled maneuver. In this section the laboratory measurement techniques are reviewed first to give a sense of measurement accuracy which can be reached statically, and then the previous work on the online measurement of c.g. height is described in detail.

The measurement and/or estimation of the longitudinal and lateral coordinates of a vehicle's sprung mass c.g. is a simple procedure that involves the measurement of axle and tire loads using a weight scale. The static tire and axle loads are then applied together with moment equilibrium to compute the longitudinal and lateral coordinates of the sprung mass c.g.. Measuring the c.g. height, however, is a far more complex process, normally conducted in laboratory using complex fixtures. Shapiro, et al. [28] described four test methods of measuring c.g. height: modified reaction method, null point method, weight

balance method and pendulum method. In the modified reaction method, the vehicle is tilted about one of its spin axes, and the c.g. height is computed from the measured longitudinal weight shift. The null point method requires a specially built platform with two parallel knife edges several inches apart on its bottom surface. The knife edges are aligned perpendicular to the longitudinal axis of the platform. The vehicle is placed on the platform so that its c.g. is located between the knife edges. The platform is tilted until it balances on one knife edge and the tilt angle is measured. This process is repeated for the opposite direction, and c.g. height is calculated from the two angles.

The weight balance method consists of a platform suspended from pivots on two sides. The vehicle is carefully located on the platform so the platform is horizontally leveled. A torque is then applied to the system, usually by adding a known weight at a known location. The platform inclination is then measured at static equilibrium to compute the c.g. height. In the pendulum method, the vehicle is placed on a suspended platform that allows the vehicle to swing through small angular displacements. The period of oscillation of the suspended vehicle is then measured and applied to obtain an estimate of the c.g. height.

Andreatta [29] described a facility designed and built for the US army for measurements of: weight; coordinates of the c.g. position, including height; roll, pitch, and yaw mass moments of inertia; and the cross products of the inertias. The facility can measure the inertial properties of vehicles ranging from light single axle trailers to long heavy vehicle combinations and tank turrets. The measurement accuracy was claimed to be within 3%.

An accurate prediction of onset of a potential rollover necessitates prior knowledge of c.g. height of the heavy vehicle, irrespective of the payload and its distribution within the trailer. The directional dynamic responses of heavy vehicles are strongly dependent upon the c.g. height, apart from the many other design and operating variables. The c.g. height may thus be estimated from the measured vehicle responses under one or more well-designed and controlled maneuvers. Thus far, only a single published study could be found on the detection of c.g. height from the measured dynamic responses [5]. The reported study considered a straight truck and attempted to identify c.g. height from different response variables. The results of the study revealed that roll rate was more sensitive to the variations in the c.g. height than the yaw rate under a lane change maneuver. Moreover, higher magnitude of roll rate was measured corresponding to a higher c.g. height. Based on this observation, a 3-D.O.F. vehicle model comprising roll, yaw and lateral velocity was formulated to derive the analytical transfer function relating the steering input to the roll output. The test data were collected under a lane change maneuver with 40 m gate length and 90 km/h forward speed to develop the experimental transfer function using the ARX model. The vehicle c.g. height was then estimated by comparing the coefficients of the analytical and experimental transfer functions. The validity of the estimated c.g. height was examined by comparing the estimated data with that measured statically using a Japanese standard. The author concluded that the vehicle c.g. height could be precisely estimated using the transfer function approach, but higher signal/noise ratio and lower rates of speed variation was the

necessary premise for the estimation method.

1.2.7 System identification techniques

Modeling is about relating the outputs and the inputs of a system through a set of mathematical equations. Two different approaches may be employed for determining these equations [30]. In the first approach the equations can be obtained by writing a set of equilibrium equations based on mass and energy balance and other physical laws. In the second approach the system is viewed as a "black-box" and the equations are determined from the past input-output records of the system. For complex and highly nonlinear systems, the second approach is often adopted for performance analyses in the absence of complete knowledge of the system behavior or some of its components. System identification is a technique that falls within the second approach, which permits for development of mathematical models of dynamic systems based on measured noisy time-series data. The procedure to determine a model of a dynamical system from observed input-output data involves three essential components [31]:

- The input-output data under representative conditions;
- A set of candidate models (the model structure);
- A criterion to select a particular model in the set, based on the information contained in the data (the identification method).

The identification process may involve repetitive selections of model structures, identifications of coefficients, and evaluations of validity. The system identification process, at its simplest level, is demonstrated in Figure 1.1.

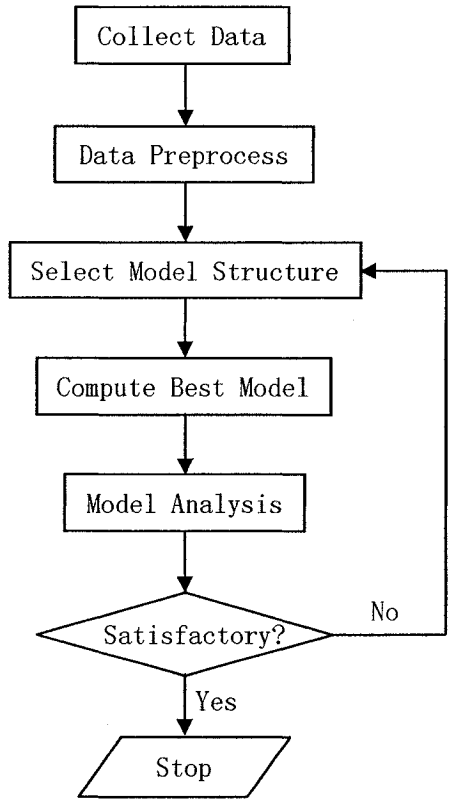

Figure 1.1: System identification process.

System Identification technique can be effectively applied to derive a reasonable estimation of the vehicle parameters [32]. The coefficients of the identified transfer function can be directly related to system parameters based on some fundamental physical laws or relationships. A number of studies have applied system identification techniques to derive simplified transfer functions describing different behaviors of the vehicle system and its subsystems. These include the tire properties, the driver behaviors, linerized handling dynamics, directional dynamics, structural properties, etc.

1.3 Scope and Objectives of the Dissertation Research

From the review of the published studies on directional dynamics and rollover potential of heavy vehicles, it is evident that the handling and directional response characteristics of vehicles are most significantly related to the c.g. height of the sprung mass. A number of concepts in prediction of onset of a potential rollover have been proposed to provide an early warning to the driver to undertake a timely preventive action in an open-loop manner. All these studies have invariably concluded that the measures directly related to onset of a rollover are dependent upon the c.g. height. The development and implementation of a rollover predictor and warning generation mechanism require prior knowledge of the c.g. height of the arbitrarily loaded vehicle. Considering that the freight transportation involves varying loading practices, the determination of c.g. height over the range of operating practices forms a formidable task. The estimation of c.g. height through known laboratory methods under different loading conditions is quite complex and expensive, and could not be implemented at the loading platforms of the freight transportation sector. Alternatively, system identification techniques could be applied to derive the c.g. height estimate on the basis of measured response behavior under carefully controlled condition. Thus far, only one reported study could be found on the online estimation of the c.g. height. This study reported by Momiyama, et al. [5] involved only one type of vehicle, a straight truck, while the accuracy of the algorithm for estimating vehicle c.g. height was found to be sensitive to the signal/noise ratio. Tractor-semitrailer accounts for the highest percentage of heavy trucks in operation in northern America. Development of an

efficient method for estimating the c.g. height of this type of vehicle would be highly desirable for developing effective early warning rollover prevention algorithms. The knowledge of vehicle c.g. height corresponding to various loading conditions further enables the operators to assess its roll stability, and may be incorporated within weight and dimensional regulations.

The scope and the overall objective of this dissertation research are thus formulated to explore different methodologies to identify the c.g. height of an arbitrarily loaded articulated freight vehicle. The specific objectives of this dissertation research are described as follows:

- Develop a model of a five-axle tractor-semitrailer combination vehicle in TruckSim.
- Identify one or more directly measurable dynamic responses that are most sensitive to variations in the c.g. height of the semitrailer sprung mass.
- Identify a simple test maneuver for generating the desirable directional response that can be directly related to the c.g. height of the vehicle.
- Perform sensitivity analyses to study the effects of various vehicle and maneuver parameters on the identified response.
- Formulate a simplified model of the five-axle tractor-semitrailer for deriving the transfer function relating the identified response to steering input.
- Examine the validity of the transfer function using the results attained from the nonlinear Yaw/Roll model.
- Collect representative and idealized test data using the Yaw/Roll model and identify experimental transfer function.

- Develop an algorithm to estimate vehicle c.g. height from the experimental transfer function, and investigate the robustness of the algorithm.

1.4 Organization of the Dissertation

In Chapter 2, the vehicle parameters representing a typical five-axle tractor-semitrailer are identified from the provincial laws and simple static analyses. The model of the five-axle tractor-semitrailer is constructed within the TruckSim platform and analyzed for identifying the dynamic responses corresponding to test maneuvers. Finally the sensitivity of the identified response to variations in selected vehicle parameters is investigated.

Owing to the limitation of the TruckSim model in deriving the system transfer function, a relatively simple but nonlinear mathematical model of the five-axle tractor-semitrailer is developed in Chapter 3. The 10-D.O.F. model incorporates nonlinear suspension and tire properties, and roll D.O.F. of the vehicle.

In Chapter 4, the proposed mathematical model is linearized to derive the transfer functions relating the desired response parameters to the test maneuver quantities. The validity of the transfer functions is examined by comparing the simulation results with those obtained from the nonlinear Yaw/Roll model.

In Chapter 5, the analytical transfer function relating the semitrailer sprung mass roll angle to the steering angle is adjusted to account for the limited roll D.O.F. considered in the analysis. An idealized experimental transfer function is identified from the results generated using the Yaw/Roll model program. The c.g. height estimation algorithm is developed and its accuracy and robustness are

examined.

Finally the conclusions and recommendations for future work are outlined in Chapter 6.

CHAPTER 2 VEHICLE PARAMETERS AND SENSITIVITY ANALYSIS

2.1 Introduction

For the reasons of economy, the transportation sector has been inclined towards the use of longer and heavier vehicle combinations. The variations in the weights and dimensions, and vehicle configurations together with the varying loading practices could yield considerable variations in the c.g. height and thus the directional responses. While the provincial laws limit the variations in the weights and dimensions for each vehicle configuration, they are not intended to limit the variations in the c.g. height. Many studies have established that the roll and yaw directional responses of heavy vehicle combinations are strongly influenced by the c.g. height, apart from many other design and operating factors. The directional responses in these studies have been reported in terms of lateral velocity and acceleration, roll deflections of the sprung and unsprung masses, tire force variations, roll and yaw rates, etc. These response quantities may exhibit different sensitivity to variations in the c.g. height. A particular directional response that exhibits extreme sensitivity to c.g. height variations may be desirable for indirect estimation of c.g. height. Moreover, the relative sensitivity of the response parameter to c.g. height may further depend upon the type of maneuver undertaken.

In this chapter, the directional response characteristics of an articulated vehicle are evaluated to identify the most sensitive vehicle dynamic response quantity to variations in the vehicle c.g. height. The analyses are performed under

different directional maneuvers and a safe and practically implementable maneuver is selected. The identified response quantity and the maneuver may then be applied for online estimation of the c.g. height. The analysis is limited to a five-axle tractor-semitrailer configuration in order to limit the variations in various design parameters. The parameters of the baseline vehicle are identified from the weights and dimensional regulations of Canada. The measurability of the determined dynamic response is also evaluated based on the available sensor technologies.

2.2 Vehicle Configuration and Parameters

A survey of the truck configurations used in Canada revealed that 77% of all heavy combination vehicles operating in Canada were tractor-semitrailers, among which 5-axle tractor-semitrailers accounted for 75% in British Columbia and 95% in Alberta and Manitoba, while 6-axle tractor-semitrailers possessed the remaining percentage [33]. A recent report, entitled, "Transportation in Canada 2003" [34], concluded that the configuration of tractor with one trailer accounted for 68.9% of the heavy trucks in Canada in 2003 on the basis of vehicle-kilometers driven. A five-axle tractor-semitrailer vehicle is thus selected for the present study. The parameters of the selected baseline vehicle are cited from those outlined in a UMTRI report [35], which conform to Canadian standards, "Weight and dimension standards for commercial vehicles in Canadian Jurisdictions" [36]. Although the parameters of suspension and tire inflation are old fashioned, this set of data is still used to configure the baseline vehicle in this

study because of its completeness and reliability. Modern air suspension and relatively higher tire inflation pressure are used for configuring non baseline vehicles for sensitivity analyses. The parameters of the baseline vehicle are summaries in Table 2.1 to Table 2.6.

Table 2.1: Parameters of the baseline tractor [35].

Parameter	Value
Wheelbase (m)	4.83
Tandem axle spread (m)	1.52
Width across outside tires (m)	2.44
Fifth wheel offset (m)	~0.41
Curb weight (kg)	8156.0
Sprung weight (kg)	5352.5
Steer axle load (ton)	5.5
Tandem axle load (ton)	17.0
Frame torsion stiffness about roll axis (N-m/deg)	7000000.0
Front suspension-Navistar (IH) COF 9670 (multiple tapered leaf steel spring)	
Load rating (ton)	5.5
Unsprung weight (kg)	544.0
Rear suspension-Hendrickson RTE 440 (multi leaf spring + walking beam tandem)	
Load rating (ton)	20.0
Unsprung weight/axle (kg)	1134.0
Tire-Michelin XZA 11R22.5/G (Radial-ply, G load rating, full tread)	
Inflation pressure (kPa)	689.5

Table 2.2: Parameters of the baseline 2-axle semitrailer [35].

Parameter	Value
Overall length (m)	14.63
Wheelbase (m)	12.34
Tandem axle spread (m)	1.22
Kingpin setback (m)	0.91
Bed/Van length (m)	14.63
Rear overhang (from trailing axle) (m)	0.76
Freight floor height (m)	1.37
Width across outside tires (m)	2.59
Payload C.G. height (m)	~2.00
Payload (ton)	25.0
Empty weight (kg)	6260.0
Sprung weight (kg)	4900.0
Tandem axle load (ton)	17.0
Suspension-Reyco 21-B (multiple leaf 4-spring tandem)	
Load rating (ton)	20.0
Unsprung weight/axle (kg)	680.0
Tire-Michelin XZA 11R22.5/G (Radial-ply, G load rating, full tread)	
Inflation pressure (kPa)	689.5

Table 2.3: Parameters of the baseline tractor front suspension [35].

Parameter		Value	
Roll moment of inertia (kgm^2)		418	
Unsprung mass (kg)		544	
Center of gravity height (m)		0.51	
Roll center height (m)		0.46	
Track width (m)		2.03	
Dual tire separation (m)		0	
Spring spread (m)		0.81	
Auxiliary roll stiffness (Nm/deg)		432.05	
Roll steer coefficient		0.000	
Left hand viscous damping coefficient		22.26	
Right hand viscous damping coefficient		22.26	
Compression Table		**Extension Table**	
Force (kN)	**Deflection (cm)**	**Force (kN)**	**Deflection (cm)**
-90.74	-38.1	-92.08	-38.1
-4.54	-1.905	-5.87	-1.905
0.0	0.000	-1.33	0.000
6.89	2.54	4.23	2.54
12.9	5.08	9.79	5.08
18.68	7.62	15.35	7.62
34.25	13.97	30.16	13.97
52.27	21.59	46.73	21.59
94.3	39.37	84.31	39.37

Table 2.4: Parameters of the baseline tractor rear suspension [35].

Parameter (Lead Axle)		**Value**	
Roll moment of inertia (km^2)		576.22	
Unsprung mass (kg)		1133.98	
Axle separation (m)		1.524	
Static load distribution		50%	
Dynamic load transfer		0%	
Center of gravity height (m)		0.508	
Roll center height (m)		0.838	
Track width (m)		1.829	
Dual tire separation (m)		0.33	
Spring spread (m)		0.965	
Auxiliary roll stiffness (Nm/deg)		3389.54	
Roll steer coefficient		0.220	
Parameter (Trailing Axle)		**Value**	
Auxiliary roll stiffness (Nm/deg)		9603.71	
Roll steer coefficient		0.230	
Compression Table		**Extension Table**	
Force (kN)	**Deflection (cm)**	**Force (kN)**	**Deflection (cm)**
-35.54	-5.08	-36.59	-5.08
0.44	-0.635	-0.67	-0.635
2.00	0.000	0.0	0.000
4.00	0.635	1.56	0.635
8.01	1.27	4.05	1.27
13.12	1.905	8.01	1.905
24.47	2.54	15.35	2.54
99.53	5.715	70.27	5.715
264.67	12.7	186.86	12.7

Table 2.5: Parameters of the baseline semitrailer suspension [35].

Parameter (Lead/Trailing Axle)		Value	
Roll moment of inertia (kgm^2)		463.24	
Unsprung mass (kg)		680.39	
Axle separation (m)		1.219	
Static load distribution		50%	
Dynamic load transfer		-10%	
Center of gravity height (m)		0.508	
Roll center height (m)		0.686	
Track width (m)		1.981	
Dual tire separation (m)		0.330	
Spring spread (m)		1.118	
Auxiliary roll stiffness (Nm/deg)		1016.86	
Roll steer coefficient		0.230	
Compression Table		**Extension Table**	
Force (kN)	**Deflection (cm)**	**Force (kN)**	**Deflection (cm)**
-118.16	-25.4	-119.02	-25.4
0.0	-3.81	-0.869	-3.81
0.0	0.000	-0.445	0.000
7.12	0.635	3.114	0.635
17.79	1.27	8.896	1.27
30.03	1.905	17.793	1.905
213.51	11.43	138.276	11.43

Table 2.6: Parameters of the baseline tire (Michelin XZA 11:00R22.50 Radial DRY [35]).

Parameter	Value
Tire radius (m)	0.508
Polar moment of inertia (kgm^2)	11.637
Lateral stiffness (N/cm)	8756.342
Vertical stiffness (N/cm)	7880.708
Camber stiffness (N/deg)	0.0
Overturning stiffness (Nm/deg)	39.793
Aligning torque stiffness (Nm/deg)	149.230
Longitudinal stiffness (N/slip)	224421.676
Cornering stiffness (N/deg)	3917.104
Peak cornering friction coefficient	0.8

Mu-y vs. Slip Angle Table (Velocity=17.892 m/sec)			
Slip Angle (deg)	Mu-y		
	Load=8820.823 N	Load=26542.538 N	Load=41995.660 N
1.00	0.18	0.14	0.10
2.00	0.32	0.27	0.19
4.00	0.54	0.47	0.36
8.00	0.77	0.66	0.55
12.00	0.91	0.73	0.61

Mu-x vs. Slip Table (Velocity=17.892 m/sec)			
Slip	Mu-x		
	Load=13433.629 N	Load=26867.258 N	Load=40300.888 N
0.04	0.51	0.33	0.22
0.10	0.79	0.69	0.55
0.24	0.85	0.79	0.73
0.25	0.85	0.79	0.73
0.50	0.77	0.72	0.67
1.00	0.56	0.48	0.41

Aligning Torque vs. Slip Angle					
Slip Angle (deg)	Aligning Torque (in-lbs) under Various Vertical Tire Loads				
	8896.4432 N	17703.922 N	26555.883 N	35363.362 N	41991.212 N
1.00	336.00	1020.00	1764.00	2484.00	3000.00
2.00	528.00	1716.00	3156.00	4608.00	5616.00
4.00	660.00	2256.00	4344.00	6720.00	8604.00
8.00	444.00	1728.00	3240.00	5304.00	7104.00
12.00	252.00	1092.00	2184.00	3576.00	4620.00

2.3 Vehicle Parameter Validation

A simple static balance analysis is conducted on the vehicle for validating the cited data. The given forces and dimensions of each unit are shown in Figure 2.1 and Figure 2.2. The vertical force balance and moment balance around a lateral axis are examined. The fifth wheel load is calculated on tractor and semitrailer separately using the given data and the results are compared to verify the vertical force balance. The coordinates of the articulation point with respect to the tractor and trailer sprung mass c.g. are then calculated using the determined fifth wheel load and compared with the cited values to verify the moment balance.

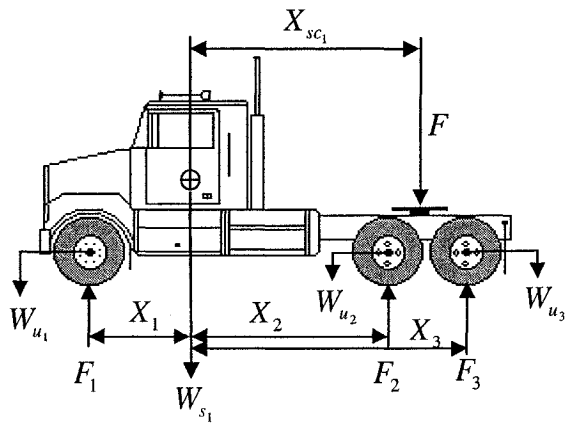

Coordinates (m)				Weight (kN)				Axle Loads (kN)		
X_1	X_2	X_3	Xsc_1	Wu_1	Wu_2	Wu_3	W_{s1}	F_1	F_2	F_3
1.397	2.667	4.191	3.041	5.338	11.121	11.121	52.489	53.935	83.355	83.355

Figure 2.1: Static force balance for the tractor.

The vertical force balance for the tractor yields:

$$F + W_{s_1} + W_{u_1} + W_{u_2} + W_{u_3} = F_1 + F_2 + F_3 \tag{2.1}$$

where F is the fifth wheel vertical load, W_{s_1} is the tractor sprung weight, W_{u_i} is unsprung weight due to axle $i\,(i=1,2,3)$, and $F_i\,(i=1,2,3)$ is the corresponding

axle load.

The moment balance around the lateral axis passing through the c.g. of tractor sprung mass yields:

$$(F_1 - W_{u_1})X_1 + FX_{sc_1} = (F_2 - W_{u_2})X_2 + (F_3 - W_{u_3})X_3 \tag{2.2}$$

where X_{sc_1} is the location of fifth wheel with respect to the sprung mass c.g.

The application of baseline vehicle data in the above equations yields $F = 140.577$ kN and $X_{sc_1} = 3.041$ m, which agree very well with the specified data, and verify for the static equilibrium for the tractor.

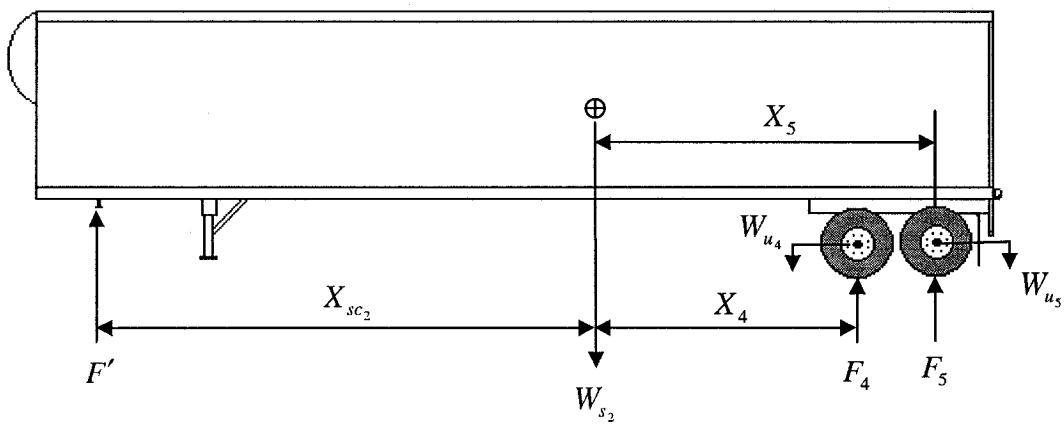

Coordinates (m)			Weight (kN)			Axle Load (kN)	
X_4	X_5	Xsc_2	Wu_4	Wu_5	Ws_2	F_4	F_5
5.294	6.513	6.441	6.672	6.672	293.943	83.355	83.355

Figure 2.2: Static force balance for the 2-axle semitrailer.

For vertical force balance of 2-axle semitrailer shown in Figure 2.2, we have:

$$W_{s_2} + W_{u_4} + W_{u_5} = F' + F_4 + F_5 \tag{2.3}$$

where W_{s_2} is the trailer sprung weight, F' is the fifth wheel reaction force, W_{u_i} is unsprung weight due to axle $i\,(i = 4, 5)$, and $F_i\ (i = 4, 5)$ is the corresponding

axle load.

The above equation yields fifth wheel reaction force $F' = 140.577$ kN, which is identical to that obtained from the tractor equilibrium.

The moment balance of the 2-axle semitrailer around the lateral axis passing through the c.g. of its sprung mass can be used to derive the longitudinal coordinate of the articulation point with respect to the sprung mass c.g. (X_{sc_2}), such that:

$$F'X_{sc_2} = (F_4 - W_{u_4})X_4 + (F_5 - W_{u_5})X_5 \tag{2.4}$$

The solution of the above equation yields $X_{sc_2} = 6.441$ m, which matches with the given data and verifies the static moment balance for the vehicle.

2.4 TruckSim Model Development and Validation

The combination vehicle model used for the preliminary feasibility study is built in TruckSim environment, which permits for analyses of directional behavior of trucks, buses, and articulated vehicles in response to steering, braking, and acceleration inputs [37]. Detailed description of the baseline vehicle TruckSim model is given in Appendix A. The simulations are initially performed to derive the axle-loads under constant speed (50 km/h) forward motion, and the resulting values are validated using the data reported in [35]. Figure 2.3 illustrates the variations in right and left tire loads of the five axles, and the mean axle loads, which are compared with the values given in [35] for the baseline vehicle considered. Figure 2.4 illustrates the percent deviation between the model outputs and the given values. The results show a maximum deviation of 1.22%,

for axle 3, while the absolute axle load difference between axle 2 and axle 3 was obtained as 1108 N, which is well below the 9810 N limit required by Canadian standard [36].

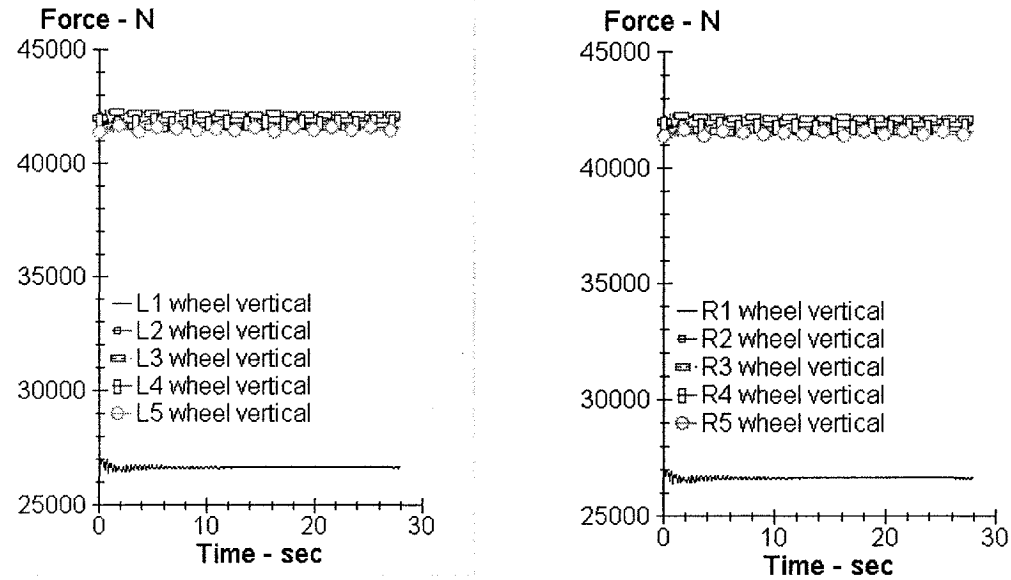

Axle 1	Axle 2	Axle 3	Axle 4	Axle 5
53274.30 N	83211.08 N	84318.94 N	83690.60 N	83045.83 N

Figure 2.3: Variations in tire forces and mean axle loads operating on a flat road.

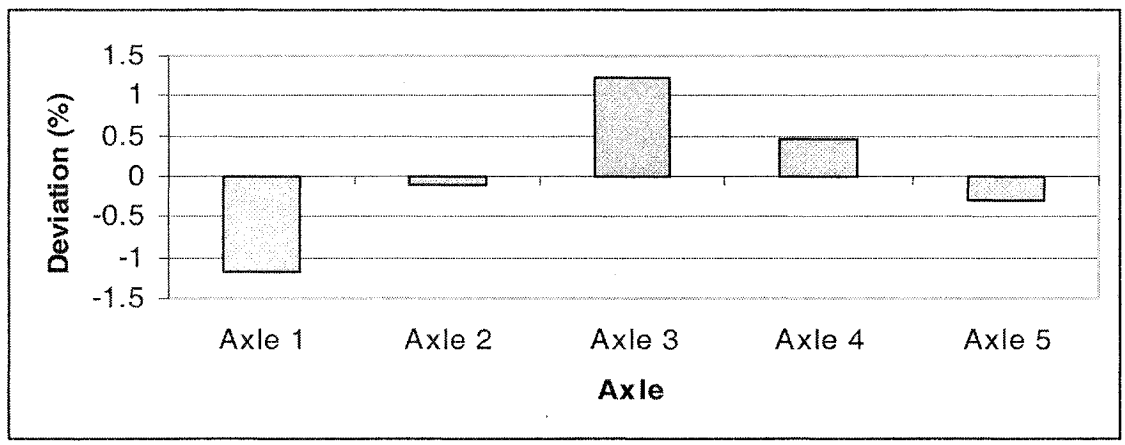

Figure 2.4: Percent deviation between the computed and specified axle loads.

2.5 Sensitivity Analysis of Dynamic Response Measures

The directional response characteristics of heavy vehicles are mostly evaluated in terms of lateral velocity and acceleration, roll and yaw rates, roll deflections of sprung and unsprung weights. These response quantities depend upon the nature of maneuver, vehicle speed and vehicle parameters. While many studies have presented the variations in these quantities with variations in the vehicle design and operating conditions, the relative sensitivities of different quantities to specific vehicle parameters have not been quantified. The consideration of a particular response that is most sensitive to variations in the c.g. height would be beneficial in obtaining an estimate of the c.g. height. The sensitivities of the response quantities to c.g. height may also depend upon the nature of steering maneuver. The vehicle model is analyzed under two typical steering maneuvers including a steady turn and a lane change maneuver. Two different values of payload c.g. height are considered: baseline and 200 mm above the baseline, to study the response parameter sensitivities to the variation in the c.g. height. The directional responses are evaluated to derive lateral accelerations and roll angles of the tractor and semitrailer sprung weights, and roll angles of the unsprung weights (axle–1 to axle–5).

Figure 2.5 illustrates the relative changes in the response quantities when payload c.g. height is increased by 200 mm under a steady turning maneuver. The maneuver is simulated by a 90° turn of 100 m radius, while traveling at a constant forward speed of 50 km/h. The units of particular response quantities are shown under the columns in Figure 2.5. The results show that the semitrailer roll

angle is most sensitive to the change in the c.g. height, followed by the roll angles of trailer axles.

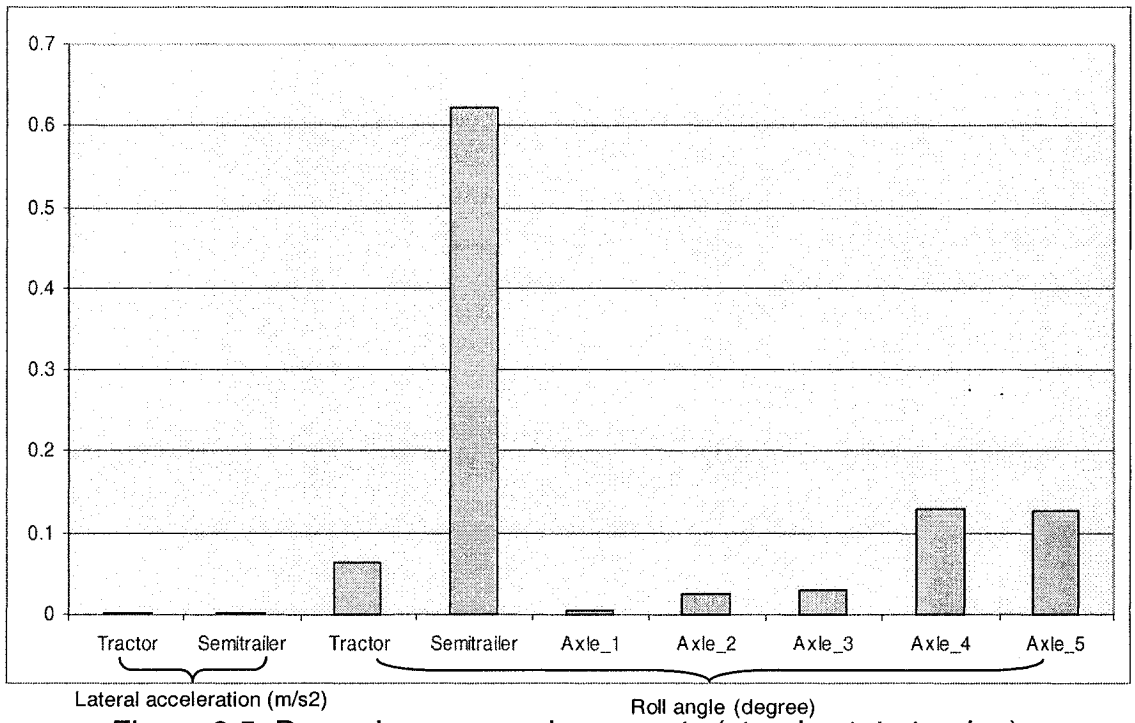

Figure 2.5: Dynamic response increments (steady-state turning).

The sensitivities of the dynamic responses are also examined under a single lane change maneuver. The lane gate is selected as 30 m long and 3.6 m wide, while the forward speed is held constant as 100 km/h. Figure 2.6 illustrates the relative increments of the dynamic responses, when the payload c.g. height is increased by 200 mm. The results show the same pattern that is the semitrailer sprung mass roll angle reveals the largest increment and is most sensitive to the change in c.g. height. The simulation results attained under both maneuvers suggest that the semitrailer sprung mass roll angle is most sensitive to the changes in the payload c.g. height and therefore could serve as the best candidate for online estimation of the c.g. height under relatively simple and

practical steering maneuvers.

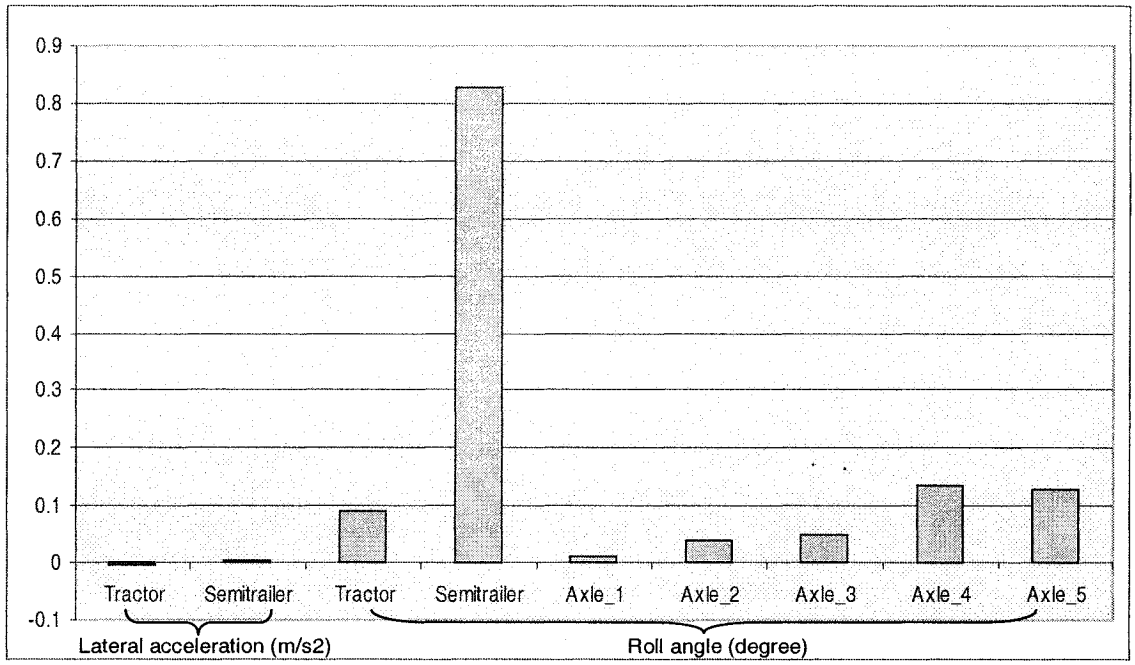

Figure 2.6: Dynamic response increments (single-lane change).

2.6 Test Maneuver Selection

The responses to steering are also known to depend upon the nature of the maneuver, although it is not quite evident from Figure 2.5 and Figure 2.6 for the two maneuvers considered. A well defined standard maneuver could also reduce the complexity of the problem and increase the accuracy of the estimation of c.g. height. A prescribed maneuver should be selected such that it does not impose any danger to the vehicles to be tested and the driver, and at the same time it should generate sufficiently large magnitude of the dynamic response of c.g. height indicator. The lateral acceleration generated under the test maneuver should be close to but not larger than the smallest rollover threshold for all different possible combinations of the vehicles. The typical five-axle

tractor-semitrailer combination, when loaded to legal gross weight, exhibits a rollover threshold as high as 0.5g with an optimal high density, low c.g. load. It could be as low as 0.25g under the worst case of loading that completely fills the volume of the trailer [38, 39]. The test maneuver for the five-axle tractor-semitrailer model should thus be designed to generate maximum lateral acceleration around 0.2g in order to permit a reasonable safety margin.

2.6.1 Steady-State Turning Maneuver

The simulation control is setup for a steady-state turning maneuver with a constant forward velocity of 50 km/h. The vehicle runs along the center line of the given road without lateral offset at a preview time of 1.5 seconds, which is the look-ahead time used by the driver controller algorithm to steer the vehicle. A shorter preview time causes the controller to steer more rapidly in response to deviations of the vehicle from the target path, and a longer one causes the vehicle to look ahead more and steer more slowly in response to changes in the target path. A realistic value of preview time is recommended as 1.5 seconds (TruckSim online help). Figure 2.7 illustrates the path used in simulation for the steady-turning maneuver. Three different cornering angles, 60°, 90° and 120° are investigated and the sensitivities of the response quantities to change in c.g. height are compared. A series of tests are initially performed to derive the coordinates of the path center lines, which are illustrated in Figure 2.8 to Figure 2.10.

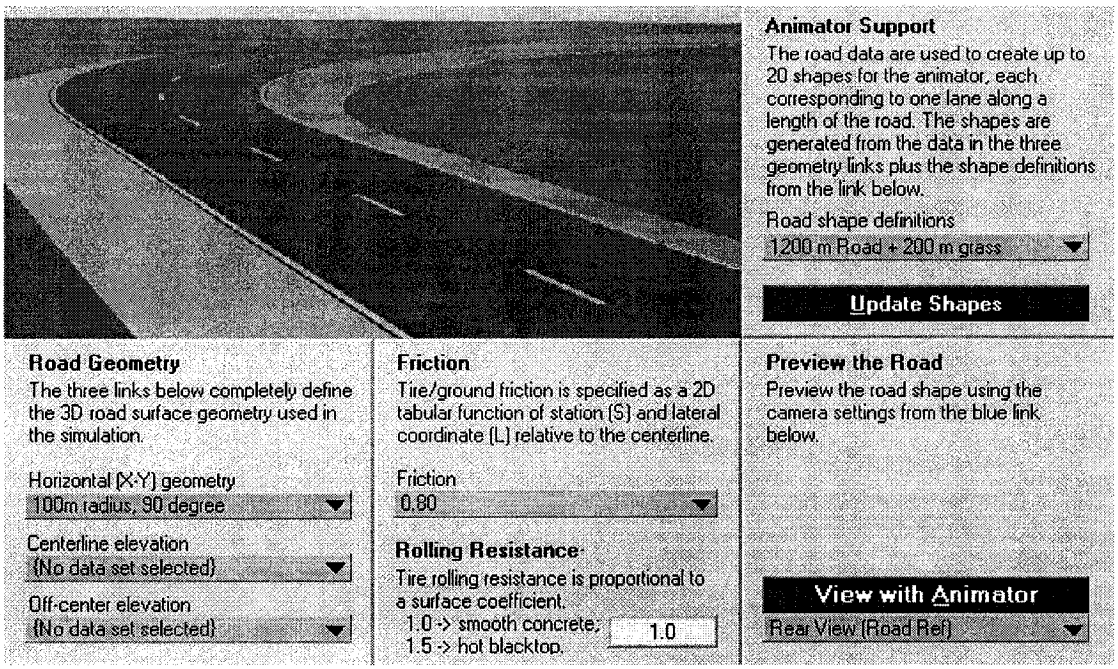

Figure 2.7: Simulation road for a steady turning maneuver.

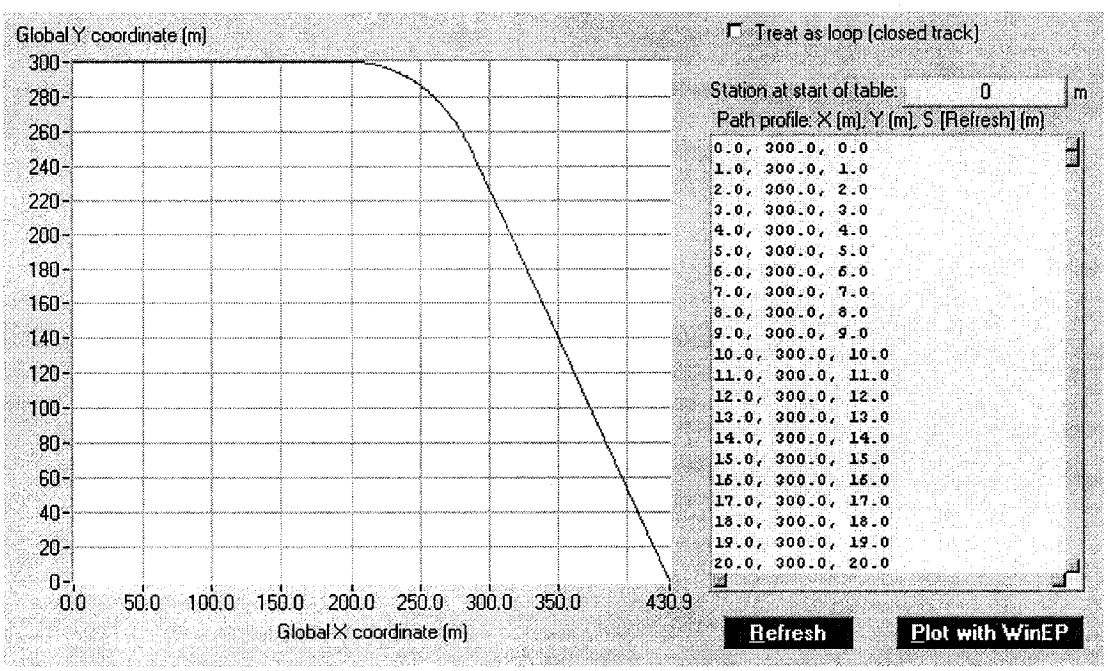

Figure 2.8: Path coordinates for a 60° cornering maneuver.

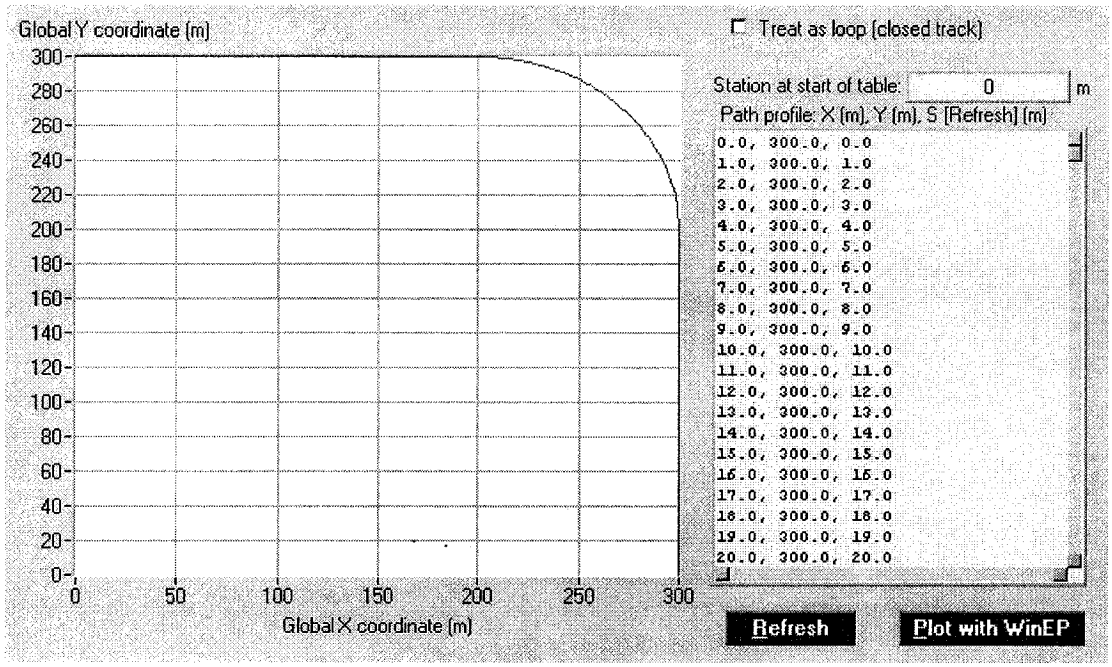

Figure 2.9: Path coordinates for a 90° cornering maneuver.

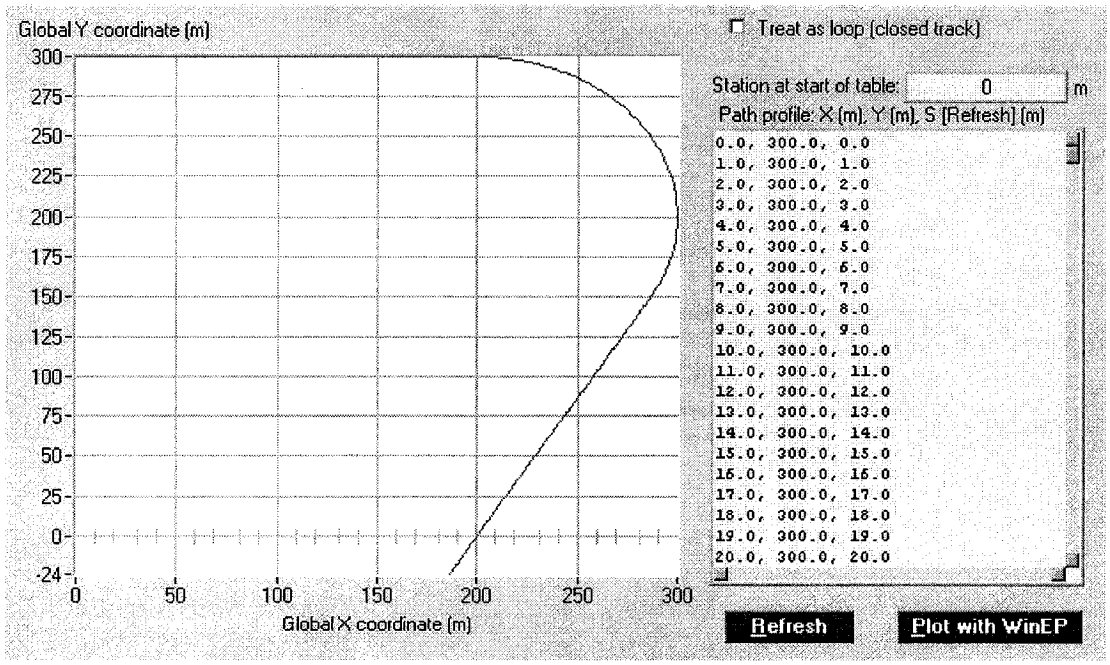

Figure 2.10: Path coordinates for a 120° cornering maneuver.

The simulations are performed by running the baseline vehicle along the

central lines shown above with a close-loop control. The simulation results in terms of the sprung mass roll angles are given in Figure 2.11 to Figure 2.13, for the three turning maneuvers at a constant forward speed of 50km/h and cornering radius of 100m. Figure 2.14 and Figure 2.15 show the comparisons of the peak values of the lateral accelerations and roll angles corresponding to the three maneuvers. The results are presented for the nominal c.g. height, where "Unit 1" and "Unit 2" refer to the tractor and semitrailer respectively. It can be seen that the variations in the steady-state turning maneuvers do not affect the peak values of semitrailer sprung mass lateral acceleration and roll angle, for the cornering radius and forward speed considered.

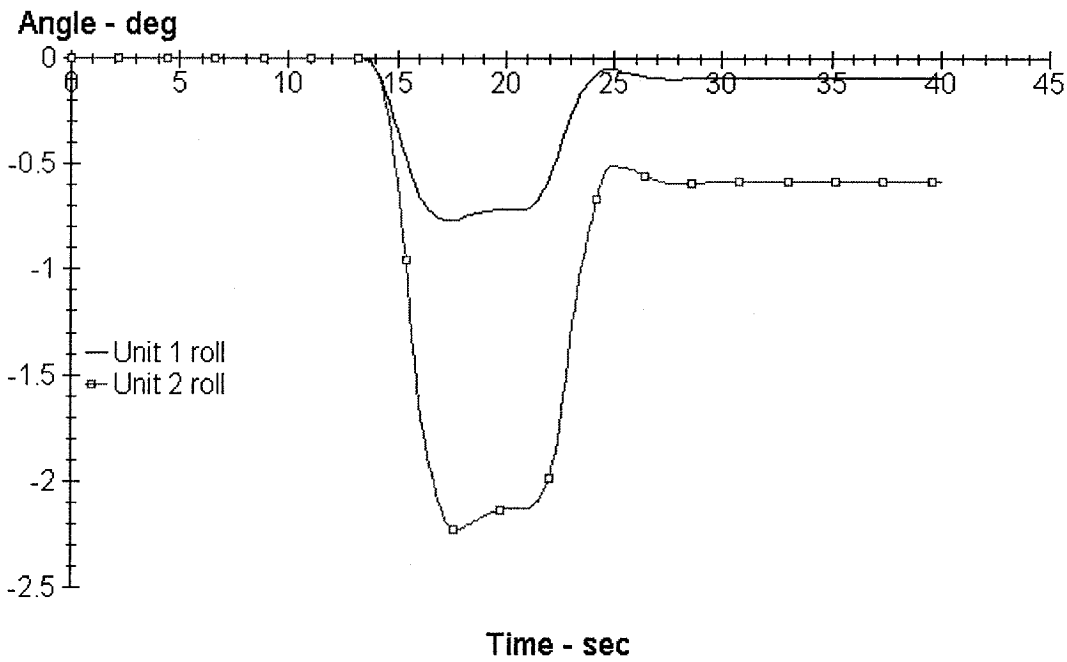

Figure 2.11: Roll angle responses of tractor (Unit 1) and semitrailer (Unit 2) sprung masses under a 60° cornering maneuver.

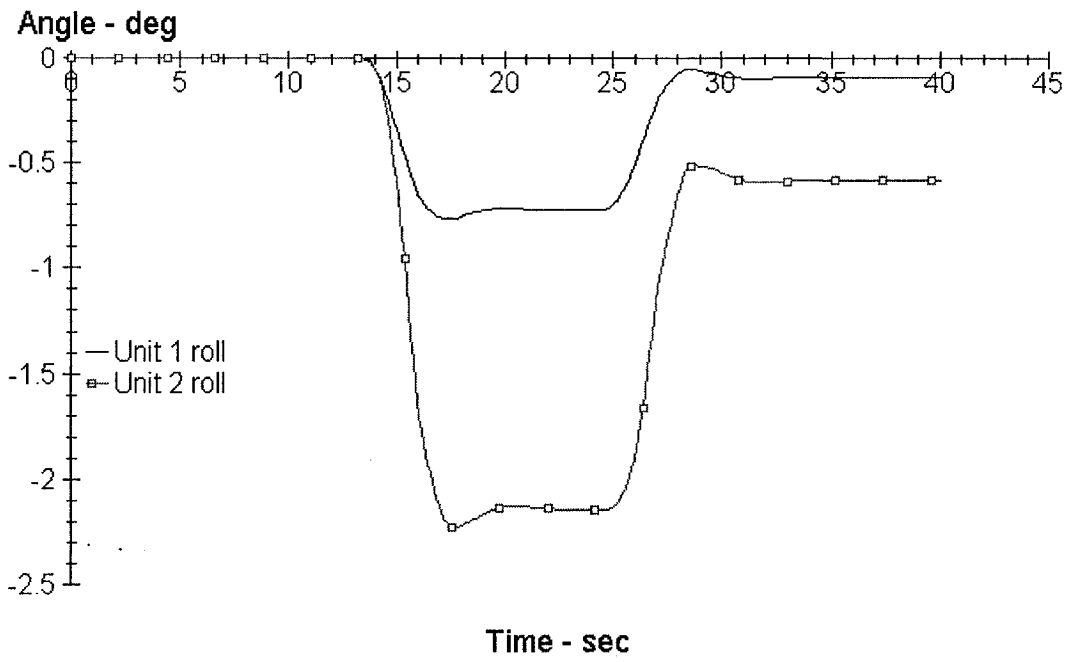

Figure 2.12: Roll angle responses of tractor (Unit 1) and semitrailer (Unit 2) sprung masses under a 90° cornering maneuver.

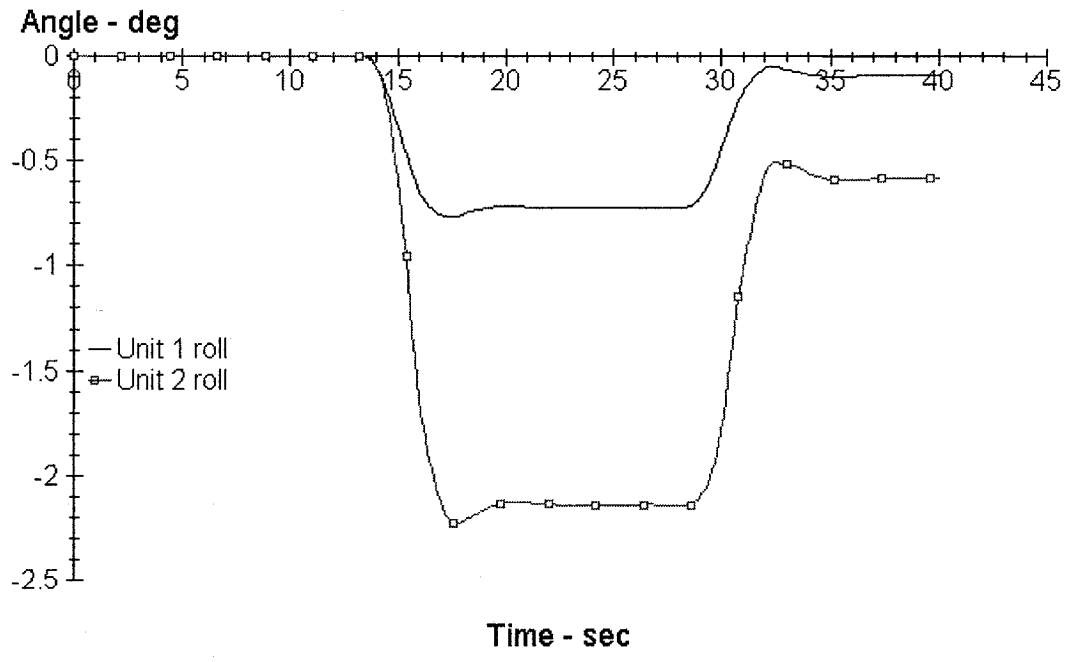

Figure 2.13: Roll angle responses of tractor (Unit 1) and semitrailer (Unit 2) sprung masses under a 120° cornering maneuver.

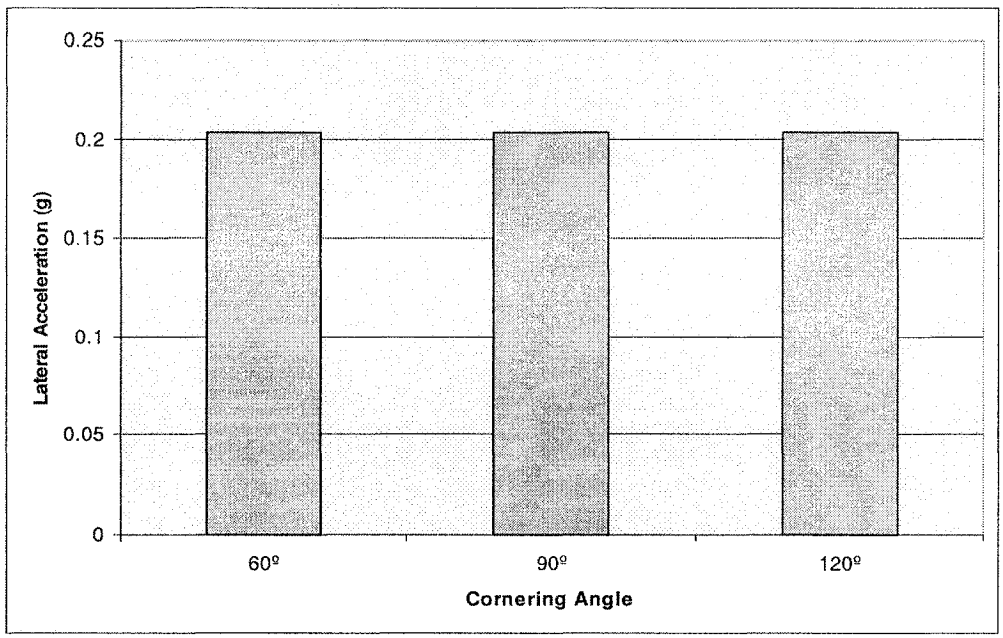

Figure 2.14: Peak semitrailer lateral acceleration responses under different cornering angles.

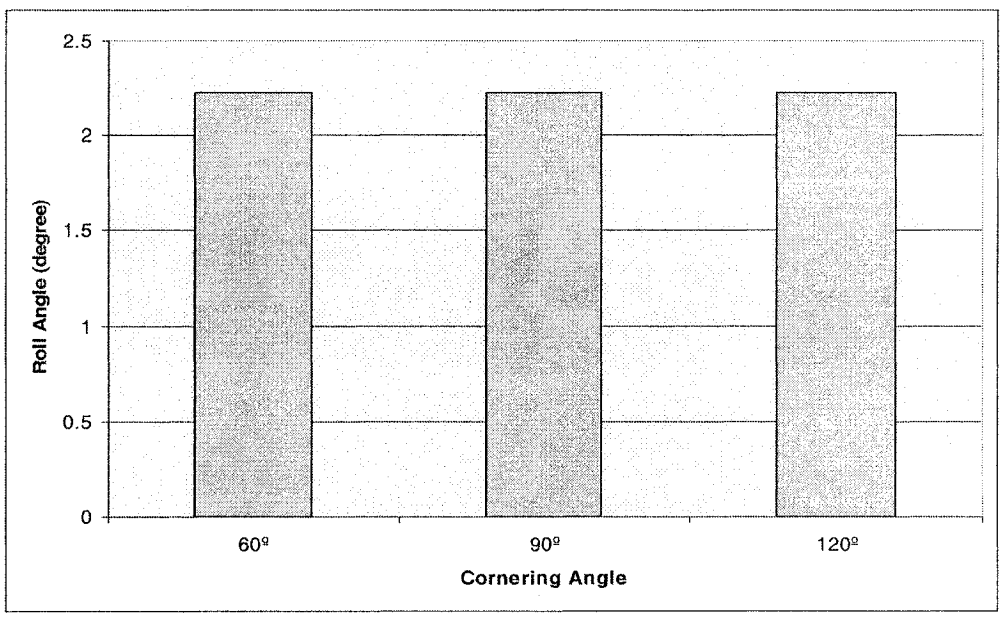

Figure 2.15: Peak semitrailer roll angle responses under different cornering angles.

2.6.2 Single-Lane Change Maneuver

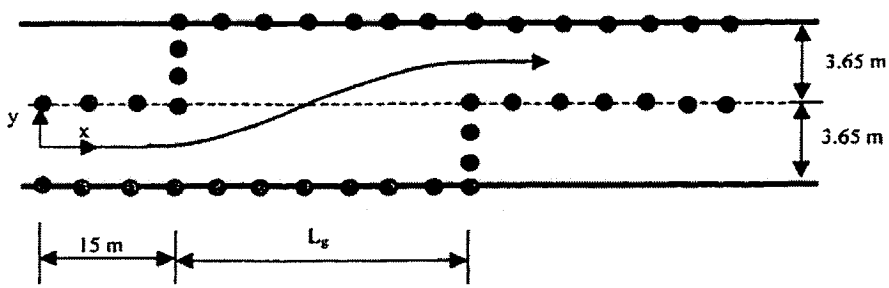

Figure 2.16: Schematic representation of the coordinates of the path followed during a single-lane change maneuver.

Figure 2.16 illustrates the trajectory of a single-lane change maneuver. The lateral coordinate (y) of the path can be expressed as a function of the gate length, lane width and the longitudinal coordinate (x). For a 3.65 m lane width, the y-coordinate is given by [4]:

$$y = \begin{cases} 0 & x \le 15\ m \\ 1.825\left[1+\sin\left(\dfrac{\pi}{L_g}(x-15)+\dfrac{3\pi}{2}\right)\right] & 15\ m < x < (15+L_g)\ m \\ 3.65 & x \ge (15+L_g)\ m \end{cases} \tag{2.5}$$

where L_g is the gate length for the path.

In this study, two different gate lengths, 20 m and 30 m, are considered, and the corresponding path coordinates are illustrated in Figure 2.17 and Figure 2.18, as derived from Equation (2.5). The simulations are performed to derive the variations in the roll angle responses, and peak values of lateral accelerations and roll angles. Figure 2.19 and Figure 2.20 show the variations in the sprung mass roll angles corresponding to the 20 m and 30 m lane changes, while the peak

values of lateral accelerations and roll angles are summarized in Figure 2.21 and Figure 2.22. It can be concluded from the simulation results that the 20 m gate length can generate a lateral acceleration of about 0.2g, while a shorter gate length can cause larger magnitudes of semitrailer sprung mass roll angle.

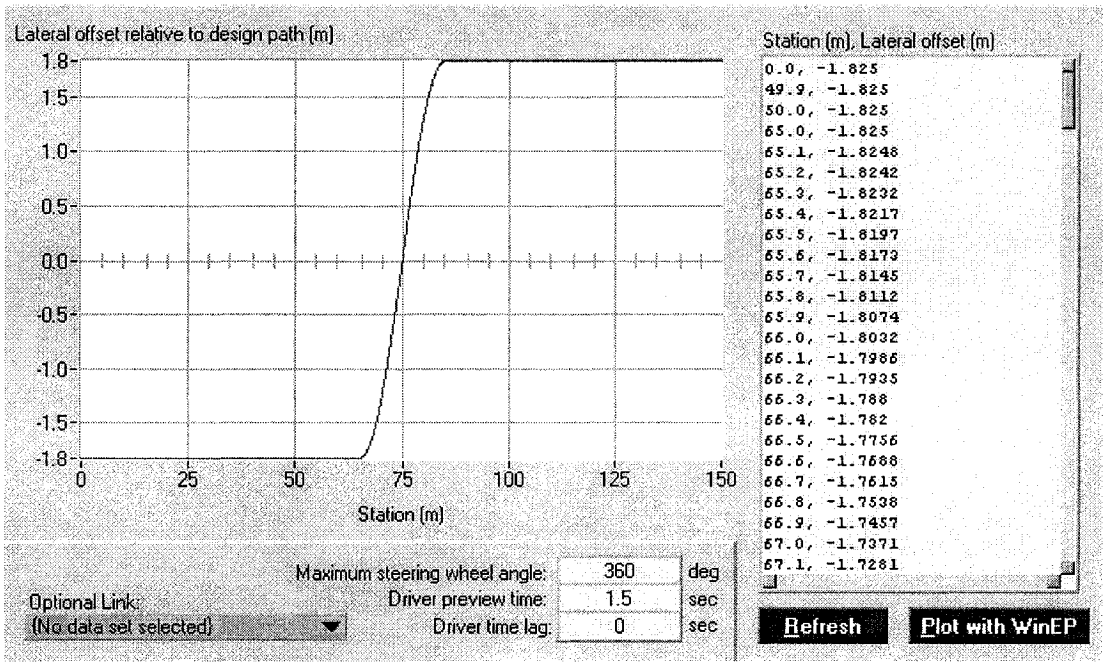

Figure 2.17: Coordinates of path followed during a single-lane change (gate length 20m).

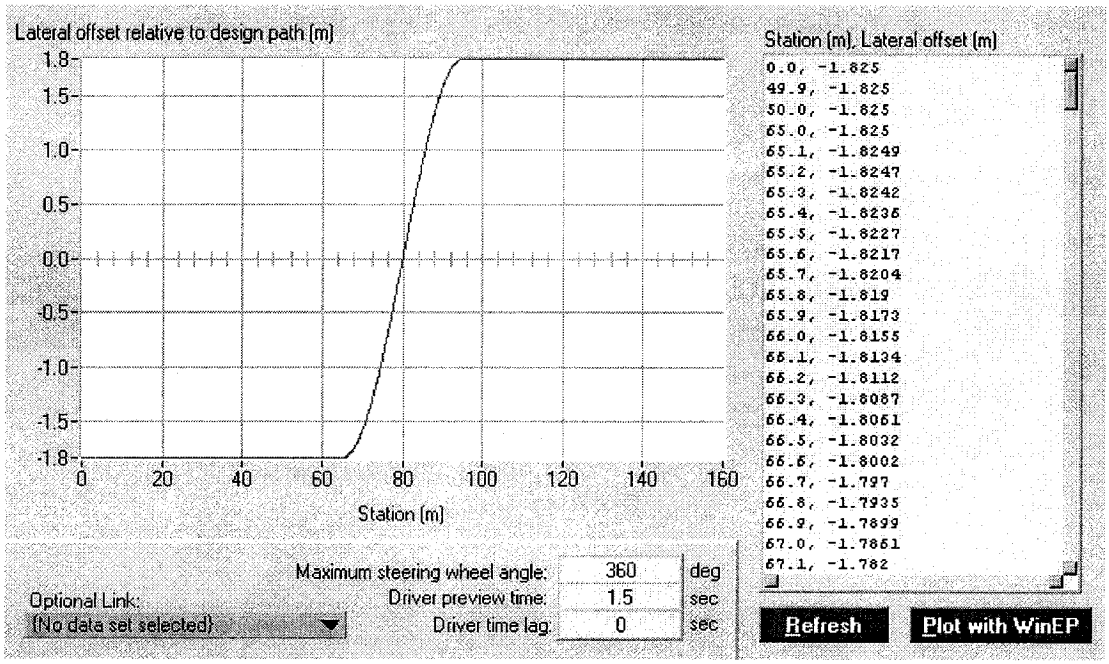

Figure 2.18: Coordinates of path followed during a single-lane change (gate length 30m).

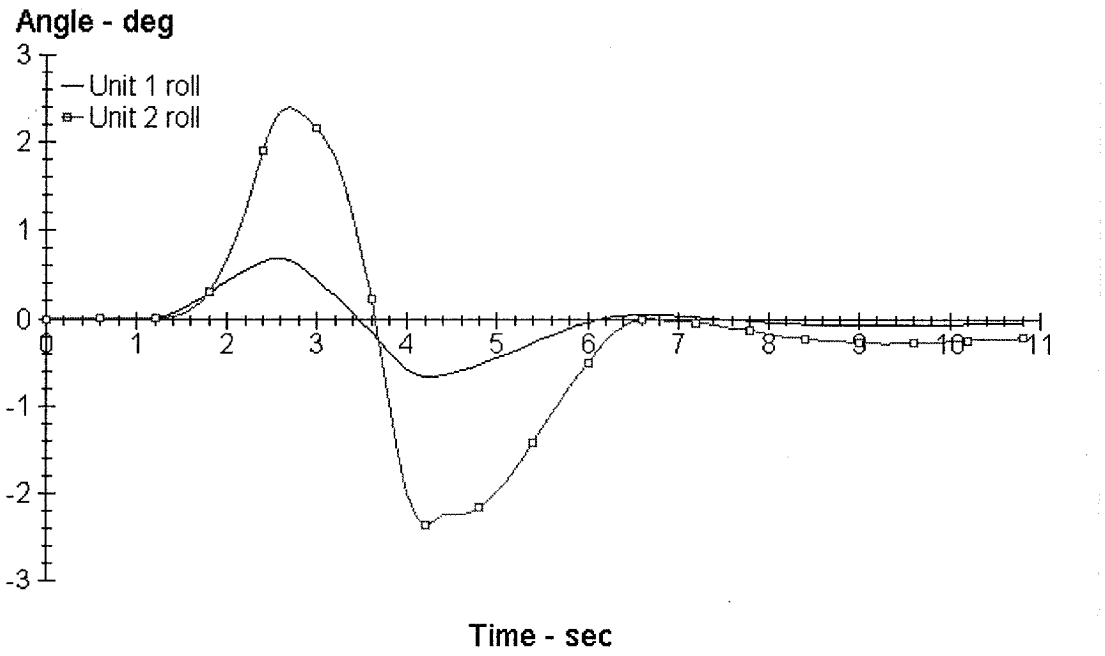

Figure 2.19: Roll angle responses of the tractor (Unit 1) and semitrailer (Unit 2) sprung masses (gate length 20m).

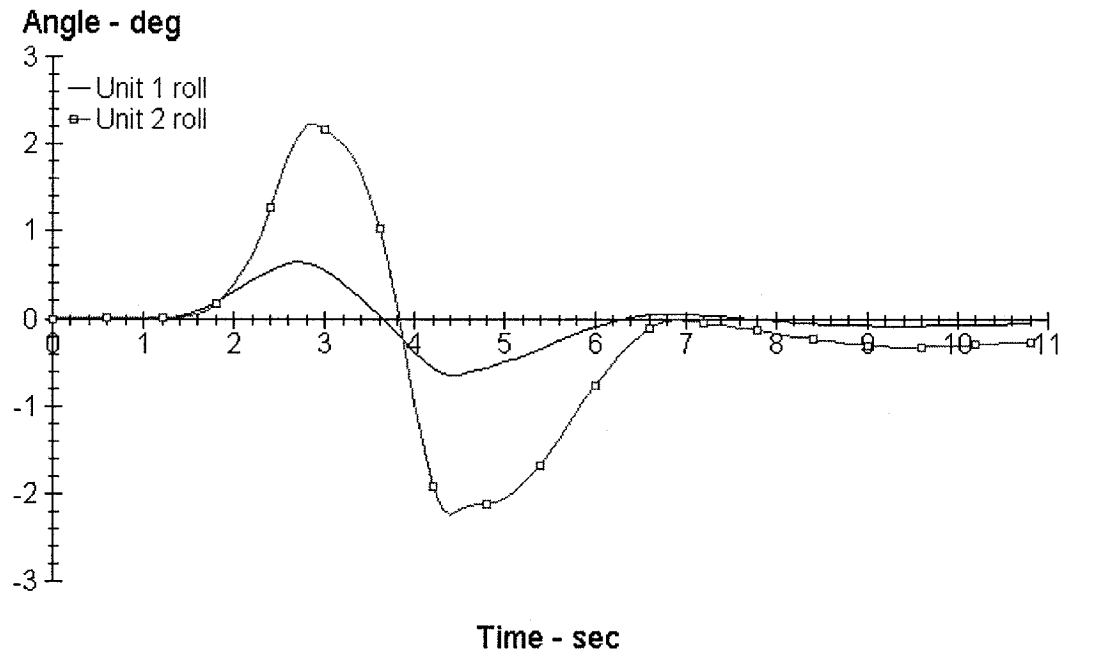

Figure 2.20: Roll angle responses of the tractor (Unit 1) and semitrailer (Unit 2) sprung masses (gate length 30m).

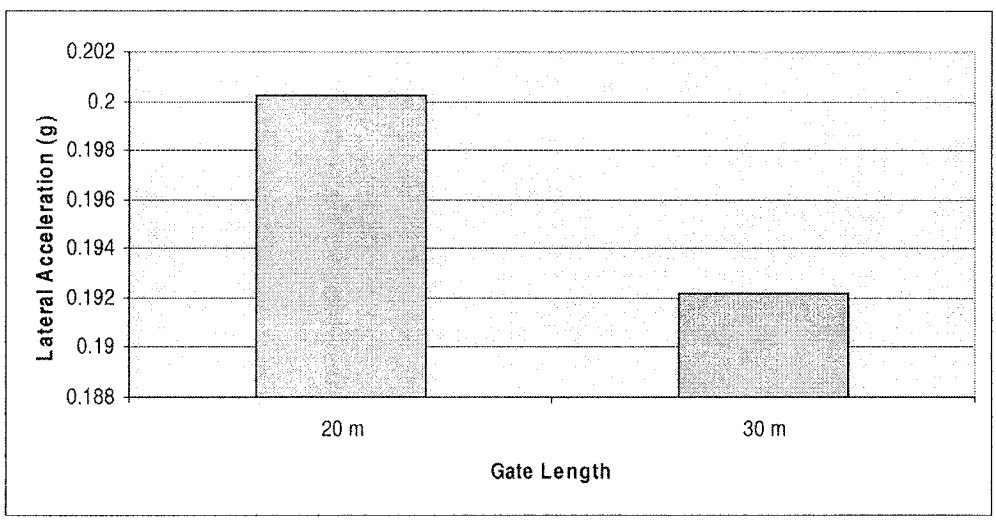

Figure 2.21: Influence of gate length on the peak lateral acceleration response.

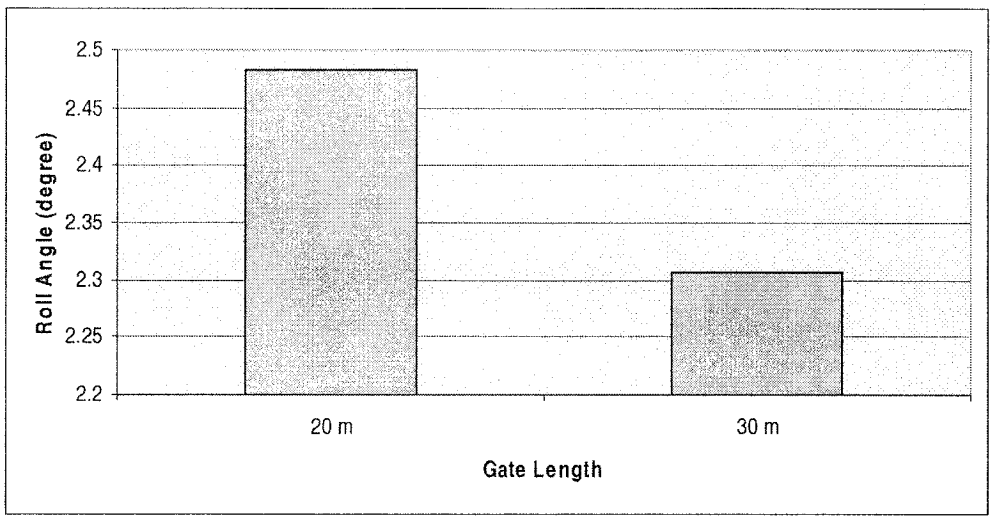

Figure 2.22: Influence of gate length on the peak roll angle response.

The 20 m lane change and the 90° cornering maneuver are thus selected as possible standardized test maneuvers for further analyses.

Figure 2.23 further displays the relationship between the peak semitrailer sprung mass roll angle and the peak lateral acceleration under the two maneuvers. The peak values are obtained corresponding to different constant speeds, varying from 70 km/h to 120 km/h for lane change maneuver and from 48 km/h to 52 km/h for cornering maneuver. The single-lane change maneuver tends to cause a larger roll angle, which is about 0.28 degree higher in average than that generated during a cornering maneuver when both maneuvers create the same peak lateral acceleration. Obviously the peak responses are dependent upon the speed. A study of the speed dependence could permit the definition of the standardized maneuver speed that is considered to be safe and yield reasonable good magnitude of the response. Figure 2.24 illustrates the variations in peak lateral acceleration with forward speed under the two maneuvers. The

results show that the vehicle may exceed the safe target lateral acceleration level of 0.2g at a much lower speed under a cornering maneuver. The test speed under a cornering maneuver, therefore, must be limited to below 50 km/h, and can be as high as 90 km/h for a lane change maneuver.

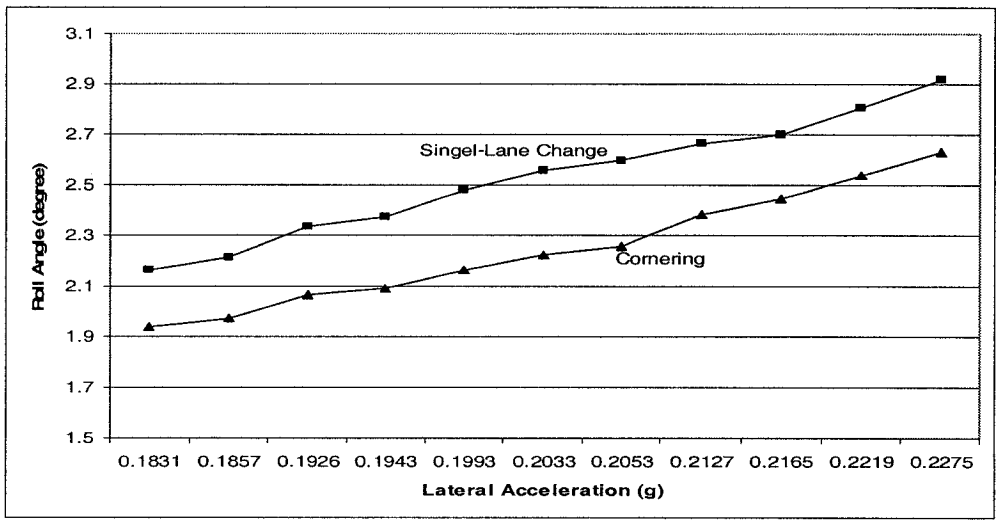

Figure 2.23: Variations in the peak roll angle with peak lateral acceleration response of semitrailer.

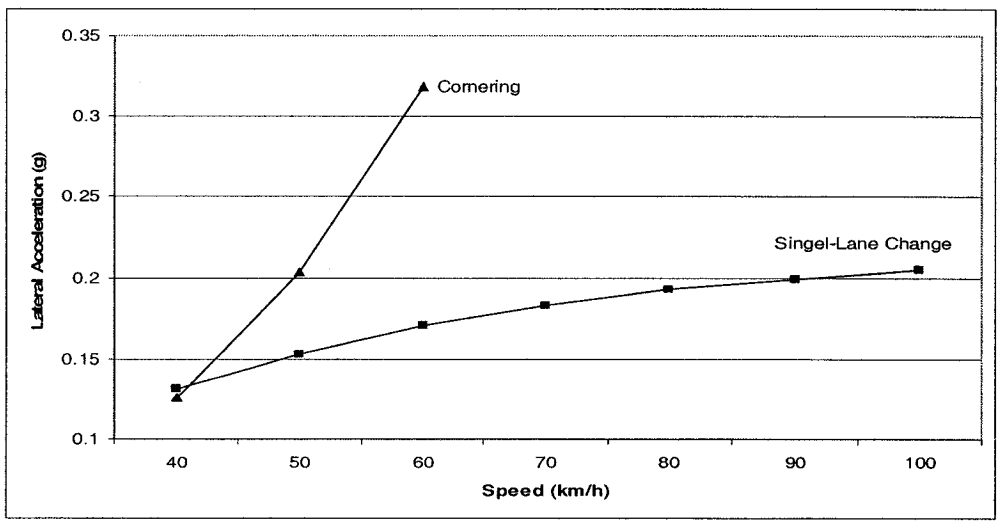

Figure 2.24: Variations in peak semitrailer lateral acceleration with speed.

Apart from the vehicle speed, the peak responses are also dependent upon the payload and roll moment of inertia of the semitrailer sprung mass. The shape of the payload is varied to attain variations in the roll mass moment of inertia ($1x10^4$ to $2.15x10^4$ kgm^2), and the effect on the peak semitrailer roll angle is investigated. Figure 2.25 displays the effect of payload roll inertial property on the peak semitrailer sprung mass roll angle. The results show that the peak response to a cornering maneuver is relatively insensitive to variations in the sprung mass moment of inertia, which is attributed to, more or less, steady-state response behavior of the vehicle. The transit mature of the response to a lane change maneuver, however, exhibits considerable sensitivity of the roll angle.

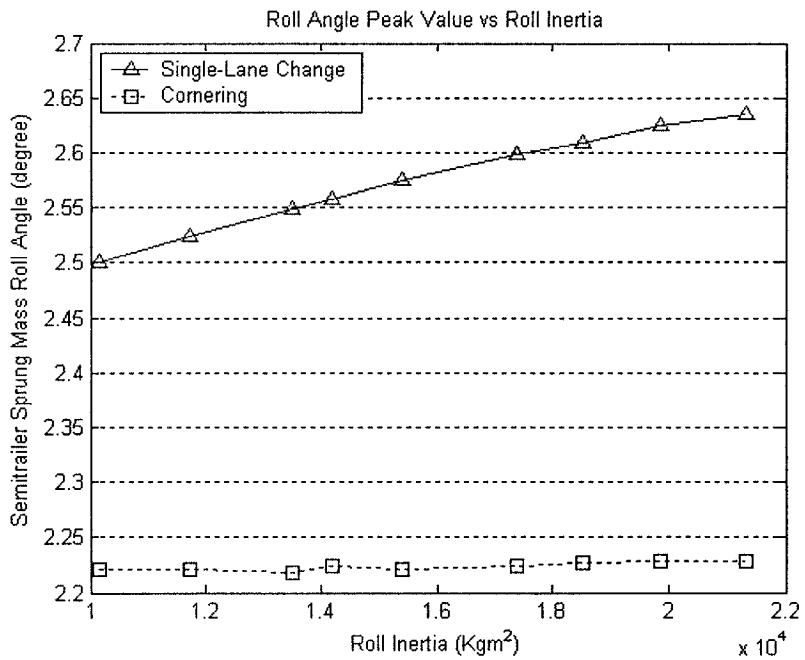

Figure 2.25: Variation in peak semitrailer sprung mass roll angle with roll inertia.

2.7 Sensitivity of Semitrailer Sprung Mass Roll Angle to CG Coordinates

Considering that a reasonable large magnitude of lateral acceleration signal can be generated at a relatively lower speed under a steady-state turning maneuver and the responses are less sensitive to variations in mass moment of inertia, this maneuver is selected for further analyses. The sensitivity of the sprung mass roll angle to variations in c.g. height and payload are investigated to identify a desirable test maneuver for online estimation of c.g. height. The relationship between c.g. height and roll angle of semitrailer sprung mass is investigated using the 90° steady-state turning maneuver at a forward speed of 50 km/h. The selected speed yields peak lateral acceleration in the vicinity of safe target value of 0.2g for the range of c.g. heights considered. Studies conducted by Miller and Barber [40] revealed that the c.g. height of sprung mass of a fully laden trailer lies around 2 meters. The sensitivity of the peak roll angle response to c.g. height is thus examined for c.g. heights varying from 1.85 m to 2.25 m, while the payload is held constant. Figure 2.26 illustrates the variations in peak roll angle response as a function of the c.g. height of semitrailer sprung mass. The results show that the peak roll angle increases in a nonlinear manner with the c.g. height, where the rate of change of roll angle with respect to the change in the c.g. height is approximately 0.0041 degree/mm or 4.1 degree/m.

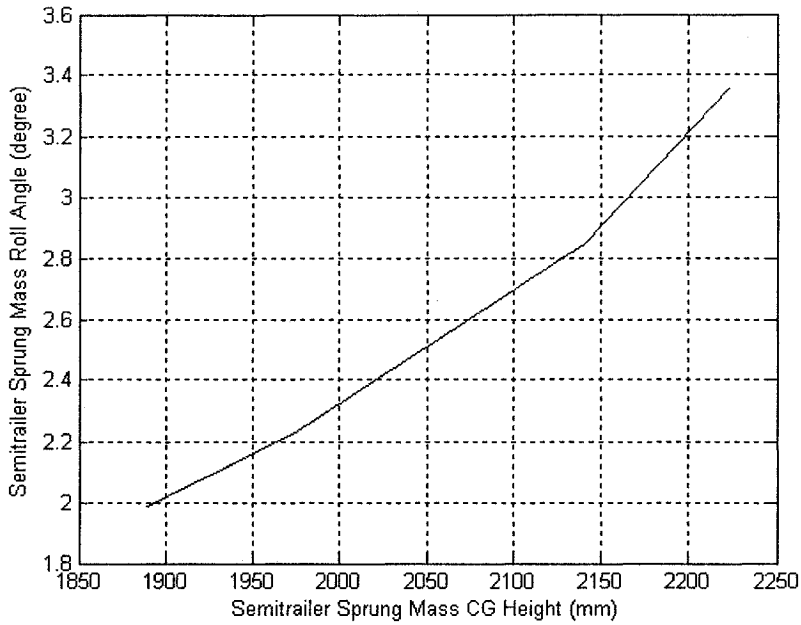

Figure 2.26: Semitrailer sprung mass roll angle and c.g. height relation.

2.7.1 Influence of payloads

Assuming that the longitudinal and lateral coordinates of the payload c.g. do not vary with the payload, and coincide with those of the unladen semitrailer sprung mass, the variations in the c.g. height of the total semitrailer sprung mass with varying payload can be derived from:

$$h = h_0 + \frac{m_p}{m_p + m_0}\left(h_p - h_0\right) \tag{2.6}$$

where h is the c.g. height of total semitrailer sprung mass, h_0 is the c.g. height of empty semitrailer sprung mass, and h_p is the c.g. height of payload, where all heights are measured from the ground. In the above equation, m_0 is the mass of the unladen semitrailer and m_p is the payload mass.

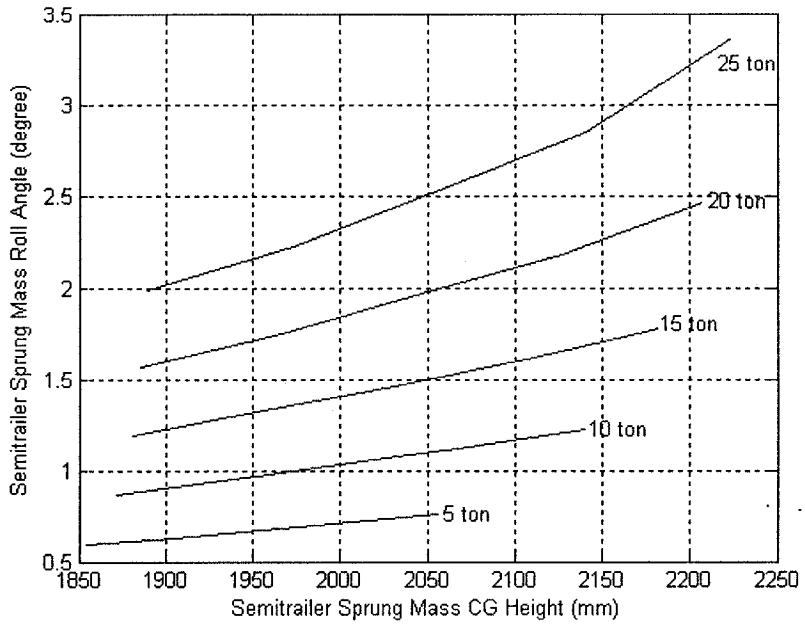

Figure 2.27: Variations in peak roll angle response with varying payload and c.g. height.

The variations in the payload cause most significant variations in the axle and tire loads, c.g. height, mass moment of inertia and the sprung weight. Such variations are thus expected to yield considerable variations in the desired response quantity, the sprung mass roll angle. For a 12.2 m dry container, the maximum payload is limited to 26.71 tons. The payloads in this study are thus varied from 5 to 25 tons, in increments of 5 tons. The simulation results are analyzed to derive the peak semitrailer sprung mass roll angles as functions of the payload and the corresponding c.g. heights. The shapes of the payloads in the study are varied to realize variations in the c.g. height and thus the roll moment of inertia. Figure 2.27 illustrates the variations in the peak roll angle as a function of the payload and the c.g. height. The results show a quasi-linear relationship between roll angle and c.g. height of the semitrailer sprung mass under various

payloads. A light payload, however, yields a lower rate of change of the roll angle with respect to c.g. height. The sensitivity of roll angle to variations in c.g. height under a payload of 5 ton is about 0.00083 degree/mm. For the resolution of a tilt sensor of nearly 0.05° (Tilt sensor CXTA02 [41]), the accuracy of the c.g. height online measurement system will be in the order of $\pm 60\,mm$ for such a payload without considering the signal noise. An accurate estimation of c.g. height of lightly loaded trailers on the basis of peak roll angle would thus be quite difficult.

2.7.2 Influence of CG lateral shift

The payload of a vehicle undergoes lateral displacement during a cornering maneuver, which may be attributed due to relative sliding of the payload when unrestrained and semitrailer roll angle. The effect of deviations of the lateral c.g. coordinate on the peak sprung mass roll angle is thus examined by shifting the payload of baseline vehicle along a lateral axis. The deviations are considered within the range of ±400 mm. The simulations are performed for vehicle operating on a straight line course and a 90° curved course. Figure 2.28 illustrates the relationship between semitrailer sprung mass roll angle and payload lateral shift, when the vehicle is running on a straight road and a curved road. The results show asymmetric behavior in the peak roll angle response. The dash-dot line represents the difference between these two situations. It is apparent that the semitrailer sprung mass roll angle is very sensitive to the lateral shift of the payload, while the results of change of the peak roll angle with the lateral shift of the payload are roughly the same for both courses. The deviations in the

differences in the peak roll angles attained for two courses, however, tend to show relatively small variations.

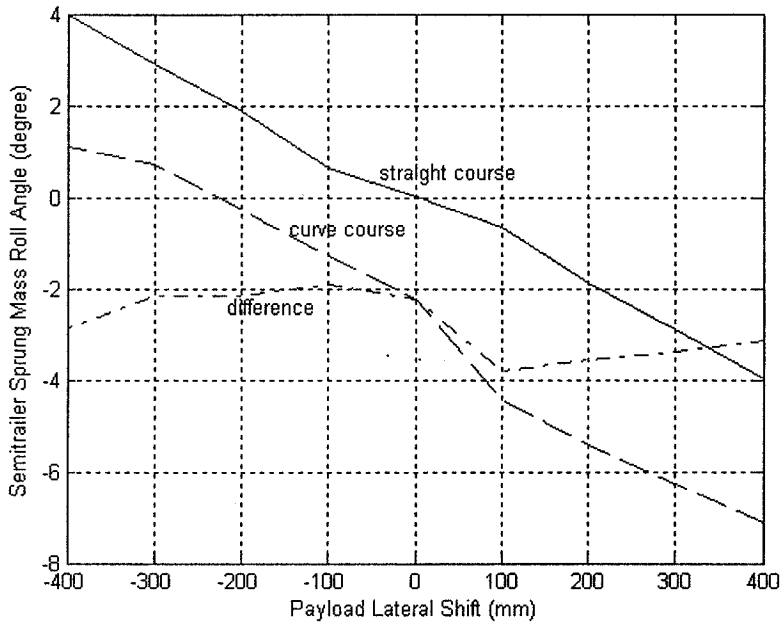

Figure 2.28: Effect of c.g. lateral shift on roll angle.

2.7.3 Influence of C.G. longitudinal shift

The influence of c.g. longitudinal shift on the peak roll angle response is further examined in a similar manner by shifting the payload of the baseline vehicle from the c.g. of the unladen sprung mass along a longitudinal axis. The variations along the longitudinal coordinate are limited to ±500 mm. The simulations are performed for vehicle operating on a 90° curved course and resulting variations in the peak roll angle response are presented in Figure 2.29. The results show only minimal variations in the peak semitrailer sprung mass roll angle response, when the longitudinal coordinate of the payload is varied. It is thus concluded that the semitrailer sprung mass roll angle response is not

sensitive to the longitudinal shift of payload. The results also suggest that an optimal longitudinal position of the payload c.g. exists to obtain the least roll deflection of the semitrailer sprung mass, which for the situation considered lies close to that of the tare semitrailer structure.

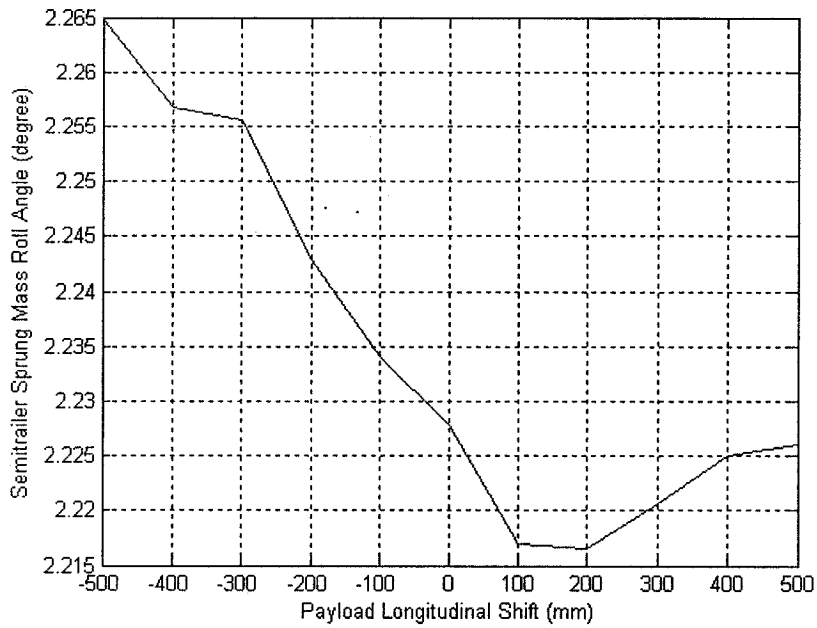

Figure 2.29: Effect of c.g. longitudinal shift on the peak roll angle of the semitrailer sprung mass.

2.7.4 Influence of suspension properties

Heavy vehicles employ a wide range of wheel suspensions, ranging from leaf-spring suspension, elastomeric suspension to air suspensions. The vertical and effective roll stiffness properties of a suspension system are directly dependent upon its construction. The left-spring and elastomeric suspensions are known to yield relatively higher vertical and roll stiffness, while the air suspensions are generally soft in vertical. Auxiliary roll stiffness mechanism is often used to enhance the roll stiffness of the vehicle. The variations in the vertical and roll

stiffness of different suspensions are known to affect the directional responses of the vehicle. In this study, the baseline vehicle is modified by introducing modern air suspensions. The properties of these air suspensions at the tractor drive and semitrailer axles are summarized in Table 2.7 and Table 2.8. The steering axle, however, is retained with the standardized left-spring suspension. The use of alternate suspension systems also yields differences in the unsprung weights and axle loads. The static force and moment balance analyses of the modified vehicle is thus performed as described in Section 2.3, the dimensions of the vehicle are appropriately adjusted, which are summarized in Table 2.9. Simulations are performed for the modified vehicle configuration equipped with air suspensions to study the effect of suspension spring rate on the peak sprung mass roll angle. The results are attained under the 90° cornering maneuver performed at a constant forward speed of 50 km/h. The results are presented to demonstrate the sensitivity of the peak roll angle to variations in c.g. height, as shown in Figure 2.30. The figure shows a comparison of the responses attained for the baseline and the modified vehicles. The air suspension vehicle yields nearly linear relationship between the peak roll angle and c.g. height of semitrailer sprung mass. Although air suspension gives a larger absolute value of the semitrailer sprung mass roll angle, the rate of change of the roll angle with the c.g. height is about the same as the baseline vehicle for the suspension data used in these two configurations.

Table 2.7: Properties of the tractor rear axle air suspension [35].

Parameter		Value	
Lead Axle			
Roll moment of inertia (kgm^2)		463.24	
Unsprung mass (kg)		680.39	
Axle separation (m)		1.219	
Static load distribution		50%	
Dynamic load transfer		0%	
Center of gravity height (m)		0.508	
Roll center height (m)		0.749	
Track width (m)		1.829	
Dual tire separation (m)		0.330	
Spring spread (m)		0.965	
Auxiliary roll stiffness (Nm/deg)		1694.772	
Roll steer coefficient		0.175	
Trailing axle			
Auxiliary roll stiffness (Nm/deg)		5762.226	
Compression Table		**Extension Table**	
Force (kN)	**Deflection (cm)**	**Force (kN)**	**Deflection (cm)**
-79.679	-10.16	-81.013	-10.16
5.783	-6.35	4.115	-6.35
10.676	-2.54	7.896	-2.54
14.234	0.000	11.121	0.000
19.461	2.54	15.235	2.54
23.576	5.08	21.574	5.08
95.386	10.16	94.608	10.16

Table 2.8: Properties of the semitrailer rear axle air suspension [35].

Parameter		Value	
Lead Axle			
Roll moment of inertia (kgm^2)		463.24	
Unsprung mass (kg)		680.39	
Axle separation (m)		1.219	
Static load distribution		50%	
Dynamic load transfer		0%	
Center of gravity height (m)		0.508	
Roll center height (m)		0.749	
Track width (m)		1.981	
Dual tire separation (m)		0.330	
Spring spread (m)		1.118	
Auxiliary roll stiffness (Nm/deg)		9377.741	
Roll steer coefficient		0	
Trailing axle			
Trailing axle data is identical to lead axle data			
Compression Table		**Extension Table**	
Force (kN)	**Deflection (cm)**	**Force (kN)**	**Deflection (cm)**
-91.745	-6.35	-92.857	-6.35
23.909	-3.493	21.463	-3.493
30.025	-1.27	26.912	-1.27
32.806	0.000	29.469	0.000
36.253	1.27	32.583	1.27
43.370	3.81	40.590	3.81
126.135	7.62	125.356	7.62

Table 2.9: Vehicle dimensions and axle loads with air suspensions.

Coordinate (m)				Weight (kN)				Axle Load (kN)		
X_1	X_2	X_3	Xsc_1	Wu_1	Wu_2	Wu_3	W_{s1}	F_1	F_2	F_3
1.397	2.819	4.039	3.053	5.338	6.672	6.672	52.489	53.935	81.131	81.131

Coordinate (m)			Weight (kN)			Axle Load (kN)	
X_4	X_5	Xsc_2	Wu_4	Wu_5	Ws_2	F_4	F_5
5.481	6.700	6.254	6.672	6.672	293.943	81.131	81.131

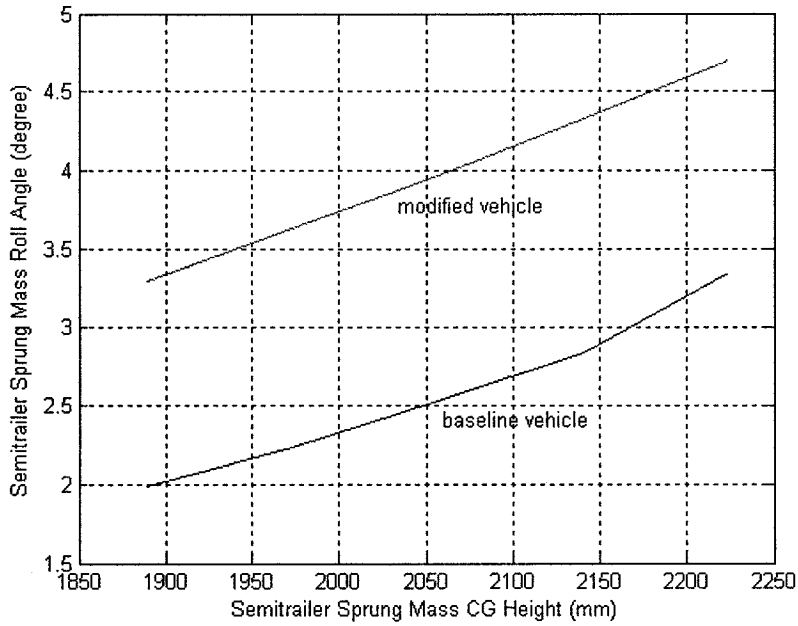

Figure 2.30: Variations in peak semitrailer sprung mass roll angle with c.g. height of the baseline and modified vehicle configurations.

2.7.5 Influence of tires

The directional response behavior of the vehicle may also be influenced by variations in the vertical stiffness and cornering properties of the tires. Heavy vehicle tires use inflation pressures ranging from 100 psi to 120 psi. A higher inflation pressure yields better fuel economy but higher vertical stiffness. Furthermore, the tire tread wear would also yield variations in the vertical stiffness. In this study, the variations in the roll angle response are investigated for different tire treads, including 1/2 and 1/3 tire tread. Figure 2.31 presents the variations in the peak roll angle of the semitrailer sprung mass with variations in the c.g. height for the baseline, 1/2 tread and 1/3 tread tires.

The results show that the change in tire vertical stiffness does not alter the trend in the peak roll angle response, and thus the relationship between the roll

angle and the c.g. height of semitrailer sprung mass. Higher tire vertical stiffness reduces the absolute value of the semitrailer sprung mass roll angle, but the rate of change of the roll angle with respect to the c.g. height does not vary. As the inflation pressure and wearing of tire are unknown factors when the vehicle is in operation, it is important to calibrate the c.g. height online measurement system using the unladen vehicle for getting an accurate estimation of its c.g, height.

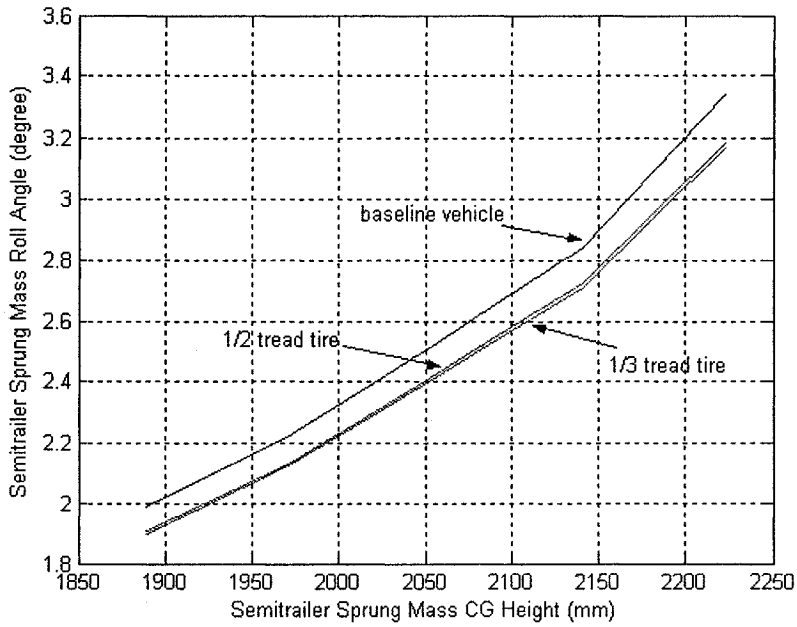

Tread wearing	1/3 tread	1/2 tread
Vertical stiffness	8744.083 N/cm	8642.509 N/cm

Figure 2.31: Semitrailer sprung mass roll angle vs. c.g. height.

2.8 Summary

A five-axle tractor-semitrailer vehicle configuration is selected for the study of c.g. height online measurement as it accounts for the mayor population of commercial vehicles in Canada. The baseline vehicle parameters are identified from the reported data on the basis of weights and dimensions regulations in

Canada. The vehicle model is formulated in the TruckSim environment and the simulations are performed under different maneuvers and parameters. The simulation results show that the semitrailer sprung mass roll angle is most sensitive to the deviations in the payload c.g. height, and therefore may serve as the candidate of indicator for the c.g. height estimation. The simulation results also show that the steady-state turning maneuver can generate sufficiently large roll angle and the target acceleration of 0.2g at a relatively lower speed, and the shape of payload has little influence on the semitrailer sprung mass roll angle under a steady-state turning maneuver. The results obtained for variations in payload, longitudinal and lateral coordinates of the c.g., and tire and suspension properties, show that the semitrailer sprung mass roll angle is quite sensitive to the lateral shift of payload c.g., but not sensitive to its longitudinal shift. The changes in the payload, suspension stiffness and tire vertical stiffness cause a vertical shift of the curve representing the relationship between roll angle and c.g. height of semitrailer sprung mass, while its slope does not change much.

CHAPTER 3 DEVELOPMENT OF SIMPLIFIED ARTICULATED VEHICLE MODEL

3.1 Introduction

Heavy vehicle models vary greatly in capability, in complexity, in the number of degrees of freedom considered, and in the amount of input data required. The choice of vehicle model relies very much on the analysis objectives. The preliminary results attained from the comprehensive TruckSim model suggest that the sprung mass roll angle response under a steady-state turning maneuver could serve as an effective measure for estimating the c.g. height. A simplified vehicle model relating the steering input to the semitrailer sprung mass roll angle may thus be developed for the purpose of estimating the c.g. height. Owing to the dependence of the roll angle response on the lateral c.g. coordinate, payload, c.g. height, and suspension and tire properties, it is essential that the simplified model should incorporate the effect of these parameters. A three-dimensional, 10-D.O.F. vehicle model is thus developed for the candidate vehicle considered to derive an analytical transfer function relating the steering angle to semitrailer sprung mass roll angle. The transfer function may then be applied to the measured roll angle response to identify the c.g. height. This vehicle model is validated against the well known Yaw/Roll model [8] after linearization in the next chapter.

3.2 Model Configuration and Axis Systems

The proposed analytical model of five-axle tractor semitrailer is a simplified

constant speed Yaw/Roll model. The tractor sprung mass is modeled to possess 3-D.O.F.: lateral, yaw and roll, while the semitrailer sprung mass has 2-D.O.F.: yaw and roll, and its forward and lateral speeds are derived from the constraint imposed by the fifth wheel articulation. The axles are permitted to roll with respect to the sprung masses to which they are attached. A 10-D.O.F. model of the articulated vehicle is thus realized, using three different axis systems, illustrated in Figure 3.1. These include: (i) an inertial axis system fixed in space ($\vec{i}_n, \vec{j}_n, \vec{k}_n$); (ii) an axis system fixed to each of the sprung masses ($\vec{i}_s, \vec{j}_s, \vec{k}_s$); (iii) and axis system fixed to each of the unsprung masses ($\vec{i}_u, \vec{j}_u, \vec{k}_u$).

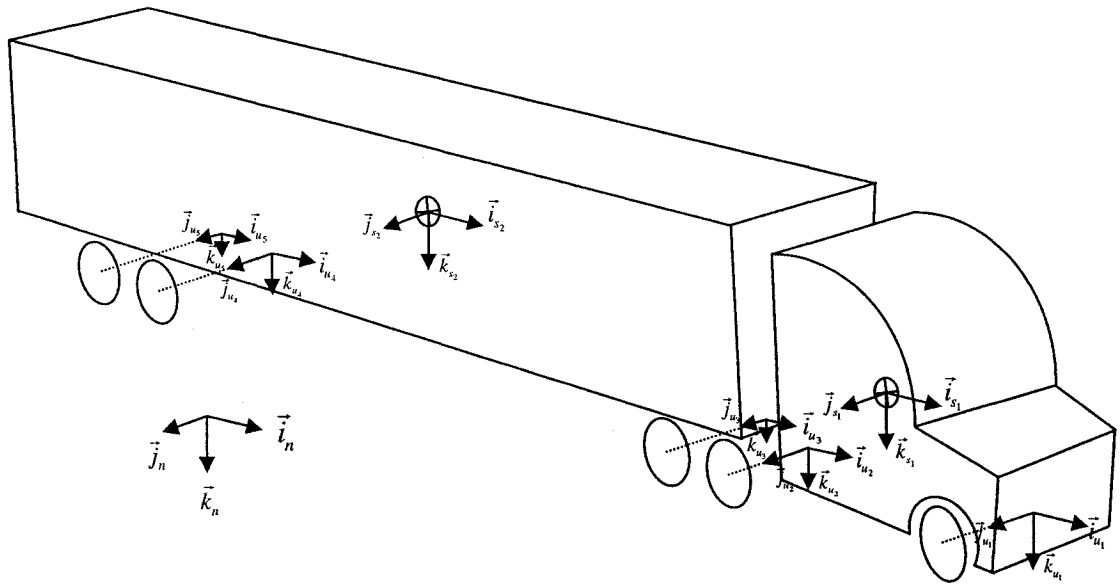

Figure 3.1: Tractor-semitrailer axis systems.

The transformation equation between the inertial and sprung mass axis systems can be derived using two sequential steps of yaw and roll motions, while neglected the pitch motions, such that:

$$\begin{Bmatrix} \vec{i}_n \\ \vec{j}_n \\ \vec{k}_n \end{Bmatrix} == \begin{bmatrix} \cos\psi_s & -\sin\psi_s\cos\phi_s & \sin\psi_s\sin\phi_s \\ \sin\psi_s & \cos\psi_s\cos\phi_s & -\cos\psi_s\sin\phi_s \\ 0 & \sin\phi_s & \cos\phi_s \end{bmatrix} \begin{Bmatrix} \vec{i}_s \\ \vec{j}_s \\ \vec{k}_s \end{Bmatrix} \tag{3.1}$$

where ψ_s and ϕ_s are the yaw and roll rotations of the sprung masses.

Similarly the transformation matrix relating the two body fixed axis systems attached to the unsprung mass and its sprung mass can be obtained as:

$$\begin{Bmatrix} \vec{i}_u \\ \vec{j}_u \\ \vec{k}_u \end{Bmatrix} = \begin{bmatrix} 1 & 0 & 0 \\ 0 & \cos(\phi_s - \phi_u) & -\sin(\phi_s - \phi_u) \\ 0 & \sin(\phi_s - \phi_u) & \cos(\phi_s - \phi_u) \end{bmatrix} \begin{Bmatrix} \vec{i}_s \\ \vec{j}_s \\ \vec{k}_s \end{Bmatrix} \tag{3.2}$$

where ϕ_u is the roll rotation of the unsprung mass.

The tractor sprung mass body fixed axis system can be transformed to the semitrailer sprung mass body fixed axis system using Equation (3.1), such that:

$$\begin{Bmatrix} \vec{i}_n \\ \vec{j}_n \\ \vec{k}_n \end{Bmatrix} = \begin{bmatrix} \cos\psi_{s_1} & -\sin\psi_{s_1}\cos\phi_{s_1} & \sin\psi_{s_1}\sin\phi_{s_1} \\ \sin\psi_{s_1} & \cos\psi_{s_1}\cos\phi_{s_1} & -\cos\psi_{s_1}\sin\phi_{s_1} \\ 0 & \sin\phi_{s_1} & \cos\phi_{s_1} \end{bmatrix} \begin{Bmatrix} \vec{i}_{s_1} \\ \vec{j}_{s_1} \\ \vec{k}_{s_1} \end{Bmatrix} \tag{3.3}$$

$$\begin{Bmatrix} \vec{i}_{s_2} \\ \vec{j}_{s_2} \\ \vec{k}_{s_2} \end{Bmatrix} = \begin{bmatrix} \cos\psi_{s_2} & \sin\psi_{s_2} & 0 \\ -\sin\psi_{s_2}\cos\phi_{s_2} & \cos\psi_{s_2}\cos\phi_{s_2} & \sin\phi_{s_2} \\ \sin\psi_{s_2}\sin\phi_{s_2} & -\cos\psi_{s_2}\sin\phi_{s_2} & \cos\phi_{s_2} \end{bmatrix} \begin{Bmatrix} \vec{i}_n \\ \vec{j}_n \\ \vec{k}_n \end{Bmatrix} \tag{3.4}$$

where ψ_{s_1} and ψ_{s_2} are the yaw rotations of the tractor and semitrailer sprung masses respectively, and ϕ_{s_1} and ϕ_{s_2} are the corresponding roll rotations. Equation (3.3) and Equation (3.4) yield the transformation of the axis systems attached to the two sprung masses:

$$\begin{Bmatrix} \vec{i}_{s_2} \\ \vec{j}_{s_2} \\ \vec{k}_{s_2} \end{Bmatrix} = \begin{bmatrix} T_{11} & T_{12} & T_{13} \\ T_{21} & T_{22} & T_{23} \\ T_{31} & T_{32} & T_{33} \end{bmatrix} \begin{Bmatrix} \vec{i}_{s_1} \\ \vec{j}_{s_1} \\ \vec{k}_{s_1} \end{Bmatrix}, \quad \begin{Bmatrix} \vec{i}_{s_1} \\ \vec{j}_{s_1} \\ \vec{k}_{s_1} \end{Bmatrix} = \begin{bmatrix} T_{11} & T_{12} & T_{13} \\ T_{21} & T_{22} & T_{23} \\ T_{31} & T_{32} & T_{33} \end{bmatrix}^T \begin{Bmatrix} \vec{i}_{s_2} \\ \vec{j}_{s_2} \\ \vec{k}_{s_2} \end{Bmatrix} \tag{3.5}$$

where

$$T_{11} = \cos(\psi_{s_2} - \psi_{s_1})$$

$$T_{12} = \cos\phi_{s_1} \sin(\psi_{s_2} - \psi_{s_1})$$

$$T_{13} = -\sin\phi_{s_1} \sin(\psi_{s_2} - \psi_{s_1})$$

$$T_{21} = -\cos\phi_{s_2} \sin(\psi_{s_2} - \psi_{s_1})$$

$$T_{22} = \cos\phi_{s_1} \cos\phi_{s_2} \cos(\psi_{s_2} - \psi_{s_1}) + \sin\phi_{s_1} \sin\phi_{s_2}$$

$$T_{23} = -\sin\phi_{s_1} \cos\phi_{s_2} \cos(\psi_{s_2} - \psi_{s_1}) + \cos\phi_{s_1} \sin\phi_{s_2}$$

$$T_{31} = \sin\phi_{s_2} \sin(\psi_{s_2} - \psi_{s_1})$$

$$T_{32} = -\cos\phi_{s_1} \sin\phi_{s_2} \cos(\psi_{s_2} - \psi_{s_1}) + \sin\phi_{s_1} \cos\phi_{s_2}$$

$$T_{33} = \sin\phi_{s_1} \sin\phi_{s_2} \cos(\psi_{s_2} - \psi_{s_1}) + \cos\phi_{s_1} \cos\phi_{s_2}$$

3.3 Suspension Forces

Each suspension is modeled as a pair of linear springs and linkages which establish a roll center R_i. Figure 3.2 illustrates the roll plane model of the vehicle. The suspension springs are assumed to remain perpendicular to the axle, and are capable of transmitting either compressive or tensile forces only. All roll plane forces, which are parallel to the axle, are assumed to act through the roll center. The roll center is located at a fixed distance beneath the sprung mass, and is permitted to slide vertically with respect to the axle. The suspension forces are computed from instantaneous spring deflections, however, the static spring deflections are initially evaluated, such that:

$$\Delta_{s0_{i1}} = \Delta_{s0_{i2}} = \left(F_i - W_{u_i}\right)/2KS_i \tag{3.6}$$

where $\Delta_{s0_{i1}}$ and $\Delta_{s0_{i2}}$ are the static deflections of the left and right suspension springs, respectively, of axle i; F_i is the static load of axle i; W_{u_i} is the weight of axle i; and KS_i is the equivalent vertical stiffness of the suspension spring of axle i.

The vehicle is assumed to operate on a highly smooth and flat road surface. The vertical and roll movements of the vehicle due to tires interacting with the road roughness are thus considered to be negligible. The forces due to suspension springs are thus evaluated from:

$$F_{i1} = KS_i\left[\Delta_{s0_{i1}} - S_i \sin\left(\phi_{s_j} - \phi_{u_i}\right)\right] \tag{3.7}$$

$$F_{i2} = KS_i\left[\Delta_{s0_{i2}} + S_i \sin\left(\phi_{s_j} - \phi_{u_i}\right)\right] \tag{3.8}$$

where ϕ_{u_i} is the roll angle of axle i and ϕ_{s_j} the roll angle of sprung mass j to which axle is attached. For $j = 1$ (tractor) $i = 1, 2, 3$; and $j = 2$ (semitrailer), $i = 4, 5$. S_i is the half of the suspension lateral spread (Figure 3.2).

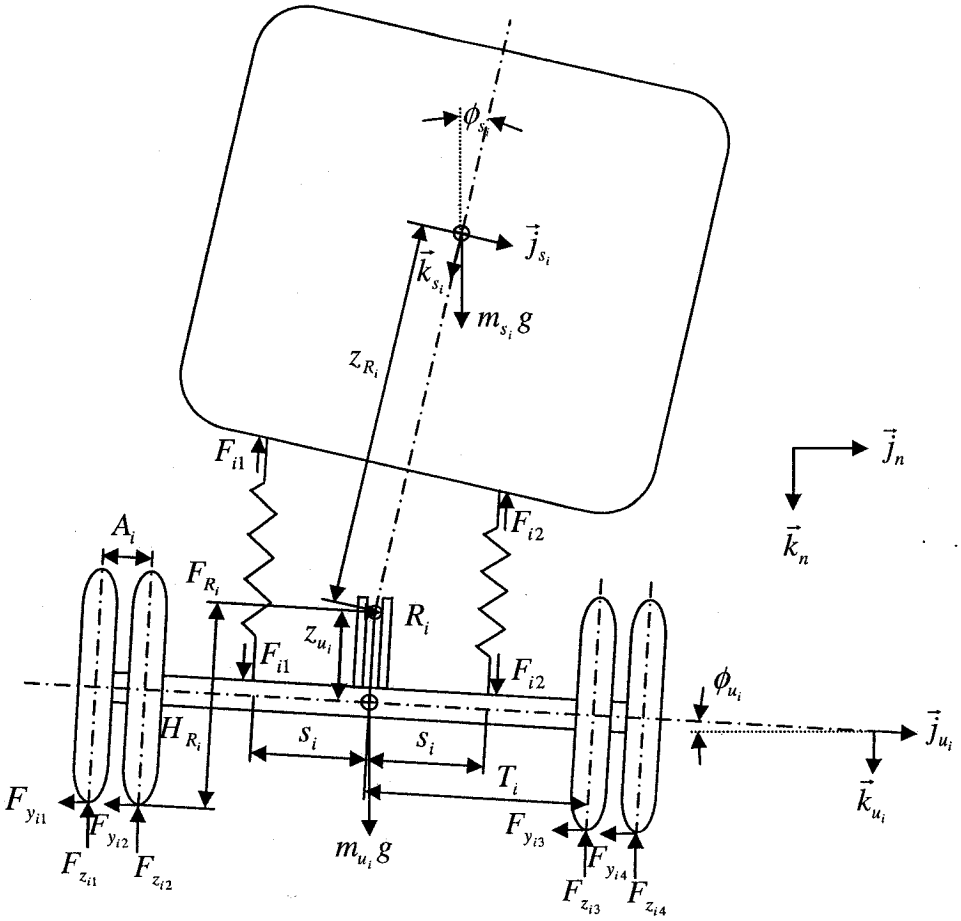

Figure 3.2: Roll plane representation of the vehicle model incorporating suspension and tire force at each axle.

3.4 Forces and Moments at the Tire-Road Interface

The simulation results attained from TruckSim model revealed tire slip angles less than 3 degrees under the selected maneuvers. The tires are known to exhibit linear cornering characteristics under such small side-slip angles. A linear tire model is thus used to compute the cornering and aligning moments developed at the tire-road interface. The tire sideslip angle is derived from the lateral and longitudinal velocities of the tire, as shown in Figure 3.3.

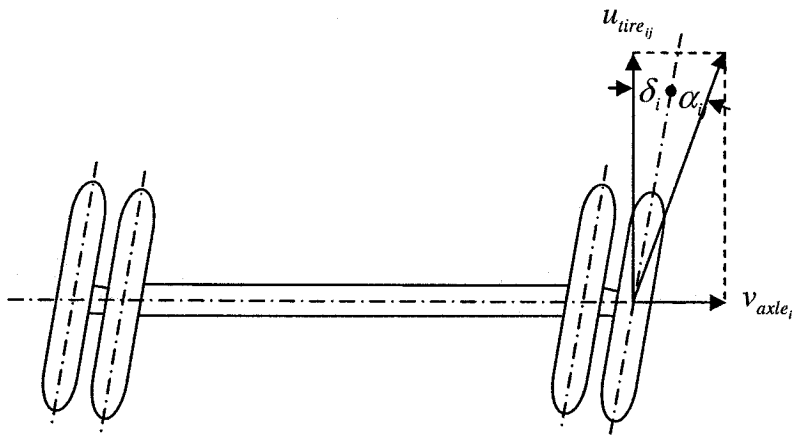

Figure 3.3: Tire sideslip angle.

The tire sideslip angle is thus expressed as:

$$\alpha_{ij} = \tan^{-1}\left(v_{axle_i} / u_{tire_{ij}}\right) - \delta_i$$
$$for\ i = 1\ \ j = 1, 2\ and\ i = 2,3,4,5\ \ j = 1,2,3,4 \tag{3.9}$$

where δ_i represents the steer angle made by the wheel plane with respect to the longitudinal axis of the sprung mass coordinate system, α_{ij} is the tire side slip angle, $u_{tire_{ij}}$ is the tire forward velocity and v_{axle_i} is the axle lateral velocity given by:

$$v_{axle_1} = \left(v_{s_1} - Z_{R_1} p_{s_1}\right)\cos\phi_{s_1} + X_1 r_{s_1}\cos\phi_{s_1} - p_{u_1} H_{R_1}\cos\phi_{u_1}$$
$$v_{axle_i} = \left(v_{s_j} - Z_{R_i} p_{s_j}\right)\cos\phi_{s_j} - X_i r_{s_j}\cos\phi_{s_j} - p_{u_i} H_{R_i}\cos\phi_{u_i}, \quad i = 2,3,4,5 \tag{3.10}$$

where X_i is the axle longitudinal distance with respect to the c.g. of the sprung mass it is attached to (Figure 3.5). p_{s_j} and r_{s_j} describe the sprung mass roll and yaw rates, and p_{u_i} is the axle roll rate. H_{R_1} and Z_{R_i} define the axle roll center height and the distance between the roll center and the sprung mass c.g. (Figure 3.2). The longitudinal speeds of tires can be related to the forward speeds

of sprung masses. For tires in axle 2-5 we have:

$$\begin{aligned} u_{tire_{i1}} &= u_{s_j} + (T_i + A_i) r_{s_j} \\ u_{tire_{i2}} &= u_{s_j} + T_i r_{s_j} \\ u_{tire_{i3}} &= u_{s_j} - T_i r_{s_j} \\ u_{tire_{i4}} &= u_{s_j} - (T_i + A_i) r \end{aligned} \tag{3.11}$$

where T_i is the half tire track, A_i is the dual tire spacing, $j = 1$ when $i = 2, 3$ and $j = 2$ when $i = 4, 5$.

For the single tire steering axle, the forward velocities of tires are given by:

$$\begin{aligned} u_{tire_{11}} &= u_{s_1} + T_1 r_{s_1} \\ u_{tire_{12}} &= u_{s_1} - T_1 r_{s_1} \end{aligned} \tag{3.12}$$

The lateral force developed by a tire is expressed as a linear function of the side-slip angle as:

$$F_{y_{ij}} = KT_{y_{ij}} \alpha_{ij} \tag{3.13}$$

where $KT_{y_{ij}}$ is the cornering stiffness of tire j in axle i, which is a constant value estimated based on the static load on the tire.

The tire vertical force is derived from the tire deflection, $\Delta_{t_{ij}}$, such that:

$$F_{z_{ij}} = KT_{z_{ij}} \Delta_{t_{ij}} \tag{3.14}$$

where $F_{z_{ij}}$ is the vertical force due to tire j on axle i and $KT_{z_{ij}}$ is its constant vertical stiffness. The tire deflections are evaluated from the static deflections and roll deflections of the unsprung masses as:

$$\begin{aligned}
\Delta_{t_{i1}} &= \Delta_{t0_{i1}} - (T_i + A_i)\sin\phi_{u_i} \\
\Delta_{t_{i2}} &= \Delta_{t0_{i2}} - T_i \sin\phi_{u_i} \\
\Delta_{t_{i3}} &= \Delta_{t0_{i3}} + T_i \sin\phi_{u_i} \\
\Delta_{t_{i4}} &= \Delta_{t0_{i4}} + (T_i + A_i)\sin\phi_{u_i}
\end{aligned} \tag{3.15}$$

The tire deflections for the steering axle are obtained as:

$$\begin{aligned}
\Delta_{t_{11}} &= \Delta_{t0_{11}} - T_1 \sin\phi_{u_1} \\
\Delta_{t_{12}} &= \Delta_{t0_{12}} + T_1 \sin\phi_{u_1}
\end{aligned} \tag{3.16}$$

The static deflection of tire $\Delta_{t0_{ij}}$ used in the above equations is evaluated from the static axle loads, such that:

$$\begin{aligned}
&\Delta_{t0_{11}} = F_1 / 2KT_{z_{11}},\ \Delta_{t0_{12}} = F_1 / 2KT_{z_{12}} \\
&\Delta_{t0_{ij}} = F_i / 4KT_{z_{ij}},\quad i = 2,3,4,5,\quad j = 1,2,3,4
\end{aligned} \tag{3.17}$$

The aligning moment due to tire j on axle i is derived assuming linear properties corresponding to small side-slip angle:

$$M_{ij} = KT_{M_{ij}} \alpha_{ij} \tag{3.18}$$

where M_{ij} is the aligning moment of tire j on axle i and $KT_{M_{ij}}$ is its aligning stiffness.

3.5 Roll Constraint of Conventional Fifth Wheel

It is assumed that the frictional coupling forces that exist along the lateral and vertical directions of the fifth wheel are sufficiently small and thus negligible. The articulation coupling thus posses a constraining roll moment acting on both coupled units. The roll compliances of the tractor and semitrailer structures, and the fifth wheel coupling are lumped to constitute the resultant torsion stiffness K_1,

as illustrated in Figure 3.4. The equivalent torsion stiffness undergoes relative roll rotations of the two sprung masses, which occur about their respective body fixed axes. The axis system $\left(\vec{i}'_{s_1}, \vec{j}'_{s_1}, \vec{k}'_{s_1}\right)$ is fixed to the fifth wheel, which has the same yaw and pitch angles as those of the tractor, but has a different roll angle ϕ'_{s_1}. The roll moment due to the fifth wheel coupling acting on the tractor can thus be expressed as:

$$\vec{M}_1 = M_{x_1}\vec{i}_{s_1}, \quad M_{x_1} = K_1\left(\phi'_{s_1} - \phi_{s_1}\right) \tag{3.19}$$

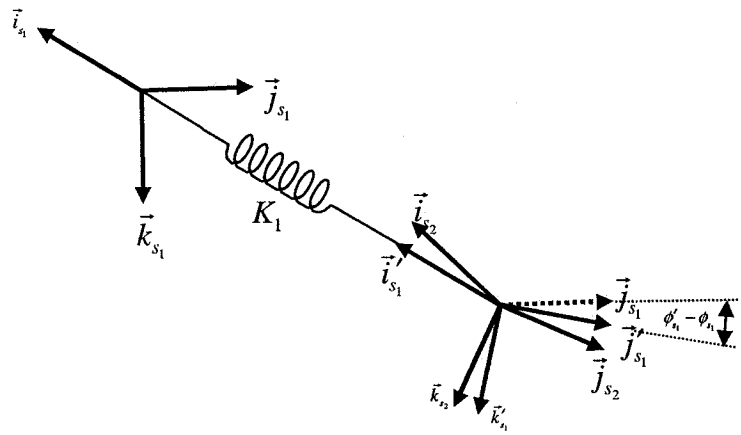

Figure 3.4: Representation of equivalent roll stiffness at the fifth wheel constraint.

Applying transformation matrix Equation (3.1), yields:

$$\vec{j}'_{s_1} = -\sin\psi_{s_1}\cos\phi'_{s_1}\vec{i}_n + \cos\psi_{s_1}\cos\phi'_{s_1}\vec{j}_n + \sin\phi'_{s_1}\vec{k}_n \tag{3.20}$$

$$\vec{k}_{s_2} = \sin\psi_{s_2}\sin\phi_{s_2}\vec{i}_n - \cos\psi_{s_2}\sin\phi_{s_2}\vec{j}_n + \cos\phi_{s_2}\vec{k}_n \tag{3.21}$$

Since $\vec{j}'_{s_1} \bullet \vec{k}_{s_2} = 0$, the above equations yield following expression of ϕ'_{s_1}:

$$\phi'_{s_1} = \tan^{-1}\left[\frac{\sin\phi_{s_2}\cos\left(\psi_{s_2} - \psi_{s_1}\right)}{\cos\phi_{s_2}}\right] \tag{3.22}$$

Equations (3.19) and (3.22) yield following expression for the roll moment imposed on the tractor due to the constraint:

$$M_{x_1} = K_1 \left\{ \tan^{-1} \left[\frac{\sin \phi_{s_2} \cos(\psi_{s_2} - \psi_{s_1})}{\cos \phi_{s_2}} \right] - \phi_{s_1} \right\} \tag{3.23}$$

The constraining moment acting on the semitrailer sprung mass can be derived from:

$$\vec{M}_2 = -M_{x_1} \vec{i}_{s_1} \tag{3.24}$$

where $\vec{M}_2$ is the constraint roll moment acting on the semitrailer sprung mass, expressed as:

$$\vec{M}_2 = M_{x_2} \vec{i}_{s_2} + M_{y_2} \vec{j}_{s_2} + M_{z_2} \vec{k}_{s_2} \tag{3.25}$$

Assuming negligible second order terms and applying the transformation Equation (3.5), yields:

$$M_{x_2} = -M_{x_1} T_{11}, \quad M_{y_2} = -M_{x_1} T_{21}, \quad M_{z_2} = -M_{x_1} T_{31} \tag{3.26}$$

3.6 Equations of Motion

The equations of motion for the simplified vehicle model are developed by applying Newton's second laws of motion, which requires the accelerations of the sprung mass c.g. along the inertial coordinates. For a given sprung mass, the linear and rotational velocities of its c.g. can be expressed as:

$$\vec{V}_s = u_s \vec{i}_s + v_s \vec{j}_s, \quad \vec{\omega}_s = p_s \vec{i}_s + r_s \vec{k}_s \tag{3.27}$$

In the above formulation, the pitch and bounce motions are ignored for the development of this vehicle model. The accelerations of the sprung mass c.g. are

further derived from above, as:

$$\vec{a}_s = \frac{d\vec{V}_s}{dt} = (\dot{u}_s - v_s r_s)\vec{i}_s + (\dot{v}_s + u_s r_s)\vec{j}_s + v_s p_s \vec{k}_s \tag{3.28}$$

For constant forward velocity considered, the accelerations of the tractor and semitrailer sprung masses () are given by:

$$\vec{a}_{s_1} = -v_{s_1} r_{s_1} \vec{i}_{s_1} + (\dot{v}_{s_1} + u_{s_1} r_{s_1})\vec{j}_{s_1} + v_{s_1} p_{s_1} \vec{k}_{s_1} \tag{3.29}$$

$$\vec{a}_{s_2} = (\dot{u}_{s_2} - v_{s_2} r_{s_2})\vec{i}_{s_2} + (\dot{v}_{s_2} + u_{s_2} r_{s_2})\vec{j}_{s_2} + v_{s_2} p_{s_2} \vec{k}_{s_2} \tag{3.30}$$

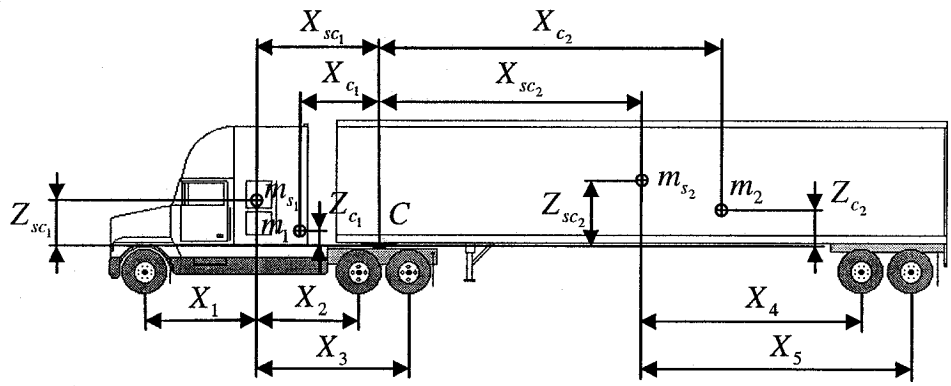

Figure 3.5: Pitch plane representation of the articulated vehicle model.

Figure 3.5 illustrates the pitch plane of the vehicle model, where c.g. of the tractor mass (m_1) is viewed as a point located on its sprung mass. The acceleration of tractor c.g. ($\vec{a}_1$) can be derived from:

$$\begin{aligned}\vec{a}_1 &= \vec{a}_{s_1} + \frac{d}{dt^2}\left[(X_{c_1} - X_{sc_1})\vec{i}_{s_1} + (Z_{sc_1} - Z_{c_1})\vec{k}_{s_1}\right] \\ &= -r_{s_1}\left[v_{s_1} + r_{s_1}(X_{c_1} - X_{sc_1}) - p_{s_1}(Z_{sc_1} - Z_{c_1})\right]\vec{i}_{s_1} + \\ &\quad \left[\dot{v}_{s_1} + u_{s_1} r_{s_1} + \dot{r}_{s_1}(X_{c_1} - X_{sc_1}) - \dot{p}_{s_1}(Z_{sc_1} - Z_{c_1})\right]\vec{j}_{s_1} + \\ &\quad p_{s_1}\left[v_{s_1} + r_{s_1}(X_{c_1} - X_{sc_1}) - p_{s_1}(Z_{sc_1} - Z_{c_1})\right]\vec{k}_{s_1}\end{aligned} \tag{3.31}$$

The acceleration of semitrailer c.g. ($\vec{a}_2$), derived in a similar manner, is

expressed as:

$$\begin{aligned}\vec{a}_2 &= \vec{a}_{s_2} + \frac{d}{dt^2}\left[\left(X_{sc_2} - X_{c_2}\right)\vec{i}_{s_2} + \left(Z_{sc_2} - Z_{c_2}\right)\vec{k}_{s_2}\right] \\ &= \left[\dot{u}_{s_2} - v_{s_2} r_{s_2} - {r_{s_2}}^2\left(X_{sc_2} - X_{c_2}\right) + r_{s_2} p_{s_2}\left(Z_{sc_2} - Z_{c_2}\right)\right]\vec{i}_{s_2} + \\ &\quad \left[\dot{v}_{s_2} + u_{s_2} r_{s_2} + \dot{r}_{s_2}\left(X_{sc_2} - X_{c_2}\right) - \dot{p}_{s_2}\left(Z_{sc_2} - Z_{c_2}\right)\right]\vec{j}_{s_2} + \\ &\quad p_{s_2}\left[v_{s_2} + r_{s_2}\left(X_{sc_2} - X_{c_2}\right) - p_{s_2}\left(Z_{sc_2} - Z_{c_2}\right)\right]\vec{k}_{s_2}\end{aligned} \tag{3.32}$$

The sprung masses due to tractor and semitrailer are constrained through the fifth wheel coupling, which is relatively rigid with respect to translational motions, but relatively compliant with respect to roll rotation. The constraint equations are obtained by equating the velocity and acceleration of point C on the tractor to those of point C on the semitrailer, which yields:

$$\vec{V}_c = \vec{V}_{s_1} + \vec{V}_{c/s_1}, \quad \vec{a}_c = \vec{a}_{s_1} + \vec{a}_{c/s_1} \tag{3.33}$$

where $\vec{V}_c$ and $\vec{a}_c$ are the velocity and acceleration at the coupling of tractor, $\vec{V}_{s_1}$ and $\vec{a}_{s_1}$ are the velocity and acceleration at the tractor sprung mass c.g., as defined in Equations (3.27) and (3.29). $\vec{V}_{c/s_1}$ and $\vec{a}_{c/s_1}$ are the relative velocity and acceleration of point C relative to the tractor sprung mass c.g., which can be derived from the position vector:

$$\vec{r}_{c/s_1} = -X_{sc_1}\vec{i}_{s_1} + Z_{sc_1}\vec{k}_{s_1} \tag{3.34}$$

Time derivations of the position vector yield:

$$\vec{V}_{c/s_1} = \dot{\vec{r}}_{c/s_1} = -X_{sc_1}\dot{\vec{i}}_{s_1} + Z_{sc_1}\dot{\vec{k}}_{s_1} = -\left(X_{sc_1} r_{s_1} + Z_{sc_1} p_{s_1}\right)\vec{j}_{s_1} \tag{3.35}$$

$$\begin{aligned}\vec{a}_{c/s_1} &= \dot{\vec{V}}_{c/s_1} = -\left(X_{sc_1}\dot{r}_{s_1} + Z_{sc_1}\dot{p}_{s_1}\right)\vec{j}_{s_1} - \left(X_{sc_1} r_{s_1} + Z_{sc_1} p_{s_1}\right)\dot{\vec{j}}_{s_1} \\ &= \left(X_{sc_1} r_{s_1} + Z_{sc_1} p_{s_1}\right) r_{s_1}\vec{i}_{s_1} - \left(X_{sc_1}\dot{r}_{s_1} + Z_{sc_1}\dot{p}_{s_1}\right)\vec{j}_{s_1} - \left(X_{sc_1} r_{s_1} + Z_{sc_1} p_{s_1}\right) p_{s_1}\vec{k}_{s_1}\end{aligned} \tag{3.36}$$

Upon substitution Equation (3.33) can thus be exploded as:

$$\vec{V}_c = u_{s_1}\vec{i}_{s_1} - \left(X_{sc_1} r_{s_1} + Z_{sc_1} p_{s_1} - v_{s_1}\right)\vec{j}_{s_1} \tag{3.37}$$

$$\begin{aligned}\vec{a}_c = &\left(X_{sc_1} r_{s_1} + Z_{sc_1} p_{s_1} - v_{s_1}\right) r_{s_1}\vec{i}_{s_1} + \\ &\left(-X_{sc_1}\dot{r}_{s_1} - Z_{sc_1}\dot{p}_{s_1} + \dot{v}_{s_1} + u_{s_1} r_{s_1}\right)\vec{j}_{s_1} + \\ &\left(-X_{sc_1} r_{s_1} - Z_{sc_1} p_{s_1} + v_{s_1}\right) p_{s_1}\vec{k}_{s_1}\end{aligned} \tag{3.38}$$

The velocity and acceleration of point C on the semitrailer are also derived in a similar manner, such that:

$$\vec{V}_c = u_{s_2}\vec{i}_{s_2} + \left(X_{sc_2} r_{s_2} - Z_{sc_2} p_{s_2} + v_{s_2}\right)\vec{j}_{s_2} \tag{3.39}$$

$$\begin{aligned}\vec{a}_c = &\left[\dot{u}_{s_2} - \left(X_{sc_2} r_{s_2} - Z_{sc_2} p_{s_2} + v_{s_2}\right) r_{s_2}\right]\vec{i}_{s_2} + \\ &\left(X_{sc_2}\dot{r}_{s_2} - Z_{sc_2}\dot{p}_{s_2} + \dot{v}_{s_2} + u_{s_2} r_{s_2}\right)\vec{j}_{s_2} + \\ &\left(X_{sc_2} r_{s_2} - Z_{sc_2} p_{s_2} + v_{s_2}\right) p_{s_2}\vec{k}_{s_2}\end{aligned} \tag{3.40}$$

Equation (3.37) can be further expressed in the semitrailer sprung mass body fixed axis system using Equation (3.5):

$$\begin{aligned}\vec{V}_c = &\left\{u_{s_1} T_{11} - \left(X_{sc_1} r_{s_1} + Z_{sc_1} p_{s_1} - v_{s_1}\right) T_{12}\right\}\vec{i}_{s_2} + \\ &\left\{u_{s_1} T_{21} - \left(X_{sc_1} r_{s_1} + Z_{sc_1} p_{s_1} - v_{s_1}\right) T_{22}\right\}\vec{j}_{s_2} + \\ &\left\{u_{s_1} T_{31} - \left(X_{sc_1} r_{s_1} + Z_{sc_1} p_{s_1} - v_{s_1}\right) T_{32}\right\}\vec{k}_{s_2}\end{aligned} \tag{3.41}$$

Relating Equation (3.41) and (3.39) yields the following speed constraint functions:

$$u_{s_2} = u_{s_1} T_{11} - \left(X_{sc_1} r_{s_1} + Z_{sc_1} p_{s_1} - v_{s_1}\right) T_{12} \tag{3.42}$$

$$v_{s_2} = u_{s_1} T_{21} - \left(X_{sc_1} r_{s_1} + Z_{sc_1} p_{s_1} - v_{s_1}\right) T_{22} - X_{sc_2} r_{s_2} + Z_{sc_2} p_{s_2} \tag{3.43}$$

Similarly, Equation (3.38) can be further expressed in the semitrailer sprung mass body fixed axis system, as:

$$\vec{a}_c = \begin{bmatrix} \left(X_{sc_1} r_{s_1} + Z_{sc_1} p_{s_1} - v_{s_1}\right) r_{s_1} T_{11} + \\ \left(-X_{sc_1} \dot{r}_{s_1} - Z_{sc_1} \dot{p}_{s_1} + \dot{v}_{s_1} + u_{s_1} r_{s_1}\right) T_{12} + \\ \left(-X_{sc_1} r_{s_1} - Z_{sc_1} p_{s_1} + v_{s_1}\right) p_{s_1} T_{13} \end{bmatrix} \vec{i}_{s_2} +$$
$$\begin{bmatrix} \left(X_{sc_1} r_{s_1} + Z_{sc_1} p_{s_1} - v_{s_1}\right) r_{s_1} T_{21} + \\ \left(-X_{sc_1} \dot{r}_{s_1} - Z_{sc_1} \dot{p}_{s_1} + \dot{v}_{s_1} + u_{s_1} r_{s_1}\right) T_{22} + \\ \left(-X_{sc_1} r_{s_1} - Z_{sc_1} p_{s_1} + v_{s_1}\right) p_{s_1} T_{23} \end{bmatrix} \vec{j}_{s_2} + \qquad (3.44)$$
$$\begin{bmatrix} \left(X_{sc_1} r_{s_1} + Z_{sc_1} p_{s_1} - v_{s_1}\right) r_{s_1} T_{31} + \\ \left(-X_{sc_1} \dot{r}_{s_1} - Z_{sc_1} \dot{p}_{s_1} + \dot{v}_{s_1} + u_{s_1} r_{s_1}\right) T_{32} + \\ \left(-X_{sc_1} r_{s_1} - Z_{sc_1} p_{s_1} + v_{s_1}\right) p_{s_1} T_{33} \end{bmatrix} \vec{k}_{s_2}$$

The coefficient comparison of Equations (3.44) and (3.40) yields:

$$\dot{u}_{s_2} = \left(X_{sc_2} r_{s_2} - Z_{sc_2} p_{s_2} + v_{s_2}\right) r_{s_2} + \left(X_{sc_1} r_{s_1} + Z_{sc_1} p_{s_1} - v_{s_1}\right) r_{s_1} T_{11} + \left(-X_{sc_1} \dot{r}_{s_1} - Z_{sc_1} \dot{p}_{s_1} + \dot{v}_{s_1} + u_{s_1} r_{s_1}\right) T_{12} + \left(-X_{sc_1} r_{s_1} - Z_{sc_1} p_{s_1} + v_{s_1}\right) p_{s_1} T_{13} \qquad (3.45)$$

$$\dot{v}_{s_2} = -X_{sc_2} \dot{r}_{s_2} + Z_{sc_2} \dot{p}_{s_2} - u_{s_2} r_{s_2} + \left(X_{sc_1} r_{s_1} + Z_{sc_1} p_{s_1} - v_{s_1}\right) r_{s_1} T_{21} + \left(-X_{sc_1} \dot{r}_{s_1} - Z_{sc_1} \dot{p}_{s_1} + \dot{v}_{s_1} + u_{s_1} r_{s_1}\right) T_{22} + \left(-X_{sc_1} r_{s_1} - Z_{sc_1} p_{s_1} + v_{s_1}\right) p_{s_1} T_{23} \qquad (3.46)$$

The unsprung mass acceleration can also be defined with respect to the sprung mass to which it is attached, such that:

$$\vec{a}_{u_i} = \vec{a}_s + \vec{a}_{R_i / m_s} + \vec{a}_{m_{u_i} / R_i} \qquad (3.47)$$

where $\vec{a}_s$ is the acceleration of sprung mass c.g.; $\vec{a}_{R_i / m_s}$ is the relative acceleration of roll center with respect to sprung mass c.g.; $\vec{a}_{m_{u_i} / R_i}$ is the relative acceleration of unsprung mass c.g. with respect to the roll center.

The sprung mass c.g. acceleration in Equation (3.28), can be further expressed in the unsprung mass axis system using Equation (3.2):

$$\vec{a}_s = \left(\dot{u}_s - v_s r_s\right) \vec{i}_{u_i} + \left[\left(\dot{v}_s + u_s r_s\right) \cos\left(\phi_s - \phi_{u_i}\right) - v_s p_s \sin\left(\phi_s - \phi_{u_i}\right)\right] \vec{j}_{u_i} + \left[\left(\dot{v}_s + u_s r_s\right) \sin\left(\phi_s - \phi_{u_i}\right) + v_s p_s \cos\left(\phi_s - \phi_{u_i}\right)\right] \vec{k}_{u_i} \qquad (3.48)$$

$\vec{a}_{R_i/m_s}$ can be derived from the position vector (Figure 3.2 and Figure 3.5):

$$\vec{r}_{R_i/m_s} = X_{R_i}\vec{i}_s + Z_{R_i}\vec{k}_s \tag{3.49}$$

which is pointing from the sprung mass c.g. to the articulation point, and thus:

$$X_{R_1} = X_1,\ X_{R_2} = -X_2,\ X_{R_3} = -X_3,\ X_{R_4} = -X_4,\ X_{R_5} = -X_5$$

Therefore,

$$\vec{v}_{R_i/m_s} = \dot{\vec{r}}_{R_i/m_s} = X_{R_i}\dot{\vec{i}}_s + Z_{R_i}\dot{\vec{k}}_s = \left(X_{R_i}r_s - Z_{R_i}p_s\right)\vec{j}_s \tag{3.50}$$

$$\begin{aligned}\vec{a}_{R_i/m_s} &= \dot{\vec{v}}_{R_i/m_s} = \left(X_{R_i}\dot{r}_s - Z_{R_i}\dot{p}_s\right)\vec{j}_s + \left(X_{R_i}r_s - Z_{R_i}p_s\right)\dot{\vec{j}}_s \\ &= \left(Z_{R_i}p_s r_s - X_{R_i}r_s^{\,2}\right)\vec{i}_s + \left(X_{R_i}\dot{r}_s - Z_{R_i}\dot{p}_s\right)\vec{j}_s + \left(X_{R_i}p_s r_s - Z_{R_i}p_s^{\,2}\right)\vec{k}_s\end{aligned} \tag{3.51}$$

$\vec{a}_{R_i/m_s}$ can be further expressed in the unsprung mass body fixed axis system using Equation (3.2), such that:

$$\begin{aligned}\vec{a}_{R_i/m_s} = &\left(Z_{R_i}p_s r_s - X_{R_i}r_s^{\,2}\right)\vec{i}_{u_i} + \\ &\left[\left(X_{R_i}\dot{r}_s - Z_{R_i}\dot{p}_s\right)\cos\left(\phi_s - \phi_{u_i}\right) - \left(X_{R_i}p_s r_s - Z_{R_i}p_s^{\,2}\right)\sin\left(\phi_s - \phi_{u_i}\right)\right]\vec{j}_{u_i} + \\ &\left[\left(X_{R_i}\dot{r}_s - Z_{R_i}\dot{p}_s\right)\sin\left(\phi_s - \phi_{u_i}\right) + \left(X_{R_i}p_s r_s - Z_{R_i}p_s^{\,2}\right)\cos\left(\phi_s - \phi_{u_i}\right)\right]\vec{k}_{u_i}\end{aligned} \tag{3.52}$$

Simularly $\vec{a}_{m_{u_i}/R_i}$ can be derived from the position vector:

$$\vec{r}_{m_{u_i}/R_i} = Z_{u_i}\vec{k}_{u_i} \tag{3.53}$$

which is pointing from the articulation point to the unsprung mass c.g., and

$$\vec{v}_{m_{u_i}/R_i} = \dot{\vec{r}}_{m_{u_i}/R_i} = Z_{u_i}\dot{\vec{k}}_{u_i} = -Z_{u_i}p_{u_i}\vec{j}_{u_i} \tag{3.54}$$

$$\begin{aligned}\vec{a}_{m_{u_i}/R_i} &= \dot{\vec{v}}_{m_{u_i}/R_i} = -Z_{u_i}\dot{p}_{u_i}\vec{j}_{u_i} - Z_{u_i}p_{u_i}\dot{\vec{j}}_{u_i} \\ &= Z_{u_i}p_{u_i}r_{u_i}\vec{i}_{u_i} - Z_{u_i}\dot{p}_{u_i}\vec{j}_{u_i} - Z_{u_i}p_{u_i}^{\,2}\vec{k}_{u_i}\end{aligned} \tag{3.55}$$

Finally the acceleration of the unsprung mass c.g. can be derived as the sum of Equations (3.48), (3.52) and (3.55):

$$\vec{a}_{u_i} = \left(\dot{u}_s - v_s r_s - X_{R_i} r_s^2 + Z_{R_i} p_s r_s + Z_{u_i} p_{u_i} r_{u_i}\right)\vec{i}_{u_i} + \left[\begin{array}{l}\left(\dot{v}_s + u_s r_s + X_{R_i}\dot{r}_s - Z_{R_i}\dot{p}_s\right)\cos\left(\phi_s - \phi_{u_i}\right) - \\ \left(X_{R_i} p_s r_s - Z_{R_i} p_s^2 + v_s p_s\right)\sin\left(\phi_s - \phi_{u_i}\right) - Z_{u_i}\dot{p}_{u_i}\end{array}\right]\vec{j}_{u_i} + \left[\begin{array}{l}\left(\dot{v}_s + u_s r_s + X_{R_i}\dot{r}_s - Z_{R_i}\dot{p}_s\right)\sin\left(\phi_s - \phi_{u_i}\right) + \\ \left(X_{R_i} p_s \dot{\psi}_s - Z_{R_i} p_s^2 + v_s p_s\right)\cos\left(\phi_s - \phi_{u_i}\right) - Z_{u_i} p_{u_i}^2\end{array}\right]\vec{k}_{u_i} \tag{3.56}$$

where the sprung mass parameters are those of the tractor for $i = 1,2,3$, and those of the semitrailer for $i = 4,5$. Suspension forces transferred to the sprung mass from any given axle i can also be expressed as:

$$F_{susp_i} = -F_{R_i}\vec{j}_{u_i} - \left(F_{i1} + F_{i2}\right)\vec{k}_{u_i} \tag{3.57}$$

where F_{i1} and F_{i2} are given the spring forces defined in Equation (3.7) and (3.8), F_{R_i} is the roll center force applied on axle i as indicated in Figure 3.2, and F_{susp_i} is the suspension force due to axle i suspension.

Equation (3.57) can be further expressed in the sprung mass axis system using Equation (3.2), such that:

$$F_{susp_i} = -\left[F_{R_i}\cos\left(\phi_s - \phi_{u_i}\right) + \left(F_{i1} + F_{i2}\right)\sin\left(\phi_s - \phi_{u_i}\right)\right]\vec{j}_s + \left[F_{R_i}\sin\left(\phi_s - \phi_{u_i}\right) - \left(F_{i1} + F_{i2}\right)\cos\left(\phi_s - \phi_{u_i}\right)\right]\vec{k}_s \tag{3.58}$$

The internal roll center force F_{R_i} can be derived from the dynamic equilibrium of axle i along the $\vec{j}_{u_i}$ direction, such that:

$$m_{u_i}\vec{a}_{u_i} \bullet \vec{j}_{u_i} = F_{R_i} - \sum_{j=1}^{n} F_{y_{ij}}\cos\phi_{u_i} - \sum_{j=1}^{n} F_{z_{ij}}\sin\phi_{u_i} + m_{u_i} g\sin\phi_{u_i} \tag{3.59}$$

where $n = 2$ for $i = 1$ and $n = 4$ for $i = 2,3,4,5$. $F_{y_{ij}}$ and $F_{z_{ij}}$ are lateral and vertical tire forces defined in Equations (3.13) and (3.14) respectively.

The acceleration component of $\vec{a}_{u_i}$ along the $\vec{j}_{u_i}$ direction can be obtained from Equation (3.56). The roll center force F_{R_i} can thus be expressed as:

$$F_{R_i} = m_{u_i}\left[\begin{array}{l}\left(\dot{v}_s + u_s r_s + X_{R_i}\dot{r}_s - Z_{R_i}\dot{p}_s\right)\cos\left(\phi_s - \phi_{u_i}\right) - \\ \left(X_{R_i} p_s r_s - Z_{R_i} {p_s}^2 + v_s p_s\right)\sin\left(\phi_s - \phi_{u_i}\right) - Z_{u_i}\dot{p}_{u_i}\end{array}\right] + \sum_{j=1}^{n} F_{y_{ij}}\cos\phi_{u_i} + \sum_{j=1}^{n} F_{z_{ij}}\sin\phi_{u_i} - m_{u_i} g\sin\phi_{u_i} \tag{3.60}$$

Lateral force equation

The force equilibrium equation for the 5-axle tractor-semitrailer along the lateral direction of tractor is obtained by applying Newton's second law to yield:

$$\vec{F} = \sum_{i=1}^{2} m_i \vec{a}_i \tag{3.61}$$

where $\vec{F}$ is the resultant of external forces. The entire vehicle is considered to consist of two units: tractor and semitrailer, with m_i and $\vec{a}_i$ representing the mass and acceleration of c.g. of unit i.

The resultant external force along the lateral direction of tractor is derived from:

$$F_y = -\sum_{i=1}^{2} F_{y_{1i}} - \sum_{j=2}^{3}\sum_{i=1}^{4} F_{y_{ji}} - \sum_{j=4}^{5}\sum_{i=1}^{4} F_{y_{ji}}\cos\left(\psi_{s_2} - \psi_{s_1}\right) \tag{3.62}$$

where $F_{y_{ji}}$ is the lateral force applied on tire i of axle j.

The inertia force of tractor along the lateral direction is obtained using Equation (3.31),

$$F_{1_y} = -m_1\left(a_{1_y}\cos\phi_{s_1} - a_{1_z}\sin\phi_{s_1}\right) \tag{3.63}$$

where

$$\vec{a}_1 = a_{1_x}\vec{i}_{s_1} + a_{1_y}\vec{j}_{s_1} + a_{1_z}\vec{k}_{s_1} \tag{3.64}$$

$$a_{1_x} = -\dot{\psi}_{s_1}\left[v_{s_1} + r_{s_1}\left(X_{c_1} - X_{sc_1}\right) - p_{s_1}\left(Z_{sc_1} - Z_{c_1}\right)\right] \tag{3.65}$$

$$a_{1_y} = \dot{v}_{s_1} + u_{s_1} r_{s_1} + \dot{r}_{s_1}\left(X_{c_1} - X_{sc_1}\right) - \dot{p}_{s_1}\left(Z_{sc_1} - Z_{c_1}\right) \tag{3.66}$$

$$a_{1_z} = p_{s_1}\left[v_{s_1} + r_{s_1}\left(X_{c_1} - X_{sc_1}\right) - p_{s_1}\left(Z_{sc_1} - Z_{c_1}\right)\right] \tag{3.67}$$

The inertia force of the semitrailer along the lateral direction is obtained in a similar manner using Equation (3.32),

$$F_{2_y} = -m_2\left[\left(a_{2_y}\cos\phi_{s_2} - a_{2_z}\sin\phi_{s_2}\right)\cos\left(\psi_{s_2} - \psi_{s_1}\right) + a_{2_x}\sin\left(\psi_{s_2} - \psi_{s_1}\right)\right] \tag{3.68}$$

where

$$\vec{a}_2 = a_{2_x}\vec{i}_{s_2} + a_{2_y}\vec{j}_{s_2} + a_{2_z}\vec{k}_{s_2} \tag{3.69}$$

$$a_{2_x} = \dot{u}_{s_2} - v_{s_2} r_{s_2} - r_{s_2}^{\ 2}\left(X_{sc_2} - X_{c_2}\right) + r_{s_2} p_{s_2}\left(Z_{sc_2} - Z_{c_2}\right) \tag{3.70}$$

$$a_{2_y} = \dot{v}_{s_2} + u_{s_2} r_{s_2} + \dot{r}_{s_2}\left(X_{sc_2} - X_{c_2}\right) - \dot{p}_{s_2}\left(Z_{sc_2} - Z_{c_2}\right) \tag{3.71}$$

$$a_{2_z} = p_{s_2}\left[v_{s_2} + r_{s_2}\left(X_{sc_2} - X_{c_2}\right) - p_{s_2}\left(Z_{sc_2} - Z_{c_2}\right)\right] \tag{3.72}$$

Thus we have:

$$F_y + F_{1_y} + F_{2_y} = 0 \tag{3.73}$$

Roll moment equations for sprung masses

The roll equilibrium equations for sprung masses are established about the longitudinal axis passing through their respective c.g.. The external moments arised from the suspension forces and constraint moment, defined in Equations (3.23) and (3.57). The roll moment equilibriums for the two sprung masses yield

$$I_{xx_{s_1}}\dot{p}_{s_1} = K_1\left\{\tan^{-1}\left[\frac{\sin\phi_{s_2}\cos(\psi_{s_2}-\psi_{s_1})}{\cos\phi_{s_2}}\right]-\phi_{s_1}\right\}+ \sum_{i=1}^{3}\left\{\begin{matrix}F_{R_i}Z_{R_i}\cos(\phi_{s_1}-\phi_{u_i})+F_{i1}[S_i+Z_{R_i}\sin(\phi_{s_1}-\phi_{u_i})]-\\ F_{i2}[S_i-Z_{R_i}\sin(\phi_{s_1}-\phi_{u_i})]-KR_i(\phi_{s_1}-\phi_{u_i})\end{matrix}\right\} \quad (3.74)$$

$$I_{xx_{s_2}}\dot{p}_{s_2} = -K_1\left\{\tan^{-1}\left[\frac{\sin\phi_{s_2}\cos(\psi_{s_2}-\psi_{s_1})}{\cos\phi_{s_2}}\right]-\phi_{s_1}\right\}\cos(\psi_{s_2}-\psi_{s_1})+ \sum_{i=4}^{5}\left\{\begin{matrix}F_{R_i}Z_{R_i}\cos(\phi_{s_2}-\phi_{u_i})+F_{i1}[S_i+Z_{R_i}\sin(\phi_{s_2}-\phi_{u_i})]-\\ F_{i2}[S_i-Z_{R_i}\sin(\phi_{s_2}-\phi_{u_i})]-KR_i(\phi_{s_2}-\phi_{u_i})\end{matrix}\right\} \quad (3.75)$$

where KR_i is the auxiliary roll stiffness of axle i, and $I_{xx_{s_1}}$ and $I_{xx_{s_2}}$ are the roll mass moment of inertia of the tractor and semitrailer sprung masses.

Roll moment equations for unsprung masses

The roll equilibrium equations for the unsprung masses are established in a similar manner and presented below:

$$I_{xx_{u_1}}\dot{p}_{u_1} = F_{R_1}Z_{u_1}-(F_{11}-F_{12})S_1+(H_{R_1}-Z_{u_1}\cos\phi_{u_1})\sum_{i=1}^{2}F_{y_{1i}}+ \sum_{i=1}^{2}F_{z_{1i}}R_{1i}\sin\phi_{u_1}+(F_{z_{11}}-F_{z_{12}})T_1\cos\phi_{u_1}+KR_1(\phi_{s_1}-\phi_{u_1}) \quad (3.76)$$

$$I_{xx_{u_2}}\dot{p}_{u_2} = F_{R_2}Z_{u_2}-(F_{21}-F_{22})S_2+(H_{R_2}-Z_{u_2}\cos\phi_{u_2})\sum_{i=1}^{4}F_{y_{2i}}+ \sum_{i=1}^{4}F_{z_{2i}}R_{2i}\sin\phi_{u_2}+(F_{z_{21}}-F_{z_{24}})(T_2+A_2)\cos\phi_{u_2}+ (F_{z_{22}}-F_{z_{23}})T_2\cos\phi_{u_2}+KR_2(\phi_{s_1}-\phi_{u_2}) \quad (3.77)$$

$$I_{xx_{u_3}}\dot{p}_{u_3} = F_{R_3}Z_{u_3}-(F_{31}-F_{32})S_3+(H_{R_3}-Z_{u_3}\cos\phi_{u_3})\sum_{i=1}^{4}F_{y_{3i}}+ \sum_{i=1}^{4}F_{z_{3i}}R_{3i}\sin\phi_{u_3}+(F_{z_{31}}-F_{z_{34}})(T_3+A_3)\cos\phi_{u_3}+ (F_{z_{32}}-F_{z_{33}})T_3\cos\phi_{u_3}+KR_3(\phi_{s_1}-\phi_{u_3}) \quad (3.78)$$

$$I_{xx_{u_4}}\dot{p}_{u_4} = F_{R_4}Z_{u_4} - (F_{41} - F_{42})S_4 + (H_{R_4} - Z_{u_4}\cos\phi_{u_4})\sum_{i=1}^{4} F_{y_{4i}} + \sum_{i=1}^{4} F_{z_{4i}} R_{4i}\sin\phi_{u_4} + (F_{z_{41}} - F_{z_{44}})(T_4 + A_4)\cos\phi_{u_4} + (F_{z_{42}} - F_{z_{43}})T_4\cos\phi_{u_4} + KR_4(\phi_{s_2} - \phi_{u_4}) \quad (3.79)$$

$$I_{xx_{u_5}}\dot{p}_{u_5} = F_{R_5}Z_{u_5} - (F_{51} - F_{52})S_5 + (H_{R_5} - Z_{u_5}\cos\phi_{u_5})\sum_{i=1}^{4} F_{y_{5i}} + \sum_{i=1}^{4} F_{z_{5i}} R_{5i}\sin\phi_{u_5} + (F_{z_{51}} - F_{z_{54}})(T_5 + A_5)\cos\phi_{u_5} + (F_{z_{52}} - F_{z_{53}})T_5\cos\phi_{u_5} + KR_5(\phi_{s_2} - \phi_{u_5}) \quad (3.80)$$

where R_{ji} is the radius of tire i of axle j, $I_{xx_{u_i}}$ is the roll mass moment of inertia of the unsprung mass j.

Yaw moment equations

The yaw equilibrium equations are defined for the two units, that is tractor and semitrailer, including their respective unsprung masses. The equations of yaw motion are established around an axis passing through the articulation point, such that:

$$X_{c_1}m_1(a_{1_y}\cos\phi_{s_1} - a_{1_z}\sin\phi_{s_1}) + I_{z_1}\dot{r}_{s_1} = -(X_1 + X_{sc_1})\sum_{i=1}^{2} F_{y_{1i}} + \sum_{i=1}^{2} M_{1i} - (X_{sc_1} - X_2)\sum_{i=1}^{4} F_{y_{2i}} + \sum_{i=1}^{4} M_{2i} + (X_3 - X_{sc_1})\sum_{i=1}^{4} F_{y_{3i}} + \sum_{i=1}^{4} M_{3i} \quad (3.81)$$

$$-X_{c_2}m_2(a_{2_y}\cos\phi_{s_2} - a_{2_z}\sin\phi_{s_2}) + I_{z_2}\dot{r}_{s_2} = \sum_{j=4}^{5}\left[(X_{sc_2} + X_j)\sum_{i=1}^{4} F_{y_{ji}} + \sum_{i=1}^{4} M_{ji}\right] \quad (3.82)$$

where I_{z_1} and I_{z_2} are the yaw mass moment inertia of the tractor and

semitrailer respectively about the articulation point.

3.7 Summary

Since the roll angle response of the semitrailer sprung mass appears to be a reasonable good indicator of its c.g. height, a simplified three dimension vehicle model is derived to establish the relationship between the steering angle in the yaw plane and the roll angle in the roll plane. The model considers the linear lateral dynamics of the vehicle with roll D.O.F. of the sprung and unsprung masses. The entire vehicle is viewed as one unit for building the equation of lateral motion, while the yaw dynamics the tractor and semitrailer are modeled as two separated rigid bodies yawing around the articulation point with respect to each other. The roll motion is most concerned and therefore modeled in more details. Each sprung mass and unsprung mass is treated independently to study its roll response. The simplified model is further linearized in the following chapter and validated against the widely used Yaw/Roll model. The validated model is then applied to build transfer function relating the steering angle to the semitrailer sprung mass roll angle.

CHAPTER 4 ANALYTICAL TRANSFER FUNCTION DEVELOPMENT AND MODEL VALIDATION

4.1 Introduction

The vehicle model developed in the previous chapter can be solved to derive the directional responses in terms of lateral velocities and accelerations, yaw and roll angles in response to a defined steer angle input. Owing to its simplicity, the model can be reduced to derive a transfer function relating the seimitrailer sprung mass roll angle to the steer angle. This dissertation intends to estimate c.g. height by comparing the coefficients of two different transfer functions derived from the model and the measured data. The analytical transfer function comprises coefficients that are functions of the unknown c.g. height, while the measured data may be treated to derive a true function using system identification techniques. Both of these two transfer functions supposedly describe the same relationship between the steering angle and the semitrailer sprung mass roll angle. The c.g. height may thus be estimated through comparisons and analyses of the analytical transfer function coefficients. The formulation of the analytical transfer function for the vehicle model, however, necessitates linear or linearized equations of motion. In this chapter the proposed vehicle model is linearized and transformed to the Laplace domain to derive the analytical transfer functions. The linearized vehicle model is validated against the widely used Yaw/Roll model through comparison of the simulation results.

4.2 Model Linearization

The equations of motion for the simplified 10-D.O.F. yaw/roll model are linearized, subject to the following assumptions:

- The roll rotations of the sprung and unsprung masses are assumed to be small, such that, $\cos\varphi \approx 1$ and $\sin\varphi \approx \varphi$.
- The yaw rotations of the vehicle units are assumed to be small.
- The second order terms involving products of the displacement responses are considered to be negligible.
- All the vehicle tires have the same radius.
- All the vehicle tires on a single axle possess the same vertical stiffness.
- All the vehicle tires on a single axle possess the same cornering stiffness.
- All the vehicle tires on a single axle possess the same aligning stiffness.
- The dual tires, on the tractor drive and semitrailer axles, possess the same tire space.

Suspension forces

The application of small angles assumption to Equations (3.6), (3.7) and (3.8) yields following expressions for the suspension forces along the k_{u_i} direction:

$$\begin{aligned} F_{i1} &= \left(F_i - W_{u_i}\right)/2 - KS_i\left(\phi_{s_j} - \phi_{u_i}\right)S_i \\ F_{i2} &= \left(F_i - W_{u_i}\right)/2 + KS_i\left(\phi_{s_j} - \phi_{u_i}\right)S_i \end{aligned} \tag{4.1}$$

where $i = 1, 2, 3$ for the tractor ($j = 1$), and $i = 4, 5$ for the semitrailer ($j = 2$).

Lateral forces at the tire-road interface

The lateral velocities of the axles, defined in Equation (3.10), can be simplified in a similar manner to yield:

$$\begin{aligned} v_{axle_1} &= v_{s_1} - Z_{R_1}\dot{\phi}_{s_1} + X_1\dot{\psi}_{s_1} - \dot{\phi}_{u_1}H_{R_1} \\ v_{axle_i} &= v_{s_j} - Z_{R_i}\dot{\phi}_{s_j} - X_i\dot{\psi}_{s_j} - \dot{\phi}_{u_i}H_{R_i} \quad (i = 2, 3, 4, 5) \end{aligned} \tag{4.2}$$

The small angle ssumption yields the following expressions for the forward and lateral velocities of the semitrailer sprung mass, defined in Equation (3.42) and (3.43),

$$\begin{aligned} u_{s_2} &= u_{s_1} \\ v_{s_2} &= u_{s_1}\left(\psi_{s_1} - \psi_{s_2}\right) - \left(X_{sc_1}\dot{\psi}_{s_1} + Z_{sc_1}\dot{\phi}_{s_1} - v_{s_1}\right) - X_{sc_2}\dot{\psi}_{s_2} + Z_{sc_2}\dot{\phi}_{s_2} \end{aligned} \tag{4.3}$$

The cornering forces developed by the tires, described in Equation (3.13), can also be simplified to yield:

$$\begin{aligned} F_{y_{i1}} &= KT_{y_1}\left(\frac{v_{axle_1}}{u_{s_1} + T_1\dot{\psi}_{s_1}} - \delta_1\right) \\ F_{y_{i2}} &= KT_{y_1}\left(\frac{v_{axle_1}}{u_{s_1} - T_1\dot{\psi}_{s_1}} - \delta_1\right) \\ F_{y_{i1}} &= \frac{KT_{y_i}v_{axle_i}}{u_{s_1} + (T_i + A)\dot{\psi}_{s_j}} \\ F_{y_{i2}} &= \frac{KT_{y_i}v_{axle_i}}{u_{s_1} + T_i\dot{\psi}_{s_j}} \\ F_{y_{i3}} &= \frac{KT_{y_i}v_{axle_i}}{u_{s_1} - T_i\dot{\psi}_{s_j}} \\ F_{y_{i4}} &= \frac{KT_{y_i}v_{axle_i}}{u_{s_1} - (T_i + A)\dot{\psi}_{s_j}} \end{aligned} \tag{4.4}$$

Vertical forces at the tire-road interface

Substituting Equations (3.15) to (3.17) into Equation (3.14) yields following

expressions for the vertical tire forces:

$$
\begin{aligned}
F_{z_{11}} &= F_1/2 - KT_{z_1}T_1\phi_{u_1} \\
F_{z_{12}} &= F_1/2 + KT_{z_1}T_1\phi_{u_1} \\
F_{z_{i1}} &= F_i/4 - KT_{z_i}(T_i + A)\phi_{u_i} \\
F_{z_{i2}} &= F_i/4 - KT_{z_i}T_i\phi_{u_i} \\
F_{z_{i3}} &= F_i/4 + KT_{z_i}T_i\phi_{u_i} \\
F_{z_{i4}} &= F_i/4 + KT_{z_i}(T_i + A)\phi_{u_i}
\end{aligned}
\tag{4.5}
$$

where $i = 2,3,4,5$.

Aligning moments at the tire-road interface

Similar to the cornering forces, the aligning moments due to tires, described in Equation (3.18), can be represented as:

$$
\begin{aligned}
M_{11} &= KT_{M_1}\left(\frac{v_{axle_1}}{u_{s_1} + T_1\dot{\psi}_{s_1}} - \delta_1\right) \\
M_{12} &= KT_{M_1}\left(\frac{v_{axle_1}}{u_{s_1} - T_1\dot{\psi}_{s_1}} - \delta_1\right) \\
M_{i1} &= \frac{KT_{M_i}v_{axle_i}}{u_{s_1} + (T_i + A)\dot{\psi}_{s_j}} \\
M_{i2} &= \frac{KT_{M_i}v_{axle_i}}{u_{s_1} + T_i\dot{\psi}_{s_j}} \\
M_{i3} &= \frac{KT_{M_i}v_{axle_i}}{u_{s_1} - T_i\dot{\psi}_{s_j}} \\
M_{i4} &= \frac{KT_{M_i}v_{axle_i}}{u_{s_1} - (T_i + A)\dot{\psi}_{s_j}}
\end{aligned}
\tag{4.6}
$$

where $i = 1, 2, 3$ for the tractor ($j = 1$), and $i = 4, 5$ for the semitrailer ($j = 2$).

Roll center forces

The roll center forces formulated in Equation (3.60) are also simplified upon consideration of the stated assumption, and summarized below:

$$
\begin{aligned}
F_{R_1} &= m_{u_1}\left(\dot{v}_{s_1} + u_{s_1}\dot{\psi}_{s_1} + X_1\ddot{\psi}_{s_1} - Z_{R_1}\ddot{\phi}_{s_1} - Z_{u_1}\ddot{\phi}_{u_1}\right) + \sum_{j=1}^{2} F_{y_{1j}} + F_1\phi_{u_1} - m_{u_1} g\phi_{u_1} \\
F_{R_2} &= m_{u_2}\left(\dot{v}_{s_1} + u_{s_1}\dot{\psi}_{s_1} - X_2\ddot{\psi}_{s_1} - Z_{R_2}\ddot{\phi}_{s_1} - Z_{u_2}\ddot{\phi}_{u_2}\right) + \sum_{j=1}^{4} F_{y_{2j}} + F_2\phi_{u_2} - m_{u_2} g\phi_{u_2} \\
F_{R_3} &= m_{u_3}\left(\dot{v}_{s_1} + u_{s_1}\dot{\psi}_{s_1} - X_3\ddot{\psi}_{s_1} - Z_{R_3}\ddot{\phi}_{s_1} - Z_{u_3}\ddot{\phi}_{u_3}\right) + \sum_{j=1}^{4} F_{y_{3j}} + F_3\phi_{u_3} - m_{u_3} g\phi_{u_3} \\
F_{R_4} &= m_{u_4}\left(\dot{v}_{s_2} + u_{s_1}\dot{\psi}_{s_2} - X_4\ddot{\psi}_{s_2} - Z_{R_4}\ddot{\phi}_{s_2} - Z_{u_4}\ddot{\phi}_{u_4}\right) + \sum_{j=1}^{4} F_{y_{4j}} + F_4\phi_{u_4} - m_{u_4} g\phi_{u_4} \\
F_{R_5} &= m_{u_5}\left(\dot{v}_{s_2} + u_{s_1}\dot{\psi}_{s_2} - X_5\ddot{\psi}_{s_2} - Z_{R_5}\ddot{\phi}_{s_2} - Z_{u_5}\ddot{\phi}_{u_5}\right) + \sum_{j=1}^{4} F_{y_{5j}} + F_5\phi_{u_5} - m_{u_5} g\phi_{u_5}
\end{aligned}
\tag{4.7}
$$

Upon substituting for cornering forces from Equation (4.4), and neglecting the product terms, yield:

$$
\begin{aligned}
F_{R_1} &= m_{u_1}\left(\dot{v}_{s_1} + u_{s_1}\dot{\psi}_{s_1} + X_1\ddot{\psi}_{s_1} - Z_{R_1}\ddot{\phi}_{s_1} - Z_{u_1}\ddot{\phi}_{u_1}\right) + \\
&\quad 2KT_{y_1}\left(v_{axle_1}/u_{s_1} - \delta_1\right) + F_1\phi_{u_1} - m_{u_1} g\phi_{u_1} \\
F_{R_2} &= m_{u_2}\left(\dot{v}_{s_1} + u_{s_1}\dot{\psi}_{s_1} - X_2\ddot{\psi}_{s_1} - Z_{R_2}\ddot{\phi}_{s_1} - Z_{u_2}\ddot{\phi}_{u_2}\right) + \\
&\quad 4KT_{y_2} v_{axle_2}/u_{s_1} + F_2\phi_{u_2} - m_{u_2} g\phi_{u_2} \\
F_{R_3} &= m_{u_3}\left(\dot{v}_{s_1} + u_{s_1}\dot{\psi}_{s_1} - X_3\ddot{\psi}_{s_1} - Z_{R_3}\ddot{\phi}_{s_1} - Z_{u_3}\ddot{\phi}_{u_3}\right) + \\
&\quad 4KT_{y_3} v_{axle_3}/u_{s_1} + F_3\phi_{u_3} - m_{u_3} g\phi_{u_3} \\
F_{R_4} &= m_{u_4}\left(\dot{v}_{s_2} + u_{s_1}\dot{\psi}_{s_2} - X_4\ddot{\psi}_{s_2} - Z_{R_4}\ddot{\phi}_{s_2} - Z_{u_4}\ddot{\phi}_{u_4}\right) + \\
&\quad 4KT_{y_4} v_{axle_4}/u_{s_1} + F_4\phi_{u_4} - m_{u_4} g\phi_{u_4} \\
F_{R_5} &= m_{u_5}\left(\dot{v}_{s_2} + u_{s_1}\dot{\psi}_{s_2} - X_5\ddot{\psi}_{s_2} - Z_{R_5}\ddot{\phi}_{s_2} - Z_{u_5}\ddot{\phi}_{u_5}\right) + \\
&\quad 4KT_{y_5} v_{axle_5}/u_{s_1} + F_5\phi_{u_5} - m_{u_5} g\phi_{u_5}
\end{aligned}
\tag{4.8}
$$

Equation of Lateral equation

Equations (3.62), (3.63) and (3.68) derived using the lateral force equilibrium can be simplified as:

$$F_y = -\sum_{i=1}^{2} F_{y_{1i}} - \sum_{j=2}^{3}\sum_{i=1}^{4} F_{y_{ji}} - \sum_{j=4}^{5}\sum_{i=1}^{4} F_{y_{ji}} \tag{4.9}$$

where $F_y = F_{1_y} + F_{2_y}$, $F_{1_y} = -m_1 a_{1_y}$ and $F_{2_y} = -m_2 a_{2_y}$

The lateral force equation can be further expressed as:

$$-\sum_{i=1}^{2} F_{y_{1i}} - \sum_{j=2}^{3}\sum_{i=1}^{4} F_{y_{ji}} - \sum_{j=4}^{5}\sum_{i=1}^{4} F_{y_{ji}} = m_1 a_{1_y} + m_2 a_{2_y} \tag{4.10}$$

Substituting for the cornering forces from Equation (4.4) into the above equation, and neglecting the product terms, yields:

$$2KT_{y_1}\left(v_{axle_1}/u_{s_1} - \delta_1\right) + 4\sum_{i=2}^{5} KT_{y_i} v_{axle_i}/u_{s_1} = -\left(m_1 a_{1_y} + m_2 a_{2_y}\right) \tag{4.11}$$

where the lateral accelerations of the two units, derived from Equations (3.66) and (3.71), are given as:

$$a_{1_y} = \dot{v}_{s_1} + u_{s_1}\dot{\psi}_{s_1} + \ddot{\psi}_{s_1}\left(X_{c_1} - X_{sc_1}\right) - \ddot{\phi}_{s_1}\left(Z_{sc_1} - Z_{c_1}\right) \tag{4.12}$$

$$a_{2_y} = \dot{v}_{s_2} + u_{s_2}\dot{\psi}_{s_2} + \ddot{\psi}_{s_2}\left(X_{sc_2} - X_{c_2}\right) - \ddot{\phi}_{s_2}\left(Z_{sc_2} - Z_{c_2}\right) \tag{4.13}$$

Roll moment equations for the sprung masses

The roll moment equilibrium, formulated in Equations (3.74) and (3.75) are simplified using small angle assumption, and given as:

$$I_{xx_{s_1}}\ddot{\phi}_{s_1} = K_1\left(\phi_{s_2} - \phi_{s_1}\right) + \sum_{i=1}^{3}\left\{\begin{matrix} F_{R_i}Z_{R_i} + F_{i1}\left[S_i + Z_{R_i}\left(\phi_{s_1} - \phi_{u_i}\right)\right] - \\ F_{i2}\left[S_i - Z_{R_i}\left(\phi_{s_1} - \phi_{u_i}\right)\right] - KR_i\left(\phi_{s_1} - \phi_{u_i}\right)\end{matrix}\right\} \tag{4.14}$$

$$I_{xx_{s_2}}\ddot{\phi}_{s_2} = -K_1\left(\phi_{s_2} - \phi_{s_1}\right) + \sum_{i=4}^{5}\left\{\begin{matrix} F_{R_i}Z_{R_i} + F_{i1}\left[S_i + Z_{R_i}\left(\phi_{s_2} - \phi_{u_i}\right)\right] - \\ F_{i2}\left[S_i - Z_{R_i}\left(\phi_{s_2} - \phi_{u_i}\right)\right] - KR_i\left(\phi_{s_2} - \phi_{u_i}\right)\end{matrix}\right\} \tag{4.15}$$

Upon substituting for sprung forces from Equation (4.1) into above equations, and neglecting the product terms, the roll moment equations are further simplified

to

$$I_{xx_{s_1}}\ddot{\phi}_{s_1} = K_1\left(\phi_{s_2} - \phi_{s_1}\right) + \sum_{i=1}^{3}\left\{\begin{matrix} F_{R_i}Z_{R_i} - 2KS_i\left(\phi_{s_1} - \phi_{u_i}\right)S_i^{\,2} + \\ Z_{R_i}\left(F_i - W_{u_i}\right)\left(\phi_{s_1} - \phi_{u_i}\right) - KR_i\left(\phi_{s_1} - \phi_{u_i}\right)\end{matrix}\right\} \tag{4.16}$$

$$I_{xx_{s_2}}\ddot{\phi}_{s_2} = -K_1\left(\phi_{s_2} - \phi_{s_1}\right) + \sum_{i=4}^{5}\left\{\begin{matrix} F_{R_i}Z_{R_i} - 2KS_i\left(\phi_{s_2} - \phi_{u_i}\right)S_i^{\,2} + \\ Z_{R_i}\left(F_i - W_{u_i}\right)\left(\phi_{s_2} - \phi_{u_i}\right) - KR_i\left(\phi_{s_2} - \phi_{u_i}\right)\end{matrix}\right\} \tag{4.17}$$

Roll moment equations for the unsprung masses

Applying small angle assumptions to equations (3.76) to (3.80), yields:

$$\begin{aligned} I_{xx_{u_1}}\ddot{\phi}_{u_1} &= F_{R_1}Z_{u_1} - \left(F_{11} - F_{12}\right)S_1 + \left(H_{R_1} - Z_{u_1}\right)\sum_{i=1}^{2}F_{y_{1i}} + \\ &\sum_{i=1}^{2}F_{z_{1i}}R_{1i}\phi_{u_1} + \left(F_{z_{11}} - F_{z_{12}}\right)T_1 + KR_1\left(\phi_{s_1} - \phi_{u_1}\right) \end{aligned} \tag{4.18}$$

$$\begin{aligned} I_{xx_{u_2}}\ddot{\phi}_{u_2} &= F_{R_2}Z_{u_2} - \left(F_{21} - F_{22}\right)S_2 + \left(H_{R_2} - Z_{u_2}\right)\sum_{i=1}^{4}F_{y_{2i}} + \sum_{i=1}^{4}F_{z_{2i}}R_{2i}\phi_{u_2} \\ &+ \left(F_{z_{21}} - F_{z_{24}}\right)\left(T_2 + A_2\right) + \left(F_{z_{22}} - F_{z_{23}}\right)T_2 + KR_2\left(\phi_{s_1} - \phi_{u_2}\right) \end{aligned} \tag{4.19}$$

$$\begin{aligned} I_{xx_{u_3}}\ddot{\phi}_{u_3} &= F_{R_3}Z_{u_3} - \left(F_{31} - F_{32}\right)S_3 + \left(H_{R_3} - Z_{u_3}\right)\sum_{i=1}^{4}F_{y_{3i}} + \sum_{i=1}^{4}F_{z_{3i}}R_{3i}\phi_{u_3} \\ &+ \left(F_{z_{31}} - F_{z_{34}}\right)\left(T_3 + A_3\right) + \left(F_{z_{32}} - F_{z_{33}}\right)T_3 + KR_3\left(\phi_{s_1} - \phi_{u_3}\right) \end{aligned} \tag{4.20}$$

$$\begin{aligned} I_{xx_{u_4}}\ddot{\phi}_{u_4} &= F_{R_4}Z_{u_4} - \left(F_{41} - F_{42}\right)S_4 + \left(H_{R_4} - Z_{u_4}\right)\sum_{i=1}^{4}F_{y_{4i}} + \sum_{i=1}^{4}F_{z_{4i}}R_{4i}\phi_{u_4} \\ &+ \left(F_{z_{41}} - F_{z_{44}}\right)\left(T_4 + A_4\right) + \left(F_{z_{42}} - F_{z_{43}}\right)T_4 + KR_4\left(\phi_{s_2} - \phi_{u_4}\right) \end{aligned} \tag{4.21}$$

$$\begin{aligned} I_{xx_{u_5}}\ddot{\phi}_{u_5} &= F_{R_5}Z_{u_5} - \left(F_{51} - F_{52}\right)S_5 + \left(H_{R_5} - Z_{u_5}\right)\sum_{i=1}^{4}F_{y_{5i}} + \sum_{i=1}^{4}F_{z_{5i}}R_{5i}\phi_{u_5} \\ &+ \left(F_{z_{51}} - F_{z_{54}}\right)\left(T_5 + A_5\right) + \left(F_{z_{52}} - F_{z_{53}}\right)T_5 + KR_5\left(\phi_{s_2} - \phi_{u_5}\right) \end{aligned} \tag{4.22}$$

Upon substituting for suspension spring forces, tire cornering forces and tire vertical forces from equation (4.1), (4.4) and (4.5), respectively, into the above

equations, following equations of roll motion for the unsprung masses are obtained:

$$I_{xx_{u_1}}\ddot{\phi}_{u_1} = F_{R_1}Z_{u_1} + 2KS_1(\phi_{s_1} - \phi_{u_1})S_1^{\,2} + 2KT_{y_1}(v_{axle_1}/u_{s_1} - \delta_1)(H_{R_1} - Z_{u_1}) + F_1R\phi_{u_1} - 2KT_{z_1}T_1^{\,2}\phi_{u_1} + KR_1(\phi_{s_1} - \phi_{u_1}) \tag{4.23}$$

$$I_{xx_{u_2}}\ddot{\phi}_{u_2} = F_{R_2}Z_{u_2} + 2KS_2(\phi_{s_1} - \phi_{u_2})S_2^{\,2} + 4KT_{y_2}v_{axle_2}(H_{R_2} - Z_{u_2})/u_{s_1} + F_2R\phi_{u_2} - 2KT_{z_2}(T_2 + A)^2\phi_{u_2} - 2KT_{z_2}T_2^{\,2}\phi_{u_2} + KR_2(\phi_{s_1} - \phi_{u_2}) \tag{4.24}$$

$$I_{xx_{u_3}}\ddot{\phi}_{u_3} = F_{R_3}Z_{u_3} + 2KS_3(\phi_{s_1} - \phi_{u_3})S_3^{\,2} + 4KT_{y_3}v_{axle_3}(H_{R_3} - Z_{u_3})/u_{s_1} + F_3R\phi_{u_3} - 2KT_{z_3}(T_3 + A)^2\phi_{u_3} - 2KT_{z_3}T_3^{\,2}\phi_{u_3} + KR_3(\phi_{s_1} - \phi_{u_3}) \tag{4.25}$$

$$I_{xx_{u_4}}\ddot{\phi}_{u_4} = F_{R_4}Z_{u_4} + 2KS_4(\phi_{s_2} - \phi_{u_4})S_4^{\,2} + 4KT_{y_4}v_{axle_4}(H_{R_4} - Z_{u_4})/u_{s_1} + F_4R\phi_{u_4} - 2KT_{z_4}(T_4 + A)^2\phi_{u_4} - 2KT_{z_4}T_4^{\,2}\phi_{u_4} + KR_4(\phi_{s_2} - \phi_{u_4}) \tag{4.26}$$

$$I_{xx_{u_5}}\ddot{\phi}_{u_5} = F_{R_5}Z_{u_5} + 2KS_5(\phi_{s_2} - \phi_{u_5})S_5^{\,2} + 4KT_{y_5}v_{axle_5}(H_{R_5} - Z_{u_5})/u_{s_1} + F_5R\phi_{u_5} - 2KT_{z_5}(T_5 + A)^2\phi_{u_5} - 2KT_{z_5}T_5^{\,2}\phi_{u_5} + KR_5(\phi_{s_2} - \phi_{u_5}) \tag{4.27}$$

Yaw moment equations

The equations of yaw moments of the two units, Equations (3.81) and (3.82), are also simplified in the similar manner, and given as:

$$X_{c_1}m_1a_{1_y} + I_{z_1}\ddot{\psi}_{s_1} = -(X_1 + X_{sc_1})\sum_{i=1}^{2}F_{y_{1i}} + \sum_{i=1}^{2}M_{1i} - (X_{sc_1} - X_2)\sum_{i=1}^{4}F_{y_{2i}} + \sum_{i=1}^{4}M_{2i} + (X_3 - X_{sc_1})\sum_{i=1}^{4}F_{y_{3i}} + \sum_{i=1}^{4}M_{3i} \tag{4.28}$$

$$-X_{c_2}m_2a_{2_y} + I_{z_2}\ddot{\psi}_{s_2} = \sum_{j=4}^{5}\left[(X_{sc_2} + X_j)\sum_{i=1}^{4}F_{y_{ji}} + \sum_{i=1}^{4}M_{ji}\right] \tag{4.29}$$

Substituting for the tire cornering forces and aligning moments from Equations

(4.4) and (4.6) into the above equations, yields:

$$\begin{aligned} X_{c_1} m_1 a_{1_y} + I_{z_1} \ddot{\psi}_{s_1} = & -2KT_{y_1}\left(X_1 + X_{sc_1}\right)\left(v_{axle_1}/u_{s_1} - \delta_1\right) + 2KT_{M_1}\left(v_{axle_1}/u_{s_1} - \delta_1\right) \\ & -4KT_{y_2}\left(X_{sc_1} - X_2\right)v_{axle_2}/u_{s_1} + 4KT_{M_2} v_{axle_2}/u_{s_1} \\ & +4KT_{y_3}\left(X_3 - X_{sc_1}\right)v_{axle_3}/u_{s_1} + 4KT_{M_3} v_{axle_3}/u_{s_1} \end{aligned} \tag{4.30}$$

$$-X_{c_2} m_2 a_{2_y} + I_{z_2} \ddot{\psi}_{s_2} = \sum_{j=4}^{5}\left[4KT_{y_j}\left(X_{sc_2} + X_j\right)v_{axle_j}/u_{s_1} + 4KT_{M_j} v_{axle_j}/u_{s_1}\right] \tag{4.31}$$

4.3 Laplace Transformation

The lateral and yaw dynamics behavior of the vehicle, and roll dynamics equilibrium for the sprung and unsprung masses are described by linear differential equations of motion in the previous section. The linearized equations of motion are transformed into Laplace domain for the derivation of analytical transfer functions for the linearized and time-invariant vehicle system.

Let

$$\begin{aligned} \Delta &= L(\delta_1) \\ V_{s_1} &= L(v_{s_1}) \\ \Psi_{s_1} &= L(\psi_{s_1}) \\ \Phi_{s_1} &= L(\phi_{s_1}) \\ \Psi_{s_2} &= L(\psi_{s_2}) \\ \Phi_{s_2} &= L(\phi_{s_2}) \\ \Phi_{u_1} &= L(\phi_{u_1}) \\ \Phi_{u_2} &= L(\phi_{u_2}) \\ \Phi_{u_3} &= L(\phi_{u_3}) \\ \Phi_{u_4} &= L(\phi_{u_4}) \\ \Phi_{u_5} &= L(\phi_{u_5}) \end{aligned} \tag{4.32}$$

where L is the Laplace operator.

Assuming zero initial values, the Laplace transforms of the derivatives of the

response vector are expressed as:

$$
\begin{aligned}
&L(\dot{v}_{s_1}) = V_{s_1} s \\
&L(\dot{\psi}_{s_1}) = \Psi_{s_1} s, L(\ddot{\psi}_{s_1}) = \Psi_{s_1} s^2 \\
&L(\dot{\phi}_{s_1}) = \Phi_{s_1} s, L(\ddot{\phi}_{s_1}) = \Phi_{s_1} s^2 \\
&L(\dot{\psi}_{s_2}) = \Psi_{s_2} s, L(\ddot{\psi}_{s_2}) = \Psi_{s_2} s^2 \\
&L(\dot{\phi}_{s_2}) = \Phi_{s_2} s, L(\ddot{\phi}_{s_2}) = \Phi_{s_2} s^2 \\
&L(\dot{\phi}_{u_1}) = \Phi_{u_1} s, L(\ddot{\phi}_{u_1}) = \Phi_{u_1} s^2 \\
&L(\dot{\phi}_{u_2}) = \Phi_{u_2} s, L(\ddot{\phi}_{u_2}) = \Phi_{u_2} s^2 \\
&L(\dot{\phi}_{u_3}) = \Phi_{u_3} s, L(\ddot{\phi}_{u_3}) = \Phi_{u_3} s^2 \\
&L(\dot{\phi}_{u_4}) = \Phi_{u_4} s, L(\ddot{\phi}_{u_4}) = \Phi_{u_4} s^2 \\
&L(\dot{\phi}_{u_5}) = \Phi_{u_5} s, L(\ddot{\phi}_{u_5}) = \Phi_{u_5} s^2
\end{aligned}
\tag{4.33}
$$

Lateral force equation

The Laplace transformation of both sides of the equation of lateral motion (4.11), yields:

$$
2KT_{y_1}\left[L\left(v_{axle_1}\right)/u_{s_1} - \Delta\right] + 4\sum_{i=2}^{5} KT_{y_i} L\left(v_{axle_i}\right)/u_{s_1} = -m_1 L\left(a_{1_y}\right) - m_2 L\left(a_{2_y}\right) \tag{4.34}
$$

where the Laplace transforms of lateral velocities and accelerations from Equations (4.2), (4.12) and (4.13), such that:

$$
\begin{aligned}
L\left(v_{axle_1}\right) &= V_{s_1} - \left(Z_{R_1}\Phi_{s_1} - X_1\Psi_{s_1} + H_{R_1}\Phi_{u_1}\right)s \\
L\left(v_{axle_i}\right) &= V_{s_j} - \left(Z_{R_i}\Phi_{s_j} + X_i\Psi_{s_j} + H_{R_i}\Phi_{u_i}\right)s
\end{aligned}
\tag{4.35}
$$

where $i = 1, 2, 3$ for the tractor ($j = 1$), and $i = 4, 5$ for the semitrailer ($j = 2$).

$$
L\left(a_{1_y}\right) = \left(V_{s_1} + u_{s_1}\Psi_{s_1}\right)s + \left[\left(X_{c_1} - X_{sc_1}\right)\Psi_{s_1} - \left(Z_{sc_1} - Z_{c_1}\right)\Phi_{s_1}\right]s^2 \tag{4.36}
$$

$$
L\left(a_{2_y}\right) = L\left(\dot{v}_{s_2}\right) + u_{s_2} s\Psi_{s_2} + \left[\left(X_{sc_2} - X_{c_2}\right)\Psi_{s_2} - \left(Z_{sc_2} - Z_{c_2}\right)\Phi_{s_2}\right]s^2 \tag{4.37}
$$

The Laplace transforms of the tractor lateral velocity and its time derivative,

described in Equations (3.43) and (3.46), are obtained as:

$$V_{s_2} = V_{s_1} + \left(u_{s_1} - X_{sc_1} s\right)\Psi_{s_1} - Z_{sc_1} s\Phi_{s_1} - \left(u_{s_1} + X_{sc_2} s\right)\Psi_{s_2} + Z_{sc_2} s\Phi_{s_2} \tag{4.38}$$

$$L\left(\dot{v}_{s_2}\right) = sV_{s_1} - \left(X_{sc_1} s^2 - u_{s_1} s\right)\Psi_{s_1} - Z_{sc_1} s^2\Phi_{s_1} - \left(X_{sc_2} s^2 + u_{s_2} s\right)\Psi_{s_2} + Z_{sc_2} s^2\Phi_{s_2} \tag{4.39}$$

Thus Equation (4.34) can be expanded and rearranged as:

$$\begin{aligned}
&\left[2KT_{y_1}/u_{s_1} + 4\left(KT_{y_2} + KT_{y_3} + KT_{y_4} + KT_{y_5}\right)/u_{s_1} + \left(m_1 + m_2\right)s\right]V_{s_1} \\
&+\left\{\begin{aligned}&4\left(KT_{y_4} + KT_{y_5}\right) + \left(m_1 X_{c_1} - m_1 X_{sc_1} - m_2 X_{sc_1}\right)s^2 \\ &+\left[\begin{aligned}&2KT_{y_1} X_1/u_{s_1} + u_{s_1}\left(m_1 + m_2\right) \\ &-4\left(KT_{y_2} X_2 + KT_{y_3} X_3 + KT_{y_4} X_{sc_1} + KT_{y_5} X_{sc_1}\right)/u_{s_1}\end{aligned}\right]s\end{aligned}\right\}\Psi_{s_1} \\
&-\left\{\begin{aligned}&\left[2KT_{y_1} Z_{R_1}/u_{s_1} + 4\left(KT_{y_2} Z_{R_2} + KT_{y_3} Z_{R_3} + KT_{y_4} Z_{sc_1} + KT_{y_5} Z_{sc_1}\right)/u_{s_1}\right]s \\ &+\left(m_1 Z_{sc_1} - m_1 Z_{c_1} + m_2 Z_{sc_1}\right)s^2\end{aligned}\right\}\Phi_{s_1} \\
&-\left\{\begin{aligned}&4\left(KT_{y_4} + KT_{y_5}\right) + m_2 X_{c_2} s^2 \\ &+4\left[KT_{y_4}\left(X_4 + X_{sc_2}\right)/u_{s_1} + KT_{y_5}\left(X_5 + X_{sc_2}\right)/u_{s_1}\right]s\end{aligned}\right\}\Psi_{s_2} \\
&+\left\{4\left[KT_{y_4}\left(Z_{sc_2} - Z_{R_4}\right)/u_{s_1} + KT_{y_5}\left(Z_{sc_2} - Z_{R_5}\right)/u_{s_1}\right]s + m_2 Z_{c_2} s^2\right\}\Phi_{s_2} \\
&-2KT_{y_1} H_{R_1} s\Phi_{u_1}/u_{s_1} - 4KT_{y_2} H_{R_2} s\Phi_{u_2}/u_{s_1} - 4KT_{y_3} H_{R_3} s\Phi_{u_3}/u_{s_1} \\
&-4KT_{y_4} H_{R_4} s\Phi_{u_4}/u_{s_1} - 4KT_{y_5} H_{R_5} s\Phi_{u_5}/u_{s_1} = 2KT_{y_1}\Delta
\end{aligned} \tag{4.40}$$

Roll moment equations of sprung masses

Laplace transformations of both sides of Equations (4.16) and (4.17), describing the roll equilibrium for the tractor and semitrailer sprung masses, yield:

$$I_{xx_{s_1}} s^2\Phi_{s_1} = K_1\left(\Phi_{s_2} - \Phi_{s_1}\right) + \sum_{i=1}^{3}\left\{\begin{aligned}&Z_{R_i} L\left(F_{R_i}\right) - 2KS_i\left(\Phi_{s_1} - \Phi_{u_i}\right)S_i^2 + \\ &Z_{R_i}\left(F_i - W_{u_i}\right)\left(\Phi_{s_1} - \Phi_{u_i}\right) - KR_i\left(\Phi_{s_1} - \Phi_{u_i}\right)\end{aligned}\right\} \tag{4.41}$$

$$I_{xx_{s_2}} s^2\Phi_{s_2} = -K_1\left(\Phi_{s_2} - \Phi_{s_1}\right) + \sum_{i=4}^{5}\left\{\begin{aligned}&Z_{R_i} L\left(F_{R_i}\right) - 2KS_i\left(\Phi_{s_2} - \Phi_{u_i}\right)S_i^2 + \\ &Z_{R_i}\left(F_i - W_{u_i}\right)\left(\Phi_{s_2} - \Phi_{u_i}\right) - KR_i\left(\Phi_{s_2} - \Phi_{u_i}\right)\end{aligned}\right\} \tag{4.42}$$

The Laplace transforms of roll center forces can be derived from Equation (4.8), such that:

$$
\begin{aligned}
L(F_{R_1}) &= m_{u_1}\left(sV_{s_1} + u_{s_1}s\Psi_{s_1} + X_1 s^2\Psi_{s_1} - Z_{R_1}s^2\Phi_{s_1} - Z_{u_1}s^2\Phi_{u_1}\right) + \\
&\quad 2KT_{y_1}\left[L(v_{axle_1})/u_{s_1} - \Delta\right] + F_1\Phi_{u_1} - m_{u_1}g\Phi_{u_1} \\
L(F_{R_2}) &= m_{u_2}\left(sV_{s_1} + u_{s_1}s\Psi_{s_1} - X_2 s^2\Psi_{s_1} - Z_{R_2}s^2\Phi_{s_1} - Z_{u_2}s^2\Phi_{u_2}\right) + \\
&\quad 4KT_{y_2}L(v_{axle_2})/u_{s_1} + F_2\Phi_{u_2} - m_{u_2}g\Phi_{u_2} \\
L(F_{R_3}) &= m_{u_3}\left(sV_{s_1} + u_{s_1}s\Psi_{s_1} - X_3 s^2\Psi_{s_1} - Z_{R_3}s^2\Phi_{s_1} - Z_{u_3}s^2\Phi_{u_3}\right) + \\
&\quad 4KT_{y_3}L(v_{axle_3})/u_{s_1} + F_3\Phi_{u_3} - m_{u_3}g\Phi_{u_3} \\
L(F_{R_4}) &= m_{u_4}\left(sV_{s_2} + u_{s_1}s\Psi_{s_2} - X_4 s^2\Psi_{s_2} - Z_{R_4}s^2\Phi_{s_2} - Z_{u_4}s^2\Phi_{u_4}\right) + \\
&\quad 4KT_{y_4}L(v_{axle_4})/u_{s_1} + F_4\Phi_{u_4} - m_{u_4}g\Phi_{u_4} \\
L(F_{R_5}) &= m_{u_5}\left(sV_{s_2} + u_{s_1}s\Psi_{s_2} - X_5 s^2\Psi_{s_2} - Z_{R_5}s^2\Phi_{s_2} - Z_{u_5}s^2\Phi_{u_5}\right) + \\
&\quad 4KT_{y_5}L(v_{axle_5})/u_{s_1} + F_5\Phi_{u_5} - m_{u_5}g\Phi_{u_5}
\end{aligned}
\tag{4.43}
$$

Thus Equation (4.41) and (4.42) can be expanded and rearranged as:

$$
\begin{aligned}
&\left[2KT_{y_1}Z_{R_1}/u_{s_1} + 4\left(KT_{y_2}Z_{R_2} + KT_{y_3}Z_{R_3}\right)/u_{s_1} + \left(m_{u_1}Z_{R_1} + m_{u_2}Z_{R_2} + m_{u_3}Z_{R_3}\right)s\right]V_{s_1} \\
&+\left\{\begin{bmatrix} u_{s_1}\left(m_{u_1}Z_{R_1} + m_{u_2}Z_{R_2} + m_{u_3}Z_{R_3}\right) + 2KT_{y_1}Z_{R_1}X_1/u_{s_1} \\ -4\left(KT_{y_2}Z_{R_2}X_2 + KT_{y_3}Z_{R_3}X_3\right)/u_{s_1} \end{bmatrix} s \right. \\
&\qquad \left. + \left(m_{u_1}Z_{R_1}X_1 - m_{u_2}Z_{R_2}X_2 - m_{u_3}Z_{R_3}X_3\right)s^2 \right\}\Psi_{s_1} \\
&+\left\{\begin{array}{l} Z_{R_1}\left(F_1 - W_{u_1}\right) + Z_{R_2}\left(F_2 - W_{u_2}\right) + Z_{R_3}\left(F_3 - W_{u_3}\right) \\ -2\left(KS_1S_1^{\,2} + KS_2S_2^{\,2} + KS_3S_3^{\,2}\right) - \left(K_1 + KR_1 + KR_2 + KR_3\right) \\ -\left[2KT_{y_1}Z_{R_1}^{\,2}/u_{s_1} + 4\left(KT_{y_2}Z_{R_2}^{\,2} + KT_{y_3}Z_{R_3}^{\,2}\right)/u_{s_1}\right]s \\ -\left(m_{u_1}Z_{R_1}^{\,2} + m_{u_2}Z_{R_2}^{\,2} + m_{u_3}Z_{R_3}^{\,2} + I_{xx_{s_1}}\right)s^2 \end{array}\right\}\Phi_{s_1} \\
&+\left[2KS_1S_1^{\,2} + KR_1 - 2KT_{y_1}Z_{R_1}H_{R_1}s/u_{s_1} - m_{u_1}Z_{R_1}Z_{u_1}s^2\right]\Phi_{u_1} \\
&+\left[2KS_2S_2^{\,2} + KR_2 - 4KT_{y_2}Z_{R_2}H_{R_2}s/u_{s_1} - m_{u_2}Z_{R_2}Z_{u_2}s^2\right]\Phi_{u_2} \\
&+\left[2KS_3S_3^{\,2} + KR_3 - 4KT_{y_3}Z_{R_3}H_{R_3}s/u_{s_1} - m_{u_3}Z_{R_3}Z_{u_3}s^2\right]\Phi_{u_3} + K_1\Phi_{s_2} = 2KT_{y_1}Z_{R_1}\Delta
\end{aligned}
\tag{4.44}
$$

$$
\begin{aligned}
&\left[4KT_{y_4}Z_{R_4}/u_{s_1}+4KT_{y_5}Z_{R_5}/u_{s_1}+\left(m_{u_4}Z_{R_4}+m_{u_5}Z_{R_5}\right)s\right]V_{s_1}\\
&+\left[\begin{array}{l}4KT_{y_4}Z_{R_4}+4KT_{y_5}Z_{R_5}-X_{sc_1}\left(m_{u_4}Z_{R_4}+m_{u_5}Z_{R_5}\right)s^2\\+\left(m_{u_4}Z_{R_4}u_{s_1}+m_{u_5}Z_{R_5}u_{s_1}-4KT_{y_4}Z_{R_4}X_{sc_1}/u_{s_1}-4KT_{y_5}Z_{R_5}X_{sc_1}/u_{s_1}\right)s\end{array}\right]\Psi_{s_1}\\
&+\left[K_1-4\left(KT_{y_4}Z_{R_4}+KT_{y_5}Z_{R_5}\right)Z_{sc_1}s/u_{s_1}-\left(m_{u_4}Z_{R_4}+m_{u_5}Z_{R_5}\right)Z_{sc_1}s^2\right]\Phi_{s_1}\\
&+\left\{\begin{array}{l}-4\left[KT_{y_4}Z_{R_4}\left(X_4+X_{sc_2}\right)+KT_{y_5}Z_{R_5}\left(X_5+X_{sc_2}\right)\right]s/u_{s_1}\\-\left[m_{u_4}Z_{R_4}\left(X_4+X_{sc_2}\right)+m_{u_5}Z_{R_5}\left(X_5+X_{sc_2}\right)\right]s^2-4\left(KT_{y_4}Z_{R_4}+KT_{y_5}Z_{R_5}\right)\end{array}\right\}\Psi_{s_2}\\
&+\left[\begin{array}{l}Z_{R_4}\left(F_4-W_{u_4}\right)-\left(K_1+KR_4+KR_5\right)-2\left(KS_4S_4{}^2+KS_5S_5{}^2\right)\\+Z_{R_5}\left(F_5-W_{u_5}\right)-4\left[KT_{y_4}Z_{R_4}\left(Z_{R_4}-Z_{sc_2}\right)+KT_{y_5}Z_{R_5}\left(Z_{R_5}-Z_{sc_2}\right)\right]s/u_{s_1}\\+\left[m_{u_4}Z_{R_4}\left(Z_{sc_2}-Z_{R_4}\right)+m_{u_5}Z_{R_5}\left(Z_{sc_2}-Z_{R_5}\right)-I_{xx_{s_2}}\right]s^2\end{array}\right]\Phi_{s_2}\\
&+\left[2KS_4S_4{}^2+KR_4-m_{u_4}Z_{R_4}Z_{u_4}s^2-4KT_{y_4}Z_{R_4}H_{R_4}s/u_{s_1}\right]\Phi_{u_4}\\
&+\left[2KS_5S_5{}^2+KR_5-m_{u_5}Z_{R_5}Z_{u_5}s^2-4KT_{y_5}Z_{R_5}H_{R_5}s/u_{s_1}\right]\Phi_{u_5}=0
\end{aligned}
\tag{4.45}
$$

Roll moment equations for the unsprung masses

The Laplace transformations of both sides of Equations (4.23) to (4.27), describing the roll moment equilibrium of the unsprung masses, yield:

$$
\begin{aligned}
I_{xx_{u_1}}s^2\Phi_{u_1}=&\,\mathrm{Z}_{\mathrm{u}_1}L\left(F_{R_1}\right)+2KS_1\left(\Phi_{s_1}-\Phi_{u_1}\right)S_1{}^2+2KT_{y_1}\left[L\left(v_{axle_1}\right)/u_{s_1}-\Delta\right]\left(H_{R_1}-Z_{u_1}\right)\\
&+F_1R\Phi_{u_1}-2KT_{z_1}T_1{}^2\Phi_{u_1}+KR_1\left(\Phi_{s_1}-\Phi_{u_1}\right)
\end{aligned}
\tag{4.46}
$$

$$
\begin{aligned}
I_{xx_{u_2}}s^2\Phi_{u_2}=&\,\mathrm{Z}_{\mathrm{u}_2}L\left(F_{R_2}\right)+2KS_2\left(\Phi_{s_1}-\Phi_{u_2}\right)S_2{}^2+4KT_{y_2}L\left(v_{axle_2}\right)\left(H_{R_2}-Z_{u_2}\right)/u_{s_1}\\
&+F_2R\Phi_{u_2}-2KT_{z_2}\left(T_2+A\right)^2\Phi_{u_2}-2KT_{z_2}T_2{}^2\Phi_{u_2}+KR_2\left(\Phi_{s_1}-\Phi_{u_2}\right)
\end{aligned}
\tag{4.47}
$$

$$
\begin{aligned}
I_{xx_{u_3}}s^2\Phi_{u_3}=&\,\mathrm{Z}_{\mathrm{u}_3}L\left(F_{R_3}\right)+2KS_3\left(\Phi_{s_1}-\Phi_{u_3}\right)S_3{}^2+4KT_{y_3}L\left(v_{axle_3}\right)\left(H_{R_3}-Z_{u_3}\right)/u_{s_1}\\
&+F_3R\Phi_{u_3}-2KT_{z_3}\left(T_3+A\right)^2\Phi_{u_3}-2KT_{z_3}T_3{}^2\Phi_{u_3}+KR_3\left(\Phi_{s_1}-\Phi_{u_3}\right)
\end{aligned}
\tag{4.48}
$$

$$
\begin{aligned}
I_{xx_{u_4}}s^2\Phi_{u_4}=&\,\mathrm{Z}_{\mathrm{u}_4}L\left(F_{R_4}\right)+2KS_4\left(\Phi_{s_2}-\Phi_{u_4}\right)S_4{}^2+4KT_{y_4}L\left(v_{axle_4}\right)\left(H_{R_4}-Z_{u_4}\right)/u_{s_1}\\
&+F_4R\Phi_{u_4}-2KT_{z_4}\left(T_4+A\right)^2\Phi_{u_4}-2KT_{z_4}T_4{}^2\Phi_{u_4}+KR_4\left(\Phi_{s_2}-\Phi_{u_4}\right)
\end{aligned}
\tag{4.49}
$$

$$
\begin{aligned}
I_{xx_{u_5}}s^2\Phi_{u_5}=&\,\mathrm{Z}_{\mathrm{u}_5}L\left(F_{R_5}\right)+2KS_5\left(\Phi_{s_2}-\Phi_{u_5}\right)S_5{}^2+4KT_{y_5}L\left(v_{axle_5}\right)\left(H_{R_5}-Z_{u_5}\right)/u_{s_1}\\
&+F_5R\Phi_{u_5}-2KT_{z_5}\left(T_5+A\right)^2\Phi_{u_5}-2KT_{z_5}T_5{}^2\Phi_{u_5}+KR_5\left(\Phi_{s_2}-\Phi_{u_5}\right)
\end{aligned}
\tag{4.50}
$$

The above equations can be further expanded and rearranged as:

$$
\begin{aligned}
&\left(2KT_{y_1}H_{R_1}/u_{s_1}+m_{u_1}Z_{u_1}s\right)V_{s_1}\\
&+\left[\left(m_{u_1}Z_{u_1}u_{s_1}+2KT_{y_1}H_{R_1}X_1/u_{s_1}\right)s+m_{u_1}Z_{u_1}X_1s^2\right]\Psi_{s_1}\\
&+\left(2KS_1S_1^{\,2}+KR_1-2KT_{y_1}H_{R_1}Z_{R_1}s/u_{s_1}-m_{u_1}Z_{u_1}Z_{R_1}s^2\right)\Phi_{s_1}\\
&+\begin{bmatrix}F_1Z_{u_1}+F_1R-m_{u_1}gZ_{u_1}-2KS_1S_1^{\,2}-2KT_{z_1}T_1^{\,2}\\-KR_1-2KT_{y_1}H_{R_1}^{\,2}s/u_{s_1}-\left(m_{u_1}Z_{u_1}^{\,2}+I_{xx_{u_1}}\right)s^2\end{bmatrix}\Phi_{u_1}\\
&=2KT_{y_1}H_{R_1}\Delta
\end{aligned}
\tag{4.51}
$$

$$
\begin{aligned}
&\left(m_{u_2}Z_{u_2}s+4KT_{y_2}H_{R_2}/u_{s_1}\right)V_{s_1}\\
&+\left[\left(m_{u_2}Z_{u_2}u_{s_1}-4KT_{y_2}X_2H_{R_2}/u_{s_1}\right)s-m_{u_2}Z_{u_2}X_2s^2\right]\Psi_{s_1}\\
&-\left(m_{u_2}Z_{u_2}Z_{R_2}s^2+4KT_{y_2}Z_{R_2}H_{R_2}s/u_{s_1}-2KS_2S_2^{\,2}-KR_2\right)\Phi_{s_1}\\
&+\begin{bmatrix}F_2\left(R+Z_{u_2}\right)-2KT_{z_2}\left(T_2+A\right)^2-2KT_{z_2}T_2^{\,2}-KR_2-2KS_2S_2^{\,2}\\-m_{u_2}gZ_{u_2}-4KT_{y_2}H_{R_2}^{\,2}s/u_{s_1}-\left(m_{u_2}Z_{u_2}^{\,2}+I_{xx_{u_2}}\right)s^2\end{bmatrix}\Phi_{u_2}=0
\end{aligned}
\tag{4.52}
$$

$$
\begin{aligned}
&\left(m_{u_3}Z_{u_3}s+4KT_{y_3}H_{R_3}/u_{s_1}\right)V_{s_1}\\
&+\left[\left(m_{u_3}Z_{u_3}u_{s_1}-4KT_{y_3}X_3H_{R_3}/u_{s_1}\right)s-m_{u_3}Z_{u_3}X_3s^2\right]\Psi_{s_1}\\
&-\left(m_{u_3}Z_{u_3}Z_{R_3}s^2+4KT_{y_3}Z_{R_3}H_{R_3}s/u_{s_1}-2KS_3S_3^{\,2}-KR_3\right)\Phi_{s_1}\\
&+\begin{bmatrix}F_3\left(R+Z_{u_3}\right)-2KT_{z_3}\left(T_3+A\right)^2-2KT_{z_3}T_3^{\,2}-KR_3-2KS_3S_3^{\,2}\\-m_{u_3}gZ_{u_3}-4KT_{y_3}H_{R_3}^{\,2}s/u_{s_1}-\left(m_{u_3}Z_{u_3}^{\,2}+I_{xx_{u_3}}\right)s^2\end{bmatrix}\Phi_{u_3}=0
\end{aligned}
\tag{4.53}
$$

$$
\begin{aligned}
&\left(m_{u_4}Z_{u_4}s+4KT_{y_4}H_{R_4}/u_{s_1}\right)V_{s_1}\\
&+\left[\left(m_{u_4}Z_{u_4}u_{s_1}-4KT_{y_4}H_{R_4}X_{sc_1}/u_{s_1}\right)s+4KT_{y_4}H_{R_4}-m_{u_4}Z_{u_4}X_{sc_1}s^2\right]\Psi_{s_1}\\
&-\left(m_{u_4}Z_{u_4}Z_{sc_1}s^2+4KT_{y_4}H_{R_4}Z_{sc_1}s/u_{s_1}\right)\Phi_{s_1}\\
&-\left[4KT_{y_4}H_{R_4}\left(X_4+X_{sc_2}\right)s/u_{s_1}+m_{u_4}Z_{u_4}\left(X_4+X_{sc_2}\right)s^2+4KT_{y_4}H_{R_4}\right]\Psi_{s_2}\\
&+\left[2KS_4S_4^{\,2}+KR_4+m_{u_4}Z_{u_4}\left(Z_{sc_2}-Z_{R_4}\right)s^2+4KT_{y_4}H_{R_4}\left(Z_{sc_2}-Z_{R_4}\right)s/u_{s_1}\right]\Phi_{s_2}\\
&+\begin{bmatrix}F_4R-2KT_{z_4}\left(T_4+A\right)^2-2KT_{z_4}T_4^{\,2}-2KS_4S_4^{\,2}-KR_4+F_4Z_{u_4}\\-m_{u_4}gZ_{u_4}-\left(I_{xx_{u_4}}+m_{u_4}Z_{u_4}^{\,2}\right)s^2-4KT_{y_4}H_{R_4}^{\,2}s/u_{s_1}\end{bmatrix}\Phi_{u_4}=0
\end{aligned}
\tag{4.54}
$$

$$
\begin{aligned}
&\left(m_{u_5}Z_{u_5}s+4KT_{y_5}H_{R_5}/u_{s_1}\right)V_{s_1}\\
&+\left[\left(m_{u_5}Z_{u_5}u_{s_1}-4KT_{y_5}H_{R_5}X_{sc_1}/u_{s_1}\right)s+4KT_{y_5}H_{R_5}-m_{u_5}Z_{u_5}X_{sc_1}s^2\right]\Psi_{s_1}\\
&-\left(m_{u_5}Z_{u_5}Z_{sc_1}s^2+4KT_{y_5}H_{R_5}Z_{sc_1}s/u_{s_1}\right)\Phi_{s_1}\\
&-\left[4KT_{y_5}H_{R_5}\left(X_5+X_{sc_2}\right)s/u_{s_1}+m_{u_5}Z_{u_5}\left(X_5+X_{sc_2}\right)s^2+4KT_{y_5}H_{R_5}\right]\Psi_{s_2}\\
&+\left[2KS_5S_5{}^2+KR_5+m_{u_5}Z_{u_5}\left(Z_{sc_2}-Z_{R_5}\right)s^2+4KT_{y_5}H_{R_5}\left(Z_{sc_2}-Z_{R_5}\right)s/u_{s_1}\right]\Phi_{s_2}\\
&+\left[\begin{array}{l}F_5R-2KT_{z_5}\left(T_5+A\right)^2-2KT_{z_5}T_5{}^2-2KS_5S_5{}^2-KR_5+F_5Z_{u_5}\\-m_{u_5}gZ_{u_5}-\left(I_{xx_{u_5}}+m_{u_5}Z_{u_5}{}^2\right)s^2-4KT_{y_5}H_{R_5}{}^2s/u_{s_1}\end{array}\right]\Phi_{u_5}=0
\end{aligned}
\tag{4.55}
$$

Yaw moment equations

Laplace transformations of both sides of Equations (4.30) and (4.31), describing the yaw moment equilibrium of the tractor and semitrailer units, yield:

$$
\begin{aligned}
X_{c_1}m_1L\left(a_{1_y}\right)+I_{z_1}s^2\Psi_{s_1}=&-2KT_{y_1}\left(X_1+X_{sc_1}\right)\left[L\left(v_{axle_1}\right)/u_{s_1}-\Delta\right]\\
&+2KT_{M_1}\left[L\left(v_{axle_1}\right)/u_{s_1}-\Delta\right]\\
&-4KT_{y_2}\left(X_{sc_1}-X_2\right)L\left(v_{axle_2}\right)/u_{s_1}+4KT_{M_2}L\left(v_{axle_2}\right)/u_{s_1}\\
&+4KT_{y_3}\left(X_3-X_{sc_1}\right)L\left(v_{axle_3}\right)/u_{s_1}+4KT_{M_3}L\left(v_{axle_3}\right)/u_{s_1}
\end{aligned}
\tag{4.56}
$$

$$
-X_{c_2}m_2L\left(a_{2_y}\right)+I_{z_2}s^2\Psi_{s_2}=\sum_{j=4}^{5}\left[\begin{array}{l}4KT_{y_j}\left(X_{sc_2}+X_j\right)L\left(v_{axle_j}\right)/u_{s_1}\\+4KT_{M_j}L\left(v_{axle_j}\right)/u_{s_1}\end{array}\right]
\tag{4.57}
$$

The above equations can be expanded and rearranged as:

$$
\begin{aligned}
&\left\{\begin{array}{l}2\left[KT_{M_1}-KT_{y_1}\left(X_1+X_{sc_1}\right)\right]/u_{s_1}+4\left[KT_{M_2}-KT_{y_2}\left(X_{sc_1}-X_2\right)\right]/u_{s_1}\\+4\left[KT_{M_3}+KT_{y_3}\left(X_3-X_{sc_1}\right)\right]/u_{s_1}-X_{c_1}m_1s\end{array}\right\}V_{s_1}+\\
&\left\{\begin{array}{l}2\left[KT_{M_1}-KT_{y_1}\left(X_1+X_{sc_1}\right)\right]X_1s/u_{s_1}-4\left[KT_{M_2}-KT_{y_2}\left(X_{sc_1}-X_2\right)\right]X_2s/u_{s_1}-\\4\left[KT_{M_3}+KT_{y_3}\left(X_3-X_{sc_1}\right)\right]X_3s/u_{s_1}-X_{c_1}m_1u_{s_1}s-\left[X_{c_1}m_1\left(X_{c_1}-X_{sc_1}\right)+I_{z_1}\right]s^2\end{array}\right\}\Psi_{s_1}\\
&+\left\{\begin{array}{l}X_{c_1}m_1s^2\left(Z_{sc_1}-Z_{c_1}\right)-2\left[KT_{M_1}-KT_{y_1}\left(X_1+X_{sc_1}\right)\right]Z_{R_1}s/u_{s_1}-\\4\left[KT_{M_2}-KT_{y_2}\left(X_{sc_1}-X_2\right)\right]Z_{R_2}s/u_{s_1}-4\left[KT_{M_3}+KT_{y_3}\left(X_3-X_{sc_1}\right)\right]Z_{R_3}s/u_{s_1}\end{array}\right\}\Phi_{s_1}\\
&-2\left[KT_{M_1}-KT_{y_1}\left(X_1+X_{sc_1}\right)\right]H_{R_1}s\Phi_{u_1}/u_{s_1}-4\left[KT_{M_2}-KT_{y_2}\left(X_{sc_1}-X_2\right)\right]H_{R_2}s\Phi_{u_2}/u_{s_1}\\
&-4\left[KT_{M_3}+KT_{y_3}\left(X_3-X_{sc_1}\right)\right]H_{R_3}s\Phi_{u_3}/u_{s_1}=\left[2KT_{M_1}-2KT_{y_1}\left(X_1+X_{sc_1}\right)\right]\Delta
\end{aligned}
\tag{4.58}
$$

$$
\begin{aligned}
&\left\{\begin{array}{l} X_{c_2} m_2 s + 4\left[KT_{y_4}\left(X_{sc_2}+X_4\right)+KT_{M_4}\right]/u_{s_1} \\ +4\left[KT_{y_5}\left(X_{sc_2}+X_5\right)+KT_{M_5}\right]/u_{s_1} \end{array}\right\} V_{s_1} \\
&+\left\{\begin{array}{l} 4\left[KT_{y_4}\left(X_{sc_2}+X_4\right)+KT_{M_4}\right]+4\left[KT_{y_5}\left(X_{sc_2}+X_5\right)+KT_{M_5}\right] \\ -4\left[KT_{y_4}\left(X_{sc_2}+X_4\right)+KT_{M_4}\right]X_{sc_1} s/u_{s_1} \\ -4\left[KT_{y_5}\left(X_{sc_2}+X_5\right)+KT_{M_5}\right]X_{sc_1} s/u_{s_1} \\ +X_{c_2} m_2 u_{s_1} s - X_{c_2} m_2 X_{sc_1} s^2 \end{array}\right\} \Psi_{s_1} \\
&-\left\{\begin{array}{l} X_{c_2} m_2 Z_{sc_1} s^2 \\ +4\left[KT_{y_4}\left(X_{sc_2}+X_4\right)+KT_{M_4}\right]Z_{sc_1} s/u_{s_1} \\ +4\left[KT_{y_5}\left(X_{sc_2}+X_5\right)+KT_{M_5}\right]Z_{sc_1} s/u_{s_1} \end{array}\right\} \Phi_{s_1} \\
&+\left\{\begin{array}{l} -\left(m_2 X_{c_2}{}^2 + I_{z_2}\right)s^2 \\ -\left[4KT_{y_4}\left(X_{sc_2}+X_4\right)+4KT_{M_4}\right]\left(X_4+X_{sc_2}\right)s/u_{s_1} \\ -\left[4KT_{y_5}\left(X_{sc_2}+X_5\right)+4KT_{M_5}\right]\left(X_5+X_{sc_2}\right)s/u_{s_1} \\ -\left[4KT_{y_4}\left(X_{sc_2}+X_4\right)+4KT_{M_4}\right] \\ -\left[4KT_{y_5}\left(X_{sc_2}+X_5\right)+4KT_{M_5}\right] \end{array}\right\} \Psi_{s_2} \\
&+\left\{\begin{array}{l} X_{c_2} m_2 s^2 Z_{c_2} \\ +\left[4KT_{y_4}\left(X_{sc_2}+X_4\right)+4KT_{M_4}\right]\left(Z_{sc_2}-Z_{R_4}\right)s/u_{s_1} \\ +\left[4KT_{y_5}\left(X_{sc_2}+X_5\right)+4KT_{M_5}\right]\left(Z_{sc_2}-Z_{R_5}\right)s/u_{s_1} \end{array}\right\} \Phi_{s_2} \\
&-\left[4KT_{y_4}\left(X_{sc_2}+X_4\right)+4KT_{M_4}\right]H_{R_4} s\Phi_{u_4}/u_{s_1} \\
&-\left[4KT_{y_5}\left(X_{sc_2}+X_5\right)+4KT_{M_5}\right]H_{R_5} s\Phi_{u_5}/u_{s_1} = 0
\end{aligned}
\tag{4.59}
$$

Equations (4.40), (4.44), (4.45), (4.51) to (4.55), (4.58), (4.58) and (4.59), describing the lateral, roll and yaw dynamics of the linearized vehicle model in the Laplace domain, can be rewritten in the matrix form as:

$$D_{10\times10} Y_{10\times1} = C_{10\times1}\Delta \tag{4.60}$$

where Δ defines the steer angle input and $Y_{10\times1}$ is the response vector, given by:

$$Y = \left[V_{s_1} \quad \Psi_{s_1} \quad \Phi_{s_1} \quad \Psi_{s_2} \quad \Phi_{s_2} \quad \Phi_{u_1} \quad \Phi_{u_2} \quad \Phi_{u_3} \quad \Phi_{u_4} \quad \Phi_{u_5}\right]^T$$

The $D_{10\times10}$ and $C_{10\times1}$ are the matrices containing vehicle parameters and their elements are given in APPENDIX B.

The above equation can be solved to define the analytical transfer functions, such that:

$$\frac{Y}{\Delta} = D^{-1}C \tag{4.61}$$

4.4 Model Validation

Equation (4.61) is solved in MATLAB using the vehicle parameters listed in Chapter 2 to derive the transfer functions. Equation (4.62), as an example, describes the general form of the analytical transfer function relating steering angle to the semitrailer sprung mass roll angle, while its coefficients are listed in Table 4.1. The pole-zero map of the analytical transfer function is shown in Figure 4.1, and Table 4.2 summarizes the values of poles, zeros and the gain. The results clearly show the stability of the transfer function corresponding to the baseline vehicle, as observed from the pole-zero map, and real components of the poles.

$$G_{\Phi_{s_2}}(s) = \frac{\Phi_{s_2}(s)}{\Delta(s)} = \frac{A_{16}s^{16} + A_{15}s^{15} + \cdots + A_2 s^2 + A_1 s + A_0}{s^{18} + B_{17}s^{17} + B_{16}s^{16} + \cdots + B_2 s^2 + B_1 s + B_0} \tag{4.62}$$

Table 4.1: Coefficients of analytical transfer function.

A_0	-4.5839e+025	A_9	-8.1600e+014	B_0	8.0754e+025	B_9	1.0346e+018
A_1	-3.1469e+024	A_{10}	-1.0676e+013	B_1	9.4037e+025	B_{10}	2.3719e+016
A_2	-5.4802e+024	A_{11}	-9.0020e+010	B_2	5.5958e+025	B_{11}	4.1120e+014
A_3	-8.4501e+023	A_{12}	-7.5645e+008	B_3	1.5906e+025	B_{12}	6.5492e+012
A_4	-1.2374e+023	A_{13}	-3.1832e+006	B_4	2.9831e+024	B_{13}	7.9242e+010
A_5	-4.2398e+021	A_{14}	-1.4555e+004	B_5	3.8434e+023	B_{14}	8.8552e+008
A_6	-1.4943e+020	A_{15}	16.6094	B_6	2.7942e+022	B_{15}	7.1043e+006
A_7	-3.0392e+018	A_{16}	0.0691	B_7	1.1477e+021	B_{16}	5.3241e+004
A_8	-6.1256e+016			B_8	4.0993e+019	B_{17}	230.9788

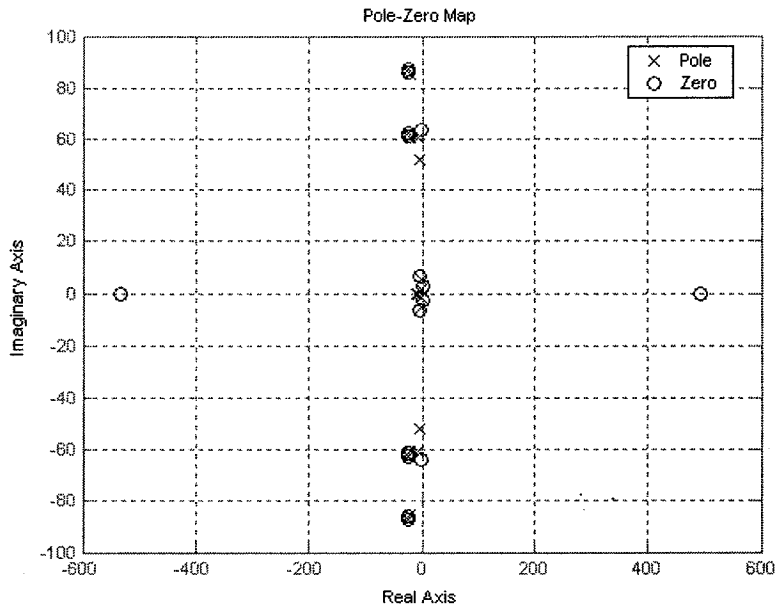

Figure 4.1: Pole-zero map of the analytical transfer function $G_{\Phi_{s_2}}$.

Table 4.2: Values of zeros, poles and the gain of the analytical transfer function.

Poles		**Zeros**	
-24.2492 ± 87.2522i	-5.0701 ± 51.9695i	-532.7544	-25.0791 ± 62.2382i
-22.1080 ± 85.3078i	-10.1493	493.8908	-24.2174 ± 61.3193i
-24.9767 ± 62.2282i	-1.3959 ± 5.5499i	-24.2487 ± 87.2532i	-3.9795 ± 6.3251i
-20.5391 ± 60.6393i	-6.2942	-23.6844 ± 86.2743i	0.4710 ± 2.9178i
-7.6665 ± 60.6146i	-1.2621 ± 1.2798i	-0.0009 ± 63.4241i	
Gain = 0.0691			

There are many definitions of stability in the control system literature, the most common one used for transfer functions is the bounded-input-bounded-output stability (BIBO), which states that for a BIBO stable system, for any bounded input, or finite amplitude input, the output of the system will also be bounded. Stability of a system is characterized by the location of its poles in the complex s-plane, meanwhile zeros characterize the system's transient responses. The complex poles always come in pairs, which imaginary parts dominate the oscillatory nature

of the system. An unstable system must have positives poles, which are in the right-hand side of the s-plane. As shown in Table 4.2 the real parts of the poles for the system represented by Equation (4.62) are all negative, and therefore the system is stable.

The step-response of the analytical transfer function is compared with that of the Yaw/Roll model for its validation as steady-state cornering maneuver is selected for estimating the unknown c.g. height. The comparison of simulation results of two models is presented in Figure 4.2, from which we can see that the response generated by the analytical transfer function is lower than that of the Yaw/Roll model. For validating the simplified analytical model the transfer functions relating steering angle and other vehicle dynamic responses are also derived and a complete comparison with the Yaw/Roll model is given in APPENDIX C.

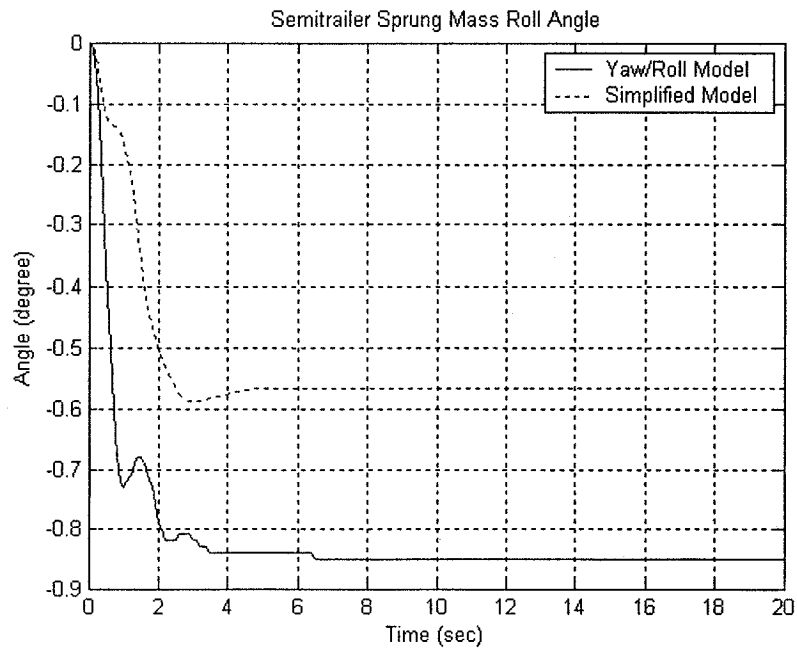

Figure 4.2: Analytical transfer function vs Yaw/Roll model comparison (semitrailer sprung mass roll angle).

4.5 Summary

In this chapter the analytical model of five-axle tractor-semitrailer is linearized and transferred to the Laplace domain for the derivation of analytical transfer functions. The analytical transfer functions are validated by comparing the responses with those derived from the Yaw/Roll model under a step steering input. This input is particularly important, since it closely represents a steady-state cornering maneuver that is desirable for estimating the unknown c.g. height. The analytical transfer function gives a conserved prediction of the semitrailer sprung mass roll angle when compared to that from the Yaw/Roll model. Therefore for an accurate estimation of the unknown c.g. height, this analytical transfer function must be compensated to make it close the Yaw/Roll model.

CHAPTER 5 ESTIMATION OF SEMITRAILER SPRUNG MASS CG HEIGHT

5.1 Introduction

System Identification techniques have been widely applied for deriving a reasonable estimates of variable vehicle and human driven parameters [32]. The parameter identification essentially involves the formulation of a true transfer function on the basis of known or measured information and comparison with the analytical transfer function of the system in terms of the coefficients. As the coefficients of analytical transfer function relate to known and/or unknown vehicle parameters, the comparison allow for estimations of the unknown vehicle parameters. The linearized transfer function relating the desired semitrailer sprung mass roll angle response to the steer angle could be applied together with the measured data attained under a prescribed maneuver to identify the unknown c.g. height.

In this chapter, the system identification technique is applied to obtain the transfer function from steering angle to semitrailer sprung mass roll angle for estimating the c.g. height of semitrailer sprung mass. First the system identification algorithm is validated with time-series data by comparing the identified transfer function with the original transfer function used for generating the data. The time-series data is composed of two parts: input data and output data. The robustness of the algorithm is examined with noise added to the output data. The c.g. height estimation algorithm is developed and validated using the data generated from the analytical transfer function with a known c.g. height.

Finally the Yaw/Roll model is used to simulate a real vehicle system for generating the idealized test data, which is applied to identify the true transfer function. The accuracy of the c.g. height estimating algorithm is further examined.

5.2 System Identification Problem

System identification is about building dynamic models which describe relationships between measured input and output signals. In most cases, the outputs are also affected by extraneous signals other than the measured inputs. The relationship among input, output and noise, representing the contributions due to the extraneous signal, can be depicted by Figure 5.1.

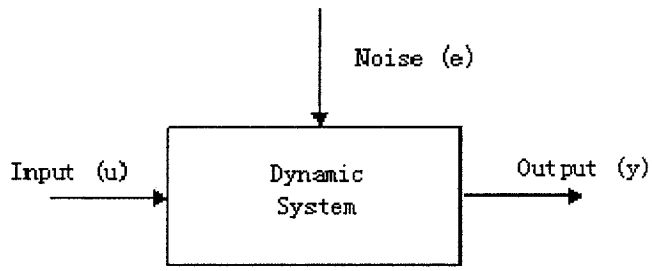

Figure 5.1: Input signal, output signal and noise.

The relationship between the input and the output can be described mathematically by linear difference equation, among which the most used model structure is ARX model as given below:

$$\begin{aligned} &y(t)+a_1 y(t-1)+\cdots+a_{na} y(t-na)= \\ &b_1 u(t-nk)+\cdots+b_{nb} u(t-nk-nb+1)+e(t) \end{aligned} \tag{5.1}$$

where na and nb are the orders of the respective polynomials. The number nk is the number of delays from input to output. The ARX model structure is thus

determined by vector $[na \quad nb \quad nk]$, and the predicted system response $\hat{y}(t)$ is a function of coefficient vector $x = [a_1, a_2, \cdots, a_{na}, b_1, b_2, \cdots, b_{nb}]^T$, when model structure and observed input-output data, $u(t)$ and $y(t)$, are given under a defined or assumed range of signal noise $e(t)$. The system identification problem thus involves the determination of a set of coefficients x to ensure that the error between the predicted response $\hat{y}(t)$ and the observed $y(t)$ is minimal. The error minimization is frequently performed using optimization algorithms. The minimization problem may be formulated to minimize the sum of squared errors corresponding the number of observations, such that:

$$\min_{x \in \Re^{na+nb}} f(x) = \sum_{i=1}^{n} [\hat{y}(x, t_i) - y(t_i)]^2 \tag{5.2}$$

where $f(x)$ is the error function and n represents the total number of observations at instants t_i $(i = 1, 2, \cdots, n)$. In this dissertation the MATLAB System Identification Toolbox is used for solving the problem.

5.3 Rounded Step Signal

For the purpose of system identification, the system has to be excited using test signals. An optimal test signal can be defined as the signal with prescribed maximum amplitude that yields the required knowledge with specified accuracy in a minimum length of time [42]. Although an input signal that approaches the properties of the impulse function is considered as an ideal signal as it yields a flat power spectrum over a wide band of frequencies, an input test signal approximating a step signal is more practical due to difficulties associated with

generation of an ideal impulse. A rounded step signal, described below, is used for exciting the vehicle system in this dissertation,

$$\delta(t) = 2\delta_m\left(2^{-e^{-at}} - 0.5\right) \tag{5.3}$$

where δ_m is the magnitude of steering angle and a is a constant which can be adjusted to make the curve to approximately follow a step function of the form:

$$\delta(t) = \begin{cases} 0, & t \le 0 \\ \delta_m, & t > 0 \end{cases} \tag{5.4}$$

5.4 Compensation Function of Analytical Transfer Function

An analytical transfer function relating the steering angle to the semitrailer sprung mass roll angle was developed in CHAPTER 4. The response characteristics of the transfer functions were compared with those derived from the well known Yaw/Roll model. The comparisons revealed that the linearized function predicts a relatively lower roll angle than the Yaw/Roll model. The difference between the results of the transfer function and the Yaw/Roll model could be attributed to many simplifications considered in the model used in this study and linearization. The analytical transfer function thus needs to be adequately compensated in order to achieve reasonable correlation with the Yaw/Roll model and to obtain more accurate c.g. height estimation. The target of the compensation is to make the output from the analytical transfer function agree reasonably well with that from the Yaw/Roll model, which is used to simulate a real vehicle. The concept underlying the development of a compensation function is shown in Figure 5.2.

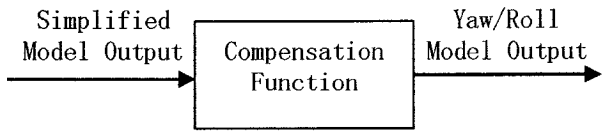

Figure 5.2: Compensation function.

The step input signal, described in Equation (5.3), is applied to both the Yaw/Roll model and the simplified model for generating the test data. The work data for system identification consists of the outputs from the two models, where the output from the simplified model works as input and the output from the Yaw/Roll model as the output for the compensation function to be identified. The compensated analytical transfer function is described as:

$$G_c(s) = F(s) * G(s) \tag{5.5}$$

where $G_c(s)$ is the compensated analytical transfer function, $F(s)$ is the compensation function and $G(s)$ is the analytical transfer function given in Equation (4.62) derived from the simplified model.

The validity of the compensated analytical transfer function is then examined using the structure indicated in Figure 5.3. The same step input signal is used to excite the Yaw/Roll model and the compensated analytical transfer function $G_c(s)$, and the dynamic semitrailer sprung mass roll angle responses from the two models are compared to examine the validity of the compensation function.

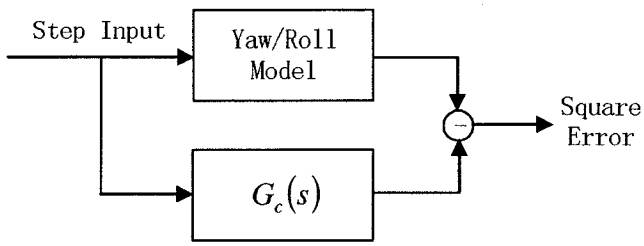

Figure 5.3: Validation of the compensated analytical transfer function.

The compensation functions of orders ranging from 1 to 6 are identified, and summarized in Table 5.1. The table also presents the magnitude of the squared errors, where tends to be lowest for the third order compensation function. A higher order compensation function yields significant transient error, as it is evident from the comparisons of the roll angle responses of the target Yaw/Roll model, the linearized transfer function and the compensated transfer function, presented in Table 5.1.

Table 5.1: Identified compensation functions and their validity.

Order	Compensation Function $F(s)$	Square Error (degree^2)	Response to Step Input
1	0.2944 s + 3.274 ---------- s + 2.163	0.0304	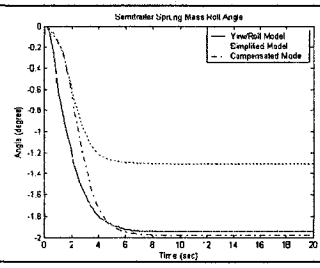
2	0.2917 s^2 + 3.364 s + 5.287 ---------- s^2 + 1.493 s + 3.607	0.0142	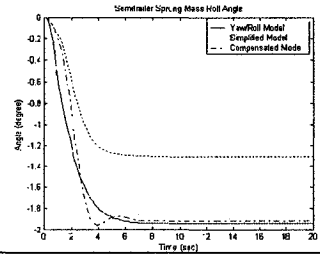
3	1.356 s^3 + 16.5 s^2 + 24.28 s + 29.55 ---------- s^3 + 3.201 s^2 + 10.87 s + 19.84	0.0016	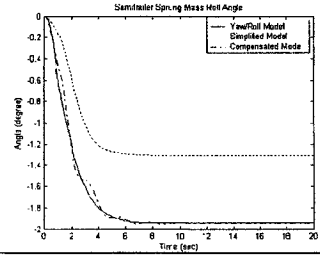
4	5.581 s^4 + 27.7 s^3 + 76.47 s^2 + 109.2 s + 54.29 ---------- s^4 + 5.058 s^3 + 17.03 s^2 + 40.27 s + 36.53	0.0141	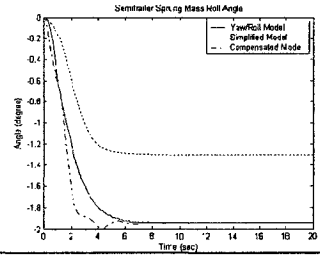
5	9.015 s^5 - 99.87 s^4 + 1923 s^3 + 7028 s^2 + 1.117e004 s + 1.6e004 ---------- s^5 + 13.06 s^4 + 749.7 s^3 + 2067 s^2 + 7698 s + 1.076e004	0.0087	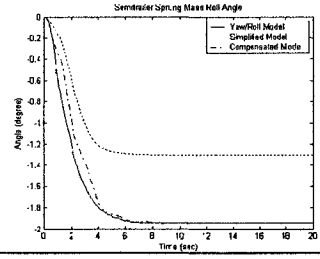
6	20.73 s^6 + 156.3 s^5 + 1.212e004 s^4 + 4.017e004 s^3 + 1.306e005 s^2 + 2.086e005 s + 4.974e004 ---------- s^6 + 23.34 s^5 + 617.5 s^4 + 3823 s^3 + 1.191e004 s^2 + 3.031e004 s + 3.35e004	0.4041	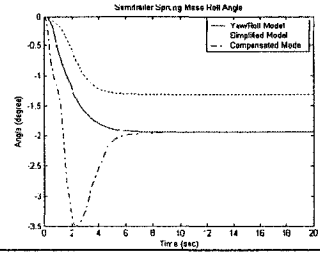

The results show that the order 3 compensation function makes the analytical transfer function corrected well with results from the Yaw/Roll model, and a higher order compensation function does not necessarily mean producing a better compensated analytical transfer function. The order 3 ARX model structure is thus selected for modeling the compensation function and the compensated analytical transfer function, given by:

$$G_c(s) = \frac{\Phi_{s_2}(s)}{\Delta(s)} = \frac{A_{19}s^{19} + A_{18}s^{18} + \cdots + A_2 s^2 + A_1 s + A_0}{s^{21} + B_{20}s^{20} + B_{19}s^{19} + \cdots + B_2 s^2 + B_1 s + B_0} \tag{5.6}$$

where the values of the coefficients of the transfer function are summarized in Table 5.2.

Table 5.2: Coefficients of the compensated analytical transfer function.

A_0	-1.35E+27	A_{11}	-9.68E+16	B_0	1.60E+27	B_{11}	4.46E+19
A_1	-1.21E+27	A_{12}	-1.28E+15	B_1	2.74E+27	B_{12}	1.11E+18
A_2	-9.95E+26	A_{13}	-1.60E+13	B_2	2.39E+27	B_{13}	2.51E+16
A_3	-2.72E+26	A_{14}	-1.35E+11	B_3	1.31E+27	B_{14}	4.33E+14
A_4	-1.19E+26	A_{15}	-1.08E+09	B_4	5.05E+26	B_{15}	6.81E+12
A_5	-2.45E+25	A_{16}	-4.56E+06	B_5	1.47E+26	B_{16}	8.21E+10
A_6	-3.30E+24	A_{17}	-1.95E+04	B_6	3.02E+25	B_{17}	9.09E+08
A_7	-2.42E+23	A_{18}	2.37E+01	B_7	4.54E+24	B_{18}	7.28E+06
A_8	-8.29E+21	A_{19}	9.37E-02	B_8	4.87E+23	B_{19}	5.40E+04
A_9	-2.54E+20			B_9	3.21E+22	B_{20}	2.34E+02
A_{10}	-5.15E+18			B_{10}	1.29E+21		

5.5 Reduction of High-Order System

As the high order of the compensated analytical transfer function poses a tedious task of computation, it would be desirable to derive a low-order model from it, which provides a reasonably good approximation to the original system. A

great deal of work has been done during the last 20 years on the subject of obtaining low-order models from high-order systems, and the tremendous different approaches can be divided into three main groups [43]. The first group of methods attempts to retain the dominant eigenvalues of the original system and the obtained low-order system responses to certain inputs in the same way as the high-order system. The second group of methods is based on obtaining a low-order model such that its responses to impulse- or step-inputs correlates with those of the original system with no restriction on the location of the eigenvalues. The third group of methods is based on matching some other properties of the responses. It has been suggested that a high-order transfer function used to describe a given system can be expanded into a continued fraction. A low-order transfer function may then be obtained by neglecting some of quotients in the expanded transfer function [44]. Consider a transfer function $T(s)$ of order n, given by:

$$T(s)=\frac{b_1 s^{n-1}+b_2 s^{n-2}+\cdots+b_n}{s^n+a_1 s^{n-1}+a_2 s^{n-2}+\cdots+a_n} \tag{5.7}$$

The polynomials in the above transfer function are rewritten in the ascending order, such that:

$$T(s)=\frac{b_n+b_{n-1}s+\cdots+b_2 s^{n-2}+b_1 s^{n-1}}{a_n+a_{n-1}s+\cdots+a_2 s^{n-2}+a_1 s^{n-1}+s^n} \tag{5.8}$$

The above transfer function may then be expanded into a continued fraction of the form:

$$T(s)=\cfrac{1}{H_1+\cfrac{1}{\cfrac{H_2}{s}+\cfrac{1}{H_3+\cfrac{1}{\cfrac{H_4}{s}+\ddots}}}}} \tag{5.9}$$

where $H_1, H_2, \cdots$ represent the constants related to the order of the transfer function. The order of the transfer function may be reduced by neglecting some quotients. For instance, a second-order transfer function can be obtained by ignoring the remaining quotients, such that the reduced transfer function can be expressed as:

$$T_2(s)=\cfrac{1}{H_1+\cfrac{1}{\cfrac{H_2}{s}+\cfrac{1}{H_3+\cfrac{1}{\cfrac{H_4}{s}}}}} \tag{5.10}$$

where $T_2(s)$ is the reduced second order transfer function, which can be simplified to yield:

$$T_2(s)=\frac{(H_2+H_4)s+H_2H_3H_4}{s^2+[H_1(H_2+H_4)+H_3H_4]s+H_1H_2H_3H_4} \tag{5.11}$$

This technique is applied in an attempt to simplify the compensated analytical transfer function $G_c(s)$ by reducing its order. The simplified transfer functions of different orders are obtained and evaluated by comparing their step responses with that of the original system, described by $G_c(s)$. Figure 5.4 displays the concept of validating the order reduced compensated analytical transfer function, under the application of a step input signal, described in Equation (5.3).

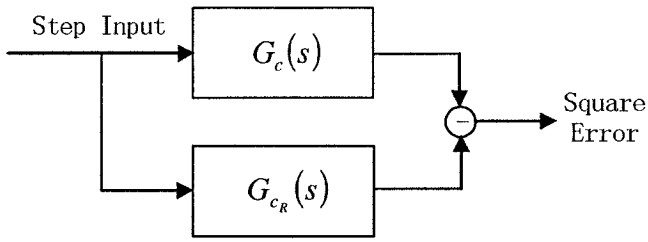

Figure 5.4: Validation of order reduced compensated analytical transfer function $G_{c_R}(s)$.

Different orders of reductions were performed using the methodology outlined in [44]. The validity of each reduction was examined by comparing the semitrailer sprung mass roll angle response of the reduced transfer function, $G_{c_R}(s)$, with that of the compensated transfer function, $G_c(s)$. Table 5.3 presents the order reduced transfer functions obtained by considering the model order of 0 to 5. Although higher order model were also attempted, the results are limited to order 5 only since no significant further improvement in the roll response was observed for the higher order models. The table also summarizes the magnitudes of squared errors between the roll responses of the original and reduced-order compensated transfer function. The step responses of the reduced-order transfer functions in terms of the semitrailer sprung mass roll angle are also compared with that of the original transfer function, $G_c(s)$. The results are also shown in Table 5.3.

Table 5.3: Different orders of the reduced compensated analytical transfer functions and their validities.

Order	Reduced-order Transfer Function	Square Error (degree^2)	Response to Step Input
0	-0.8456	0.0334	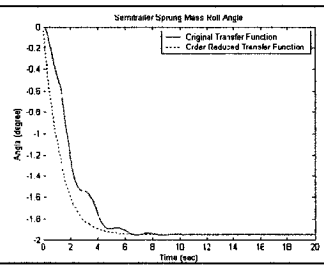
1	0.03267 s - 1.029 ---------- 0.9614 s + 1.216	9.7715e-004	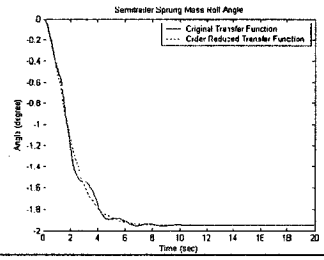
2	0.2204 s^2 - 7.905 s - 1.962 ---------- 7.485 s^2 + 11.26 s + 2.32	9.7995e-004	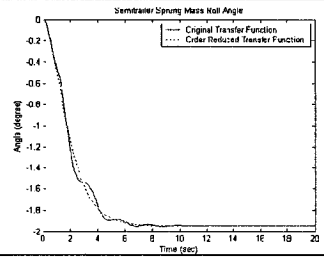
3	0.04003 s^3 - 0.41 s^2 - 0.5328 s – 0.5307 ---------- 0.3596 s^3 + 1.019 s^2 + 1.146 s + 0.6275	9.3233e-004	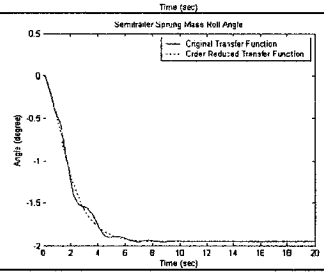
4	-0.07295 s^4 + 0.03231 s^3 – 2.038 s^2 - 2.642 s - 4.123 ---------- 0.3446 s^4 + 1.962 s^3 + 5.107 s^2 + 7.133 s + 4.876	7.2353e-004	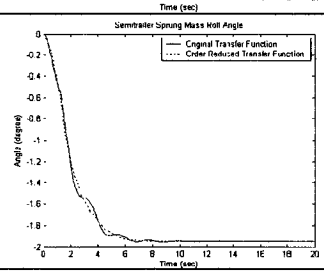
5	0.1157 s^5 - 1.181 s^4 + 0.4086 s^3 – 11.02 s^2 - 12.62 s - 23.47 ---------- 0.4533 s^5 + 2.668 s^4 + 10.26 s^3 + 26.02 s^2 + 37.74 s + 27.75	6.9315e-005	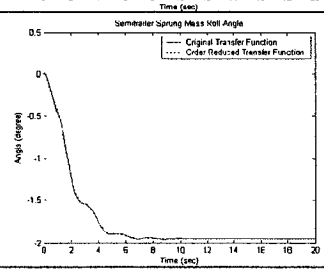

The results indicate that expressing the original compensated analytical transfer function by a fifth-order transfer function yields satisfactory results in terms of the semitrailer sprung mass roll angle response to a step steering input. A reduced-order compensated analytical transfer function is thus formulated as:

$$G_{c_R}(s) = \frac{\Phi_{s_2}(s)}{\Delta(s)} = \frac{A_5 s^5 + A_4 s^4 + A_3 s^3 + A_2 s^2 + A_1 s + A_0}{s^5 + B_4 s^4 + B_3 s^3 + B_2 s^2 + B_1 s + B_0} \tag{5.12}$$

where,

A_0	A_1	A_2	A_3	A_4	A_5
-51.7785	-27.8430	-24.3105	0.9015	-2.6063	0.2554
B_0	B_1	B_2	B_3	B_4	
61.2322	83.2666	57.4175	22.6413	5.8858	

The reduced-order transfer function, described in Equation (5.12), can facilitate the implementation for the online assessment of c.g. height, when the estimation is based upon the measure of semitrailer sprung mass roll angle under a rounded step cornering maneuver. The validity of the reduced transfer function, however, needs to be examined under a range of test condition.

5.6 CG Height Estimation Algorithm and Validation

The analytical transfer function for the prediction of the semitrailer sprung mass roll angle can be established using the simplified vehicle model developed in Chapter 4. Its coefficients are functions of various vehicle parameters, where the semitrailer sprung mass c.g. height is considered as the only unknown parameter. The simulation results revealed that the analytical transfer function yields an under estimate of the semitrailer sprung mass roll angle than when

compared to that derived from the proven Yaw/Roll model, due to the many simplifications considered in the model development. Further more, a heavy vehicle may exhibit parameter changes may change during the usage of the vehicle, for instance, suspension stiffness and tire stiffness. The analytical transfer function thus needs to be compensated in order to achieve a reasonable estimation of the unknown c.g. height, when variations in some of the vehicle parameters are considered. The compensation functions, defined in Table 5.1, can be considered applicable for the baseline vehicle considered with parameters defined in Chapter 2. The development of a generally applicable c.g. height estimation algorithm would require considerable systematic efforts to derive a robust transfer function that could be considered valid when one or more key parameters of the vehicle are varied. The key parameters refer to those to which relatively high sensitivity of a measured response is observed. The results presented in CHAPTER 2 revealed that the desired semitrailer sprung mass roll angle response would be sensitive to deviations in the lateral coordinate of the payload c.g., and suspension and tire properties. The efforts in this dissertation research are limited to the development of the methodology and the algorithm, while the variations are limited to the unknown c.g. height. Furthermore, the Yaw/Roll model results are considered as the measured data due to lack of available measured data. The robustness of the algorithm, however, is examined for different levels of signal-to-noise ratio (SNR) and wide variations in the c.g. height. The methodology involves the identification of the true transfer function relating the measured (Yaw/Roll model results) semitrailer sprung mass roll angle

response to a rounded step steering input. The unknown semitrailer sprung mass c.g. height is then estimated by comparing the coefficients of the reduced-order compensated analytical transfer function and the one built from test data. An overview the c.g. height estimation algorithm is described in Figure 5.5.

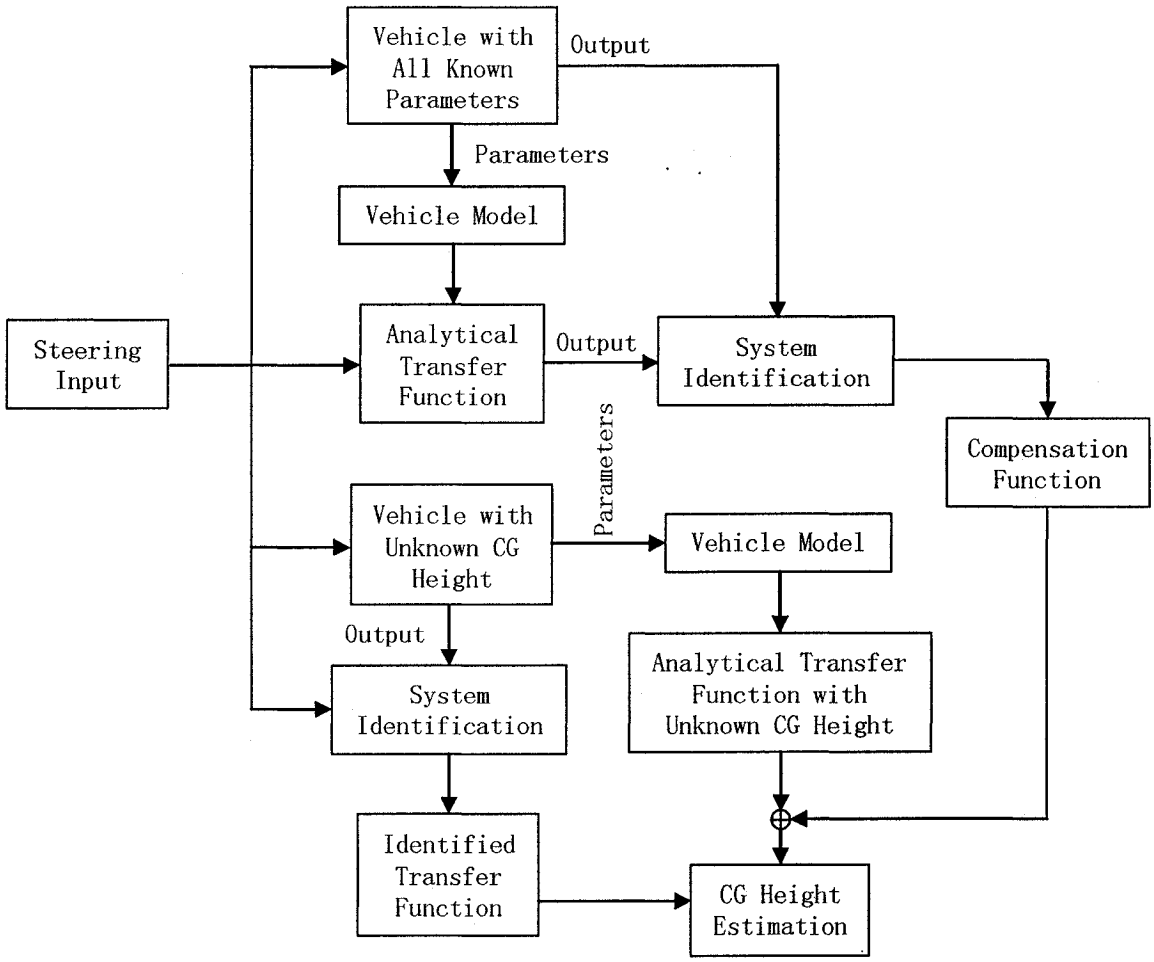

Figure 5.5: CG height estimation algorithm.

5.6.1 Sensitivity of transfer function coefficients to input signal

The influence of the input signal on the identified transfer function and thus the system identification algorithm is examined by varying the rate of change of

the steering input. As shown in Figure 5.6, the transfer function $G_i(s)$ is identified using the data set generated from the reduced-order compensated analytical transfer function $G_{c_R}(s)$, defined in Equation (5.12). The validity of the identified transfer function $G_i(s)$ is then examined by comparing its response with that of the original transfer function $G_{c_R}(s)$ under varying inputs.

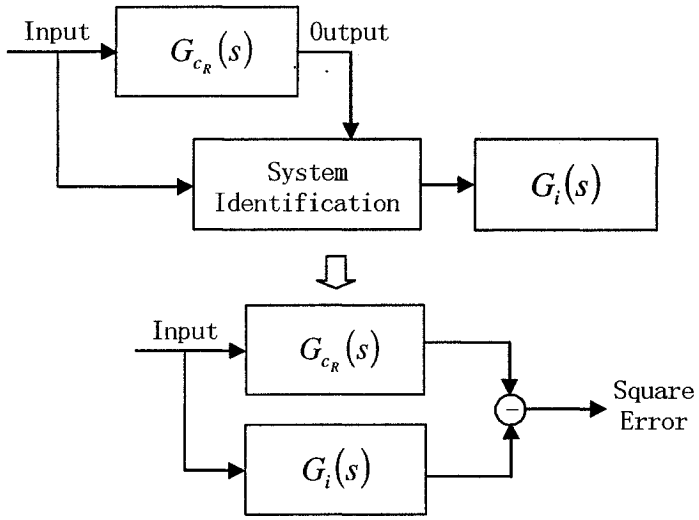

Figure 5.6: Sensitivity to input signal of system identification algorithm.

The input signal, described in Equation (5.3), is applied, where the constant a is adjusted to generate different sets of input-output data for system identification. It should be noted that the variations in constant a would yield different rate of change of the steering input in the vicinity of $t=0$, as evident in Table 5.4. A higher value of a yields rapid change in the steering, which may not be practically realizable in a test course. Table 5.4 also presents the identified transfer functions corresponding to different step inputs, while the order is limited to 5. The results show that the coefficients of the identified transfer function are

quite sensitive to the input signal used to excite the system, and they do not necessarily match the corresponding ones of the original transfer function used for generating the test data in order to give a reasonable good fit of the output under the step input signal. The steady state value of the transfer function, ratio A_0 / B_0, however remains relatively unchanged under the first four variations in a (1 to 4). This would more clearly represent a steady state turning maneuver.

Table 5.4: Influence of input signal to system identification algorithm.

Input Signal	Identified Transfer Function	Response to Step Input
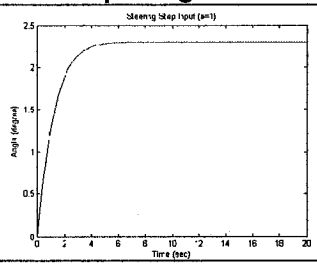	-0.116 s^5 - 1.358 s^4 - 1.767 s^3 - 15.7 s^2 - 16.65 s - 39.79 --- s^5 + 3.263 s^4 + 16.96 s^3 + 32.25 s^2 + 56.41 s + 47.04	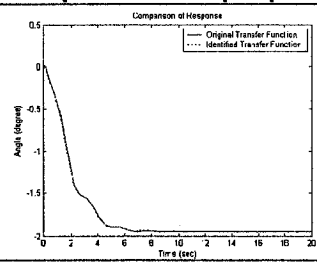
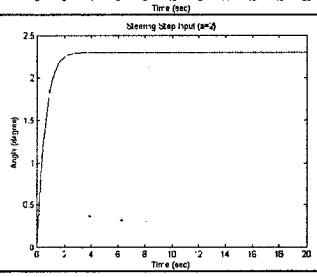	-0.1143 s^5 - 1.356 s^4 - 2.178 s^3 - 15.84 s^2 - 19.65 s - 45.89 --- s^5 + 3.285 s^4 + 18.13 s^3 + 34.25 s^2 + 65.68 s + 54.23	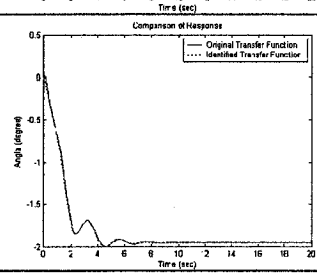
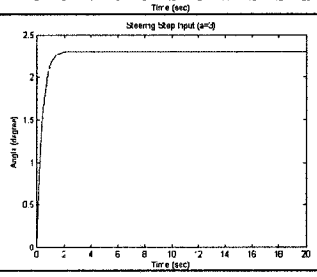	-0.1124 s^5 - 1.352 s^4 - 2.56 s^3 - 15.94 s^2 - 22.52 s - 51.33 --- s^5 + 3.318 s^4 + 19.21 s^3 + 36.16 s^2 + 74.21 s + 60.66	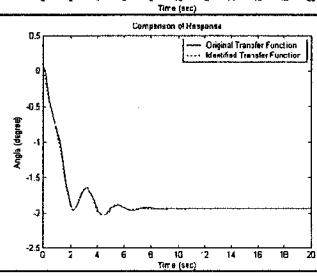
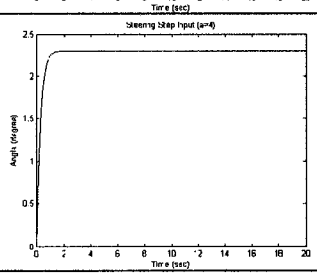	-0.1104 s^5 - 1.345 s^4 - 2.901 s^3 - 15.99 s^2 - 25.15 s - 55.94 --- s^5 + 3.359 s^4 + 20.17 s^3 + 37.91 s^2 + 81.68 s + 66.1	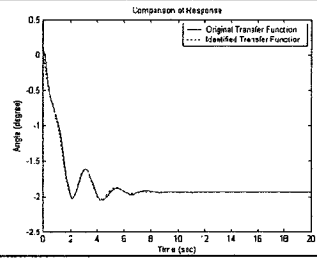
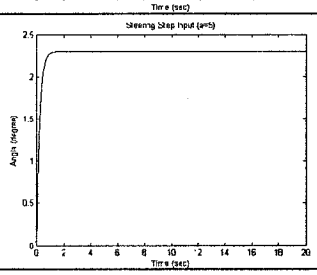	-0.1085 s^5 - 1.337 s^4 - 3.201 s^3 - 16.01 s^2 - 27.51 s - 59.84 --- s^5 + 3.405 s^4 + 20.99 s^3 + 39.48 s^2 + 88.18 s + 70.7	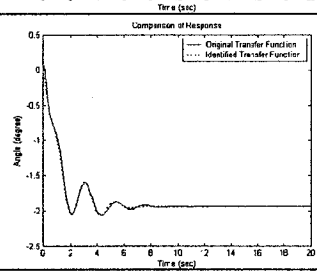
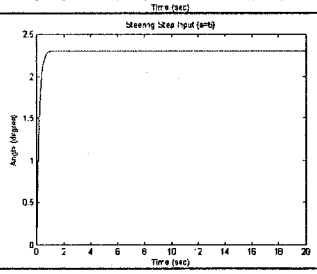	-0.1066 s^5 - 1.33 s^4 - 3.465 s^3 - 16.01 s^2 - 29.61 s - 63.15 --- s^5 + 3.45 s^4 + 21.72 s^3 + 40.88 s^2 + 93.83 s + 74.61	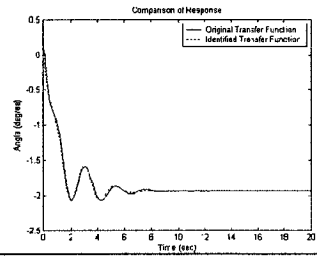

5.6.2 CG height estimation algorithm

The sensitivity of the coefficients of the identified transfer function to variations in the input signal posed considerable difficulties in applying the algorithm suggested by Yang [32] for estimating the unknown semitrailer sprung mass c.g. height. In his algorithm the coefficients of the identified transfer function are supposed to be equal to the corresponding ones of the original transfer function. The unknown vehicle parameters are thus derived by solving the following group of equations:

$$\begin{cases} A_i = A_i' \\ B_j = B_j' \end{cases} \tag{5.13}$$

where A_i, B_j and A_i', B_j' are the coefficients of the analytical and identified transfer functions, respectively.

A transfer function of the form used in this study is a low pass filter by nature. For the vehicle system excited with a step input signal the steady state of the system is most concerned, which property is reflected by the ratio of A_0 / B_0, where A_0 and B_0 are defined in Equation (5.12). Mathematically, for two transfer functions given below:

$$G_1(s) = \frac{A_{1m_1} s^{m_1} + \cdots + A_{11} s + A_{10}}{s^4 + B_{1n_1} s^{n_1} + \cdots B_{11} s + B_{10}}, \quad G_2(s) = \frac{A_{2m_2} s^{m_2} + \cdots + A_{21} s + A_{20}}{s^4 + B_{2n_2} s^{n_2} + \cdots B_{21} s + B_{20}} \tag{5.14}$$

a reasonable good agreement between their outputs in the steady state under the same step input would imply that:

$$A_{10} / B_{10} = A_{20} / B_{20} \tag{5.15}$$

The above would hold irrespective of the orders of the two transfer functions

and the values of their coefficients. This relationship can be examined with the identified transfer functions presented in Table 5.4. The ratios A_0 / B_0 of the different identified transfer functions are compared and summarized in Table 5.5. Although each identified transfer function exhibits different values of the coefficients, the ratio A_0 / B_0 is convergent at the ratio value of the original transfer function used for generating the test data, irrespective of the type of input used. This ratio relates to the steady state response and thus the peak value of the roll angle response.

Table 5.5: Comparisons of ratio A_0 / B_0 of the transfer functions attained under different step inputs.

		A_0	B_0	A_0 / B_0
Original Transfer Function (5.12)		-51.7785	61.2322	-0.8456
Identified Transfer Function	a=1	- 39.79	47.04	-0.8459
	a=2	- 45.89	54.23	-0.8462
	a=3	- 51.33	60.66	-0.8462
	a=4	- 55.94	66.1	-0.8463
	a=5	- 59.84	70.7	-0.8464
	a=6	- 63.15	74.61	-0.8464

For the analytical transfer function the coefficients A_0 and B_0 are functions of the unknown semitrailer sprung mass c.g. height h, that is:

$$A_0 = f_A(h)$$
$$B_0 = f_B(h) \tag{5.16}$$

For the baseline vehicle, defined in Chapter 2, these coefficients of the analytical transfer function were obtained as:

$$A_0 = a_1 h + a_0$$
$$B_0 = b_1 h + b_0 \tag{5.17}$$

where

$$a_0 = -1.9772e + 270$$
$$a_1 = -1.0268e + 270$$
$$b_0 = 1.6703e + 272$$
$$b_1 = -2.9656e + 269$$

are derived from the linearized model program implemented in MATLAB.

Now let R_a, R_c and R_i represent the ratios A_0 / B_0 of the analytical transfer function, compensation function and identified transfer function, respectively. The coefficients of the analytical transfer function, given in Equation (5.17), yields the ratio as:

$$R_a = \frac{a_1 h + a_0}{b_1 h + b_0} \tag{5.18}$$

The compensation function of order 3, defined in Table 5.1, yields the ratio as:

$$R_c = \frac{29.55}{19.84} = 1.4894 \tag{5.19}$$

The above two ratios can be applied to estimate the unknown semitrailer sprung mass c.g. height by solving the following equation:

$$R_c R_a = R_i \tag{5.20}$$

Equation (5.20) is applied to the identified transfer functions given in Table 5.4, and the semitrailer sprung mass c.g. height h solved corresponding to each input. Table 5.6 lists the coefficients A_0 and B_0 of the identified transfer functions, the ratio A_0 / B_0, and the estimated values of c.g. height. Comparisons of the estimated values with the true value of h=1.973 m for the baseline vehicle suggests that the proposed c.g. height estimation algorithm can yield an accurate

estimation of the unknown semitrailer sprung mass c.g. height, irrespective of the step input rate.

Table 5.6: Estimated semitrailer sprung mass c.g. height (without noise).

True Value h =77.68 in (1.973 m)	A_0	B_0	A_0 / B_0	h (in)	Bias (%)
a=1	- 39.79	47.04	-0.8459	77.7147 (1.974 m)	0.04467
a=2	- 45.89	54.23	-0.8462	77.7390 (1.975 m)	0.075953
a=3	- 51.33	60.66	-0.8462	77.7390 (1.975 m)	0.075953
a=4	- 55.94	66.1	-0.8463	77.7470 (1.975 m)	0.086251
a=5	- 59.84	70.7	-0.8464	77.7551 (1.975 m)	0.096679
a=6	- 63.15	74.61	-0.8464	77.7551 (1.975 m)	0.096679

5.6.3 Robustness of the CG height estimation algorithm

The validity of the above described semitrailer sprung mass c.g. height estimation algorithm is further examined with noise added to the output data used for system identification, as shown in Figure 5.7. Table 5.8 lists the coefficients of the identified transfer functions corresponding to different levels of noise added to the output data from $G_{c_R}(s)$. The signal to noise ratio is varied from 5 to 30 dB. It can be seen that the coefficients of the identified transfer function change with the variations in the noise level, but the ratio A_0 / B_0 tends to converge towards that of the original transfer function $G_{c_R}(s)$, defined in Equation (5.12). The table also shows the estimated c.g. height and deviations with respect to the known c.g. height. The estimation error tends to grow under low values of SNR. The results demonstrate the robustness of the c.g. height estimation algorithm to the noise in the test data.

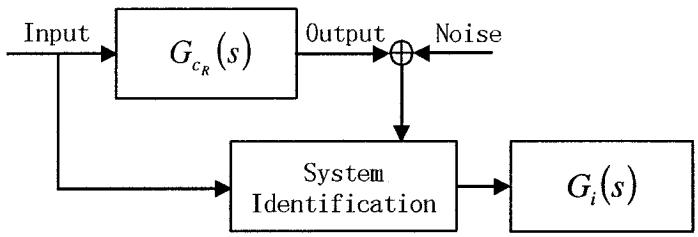

Figure 5.7: Evaluation of the robustness of the c.g. height estimation algorithm to the noise present in the test data.

Table 5.7: Estimated semitrailer sprung mass c.g. height (with noise).

True Value =77.68 in (1.973 m)			A_0	B_0	A_0 / B_0	h (in)	Bias (%)
Original Transfer Function $G_{c_R}(s)$			-51.7785	61.2322	-0.8456	77.69 (1.973 m	0.01
Identified Transfer Function	SNR (dB)	30	- 5428	6439	-0.8430	77.48 (1.968 m)	-0.26
		25	- 1.645e004	1.943e004	-0.8466	77.77 (1.975 m)	0.12
		20	- 7.615e004	9.06e004	-0.8405	77.28 (1.963 m)	-0.51
		15	- 6.921e004	8.175e004	-0.8466	77.77 (1.975 m)	0.12
		10	- 2.716e004	3.256e004	-0.8342	76.77 (1.975 m)	-1.17
		5	- 1.88e005	2.209e005	-0.8511	78.13 (1.985 m)	0.58

Table 5.8: Influence of signal noise on the coefficients of the identified transfer function.

SNR (dB)	Identified Transfer Function	Response to Step Input
30	0.02165 s^5 - 1.637 s^4 - 84.5 s^3 - 599.6 s^2 - 2659 s - 5428 --- s^5 + 13.52 s^4 + 425 s^3 + 3058 s^2 + 7724 s + 6439	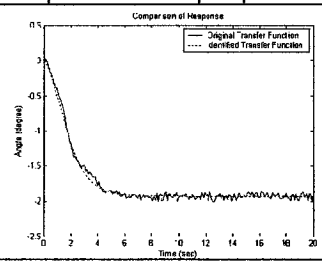
25	0.04855 s^5 - 4.73 s^4 - 240.5 s^3 - 1509 s^2 - 6219 s - 1.645e004 --- s^5 + 27.65 s^4 + 549.7 s^3 + 5733 s^2 + 2.001e004 s + 1.943e004	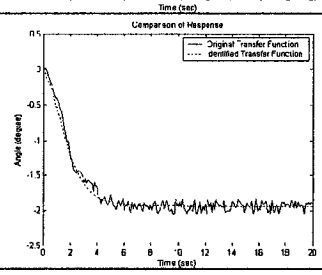
20	-0.01281 s^5 - 8.075 s^4 - 453.2 s^3 - 5275 s^2 - 1.758e004 s - 7.615e004 --- s^5 + 45.71 s^4 + 845.2 s^3 + 1.459e004 s^2 + 7.887e004 s + 9.06e004	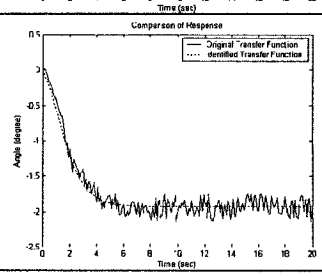
15	0.1578 s^5 - 29.61 s^4 - 1389 s^3 - 6778 s^2 - 2.814e004 s - 6.921e004 --- s^5 + 37.08 s^4 + 733.3 s^3 + 9034 s^2 + 4.702e004 s + 8.175e004	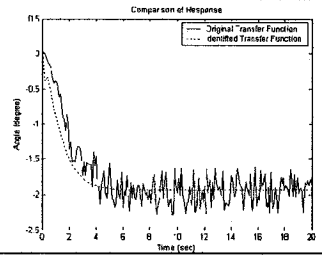
10	0.3871 s^5 - 24.24 s^4 - 955.2 s^3 + 811.8 s^2 - 3.48e004 s - 2.716e004 --- s^5 + 14 s^4 + 478.1 s^3 + 3300 s^2 + 2.374e004 s + 3.256e004	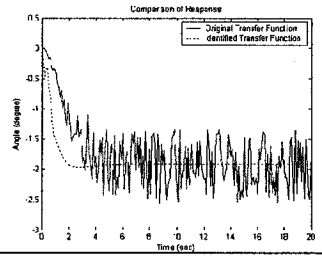
5	-0.2731 s^5 + 14.85 s^4 - 92.06 s^3 - 4225 s^2 + 5.476e004 s - 1.88e005 --- s^5 + 16.34 s^4 + 825.9 s^3 + 7866 s^2 + 1.134e005 s + 2.209e005	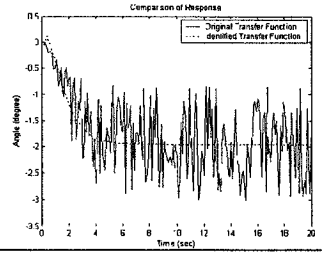

5.7 CG Height Estimation Using Vehicle Response Data

Owing to the lack of available experimental data for testing the c.g. height estimation algorithm, a representative data set is generated using the well known Yaw/Roll model. The baseline vehicle is analyzed under the cornering maneuver performed at a speed of 50 km/h. The response evaluated in terms of semitrailer sprung mass roll deflection is applied to identify a transfer function and c.g. height using the algorithm described in the previous section. The robustness of the estimation algorithm is further examined by introducing different levels of noise to the data set derived from the Yaw/Roll model. The estimated values of the c.g. height for different levels of SNR are compared with the baseline data, which is identical to that derived from the coefficients A_0 and B_0 of the analytical transfer function, described in Equation (5.18). The accuracy of the semitrailer sprung mass c.g. height estimation algorithm is also investigated using the measured responses established from the Yaw/Roll model.

As concluded earlier in Chapter 2, the test maneuver should be selected to generate reasonable magnitude of the response quantity to be measured, while the lateral acceleration should not exceed 0.2 g to ensure safety of the vehicle and the driver. A higher value of lateral acceleration, however, is desirable to produce higher magnitude of the quantity to be measured, such as semitrailer sprung mass roll angle. The maneuver should thus be selected to realize lateral acceleration close to 0.2 g. Furthermore, the steering input required for steady cornering maneuver closely resembles a rounded step input defined in Equation (5.3). The measured response data to be applied in system identification is thus

derived from the Yaw/Roll model under a rounded step steering input at a forward speed of 50 km/h. Figure 5.8 illustrates time histories of the step input, semitrailer sprung mass roll angle, and lateral accelerations of the tractor and semitrailer of the Yaw/Roll model. The vehicle model in Yaw/Roll program is configured on the basis of the baseline vehicle parameters, while the forward speed is held constant at 50km/h. The results show that the semitrailer roll angle and lateral acceleration responses approach steady values after approximately 5 sec, while the peak acceleration is close to 0.2 g. This particularly steering input is thus considered adequate for generating the representative data set for the identification task.

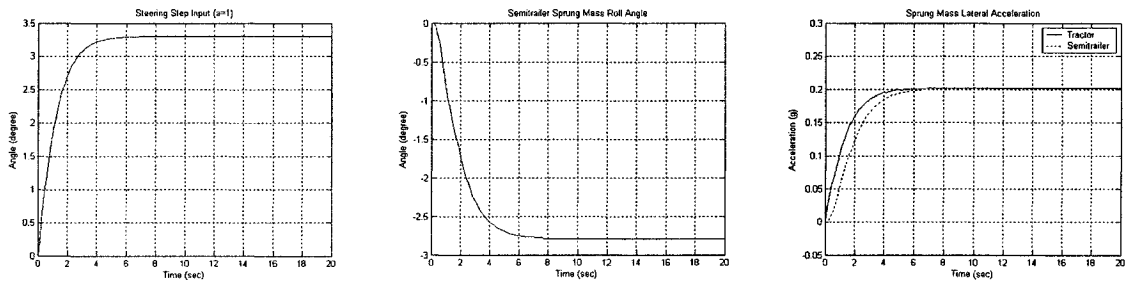

Figure 5.8: Time histories of representative data set generated from the Yaw/Roll model.

The sensitivity of the estimation algorithm to signal noise is investigated by adding different levels of noise to the test data generated from the Yaw/Roll model. Figure 5.9 illustrates the algorithm for estimating the transfer function and thus the c.g. height in the presence of the signal noise. The SNR is varied from ∞ to 5 dB, and the algorithm is applied to identify the transfer function R_i. The analytical transfer function, R_a, and the compensation function, R_c, are then applied to obtain an estimate of the c.g. height, using Equation (5.20), where R_a and R_c

are given in Equations (5.18) and (5.19). The system identification in the presence of the noise is conducted using different orders of ARX model, ranging from 1 to 5. The estimated values of semitrailer sprung mass c.g. heights corresponding to different orders of the ARX model and SNR values are presented in Table 5.9. The table also presents the estimation error in relation to the true value used in the Yaw/Roll model. The simulation results show that the estimation accuracy is not dependent upon the order of ARX model selected for system identification. An increase in the noise level generally yields higher estimation error, although some exceptions exist. A higher order also generally yields lower degree of estimation error.

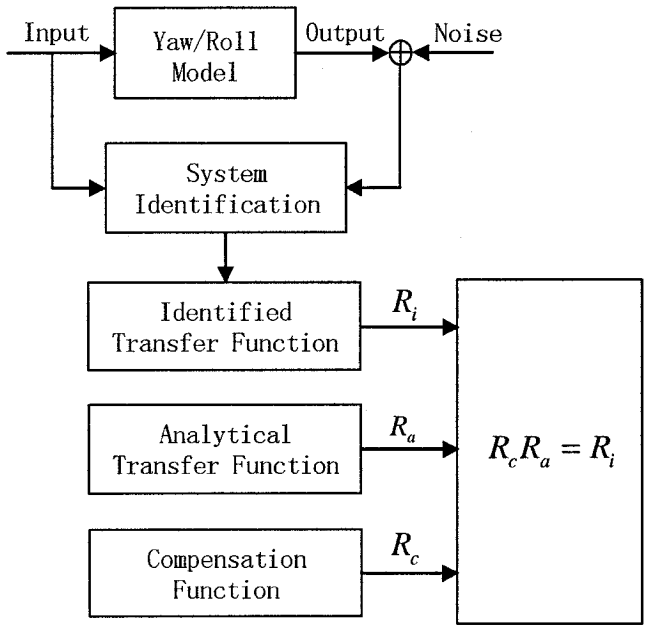

Figure 5.9: CG height estimation algorithm based on the representative data set generated from the Yaw/Roll model.

Table 5.9: The influence of SNR on the effectiveness of the CG height estimation algorithm.

Order	True value	SNR (dB)						
	h=77.68in	∞	30	25	20	15	10	5
1	h (in)	77.6621	77.7982	77.7962	78.1241	75.9020	76.2672	77.0400
	h (m)	1.973	1.976	1.976	1.984	1.928	1.937	1.957
	Bias (%)	-0.0231	0.1522	0.1495	0.5717	-2.2889	-1.8187	-0.8239
2	h (in)	77.7452	77.5138	77.5314	77.3811	77.4894	76.9465	78.5420
	h (m)	1.975	1.969	1.969	1.965	1.968	1.954	1.995
	Bias (%)	0.0839	-0.2139	-0.1912	-0.3847	-0.2453	-0.9442	1.1097
3	h (in)	77.6870	77.6972	77.4536	77.5077	77.0540	76.6206	76.9924
	h (m)	1.973	1.974	1.967	1.969	1.957	1.946	1.956
	Bias (%)	0.0090	0.0221	-0.2914	-0.2218	-0.8059	-1.3637	-0.8852
4	h (in)	77.6860	77.6347	77.5212	77.6079	77.1141	76.9584	79.2048
	h (m)	1.973	1.972	1.969	1.971	1.959	1.955	2.012
	Bias (%)	0.0078	-0.0583	-0.2045	-0.0928	-0.7285	-0.9289	1.9629
5	h (in)	77.6858	77.5512	77.7160	77.6020	76.8246	78.0673	79.0832
	h (m)	1.973	1.970	1.974	1.971	1.951	1.983	2.009
	Bias (%)	0.0075	-0.1658	0.0463	-0.1003	-1.1012	0.4986	1.8063

5.7.1 Sensitivity to variations in the vehicle parameters

A heavy vehicle in service may exhibit considerable deviations in the design and operating parameters from the baseline vehicle. Apart from the payload and c.g. height, which are known to vary most frequently, the suspension and tire properties form the important variations of the second order. The variations in these parameters pose considerable difficulties in applying the proposed algorithm, More specifically, the analytical transfer function (based upon the either the simplified model or the reduced-order) can only be built using either the known or the nominal values of the vehicle parameters. The analytical transfer function may not be considered applicable when considerable changes in the suspension and/or tire properties are encountered. The effect of such variations, however, could be incorporated through the compensation function. It would be desirable to update the compensation transfer function routinely. This task can be

accomplished by performing a test run on the vehicle with the semitrailer either unladen or loaded with known c.g. height. The methodology described in section 5.4 may then be applied to derive an updated compensation function that would adequately account for variations in the vehicle parameters arising from either normal wear or due to changes in some of the component, such as tires, suspension springs and dampers.

In this study, the effect of variations in suspension stiffness on the c.g. height estimation algorithm is considered. The stiffness due to the tractor drive and trailer axles suspensions are varied by ±10, ±20, and ±30% of the baseline values. The responses attained corresponding to these variations in the Yaw/Roll program are applied to update the compensation function for the analytical transfer function, while the order of the function is held as 3, as concluded earlier in section 5.4. Both the original and the updated compensation function corresponding to each variation are presented in Table 5.10. The updated compensation functions reaveal gradual changes in their coefficients, as the deviations in the spring rates progress. The table also presents the estimated c.g. heights on the basis of the original as well as updated compensation functions together with percent errors. It is evident that the application of the basic compensation function yields considerable estimation error when suspension stiffness deviate from the baseline values. The magnitude of the error grows with the magnitude of the deviation. The applications of the updated compensation functions, however, permit for the c.g. height estimation with higher degree of accuracy. The concept of updated compensation functions could also be applied for variations in other

design parameters of the vehicle involving structure modifications, upgrading of the roll stiffness, inflation pressure variations, etc.

Table 5.10: Updated compensation functions and CG height estimations under variations in the suspension stiffness.

Suspension Stiffness Deviation(%)	Baseline Compensation Function	Estimated h (in)	Bias (%)	Updated Compensation Function	Estimated h (in)	Bias (%)
-30	Order 3 Compensation Function in Table 5.1: 1.356 s^3 + 16.5 s^2 + 24.28 s + 29.55 --- s^3 + 3.201 s^2 + 10.87 s + 19.84	92.40 (2.347m)	18.95	1.456 s^3 + 17.33 s^2 + 25.36 s + 28.39 --- s^3 + 2.716 s^2 + 10.29 s + 15.55	77.47 (1.968m)	-0.2
-20		86.58 (2.199m)	11.46	1.396 s^3 + 16.75 s^2 + 24.89 s + 28.38 --- s^3 + 2.869 s^2 + 10.48 s+ 16.78	77.50 (1.969m)	-0.23
-10		81.80 (2.078m)	5.31	1.321 s^3 + 15.86 s^2 + 23.37 s + 26.89 --- s^3 + 2.911 s^2 + 10.53 s + 16.98	77.52 (1.969m)	-0.20
0		77.69 (1.973m)	0.01	1.271 s^3 + 15.36 s^2 + 22.9 s + 26.77 --- s^3 + 3.035 s^2 + 10.68 s + 17.93	77.52 (1.969m)	-0.21
+10		74.21 (1.885m)	-4.47	1.19 s^3 + 14.37 s^2 + 21.29 s + 25.13 --- s^3 + 3.029 s^2 + 10.65 s + 17.73	77.53 (1.969m)	-0.19
+20		70.99 (1.803m)	-8.61	1.184 s^3 + 14.44 s^2 + 21.87 s + 26.19 --- s^3 + 3.201 s^2 + 10.88 s + 19.43	77.57 (1.970m)	-0.14
+30		68.43 (1.738m)	-11.91	1.1 s^3 + 13.33 s^2 + 19.62 s + 23.43 --- s^3 + 3.098 s^2 + 10.76 s + 18.1	77.53 (1.969m)	-0.19

5.7.2 Sensitivity to c.g. height variation

The c.g height estimation algorithm, described in Figure 5.5, involves two steps: (i) formulation of a compensation function on the basis of the measured response of the vehicle with known c.g. height; and (ii) application of the compensated analytical transfer function for predicting the semitrailer sprung mass c.g. height during future operations under arbitrary loading conditions. The analytical transfer function and compensation function are thus derived on the basis of a single known c.g. height. Owing to the nonlinear directional behaviors of the heavy vehicles, the application of compensated function may lead to errors when particular loading conditions involve extreme variations in the c.g. height. The variations in the c.g. height on the effectiveness of the estimation algorithm is thus investigated by generating measured data sets from the Yaw/Roll program for different c.g. heights, ranging from 1.854 m to 2.210 m. The transfer function identified for each measured data set is then used in conjunction with the baseline compensation function to estimate the c.g. height. The baseline compensated analytical transfer function was derived for the baseline c.g. height of 1.973 m. The results, presented in

Table 5.11, show that the estimation error increases as the c.g. height deviates from the baseline value. The peak error, however, remains in the order of 5.5% under extreme variation considered in the study. The results suggest the need for developing a robust compensation function calibrated over the desired range of variations in the c.g. height.

Table 5.11: CG height estimation algorithm sensitivity to c.g. height variation.

True Value (m)	Estimated Value (m)	Bias (%)
1.854	1.797	-3.1078
1.905	1.873	-1.6966
1.973	1.973	0.0075
2.007	2.023	0.8131
2.057	2.097	1.9157
2.108	2.175	3.1803
2.159	2.253	4.3397
1.854	1.797	5.4368

5.8 Summary

System identification technique is applied for the development of semitrailer sprung mass c.g. height estimation algorithm. The analytical transfer function relating the steering angle to the semitrailer sprung mass roll angle, derived from the simplified vehicle model is modified using a compensation function, in order to achieve responses that agree reasonably well with those attained from the widely used Yaw/Roll model. The effectiveness and limitations of the proposed algorithm are demonstrated through consideration of variations in signal-to-noise ratio, suspension properties, and c.g. height.

CHAPTER 6 CONCLUSIONS AND RECOMMENDATIONS FOR FUTURE WORK

6.1 Highlights and Major Contributions

This dissertation research presents a systematic but preliminary effort for estimation of center of gravity height of a semitrailer used in the five-axle tractor-semitrailer configuration. The highlights and notable contributions of the investigation are summarized below:

- A measurable directional dynamic response of the vehicle that is most sensitive to variations in the c.g. height of the semitrailer sprung mass is identified on the basis of parametric analyses. Furthermore, a simple and practically implementable test maneuver in the form of a steady turn is determined for the purpose of the c.g. height estimation.
- The directional dynamics of the five-axle tractor-semitrailer is described by a simplified 10-D.O.F. analytical model, which is further linearized to derive the transfer function relating the steering angle to the identified response, namely the semitrailer sprung mass roll angle.
- The linearized transfer function is reduced to a fifth order function to facilitate its implementation for system identification.
- A compensation function is further identified to account for possible errors caused by model simplification and order-reduction. The validity of the resulting compensated function is demonstrated by comparing the responses with those gained from the well-known Yaw/Roll model. A

methodology for deriving reduced-order compensated function is developed.

- A system identification based methodology is formulated to estimate the c.g. height from the measured data acquired under controlled maneuvers. The effectiveness and limitation of the estimation algorithm are systematically presented and discussed.

6.2 Major Conclusions

Based on the results attained from the study, following major conclusions are drawn:

- The semitrailer sprung mass roll angle response to a steering maneuver exhibits most sensitivity to changes in c.g. height, and may thus be considered for online c.g. identification.
- The roll angle response to a steady-state turning maneuver is considered to be well-suited for estimating the c.g. height. This maneuver ensures safety of the vehicle and driver due to its lower speed, and yields reasonable magnitudes of the semitrailer roll angle.
- The semitrailer sprung mass roll angle response is insensitive to the shape of the payload and thus the roll moment of inertia but moderately sensitive to variations in lateral coordinate of the payload c.g., and suspension and tire properties.
- The vehicle's c.g. height can be directly related to its semitrailer sprung mass roll angle, which can be easily measured.

- The relationship between the semitrailer sprung mass roll angle response and the steering angle could be described by a linearized transfer function of a simplified 10-D.O.F. vehicle model.
- The validity and effectiveness of the linearized reduced-order transfer function could be significantly enhanced through identification and integration of a compensated function.
- The c.g. height of the vehicle can be directly derived from the constant coefficients, A_0 and B_0, of the compensated analytical transfer function.
- The System Identification technique can be effectively applied for estimation of the vehicle c.g. height.
- The coefficients of the identified transfer function are quite sensitive to the input signal used to excite the system to be identified.
- The ratio of the constant term of the numerator to the constant term of the denominator of the identified transfer function remains quite stable, irrespective to variations in the input signals, while the ratio of the two constants directly relates to the c.g. height.
- The unknown vehicle c.g. height can be derived by comparing the ratio of the constant term of the numerator to the constant term of the denominator of the analytical transfer function and the identified transfer function. The estimated c.g. height reveals a strong robustness to the noise present in the test data used for System Identification.
- A calibration procedure can be used to eliminate the influence of variations in various other vehicle parameters on the estimation accuracy of the

vehicle c.g. height.

6.3 Recommendation for Future Work

The study proposes an algorithm for the estimation of c.g. height of a five-axle tractor-semitrailer. A 10-D.O.F. vehicle model is used for the development of the analytical transfer functions, which are considered cumbersome for practical application. The study represents a preliminary effort in the field, and requires considerable efforts, which are suggested below:

- Alternate simple models would be desirable to describe the roll behavior through a reduced-order analytical transfer function to facilitate implementation.
- Alternate methodologies for deriving the compensation function for wide variations in the design and operating conditions would be desirable.
- Further developments in the c.g. height estimation algorithm would necessitate extensive field measured data under varying loading conditions and number of vehicles with different tires and suspensions. The test data would form the vital component for identifying a generally applicable compensation function, and possibly the envelopes describing the range of variations.
- The proposed algorithm needs to be thoroughly tested on the basis of the field-measured data.
- An application program, which can be embedded in the vehicle's PC, should be developed to realize the algorithm.

- The means to integrate the algorithm into the Rollover Warning/Control devices also need to be investigated.

REFERENCES

1. http://www-nrd.nhtsa.dot.gov/pdf/nrd-30/NCSA/TSFAnn/TSF2002EE.pdf.
2. Chrstos, J. P., Guenther, D. A. (1992) "The Measurement of Static Rollover Metrics", SAE 920582.
3. Lund, Y. I., and Bernard, J. E. (1995) "Analysis of Simple Rollover Metrics", SAE paper 950306.
4. Liu, P. J. (1999) "Analysis, Detection and Early Warning Control of Dynamic Rollover of Heavy Freight Vehicles", PhD thesis, Concordia University.
5. Fujio Momiyama, et al. (1999) "Gravity Center Height Estimation for the Rollover Compensation System of Commercial Vehicles", JSAE Review 20 (1999) 493-497.
6. Verma, M. K., and Gillespie, T. D. (1980) "Roll Dynamics of Commercial Vehicles", Vehicle System Dynamics, pp. 1-17.
7. Mallikarjunarao, C. et al. (1982), "Roll Response of Articulated Motor Trucks during Steady-Turning Maneuver", Computation Method in Ground Transportation Vehicles, ASME Winter Annual Meeting, (November), pp. 133-152.
8. Gillespie, T. D. and MacAdam, C.C. (1982), "Constant velocity yaw/roll program: user's manual", Transportation Research Institute, The University of Michigan.
9. Winkler, C. B. et al. (1978), "Testing the Michigan Double-Bottom Tanker", SAE Paper 781066.

10. El-Gindy, M., and Wong, J. Y. (1987), "A comparison of Various Computer Simulation Models for Predicting the Directional Responses of Articulated Vehicles", Vehicle System Dynamics, 16, pp. 249-268.
11. Mueller, T. H.., Depont, J. J., Bass, P. H., (1999) "Heavy Vehicle Stability Versus Crash Rates", Transport Engineering Research New Zealand Limited , http://www.ltsa.govt.nz/publications/docs/stability.pdf
12. Winkler, C. B., et al. (1993) "Repeatability of the Tilt-Table Test Method", SAE paper 930832.
13. Nalecz, A. G. et al. (1993) "An investigation into Dynamic Measure of Vehicle Rollover Propensity", SAE Paper No. 930831.
14. Hinch, J., et al. (1992) "NHTSA's Rollover Rulemaking Program Results of Testing and Analysis", SAE 920581.
15. Preston-Thomas, J. and Woodrooffe, J. H. F. (1990), "A Feasibility Study of A Rollover Warning Device for Heavy Trucks", Transport Canada Publication No. TP 10610, (September).
16. El Gindy, M. (1995) "An Overview of Performance Measures for Heavy Commercial Vehicles in North America", Int. J. of Vehicle Design, Vol. 16, Nos 4/5, pp. 441-463.
17. Piche, A. (1990), "Detection of Onset of Instability for an Early Warning Safety Monitor for Articulated Freight Vehicles", M. Thesis, Concordia University.
18. Chen, B. and Peng, H. (1999a) "Rollover Warning for Articulated Vehicles Based on A Time-To-Rollover Metric", to appear in the Proceedings of the

1999 International Mechanical Engineering Congress and Exposition, (November).

19. Chen, B. and Peng, H. (1999b) "A Real-time Rollover Threat Index for Sport Utility Vehicles", Proceedings of the American Control Conference, San Diego, California, (June).
20. Trent, V., and Greene, M. (2002), "A Genetic Algorithm Predictor for Vehicle Rollover", Archangle System Inc and Auburn University.
21. Rakheja, S., and Piche, A. (1990) "Development of Directional Stability Criteria for an Early Warning Safety Device", SAE paper no. 902265, SP-843, pp. 1-13.
22. Dunwoody, A. B. and Froese, S. (1993) "Active Roll Control of A Semi-trailer", SAE Transactions, 102 (933045): 999-1004.
23. Lin, R. C., Cebon, D., and Cole, D., J. (1996) "Active Roll Control of Articulated Vehicles", Vehicle System Dynamics, 26 (1): 17-43.
24. Palkovics, L., Semsey, A., and Gerum, E. (1999) "Rollover Prevention System for Commercial Vehicles—Additional Sensorless Function of the Electronic Brake System", Vehicle System Dynamics, 32, pp. 285-297.
25. Wielenga, T. J. (1999) "A Method for Reducing On-Road Rollovers—Anti-rollover Braking", SAE Paper No. 1999-01-0123.
26. Wielenga, T. J. and Chace, M. A. (2000) "A Study of Rollover Prevention Using Anti-rollover Braking", SAE Paper No. 2000-01-1642.
27. Lewis, A. S. and El-Gindy, M. (2001) "Nonlinear Active Rollover Prevention Control Strategies for A 5-axle Tractor Semi-trailer", ASME International

Mechanical Engineering Congress and Exposition, New York, (November).

28. Shapiro, S. C., et al. (1995), "Error Analysis of Center-of-Gravity Measurement Techniques", SAE Paper No. 950027.
29. Andreatta, D. A. et al. (2001), "Inertia Measurement of Large Military Vehicles", SAE Paper No. 2001-01-0792.
30. Sinha, N. K. and Kuszta, B., Modeling and Identification of Dynamic Systems, Van Nostrand Reinhold, 1983.
31. Ljung, L., System Identification Toolbox for Use with MATLAB, The Math Works Inc., 1995.
32. Yang, X. (1999), "A closed-loop driver/vehicle directing dynamics predictor", PhD thesis, Concordia University.
33. Erin, R. D. (1986) "The Dependence of Truck Roll Stability on Size and Weight Variables", Int. J. of Vehicle Design, Special Issue on Vehicle Safety, pp. 192-208.
34. http://www.tc.gc.ca/pol/en/Report/anre2003/toc_e.htm.
35. Ervin, R. D., et al. (1986), "The influence of weights and dimensions on the stability and control of heavy duty trucks in Canada", The University of Michigan Transportation Research Institute. Report No. UMTRI-86-35.
36. http://www.comt.ca/english/programs/trucking/MOU99.PDF.
37. http://www.carsim.com/trucksim.
38. El Gindy, M., and Hosamel Deen, Y. H. (1989) "Sensitivity Parametric Analysis of UMTRI Static Roll Model", Int. J. of Vehicle Design, vol. 10, no. 2, pp. 187-189.

39. Ervin, R. D., Nisenger, R. L. (1982), "Analysis of the roll stability of cryogenic tankers", The University of Michigan Transportation Research Institute. Report No. UM-HSRI-82-32.

40. Miller, D.W.G. and Barber, N.F. (1973), "Roll-over of Articulated Vehicles", Proc. Of the Inst. Of Mech. Engrs., Paper C203/73.

41. http://www.xbow.com/Products/productsdetails.aspx?sid=41(Crossbow Smarter Sensors in Silicon).

42. Eykhoff, P., System Identification, Parameter and State Estimation, John Wiley & Sons, 1977.

43. Sinha, N. K. and Kuszta, B., Modeling and Identification of Dynamic Systems, Van Nostrand Reinhold, 1983.

44. Chen, C. F. and Shieh, L. S., A Novel Approach to Linear Model Simplification, Int. J. Control, 1968, vol. 8, No. 6, 561-570.

APPENDIX A FIVE-AXLE TRACTOR-SEMITRAILER TRUCKSIM MODEL

A.1 Tractor

The baseline power-unit used is a 3-axle 6x4 tractor equipped with a conventional fifth wheel providing for semitrailer motion which is fully coupled in roll and fully uncoupled in pitch and yaw to that of the tractor. The tractor configuration of TruckSim model is shown in Figure A.1. The aerodynamics conditions, power train and brakes are chosen by referring to the built-in TruckSim tractor-semitrailer model.

The inertial properties, c.g. position and coordinate system of sprung mass are shown in Figure A.2. The coordinate system is used to define points and distances to parts of the vehicle, such as the wheel centers. As with other coordinate systems, the X axis is forward, the Z axis is up, and the Y axis points to the left-hand side of the vehicle. The location of the origin is in an X-Z plane that splits the sprung mass laterally (the plane of symmetry), and also in a Y-Z plane containing the spin axis of the front wheels. The vertical location of the origin point is fixed with respect to the sprung mass. Because the sprung mass height relative to the ground depends on the tire sizes and the loads carried in the vehicle, the height of the sprung mass origin point relative to the ground varies when tire properties or load conditions are changed.

Most heights of points of interest are specified relative to the origin of the sprung mass when the vehicle is in a design load condition, which is a load condition used to define vertical locations of various points in the vehicle relative

to the origin of the sprung mass coordinate system. The specific conditions that define the design load are not specified for TruckSim, but it is important that all heights apply for the same load condition. In the case of this simulation study, the design load condition is the vehicle fully loaded.

The roll stiffness of the fifth wheel coupling is 999999.88 in-lb/deg [35], the tractor frame torsion stiffness about roll axis is 40000.0 in-lb/deg [35], and the fifth wheel lash is ±3° [39]. The combined torsion stiffness of the tractor frame and the fifth wheel roll coupling is shown in Figure A.3, in which the right hand side is the two-column table of values for roll angles and resulting moments.

The tractor steer axle is shown in Figure A.4. Tractor steer axle suspension spring and shock absorber are shown in Figure A.5 and Figure A.6. Figure A.7 is tractor steer axle auxiliary roll moment, which accounts for the difference between the overall roll stiffness and the stiffness provided by the springs alone.

The tractor leading drive axle and its related property features are shown in Figure A.8 to Figure A.10. The tractor trailing drive axle and its related property features are shown in Figure A.11 to Figure A.13.

The tire configuration of tractor model is shown in Figure A.14, in which same tires are used for all the axles.

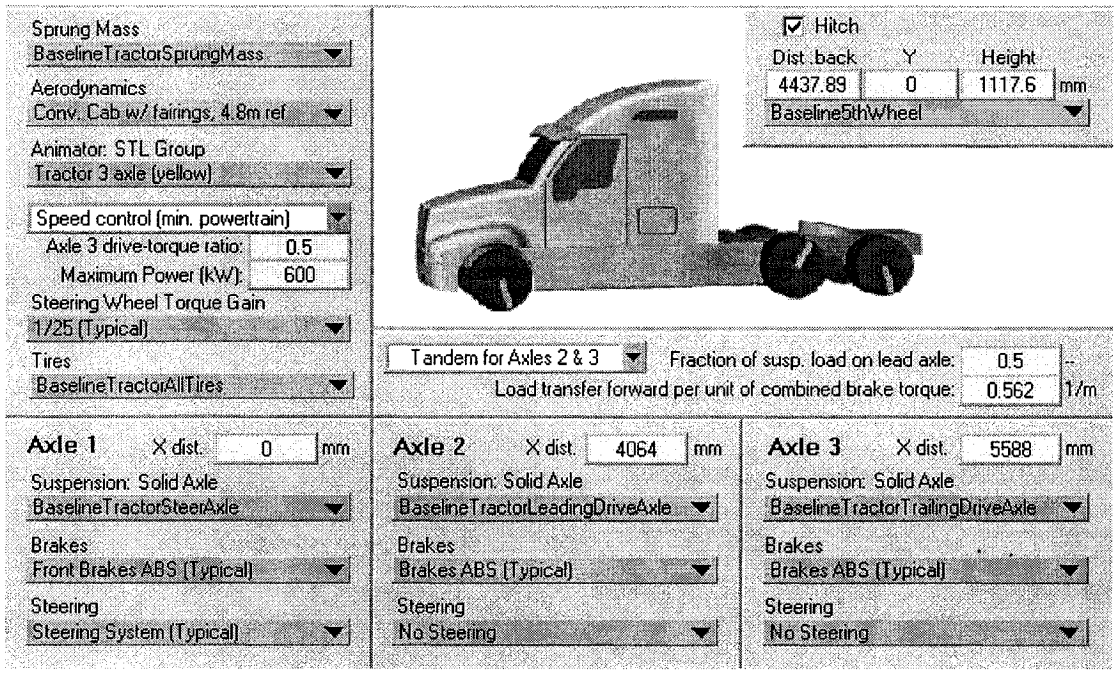

Figure A.1: Tractor configuration.

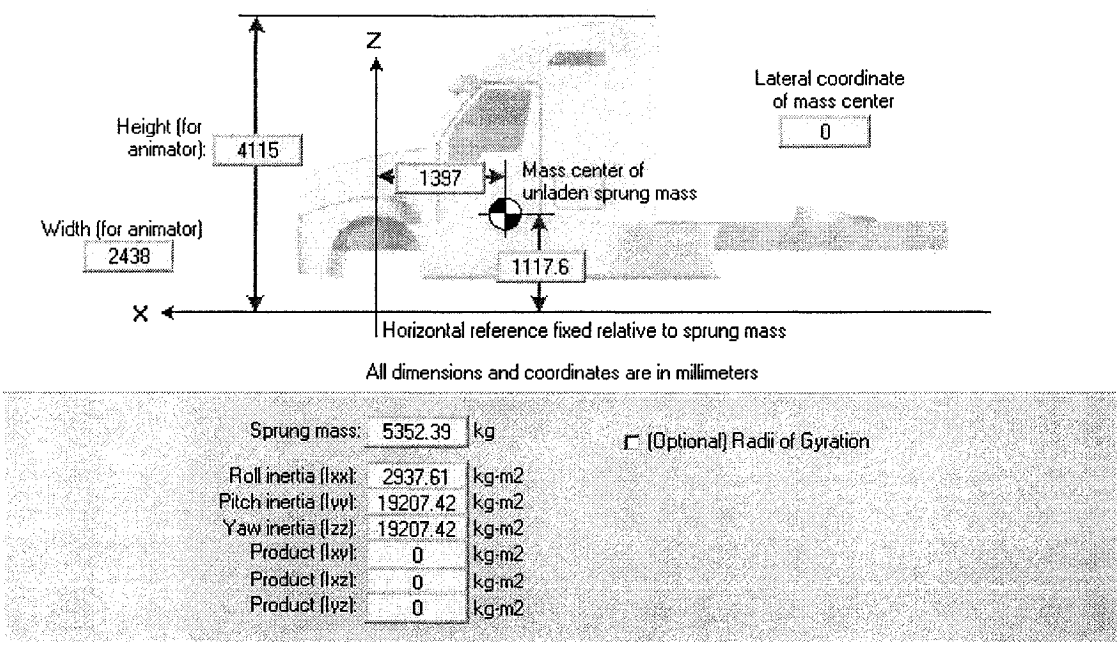

Figure A.2: Tractor unladen sprung mass.

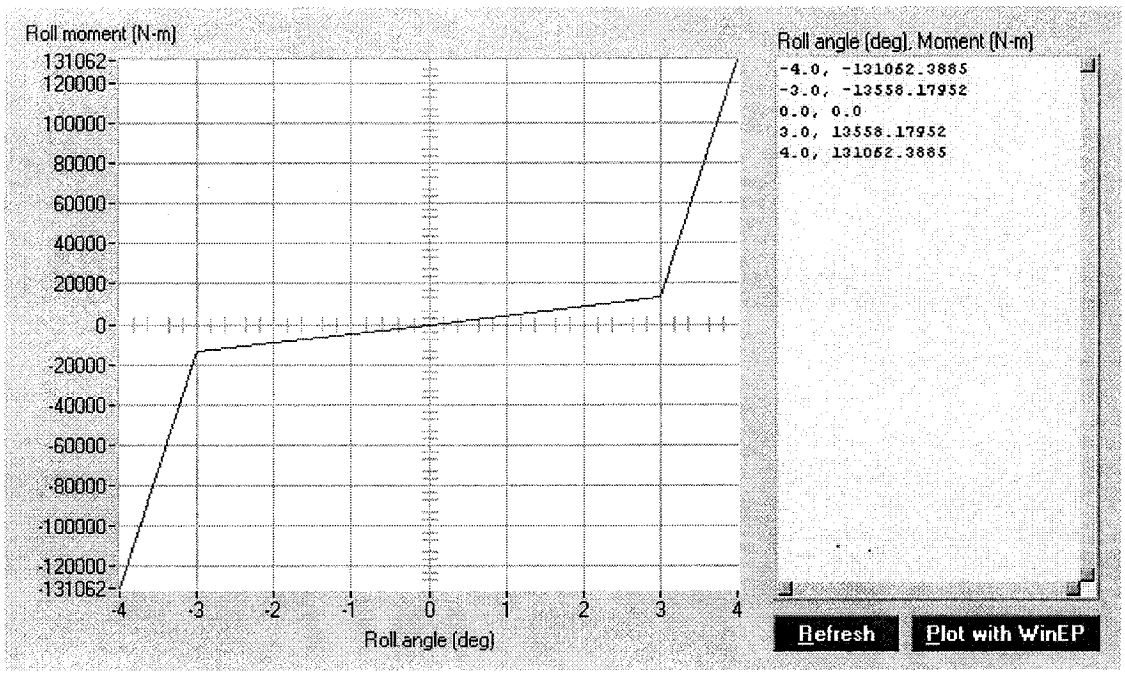

Figure A.3: Hitch roll stiffness.

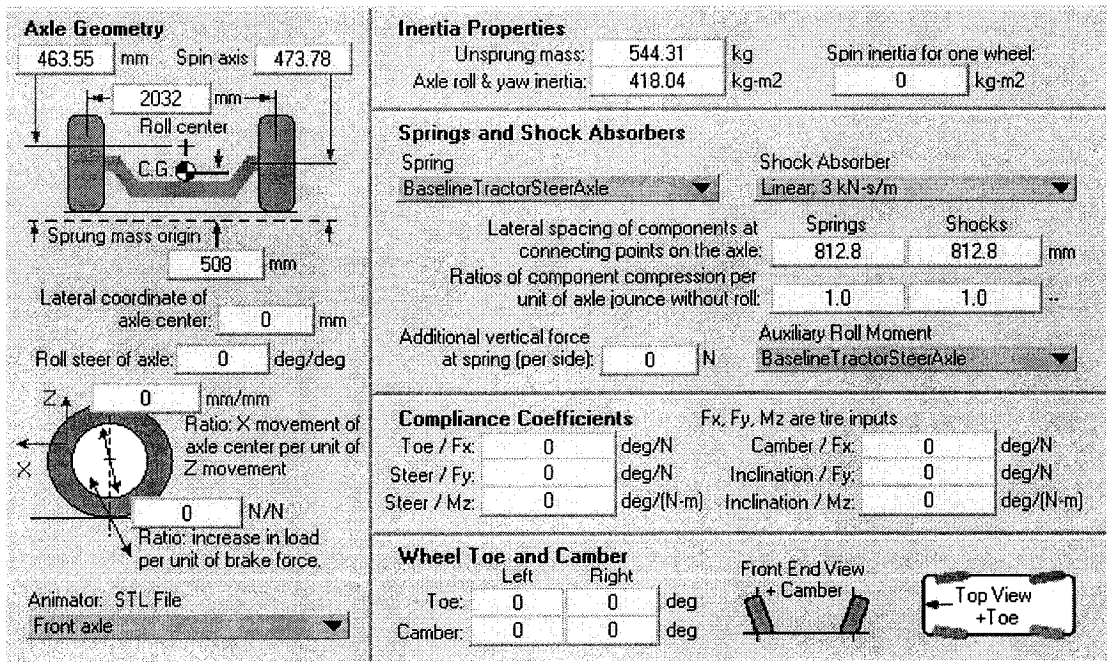

Figure A.4: Tractor steer axle configuration.

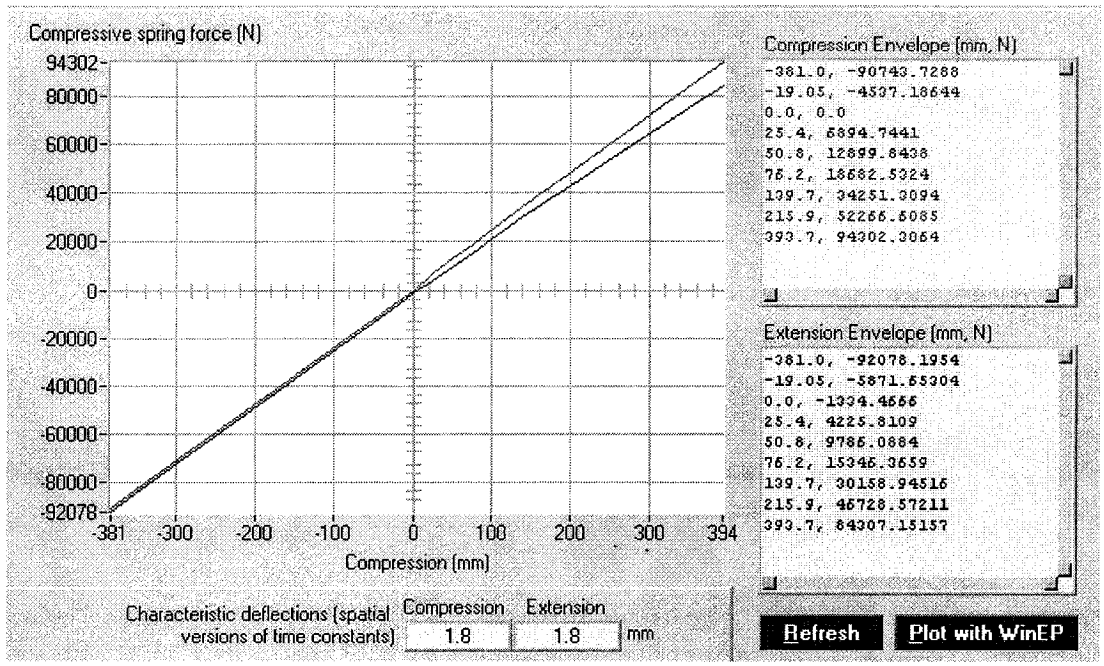

Figure A.5: Tractor steer axle suspension spring.

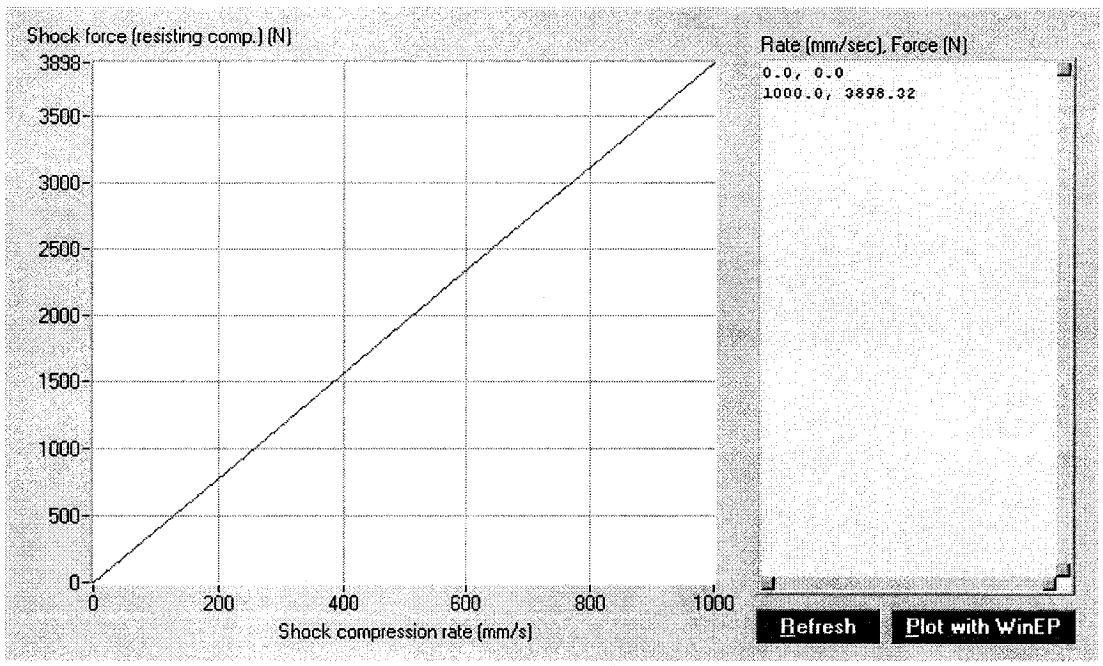

Figure A.6: Tractor steer axle shock absorber.

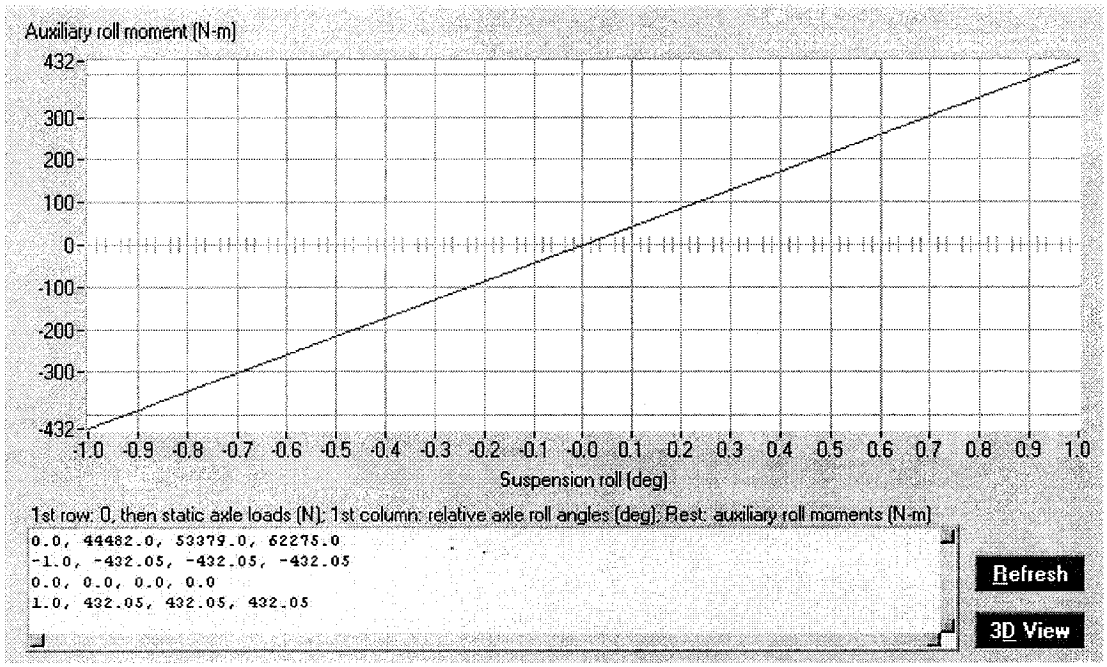

Figure A.7: Tractor steer axle auxiliary roll moment.

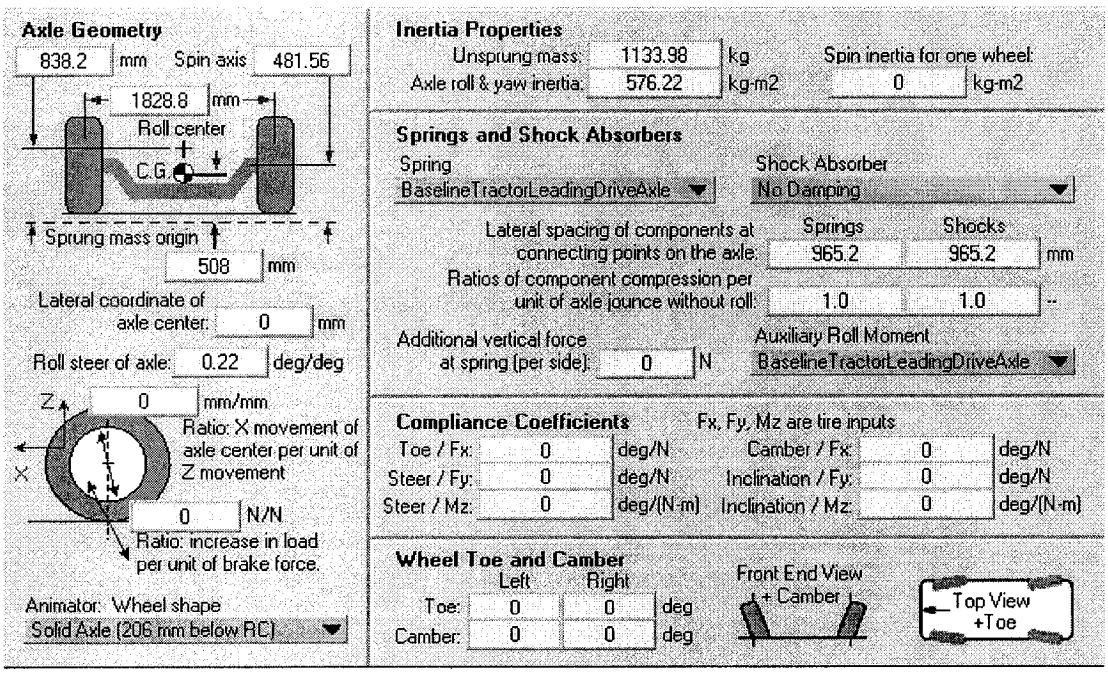

Figure A.8: Tractor leading drive axle configuration.

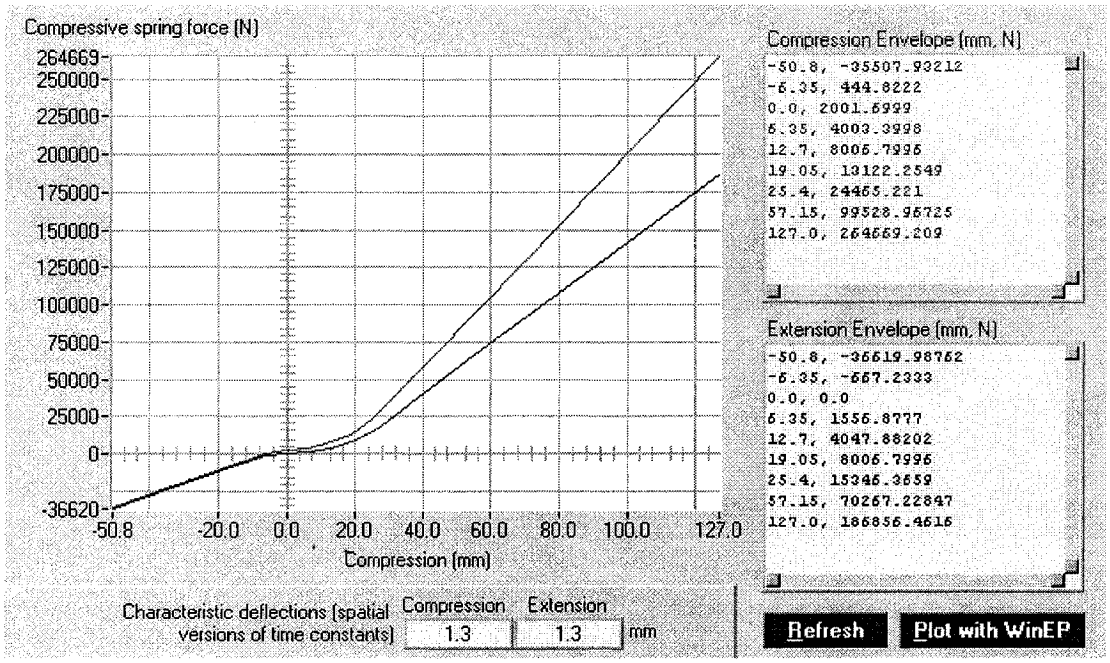

Figure A.9: Tractor leading drive axle suspension spring.

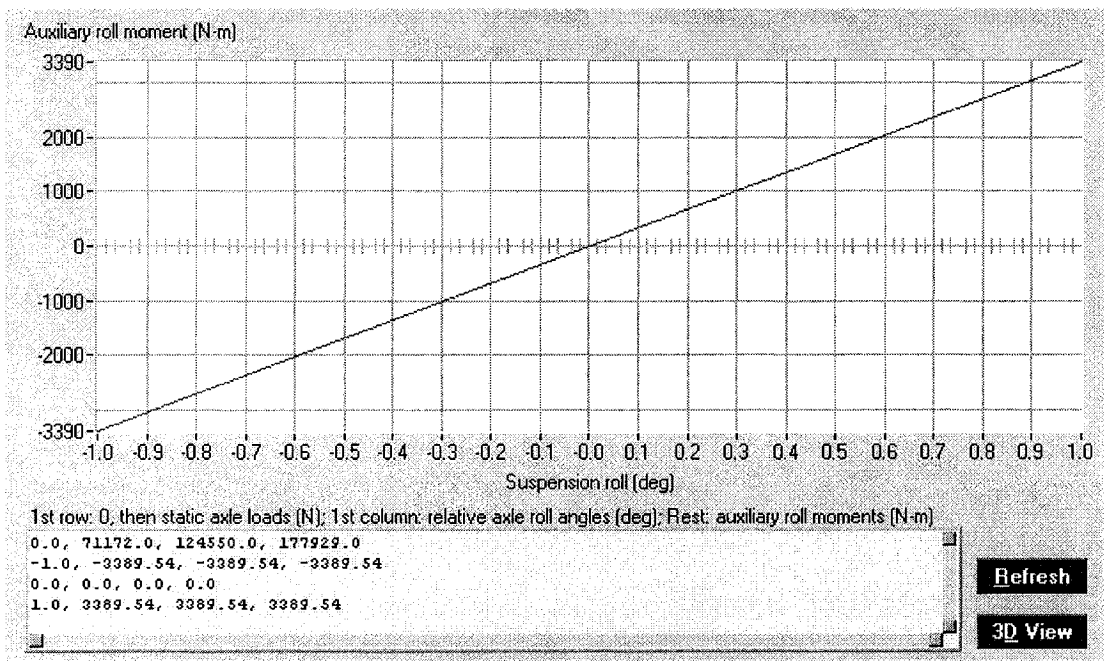

Figure A.10: Tractor leading drive axle auxiliary roll moment.

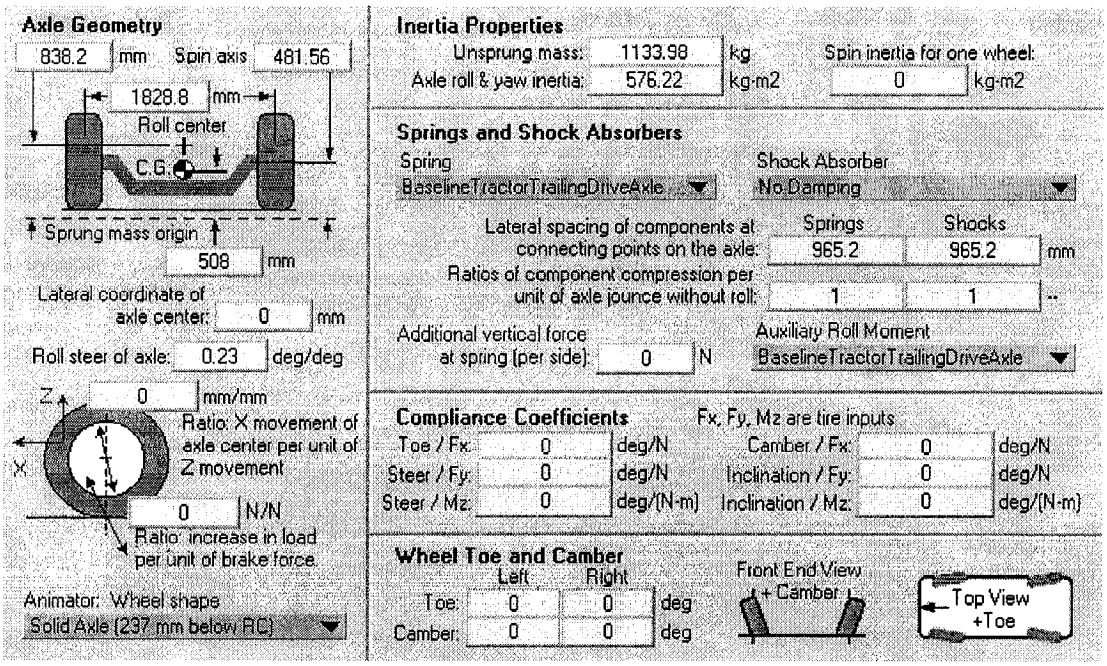

Figure A.11: Tractor trailing drive axle configuration.

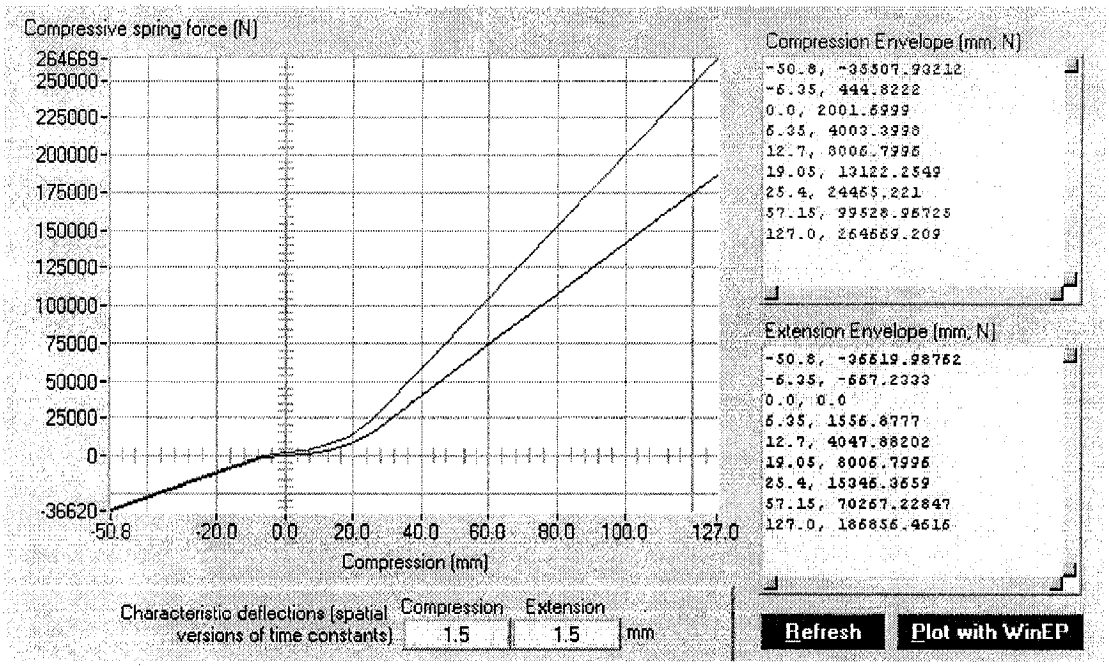

Figure A.12: Tractor trailing drive axle suspension spring.

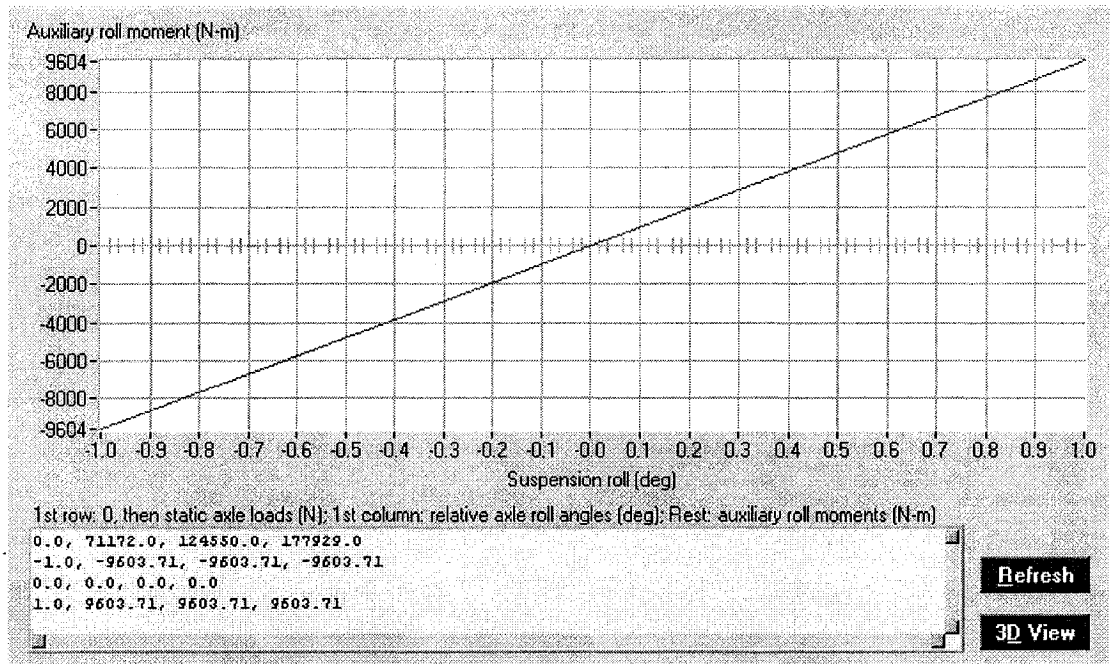

Figure A.13: Tractor trailing drive axle auxiliary roll moment.

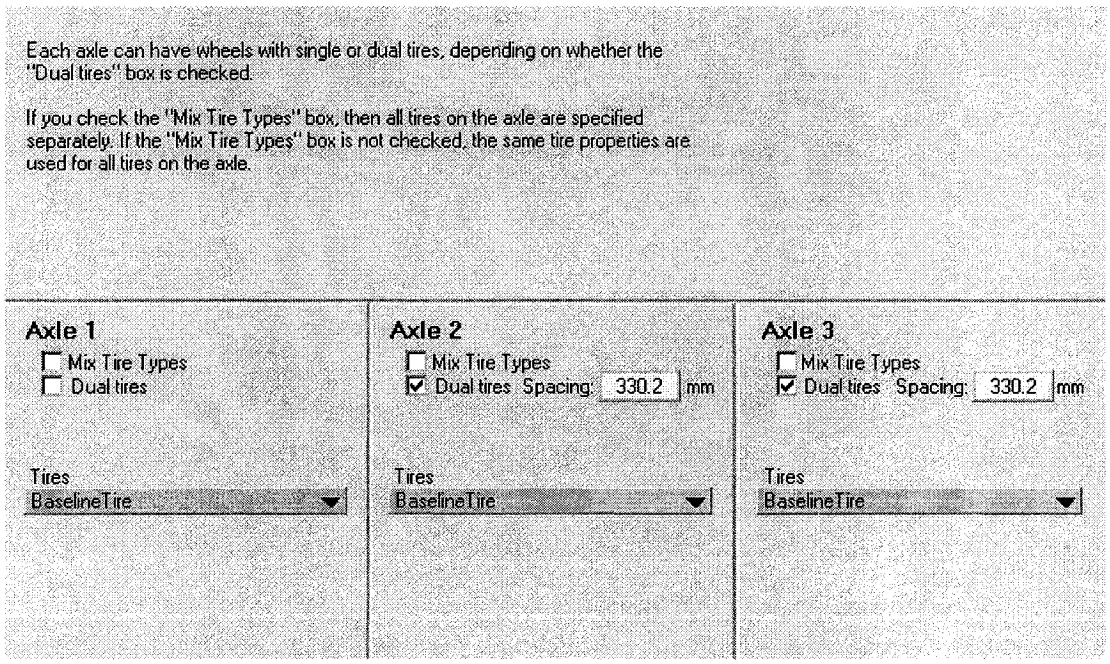

Figure A.14: All tractor tires.

A.2 Two-Axle Semitrailer

Figure A.15 is the configuration of 2-axle semitrailer. The semitrailer inertial properties, c.g. position and coordinate system of sprung mass are shown in Figure A.16. The leading trailer axle and its related property features are shown in Figure A.17 to Figure A.19. The trailing trailer axle has the same properties as the leading trailer axle except its spring characteristic deflections are 0.26 mm both for compression and extension. The tire configuration of 2-axle trailer model is shown in Figure A.20 , in which same tires as those of the trailer are used for all the axles. The payload box of the 2-axle semitrailer is shown in Figure A.21.

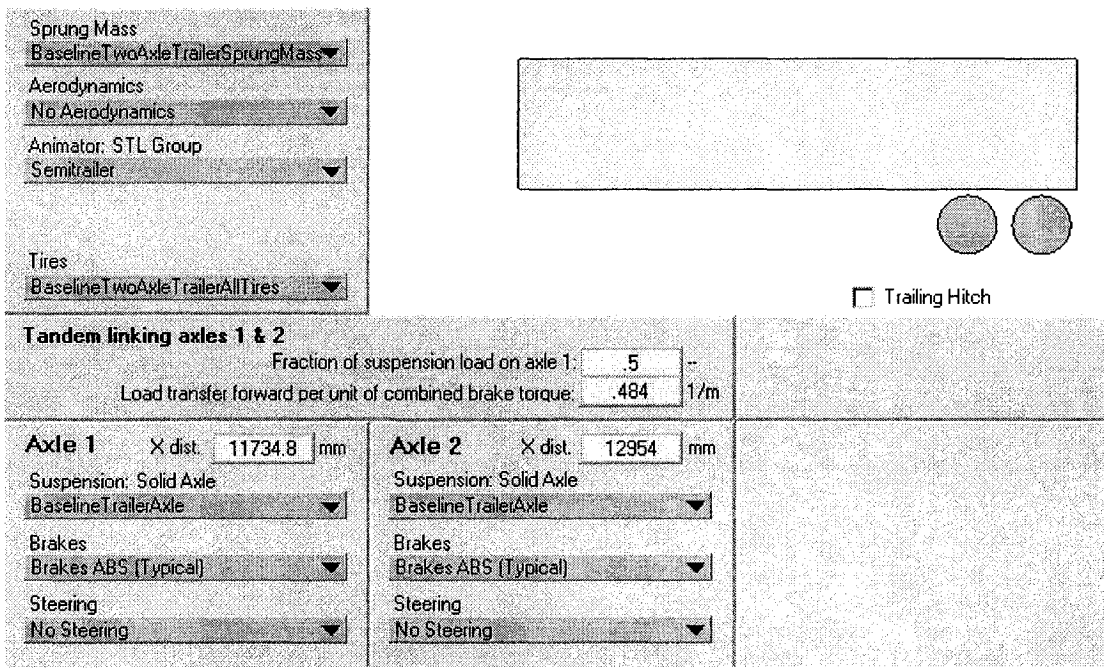

Figure A.15: Semitrailer configuration.

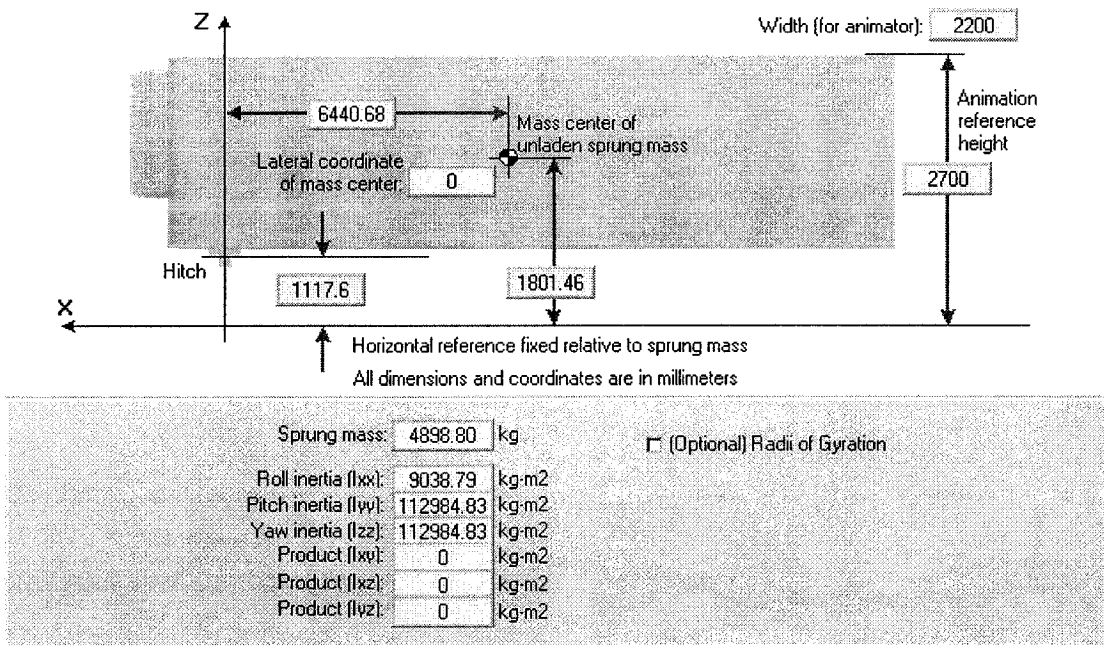

Figure A.16: Semitrailer unladen sprung mass.

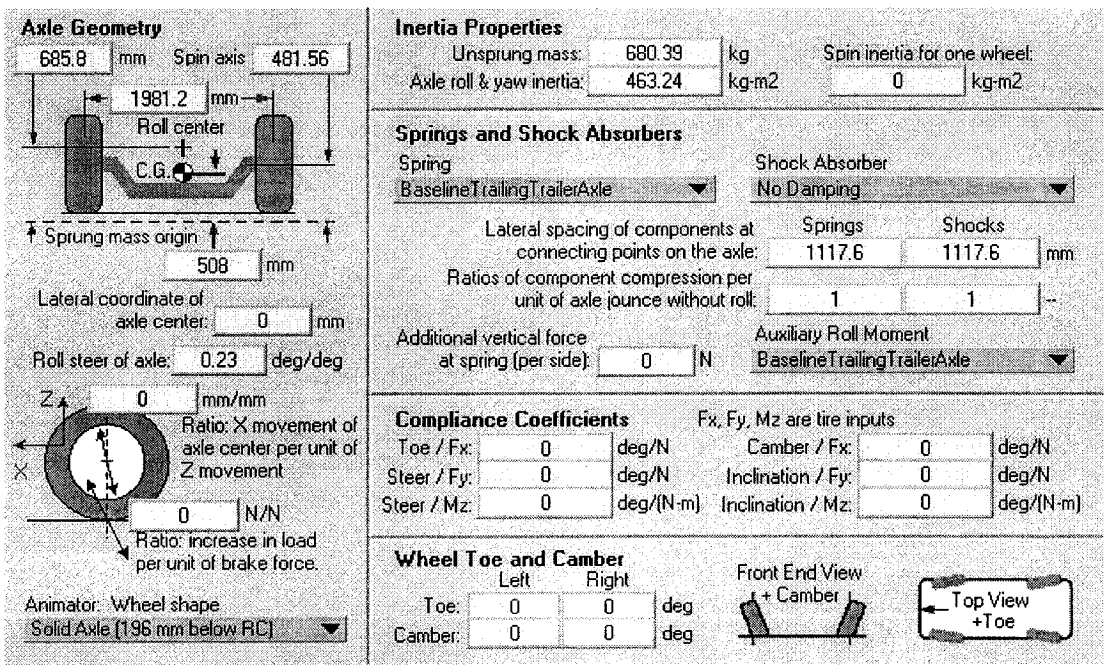

Figure A.17: Semitrailer axle configuration.

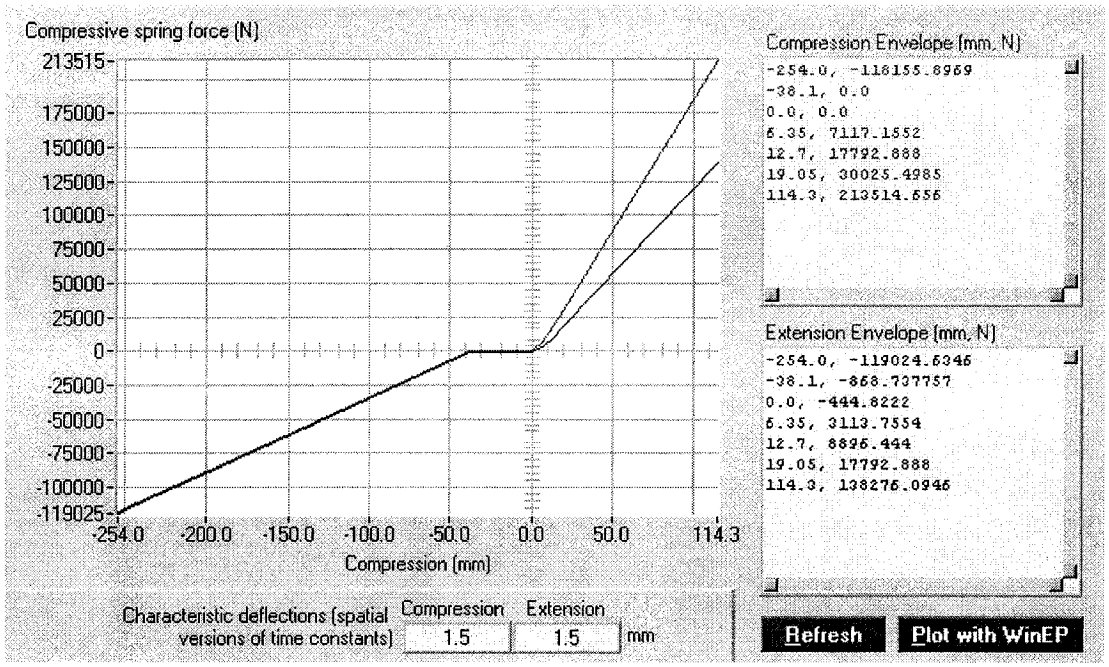

Figure A.18: Semitrailer axle suspension spring.

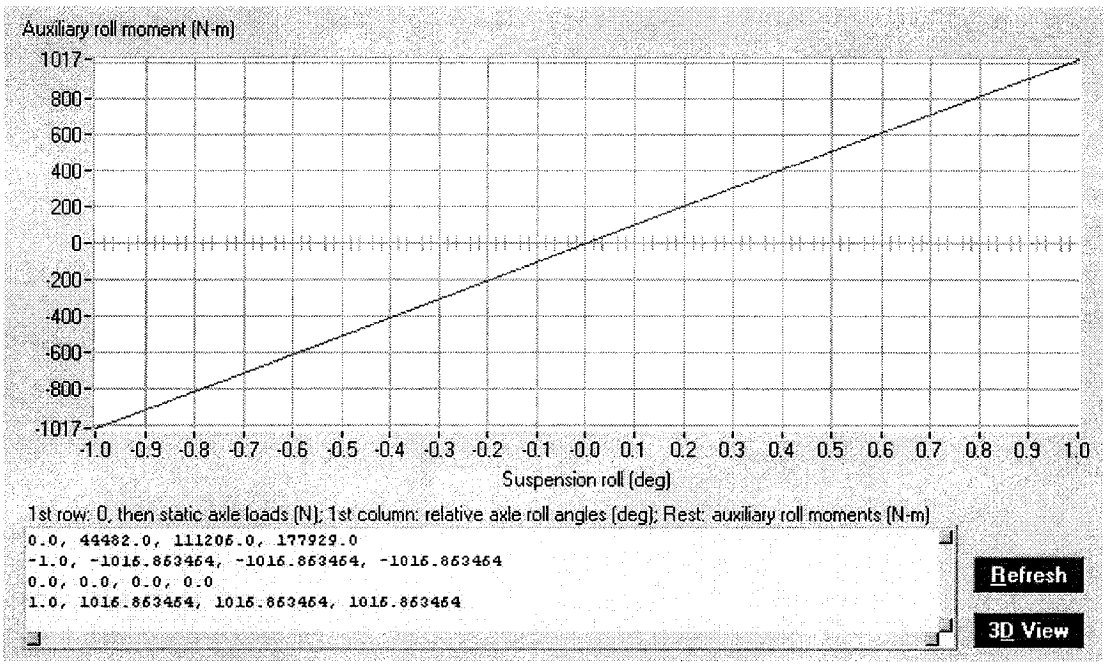

Figure A.19: Semitrailer axle auxiliary roll moment.

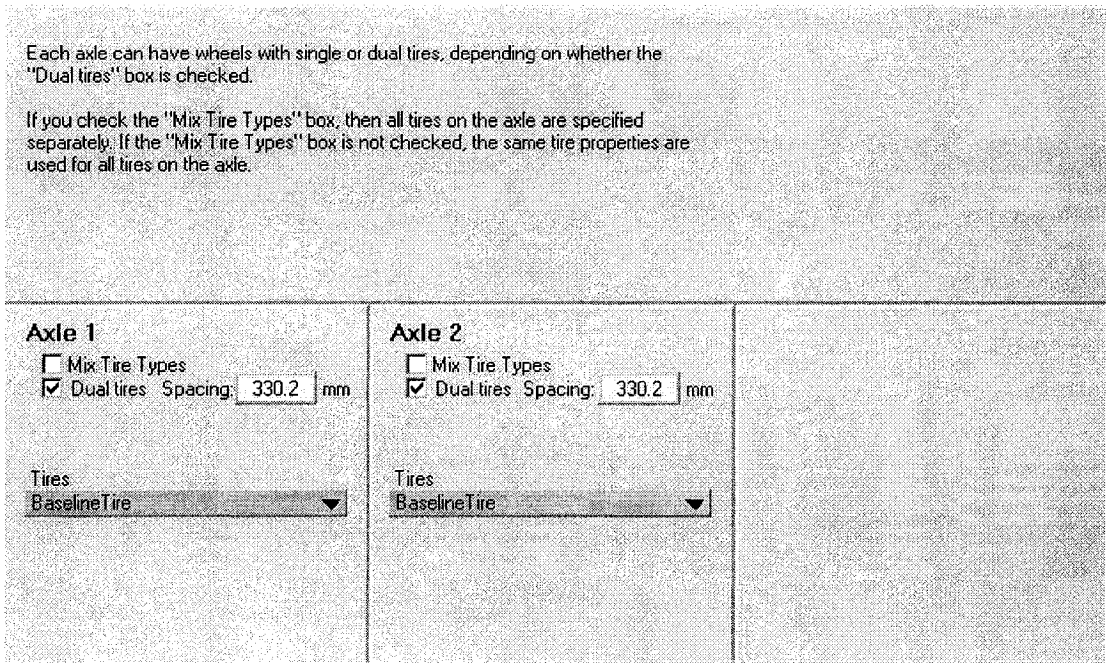

Figure A.20: All trailer tires.

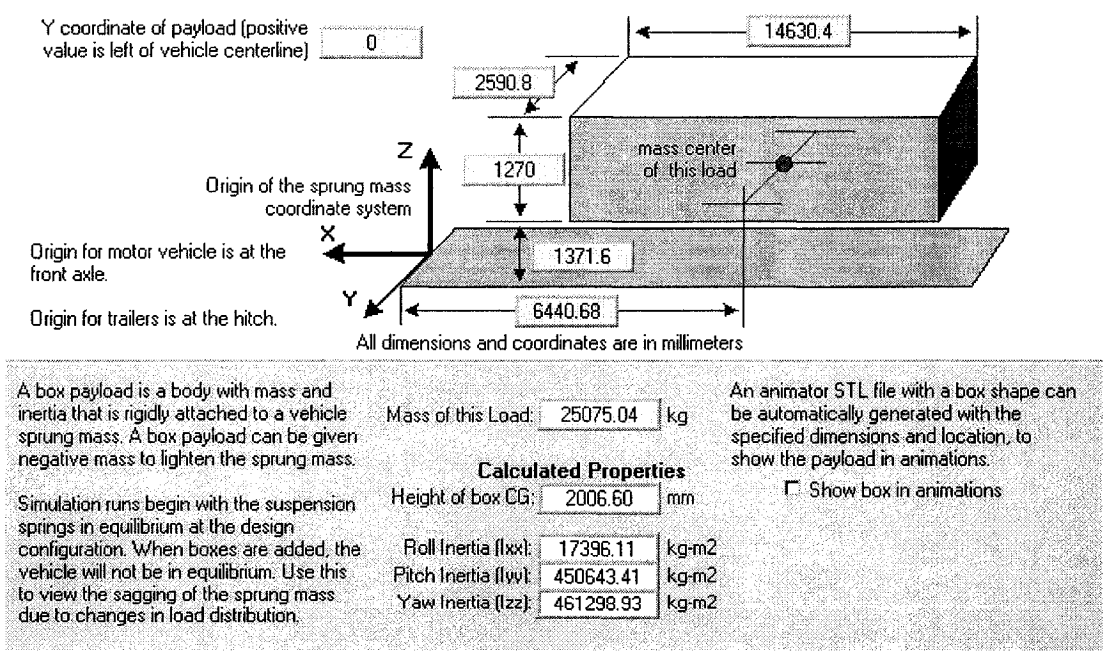

Figure A.21: Payload configuration.

A.3 Tire

The tire model is shown in Figure A.22. Figure A.23 to Figure A.25 are the longitudinal force, lateral force and aligning moment properties of the tire.

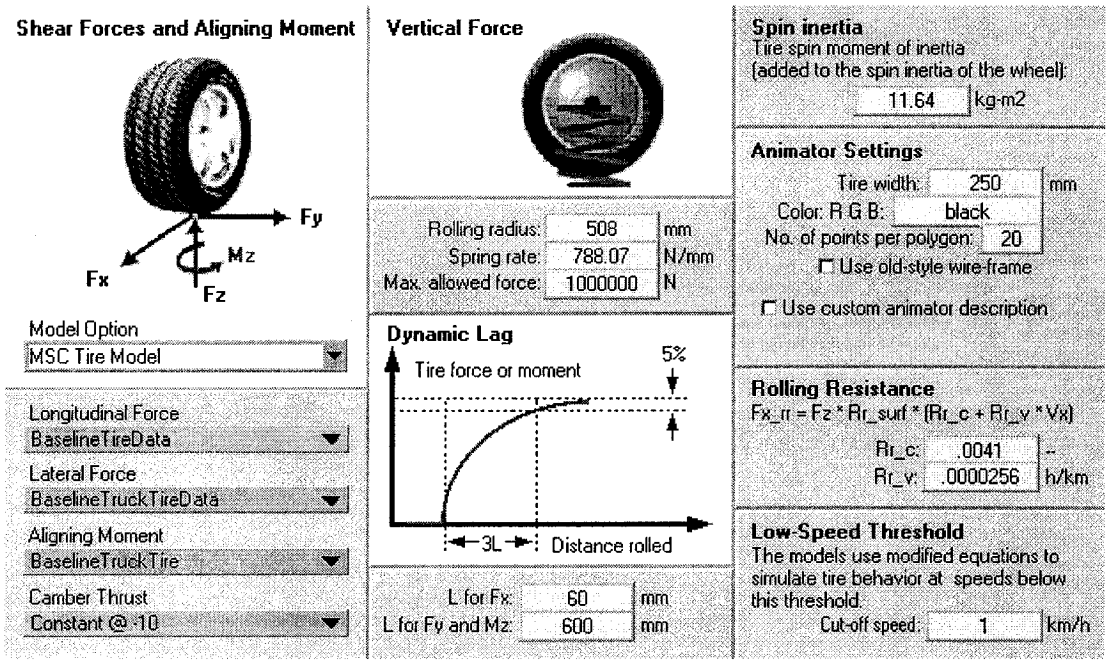

Figure A.22: Tire configuration.

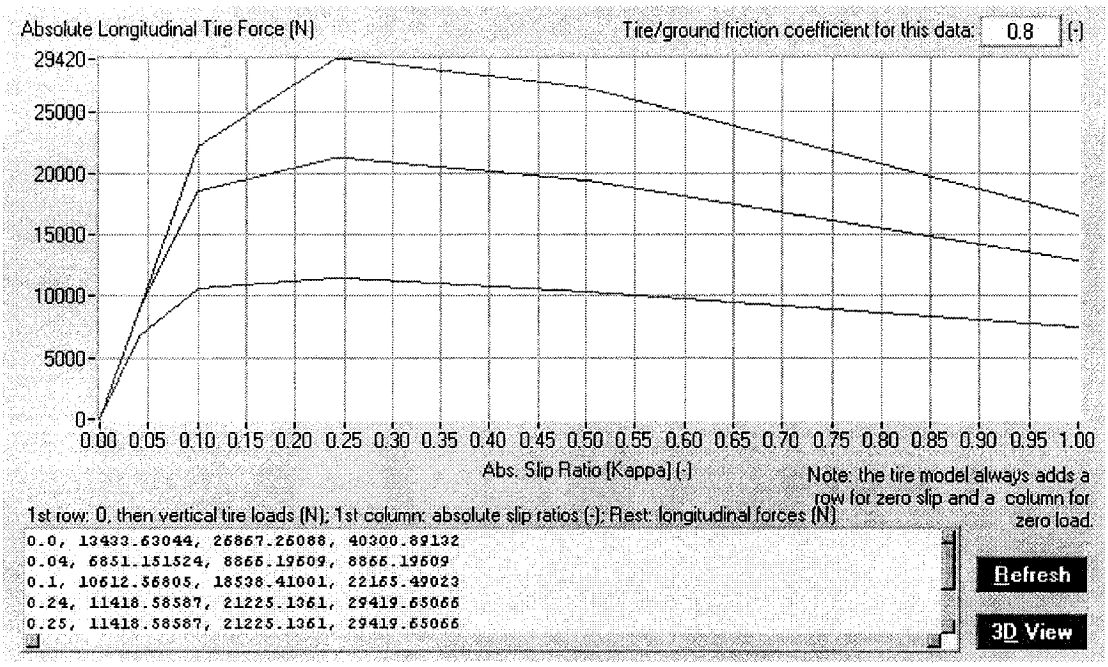

Figure A.23: Tire longitudinal force (Velocity=58.7 ft/sec).

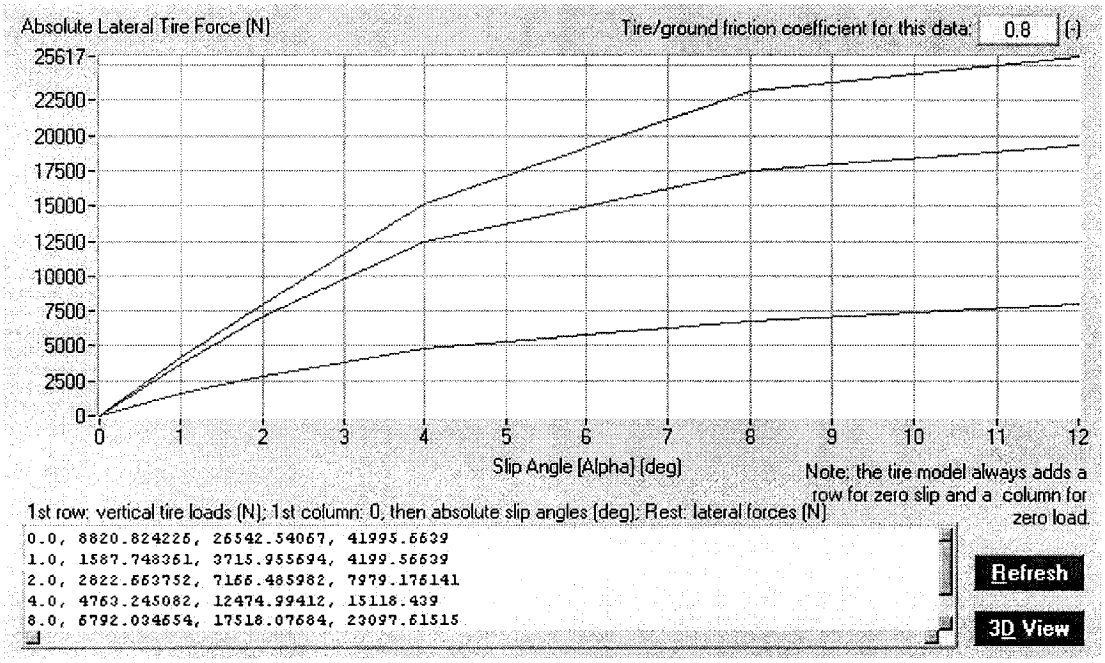

Figure A.24: Tire lateral force (Velocity=58.7 ft/sec).

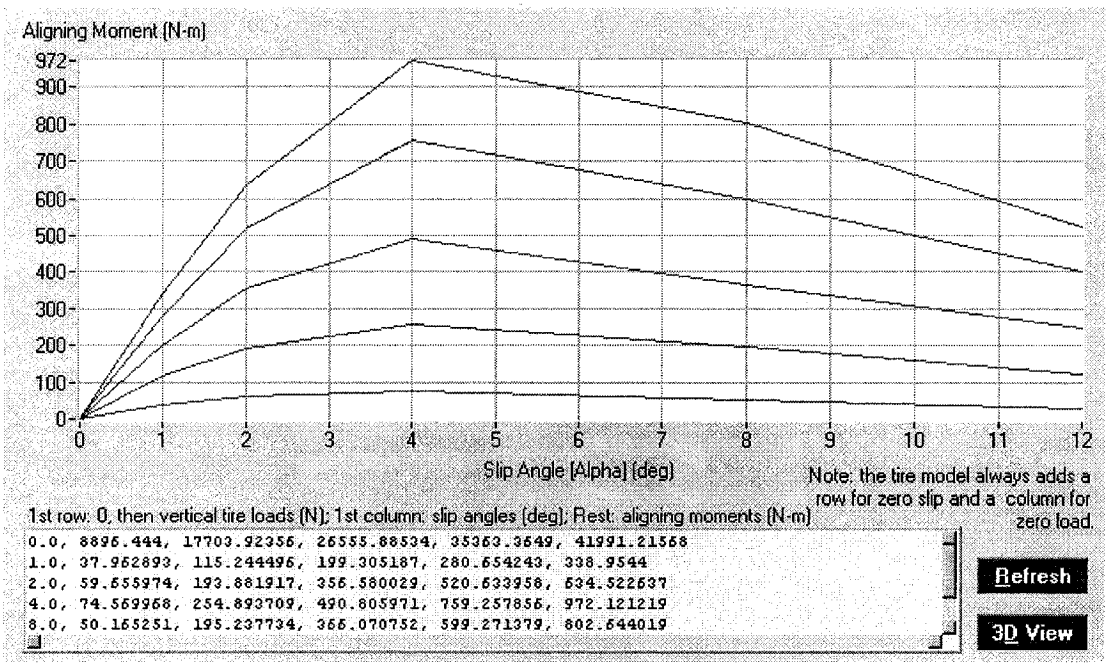

Figure A.25: Tire aligning moment.

APPENDIX B ELEMENTS OF MATRICES $D_{10\times10}$ AND $C_{10\times1}$

$$D(1,1) = 2KT_{y_1}/u_{s_1} + 4\left(KT_{y_2} + KT_{y_3} + KT_{y_4} + KT_{y_5}\right)/u_{s_1} + (m_1 + m_2)s \tag{B.1}$$

$$\begin{aligned} D(1,2) &= 4\left(KT_{y_4} + KT_{y_5}\right) + \left(m_1X_{c_1} - m_1X_{sc_1} - m_2X_{sc_1}\right)s^2 \\ &+ \left[\begin{matrix} 2KT_{y_1}X_1/u_{s_1} + u_{s_1}(m_1 + m_2) \\ -4\left(KT_{y_2}X_2 + KT_{y_3}X_3 + KT_{y_4}X_{sc_1} + KT_{y_5}X_{sc_1}\right)/u_{s_1} \end{matrix}\right]s \end{aligned} \tag{B.2}$$

$$\begin{aligned} D(1,3) &= -\left(m_1Z_{sc_1} - m_1Z_{c_1} + m_2Z_{sc_1}\right)s^2 \\ &- \left[2KT_{y_1}Z_{R_1}/u_{s_1} + 4\left(KT_{y_2}Z_{R_2} + KT_{y_3}Z_{R_3} + KT_{y_4}Z_{sc_1} + KT_{y_5}Z_{sc_1}\right)/u_{s_1}\right]s \end{aligned} \tag{B.3}$$

$$\begin{aligned} D(1,4) &= -4\left(KT_{y_4} + KT_{y_5}\right) - m_2X_{c_2}s^2 \\ &- 4\left[KT_{y_4}\left(X_4 + X_{sc_2}\right)/u_{s_1} + KT_{y_5}\left(X_5 + X_{sc_2}\right)/u_{s_1}\right]s \end{aligned} \tag{B.4}$$

$$D(1,5) = 4\left[KT_{y_4}\left(Z_{sc_2} - Z_{R_4}\right)/u_{s_1} + KT_{y_5}\left(Z_{sc_2} - Z_{R_5}\right)/u_{s_1}\right]s + m_2Z_{c_2}s^2 \tag{B.5}$$

$$D(1,6) = -2KT_{y_1}H_{R_1}s/u_{s_1} \tag{B.6}$$

$$D(1,7) = -4KT_{y_2}H_{R_2}s/u_{s_1} \tag{B.7}$$

$$D(1,8) = -4KT_{y_3}H_{R_3}s/u_{s_1} \tag{B.8}$$

$$D(1,9) = -4KT_{y_4}H_{R_4}s/u_{s_1} \tag{B.9}$$

$$D(1,10) = -4KT_{y_5}H_{R_5}s/u_{s_1} \tag{B.10}$$

$$\begin{aligned} D(2,1) &= 4\left[KT_{M_3} + KT_{y_3}\left(X_3 - X_{sc_1}\right)\right]/u_{s_1} - X_{c_1}m_1s \\ &+ 2\left[KT_{M_1} - KT_{y_1}\left(X_1 + X_{sc_1}\right)\right]/u_{s_1} + 4\left[KT_{M_2} - KT_{y_2}\left(X_{sc_1} - X_2\right)\right]/u_{s_1} \end{aligned} \tag{B.11}$$

$$\begin{aligned} D(2,2) &= 2\left[KT_{M_1} - KT_{y_1}\left(X_1 + X_{sc_1}\right)\right]X_1s/u_{s_1} \\ &- 4\left[KT_{M_2} - KT_{y_2}\left(X_{sc_1} - X_2\right)\right]X_2s/u_{s_1} \\ &- 4\left[KT_{M_3} + KT_{y_3}\left(X_3 - X_{sc_1}\right)\right]X_3s/u_{s_1} \\ &- X_{c_1}m_1u_{s_1}s - \left[X_{c_1}m_1\left(X_{c_1} - X_{sc_1}\right) + I_{z_1}\right]s^2 \end{aligned} \tag{B.12}$$

$$
\begin{aligned}
D(2,3) &= X_{c_1} m_1 s^2 \left(Z_{sc_1} - Z_{c_1}\right) \\
&- 2\left[KT_{M_1} - KT_{y_1}\left(X_1 + X_{sc_1}\right)\right] Z_{R_1} s / u_{s_1} \\
&- 4\left[KT_{M_2} - KT_{y_2}\left(X_{sc_1} - X_2\right)\right] Z_{R_2} s / u_{s_1} \\
&- 4\left[KT_{M_3} + KT_{y_3}\left(X_3 - X_{sc_1}\right)\right] Z_{R_3} s / u_{s_1}
\end{aligned}
\tag{B.13}
$$

$$D(2,4) = 0 \tag{B.14}$$

$$D(2,5) = 0 \tag{B.15}$$

$$D(2,6) = -2\left[KT_{M_1} - KT_{y_1}\left(X_1 + X_{sc_1}\right)\right] H_{R_1} s / u_{s_1} \tag{B.16}$$

$$D(2,7) = -4\left[KT_{M_2} - KT_{y_2}\left(X_{sc_1} - X_2\right)\right] H_{R_2} s / u_{s_1} \tag{B.17}$$

$$D(2,8) = -4\left[KT_{M_3} + KT_{y_3}\left(X_3 - X_{sc_1}\right)\right] H_{R_3} s / u_{s_1} \tag{B.18}$$

$$D(2,9) = 0 \tag{B.19}$$

$$D(2,10) = 0 \tag{B.20}$$

$$
\begin{aligned}
D(3,1) &= 2KT_{y_1} Z_{R_1} / u_{s_1} + 4\left(KT_{y_2} Z_{R_2} + KT_{y_3} Z_{R_3}\right) / u_{s_1} \\
&+ \left(m_{u_1} Z_{R_1} + m_{u_2} Z_{R_2} + m_{u_3} Z_{R_3}\right) s
\end{aligned}
\tag{B.21}
$$

$$
\begin{aligned}
D(3,2) &= \left(m_{u_1} Z_{R_1} X_1 - m_{u_2} Z_{R_2} X_2 - m_{u_3} Z_{R_3} X_3\right) s^2 \\
&+ \left[\begin{array}{l} u_{s_1}\left(m_{u_1} Z_{R_1} + m_{u_2} Z_{R_2} + m_{u_3} Z_{R_3}\right) + 2KT_{y_1} Z_{R_1} X_1 / u_{s_1} \\ -4\left(KT_{y_2} Z_{R_2} X_2 + KT_{y_3} Z_{R_3} X_3\right) / u_{s_1} \end{array}\right] s
\end{aligned}
\tag{B.22}
$$

$$
\begin{aligned}
D(3,3) &= Z_{R_1}\left(F_1 - W_{u_1}\right) + Z_{R_2}\left(F_2 - W_{u_2}\right) + Z_{R_3}\left(F_3 - W_{u_3}\right) \\
&- 2\left(KS_1 S_1{}^2 + KS_2 S_2{}^2 + KS_3 S_3{}^2\right) - \left(K_1 + KR_1 + KR_2 + KR_3\right) \\
&- \left[2KT_{y_1} Z_{R_1}{}^2 / u_{s_1} + 4\left(KT_{y_2} Z_{R_2}{}^2 + KT_{y_3} Z_{R_3}{}^2\right) / u_{s_1}\right] s \\
&- \left(m_{u_1} Z_{R_1}{}^2 + m_{u_2} Z_{R_2}{}^2 + m_{u_3} Z_{R_3}{}^2 + I_{xx_{s_1}}\right) s^2
\end{aligned}
\tag{B.23}
$$

$$D(3,4) = 0 \tag{B.24}$$

$$D(3,5) = K_1 \tag{B.25}$$

$$D(3,6) = 2KS_1 S_1{}^2 + KR_1 - 2KT_{y_1} Z_{R_1} H_{R_1} s / u_{s_1} - m_{u_1} Z_{R_1} Z_{u_1} s^2 \tag{B.26}$$

$$D(3,7) = 2KS_2S_2{}^2 + KR_2 - 4KT_{y_2}Z_{R_2}H_{R_2}s/u_{s_1} - m_{u_2}Z_{R_2}Z_{u_2}s^2 \quad \text{(B.27)}$$

$$D(3,8) = 2KS_3S_3{}^2 + KR_3 - 4KT_{y_3}Z_{R_3}H_{R_3}s/u_{s_1} - m_{u_3}Z_{R_3}Z_{u_3}s^2 \quad \text{(B.28)}$$

$$D(3,9) = 0 \quad \text{(B.29)}$$

$$D(3,10) = 0 \quad \text{(B.30)}$$

$$\begin{aligned} D(4,1) &= 4\left[KT_{y_5}\left(X_{sc_2} + X_5\right) + KT_{M_5}\right]/u_{s_1} \\ &+ X_{c_2}m_2s + 4\left[KT_{y_4}\left(X_{sc_2} + X_4\right) + KT_{M_4}\right]/u_{s_1} \end{aligned} \quad \text{(B.31)}$$

$$\begin{aligned} D(4,2) &= X_{c_2}m_2u_{s_1}s - X_{c_2}m_2X_{sc_1}s^2 \\ &+ 4\left[KT_{y_4}\left(X_{sc_2} + X_4\right) + KT_{M_4}\right] + 4\left[KT_{y_5}\left(X_{sc_2} + X_5\right) + KT_{M_5}\right] \\ &- 4\left[KT_{y_4}\left(X_{sc_2} + X_4\right) + KT_{M_4}\right]X_{sc_1}s/u_{s_1} \\ &- 4\left[KT_{y_5}\left(X_{sc_2} + X_5\right) + KT_{M_5}\right]X_{sc_1}s/u_{s_1} \end{aligned} \quad \text{(B.32)}$$

$$D(4,3) = -\left\{\begin{aligned} &X_{c_2}m_2Z_{sc_1}s^2 \\ &+ 4\left[KT_{y_4}\left(X_{sc_2} + X_4\right) + KT_{M_4}\right]Z_{sc_1}s/u_{s_1} \\ &+ 4\left[KT_{y_5}\left(X_{sc_2} + X_5\right) + KT_{M_5}\right]Z_{sc_1}s/u_{s_1} \end{aligned}\right\} \quad \text{(B.33)}$$

$$\begin{aligned} D(4,4) &= -\left(m_2X_{c_2}{}^2 + I_{z_2}\right)s^2 \\ &- \left[4KT_{y_4}\left(X_{sc_2} + X_4\right) + 4KT_{M_4}\right]\left(X_4 + X_{sc_2}\right)s/u_{s_1} \\ &- \left[4KT_{y_5}\left(X_{sc_2} + X_5\right) + 4KT_{M_5}\right]\left(X_5 + X_{sc_2}\right)s/u_{s_1} \\ &- \left[4KT_{y_4}\left(X_{sc_2} + X_4\right) + 4KT_{M_4}\right] \\ &- \left[4KT_{y_5}\left(X_{sc_2} + X_5\right) + 4KT_{M_5}\right] \end{aligned} \quad \text{(B.34)}$$

$$\begin{aligned} D(4,5) &= X_{c_2}m_2s^2Z_{c_2} \\ &+ \left[4KT_{y_4}\left(X_{sc_2} + X_4\right) + 4KT_{M_4}\right]\left(Z_{sc_2} - Z_{R_4}\right)s/u_{s_1} \\ &+ \left[4KT_{y_5}\left(X_{sc_2} + X_5\right) + 4KT_{M_5}\right]\left(Z_{sc_2} - Z_{R_5}\right)s/u_{s_1} \end{aligned} \quad \text{(B.35)}$$

$$D(4,6) = 0 \quad \text{(B.36)}$$

$$D(4,7) = 0 \quad \text{(B.37)}$$

$$D(4,8) = 0 \quad \text{(B.38)}$$

$$D(4,9) = -\left[4KT_{y_4}\left(X_{sc_2} + X_4\right) + 4KT_{M_4}\right]H_{R_4}s/u_{s_1} \tag{B.39}$$

$$D(4,10) = -\left[4KT_{y_5}\left(X_{sc_2} + X_5\right) + 4KT_{M_5}\right]H_{R_5}s/u_{s_1} \tag{B.40}$$

$$D(5,1) = 4KT_{y_4}Z_{R_4}/u_{s_1} + 4KT_{y_5}Z_{R_5}/u_{s_1} + \left(m_{u_4}Z_{R_4} + m_{u_5}Z_{R_5}\right)s \tag{B.41}$$

$$\begin{aligned} D(5,2) &= 4KT_{y_4}Z_{R_4} + 4KT_{y_5}Z_{R_5} - X_{sc_1}\left(m_{u_4}Z_{R_4} + m_{u_5}Z_{R_5}\right)s^2 \\ &+ \left(m_{u_4}Z_{R_4}u_{s_1} + m_{u_5}Z_{R_5}u_{s_1} - 4KT_{y_4}Z_{R_4}X_{sc_1}/u_{s_1} - 4KT_{y_5}Z_{R_5}X_{sc_1}/u_{s_1}\right)s \end{aligned} \tag{B.42}$$

$$D(5,3) = K_1 - 4\left(KT_{y_4}Z_{R_4} + KT_{y_5}Z_{R_5}\right)Z_{sc_1}s/u_{s_1} - \left(m_{u_4}Z_{R_4} + m_{u_5}Z_{R_5}\right)Z_{sc_1}s^2 \tag{B.43}$$

$$\begin{aligned} D(5,4) &= -4\left[KT_{y_4}Z_{R_4}\left(X_4 + X_{sc_2}\right) + KT_{y_5}Z_{R_5}\left(X_5 + X_{sc_2}\right)\right]s/u_{s_1} \\ &- \left[m_{u_4}Z_{R_4}\left(X_4 + X_{sc_2}\right) + m_{u_5}Z_{R_5}\left(X_5 + X_{sc_2}\right)\right]s^2 - 4\left(KT_{y_4}Z_{R_4} + KT_{y_5}Z_{R_5}\right) \end{aligned} \tag{B.44}$$

$$\begin{aligned} D(5,5) &= Z_{R_4}\left(F_4 - W_{u_4}\right) + Z_{R_5}\left(F_5 - W_{u_5}\right) - 2\left(KS_4{S_4}^2 + KS_5{S_5}^2\right) \\ &- \left(K_1 + KR_4 + KR_5\right) - 4\left[KT_{y_4}Z_{R_4}\left(Z_{R_4} - Z_{sc_2}\right) + KT_{y_5}Z_{R_5}\left(Z_{R_5} - Z_{sc_2}\right)\right]s/u_{s_1} \\ &+ \left[m_{u_4}Z_{R_4}\left(Z_{sc_2} - Z_{R_4}\right) + m_{u_5}Z_{R_5}\left(Z_{sc_2} - Z_{R_5}\right) - I_{xx_{s_2}}\right]s^2 \end{aligned} \tag{B.45}$$

$$D(5,6) = 0 \tag{B.46}$$

$$D(5,7) = 0 \tag{B.47}$$

$$D(5,8) = 0 \tag{B.48}$$

$$D(5,9) = 2KS_4{S_4}^2 + KR_4 - m_{u_4}Z_{R_4}Z_{u_4}s^2 - 4KT_{y_4}Z_{R_4}H_{R_4}s/u_{s_1} \tag{B.49}$$

$$D(5,10) = 2KS_5{S_5}^2 + KR_5 - m_{u_5}Z_{R_5}Z_{u_5}s^2 - 4KT_{y_5}Z_{R_5}H_{R_5}s/u_{s_1} \tag{B.50}$$

$$D(6,1) = 2KT_{y_1}H_{R_1}/u_{s_1} + m_{u_1}Z_{u_1}s \tag{B.51}$$

$$D(6,2) = \left(m_{u_1}Z_{u_1}u_{s_1} + 2KT_{y_1}H_{R_1}X_1/u_{s_1}\right)s + m_{u_1}Z_{u_1}X_1s^2 \tag{B.52}$$

$$D(6,3) = 2KS_1{S_1}^2 + KR_1 - 2KT_{y_1}H_{R_1}Z_{R_1}s/u_{s_1} - m_{u_1}Z_{u_1}Z_{R_1}s^2 \tag{B.53}$$

$$D(6,4) = 0 \tag{B.54}$$

$$D(6,5) = 0 \tag{B.55}$$

$$D(6,6) = F_1 Z_{u_1} + F_1 R - m_{u_1} g Z_{u_1} - 2KS_1 S_1^{\,2} - 2KT_{z_1} T_1^{\,2} - KR_1 - 2KT_{y_1} H_{R_1}^{\,2} s/u_{s_1} - \left(m_{u_1} Z_{u_1}^{\,2} + I_{xx_{u_1}}\right)s^2 \quad \text{(B.56)}$$

$$D(6,7) = 0 \quad \text{(B.57)}$$

$$D(6,8) = 0 \quad \text{(B.58)}$$

$$D(6,9) = 0 \quad \text{(B.59)}$$

$$D(6,10) = 0 \quad \text{(B.60)}$$

$$D(7,1) = m_{u_2} Z_{u_2} s + 4KT_{y_2} H_{R_2}/u_{s_1} \quad \text{(B.61)}$$

$$D(7,2) = \left(m_{u_2} Z_{u_2} u_{s_1} - 4KT_{y_2} X_2 H_{R_2}/u_{s_1}\right)s - m_{u_2} Z_{u_2} X_2 s^2 \quad \text{(B.62)}$$

$$D(7,3) = -\left(m_{u_2} Z_{u_2} Z_{R_2} s^2 + 4KT_{y_2} Z_{R_2} H_{R_2} s/u_{s_1} - 2KS_2 S_2^{\,2} - KR_2\right) \quad \text{(B.63)}$$

$$D(7,4) = 0 \quad \text{(B.64)}$$

$$D(7,5) = 0 \quad \text{(B.65)}$$

$$D(7,6) = 0 \quad \text{(B.66)}$$

$$D(7,7) = -m_{u_2} g Z_{u_2} - 4KT_{y_2} H_{R_2}^{\,2} s/u_{s_1} - \left(m_{u_2} Z_{u_2}^{\,2} + I_{xx_{u_2}}\right)s^2 + F_2\left(R + Z_{u_2}\right) - 2KT_{z_2}\left(T_2 + A\right)^2 - 2KT_{z_2} T_2^{\,2} - KR_2 - 2KS_2 S_2^{\,2} \quad \text{(B.67)}$$

$$D(7,8) = 0 \quad \text{(B.68)}$$

$$D(7,9) = 0 \quad \text{(B.69)}$$

$$D(7,10) = 0 \quad \text{(B.70)}$$

$$D(8,1) = m_{u_3} Z_{u_3} s + 4KT_{y_3} H_{R_3}/u_{s_1} \quad \text{(B.71)}$$

$$D(8,2) = \left(m_{u_3} Z_{u_3} u_{s_1} - 4KT_{y_3} X_3 H_{R_3}/u_{s_1}\right)s - m_{u_3} Z_{u_3} X_3 s^2 \quad \text{(B.72)}$$

$$D(8,3) = -\left(m_{u_3} Z_{u_3} Z_{R_3} s^2 + 4KT_{y_3} Z_{R_3} H_{R_3} s/u_{s_1} - 2KS_3 S_3^{\,2} - KR_3\right) \quad \text{(B.73)}$$

$$D(8,4) = 0 \quad \text{(B.74)}$$

$$D(8,5)=0 \tag{B.75}$$

$$D(8,6)=0 \tag{B.76}$$

$$D(8,7)=0 \tag{B.77}$$

$$\begin{aligned} D(8,8) &= -m_{u_3} g Z_{u_3} - 4KT_{y_3} {H_{R_3}}^2 s/u_{s_1} - \left(m_{u_3} {Z_{u_3}}^2 + I_{xx_{u_3}}\right)s^2 \\ &+ F_3\left(R + Z_{u_3}\right) - 2KT_{z_3}\left(T_3 + A\right)^2 - 2KT_{z_3} {T_3}^2 - KR_3 - 2KS_3 {S_3}^2 \end{aligned} \tag{B.78}$$

$$D(8,9)=0 \tag{B.79}$$

$$D(8,10)=0 \tag{B.80}$$

$$D(9,1)=m_{u_4} Z_{u_4} s + 4KT_{y_4} H_{R_4}/u_{s_1} \tag{B.81}$$

$$D(9,2)=\left(m_{u_4} Z_{u_4} u_{s_1} - 4KT_{y_4} H_{R_4} X_{sc_1}/u_{s_1}\right)s + 4KT_{y_4} H_{R_4} - m_{u_4} Z_{u_4} X_{sc_1} s^2 \tag{B.82}$$

$$D(9,3)=-\left(m_{u_4} Z_{u_4} Z_{sc_1} s^2 + 4KT_{y_4} H_{R_4} Z_{sc_1} s/u_{s_1}\right) \tag{B.83}$$

$$D(9,4)=-\left[4KT_{y_4} H_{R_4}\left(X_4 + X_{sc_2}\right)s/u_{s_1} + m_{u_4} Z_{u_4}\left(X_4 + X_{sc_2}\right)s^2 + 4KT_{y_4} H_{R_4}\right] \tag{B.84}$$

$$D(9,5)=2KS_4 {S_4}^2 + KR_4 + m_{u_4} Z_{u_4}\left(Z_{sc_2} - Z_{R_4}\right)s^2 + 4KT_{y_4} H_{R_4}\left(Z_{sc_2} - Z_{R_4}\right)s/u_{s_1} \tag{B.85}$$

$$D(9,6)=0 \tag{B.86}$$

$$D(9,7)=0 \tag{B.87}$$

$$D(9,8)=0 \tag{B.88}$$

$$\begin{aligned} D(9,9) &= -m_{u_4} g Z_{u_4} - \left(I_{xx_{u_4}} + m_{u_4} {Z_{u_4}}^2\right)s^2 - 4KT_{y_4} {H_{R_4}}^2 s/u_{s_1} \\ &+ F_4 R - 2KT_{z_4}\left(T_4 + A\right)^2 - 2KT_{z_4} {T_4}^2 - 2KS_4 {S_4}^2 - KR_4 + F_4 Z_{u_4} \end{aligned} \tag{B.89}$$

$$D(9,10)=0 \tag{B.90}$$

$$D(10,1)=m_{u_5} Z_{u_5} s + 4KT_{y_5} H_{R_5}/u_{s_1} \tag{B.91}$$

$$D(10,2)=\left(m_{u_5} Z_{u_5} u_{s_1} - 4KT_{y_5} H_{R_5} X_{sc_1}/u_{s_1}\right)s + 4KT_{y_5} H_{R_5} - m_{u_5} Z_{u_5} X_{sc_1} s^2 \tag{B.92}$$

$$D(10,3) = -\left(m_{u_5} Z_{u_5} Z_{sc_1} s^2 + 4KT_{y_5} H_{R_5} Z_{sc_1} s / u_{s_1}\right) \quad \text{(B.93)}$$

$$D(10,4) = -\left[4KT_{y_5} H_{R_5}\left(X_5 + X_{sc_2}\right)s / u_{s_1} + m_{u_5} Z_{u_5}\left(X_5 + X_{sc_2}\right)s^2 + 4KT_{y_5} H_{R_5}\right] \quad \text{(B.94)}$$

$$D(10,5) = 2KS_5 S_5{}^2 + KR_5 + m_{u_5} Z_{u_5}\left(Z_{sc_2} - Z_{R_5}\right)s^2 + 4KT_{y_5} H_{R_5}\left(Z_{sc_2} - Z_{R_5}\right)s / u_{s_1} \quad \text{(B.95)}$$

$$D(10,6) = 0 \quad \text{(B.96)}$$

$$D(10,7) = 0 \quad \text{(B.97)}$$

$$D(10,8) = 0 \quad \text{(B.98)}$$

$$D(10,9) = 0 \quad \text{(B.99)}$$

$$D(10,10) = -m_{u_5} g Z_{u_5} - \left(I_{xx_{u_5}} + m_{u_5} Z_{u_5}{}^2\right)s^2 - 4KT_{y_5} H_{R_5}{}^2 s / u_{s_1} + F_5 R - 2KT_{z_5}\left(T_5 + A\right)^2 - 2KT_{z_5} T_5{}^2 - 2KS_5 S_5{}^2 - KR_5 + F_5 Z_{u_5} \quad \text{(B.100)}$$

$$C(1) = 2KT_{y_1} \quad \text{(B.101)}$$

$$C(2) = 2KT_{M_1} - 2KT_{y_1}\left(X_1 + X_{sc_1}\right) \quad \text{(B.102)}$$

$$C(3) = 2KT_{y_1} Z_{R_1} \quad \text{(B.103)}$$

$$C(4) = 0 \quad \text{(B.104)}$$

$$C(5) = 0 \quad \text{(B.105)}$$

$$C(6) = 2KT_{y_1} H_{R_1} \quad \text{(B.106)}$$

$$C(7) = 0 \quad \text{(B.107)}$$

$$C(8) = 0 \quad \text{(B.108)}$$

$$C(9) = 0 \quad \text{(B.109)}$$

$$C(10) = 0 \quad \text{(B.110)}$$

APPENDIX C Comparison of analytical model and Yaw/Roll model

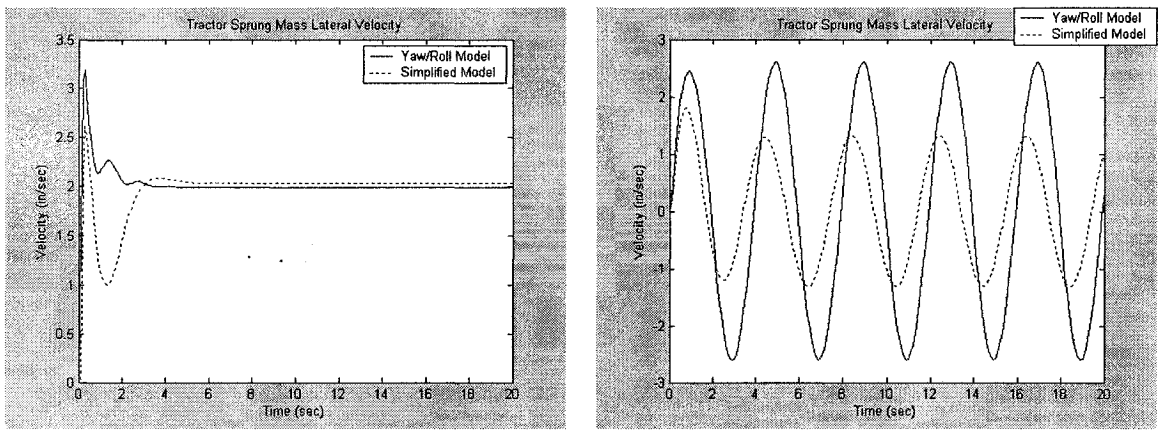

Figure C.1: Analytical transfer function vs Yaw/Roll model comparison (tractor sprung mass lateral velocity).

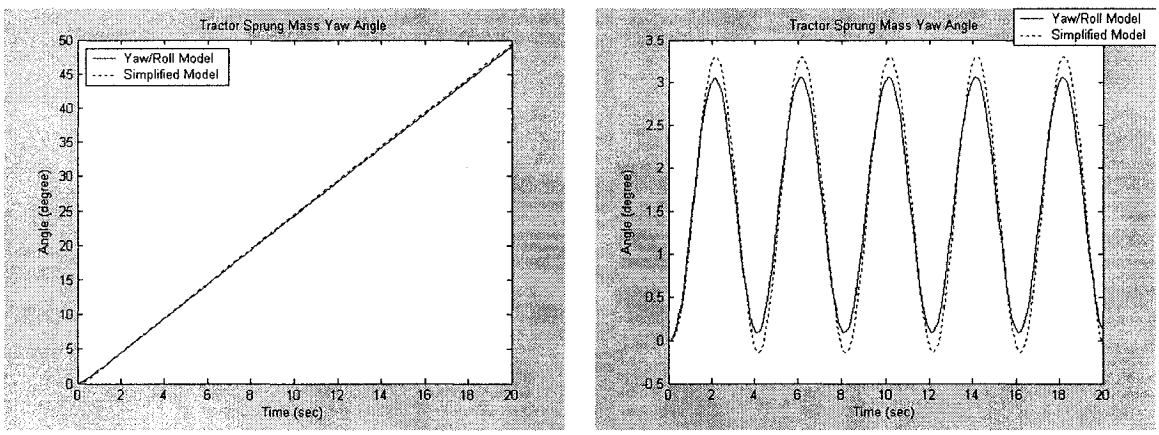

Figure C.2: Analytical transfer function vs Yaw/Roll model comparison (tractor sprung mass yaw angle).

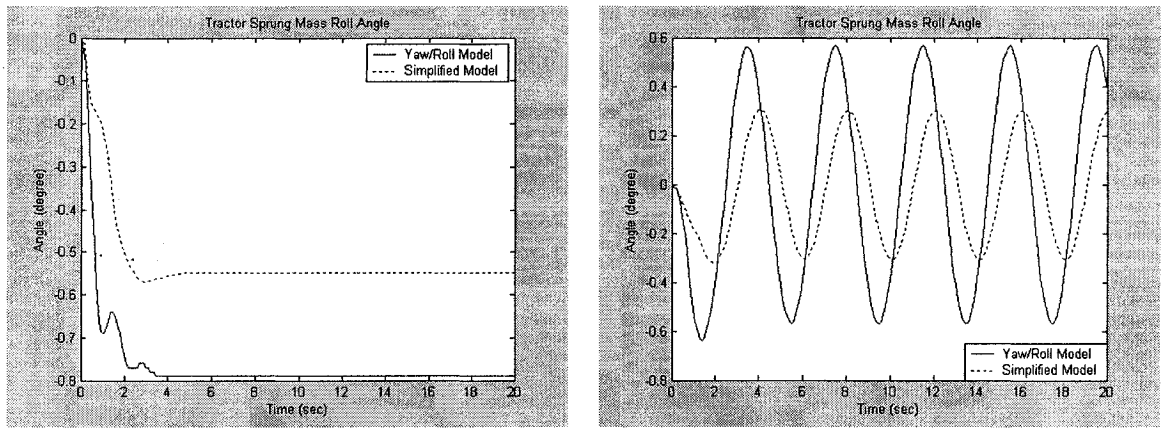

Figure C.3: Analytical transfer function vs Yaw/Roll model comparison (tractor sprung mass roll angle).

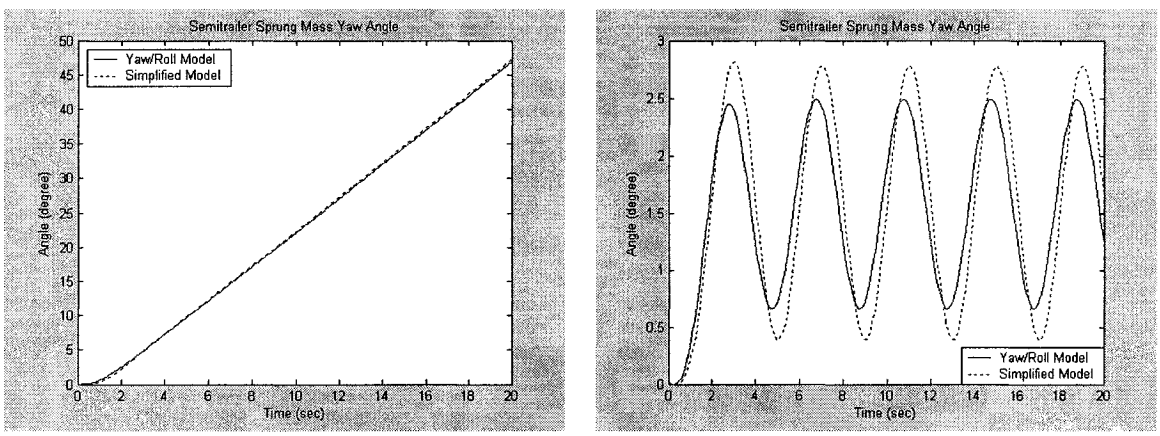

Figure C.4: Analytical transfer function vs Yaw/Roll model comparison (semitrailer sprung mass yaw angle).

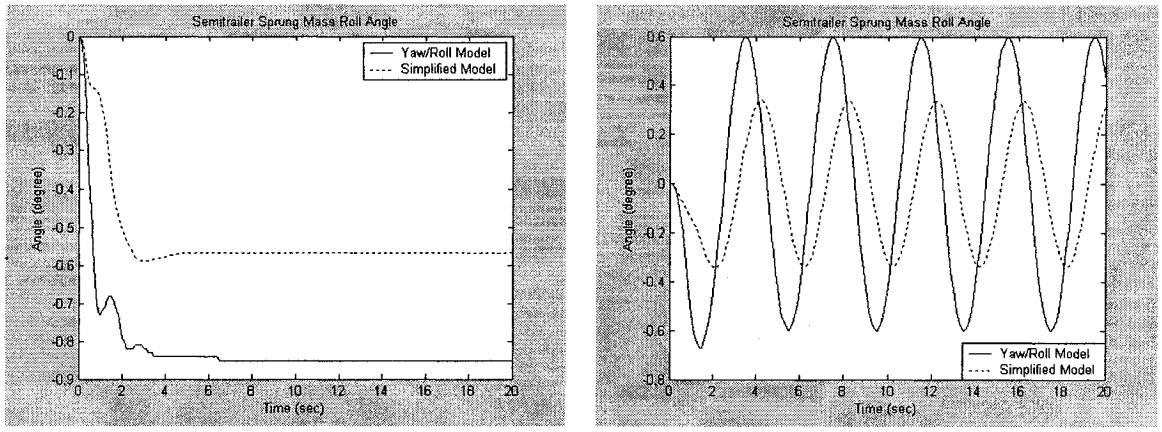

Figure C.5: Analytical transfer function vs Yaw/Roll model comparison (semitrailer sprung mass roll angle).

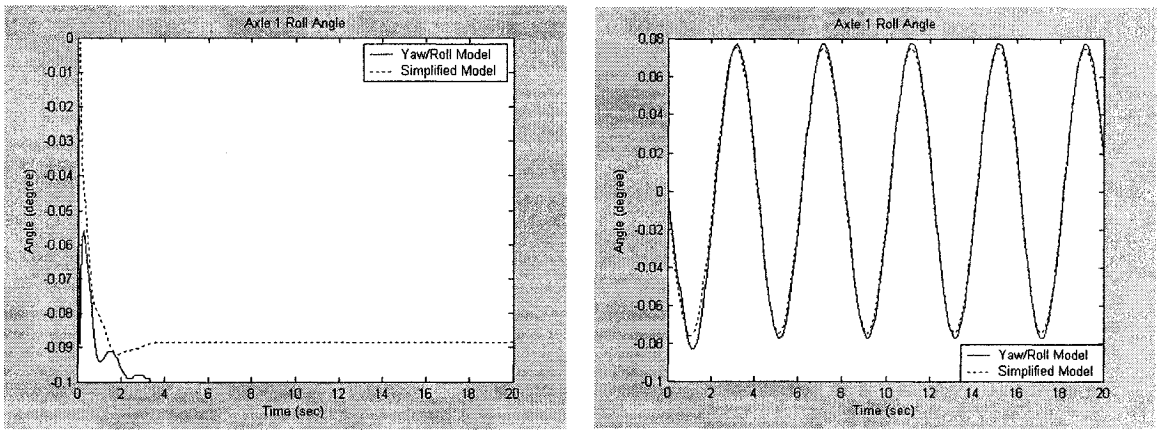

Figure C.6: Analytical transfer function vs Yaw/Roll model comparison (axle 1 roll angle).

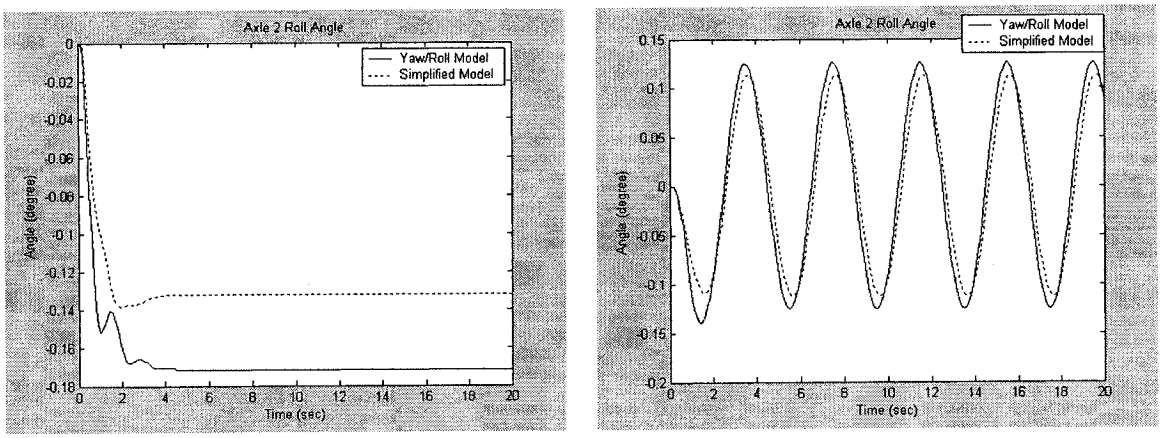

Figure C.7: Analytical transfer function vs Yaw/Roll model comparison (axle 2 roll angle).

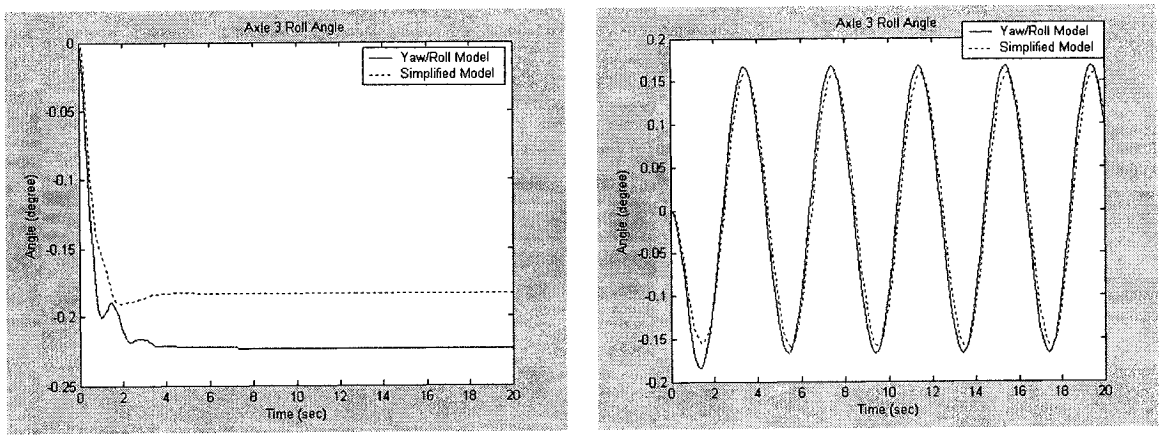

Figure C.8: Analytical transfer function vs Yaw/Roll model comparison (axle 3 roll angle).

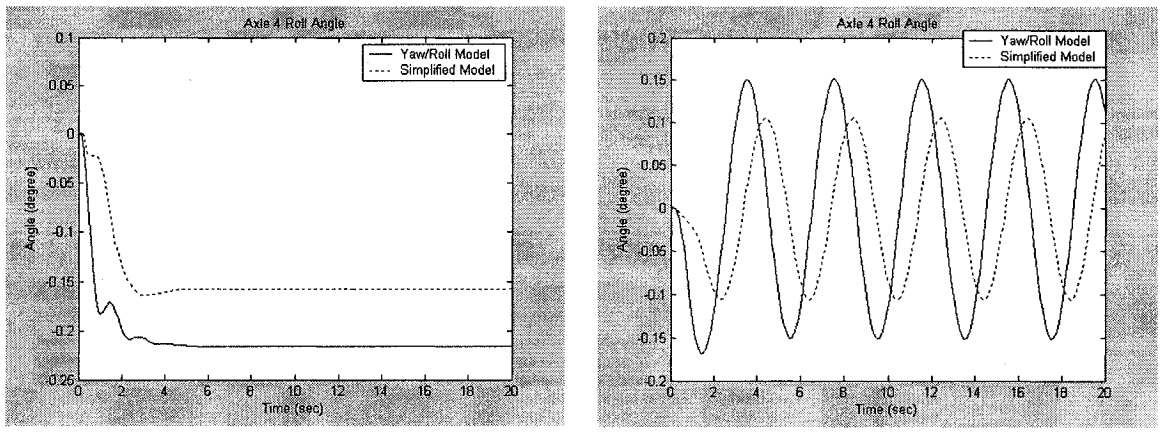

Figure C.9: Analytical transfer function vs Yaw/Roll model comparison (axle 4 roll angle).

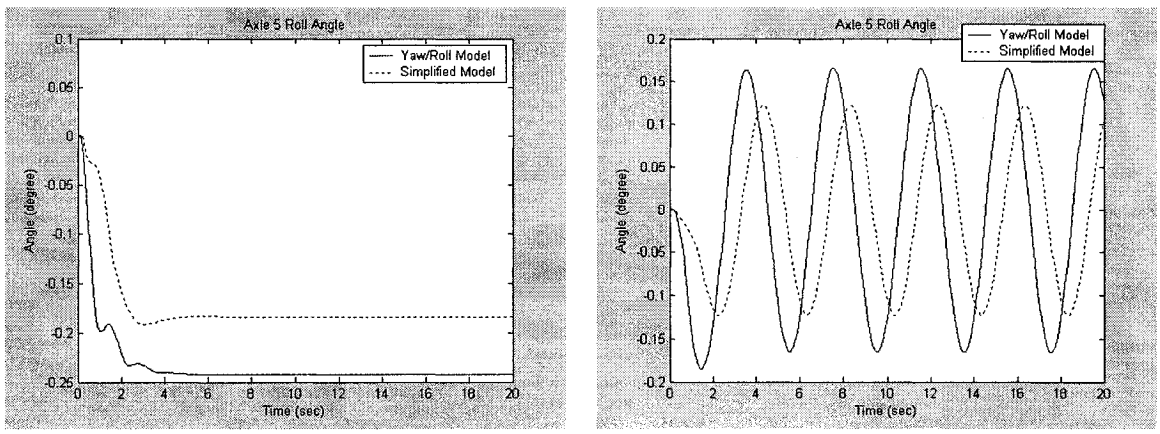

Figure C.10: Analytical transfer function vs Yaw/Roll model comparison (axle 5 roll angle).